PRIMARY PRODUCTION AND THE SETTLING FLUX IN TWO FJORDS OF BRITISH COLUMBIA, CANADA

by

David Andrew Timothy

M.Sc. Oceanography, U.B.C., 1994

B.Sc. Environmental Engineering, M.I.T., 1989

A THESIS SUBMITTED IN PARTIAL FULFILLMENT OF

THE REQUIREMENTS FOR THE DEGREE OF

DOCTOR OF PHILOSOPHY

in

THE FACULTY OF GRADUATE STUDIES

DEPARTMENT OF EARTH AND OCEAN SCIENCES

We accept this thesis as conforming

to the required standard

THE UNIVERSITY OF BRITISH COLUMBIA

July 2001

In presenting this thesis in partial fulfilment of the requirements for an advanced degree at the University of British Columbia, I agree that the Library shall make it freely available for reference and study. I further agree that permission for extensive copying of this thesis for scholarly purposes may be granted by the head of my department or by his or her representatives. It is understood that copying or publication of this thesis for financial gain shall not be allowed without my written permission.

Department of Earth + Ocean Sciences

The University of British Columbia
Vancouver, Canada

Date July 6, 2001

Abstract

A time series of primary production and sediment trap flux measurements was carried out in two fjords of British Columbia, Canada between 1983 and 1989. The fjords, periodically anoxic Saanich Inlet and oxygen-replete Jervis Inlet, were chosen in order to compare organic matter formation and particle flux in these environments with largely differing redox conditions. Two sediment-trap moorings were deployed in each fjord, and each mooring had sediment traps at three depths. The moorings were serviced monthly, when primary production was also measured using the ^{14}C-uptake technique. Hydrographic and nutrient data were collected during portions of the experiment, and ^{210}Pb profiling of bottom sediments allowed comparison of water-column fluxes and sedimentary accumulation rates.

Saanich Inlet (490 g C m^{-2} y^{-1}) was 1.7 times more productive than Jervis Inlet (290 g C m^{-2} y^{-1}) and primary production toward the mouths of both fjords was 1.4 times higher than at the heads of the fjords. The elevated rates of primary production in Saanich Inlet were probably due to exchange with the nutrient-rich surface waters of the passages leading to the Pacific Ocean, and the up-inlet gradients in both fjords reflected the relative nutrient supply. The sediment-trap material was dominated by biogenic silica, especially in the spring and early summer but also in the late summer and fall, while organic carbon fluxes tended to peak in the summer. While winter fluxes were usually dominated by aluminosilicates, at the mouth of Jervis Inlet organic matter often comprised most of the mass flux to the 50 m sediment traps, as wintertime sources of biogenic silica and aluminosilicates were small. At the head of Saanich Inlet, the aluminosilicate flux closely followed the pattern of local rainfall and flow from the Cowichan

River, a distinct difference from the other stations where turbulent resuspension from topographic boundaries and particle focusing appear to have dominated the lithogenic flux. $\delta^{13}C$ of the trapped material was heavier in the summer than in the winter, reflecting a higher ratio of marine to terrestrial organic matter at that time. The relationship between stable carbon isotope ratios and BSi content revealed that 70-80% of the marine OC in these fjords is diatomaceous. This relationship was furthermore used to estimate the $\delta^{13}C$ endmember of the marine organic matter and the proportion of terrigenous material to the total organic matter flux. Export ratios of organic carbon were low, likely because of solubilisation within the traps, while export ratios of biogenic silica were high. Sediment-trap fluxes at the mouth of Saanich Inlet were strongly affected by a sediment plume that extended off the nearby sill. However, compared to the other stations, this plume did not result in excess sedimentary accumulation of biogenic silica and organic carbon relative to local primary production. At each station, similar proportions of local primary production ($\sim$5%) were buried in the sediments below, suggesting that the bulk of the marine organic matter was not preferentially preserved in the intensely anoxic sediments of Saanich Inlet.

The possibility of organic matter solubilisation within the sediment traps, and the excessive water-column fluxes at the mouth of Saanich Inlet, confuse comparison of organic carbon fluxes in Saanich and Jervis Inlets. However, away from the mouth of Saanich Inlet water-column fluxes of biogenic silica were proportional to local primary production. If the biogenic silica carried proportional amounts of organic matter, then the heightened primary production in Saanich Inlet resulted in a large delivery of organic matter to depth. Combined with the high primary production and export flux, low rates of vertical mixing and particle-entrapment within the fjord, factors associated with the weak estuarine circulation and weak winds of Saanich Inlet, may have also stimulated

anoxia. Although in Jervis Inlet there is more stagnant water behind the sill and deep-water renewals were less frequent than in Saanich Inlet, the deep sill allows oxidation of a significant fraction of the sinking organic matter before the stagnant waters are reached, reducing the chances of oxygen depletion in the bottom waters.

A model that estimates rates of water-column decay from sediment-trap data showing increases in flux with depth was used with the time series from Saanich and Jervis Inlets. Model results from Saanich Inlet were not conclusive, possibly because the depth interval between sediment traps was too small to resolve water-column rates of decay. However, the model fit well to the time series from Jervis Inlet, and rate constants for organic carbon and nitrogen agree well with previous estimates made from oceanic settings. The model has also allowed some of the first estimates of depth-dependent dissolution rates of sinking biogenic silica, and translation to time-dependent dissolution using a nominal sinking rate suggests the diatomaceous opal in Jervis Inlet was dissolving rapidly. Changes with depth of rate constants for organic carbon, nitrogen and biogenic silica are well described by the power function, suggesting that organic matter and biogenic silica are composed of a set of multiple components that decay at varying rates. This model for decay has been explained for organic matter, and for the biogenic silica may be caused by the presence of various diatom species or degrees of frustule fragmentation that result in a number of fractions with different dissolution rates. The model has also allowed a description of the material that causes increases in flux with depth. This sediment was depleted of organic carbon and nitrogen and thus appeared diagenetically altered, and its aluminosilicate and biogenic silica contents were characteristic of hydrodynamically sorted resuspended material. Additional material was delivered to the deepest sediment traps during deepwater renewals, but a continual process such as tidal resuspension, particle focusing, or increases in trapping efficiency with depth resulted in additional fluxes to the mid-depth sediment traps.

Table of Contents

List of Tables

List of Figures

Preface

The results of the primary production time series have been published (Timothy and Soon, 2001); Chapter 2 is a slightly modified version to accommodate the structure of this dissertation. The descriptive portion of the sediment trap experiment (the majority of Chapter 3) will be submitted to *Progress in Oceanography.* The principles of the sediment-trap model used in Chapter 4 were first described by Timothy (1994) and a version of the model was published by Timothy and Pond (1997). The results of this model applied to the time series from Jervis Inlet will be submitted to the *Journal of Geophysical Research* or *Global Biogeochemical Cycles.*

Acknowledgements

From the beginning of this project, my supervisor, Steve Calvert, has been extremely supportive intellectually and personally, and through many surprising circumstances he somehow maintained his calm. I am grateful to Steve and committee member Ken Denman for quickly commenting on chapters of the dissertation. The rest of my committee, Paul Harrison and C.S. Wong, were always supportive and Paul gave very good advice at various stages. I am very grateful to Steve Pond who encouraged me to think critically in the early stages of my work.

Collecting the data presented here was truly a Herculean endeavor, tackled almost entirely by Maureen Soon. I can't thank her enough for her commitment, and for the constructive and pleasant environment she created in the lab. Ram and Hugh, and the officers and crew of the *C.S.S. Vector*, provided excellent help and good humour during the field program, so I'm told! Bente Nielsen, Christine Elliott, Kathy Gordon and Bert Mueller were also very helpful with laboratory analyses. I am thankful to everybody in the Annex for their help and patience. Roger Pieters, Rich Pawlowicz, Susan Allen and Lionel Pandolfo have answered questions and allowed me to work on their computers. Tom Pedersen was always available for questions and advice, and Kristin Orians helped establish methods on the ICP-MS. Yuval gave very efficient lessons in matlab particular to the modelling - thanks! Don Murray and Jesse Hoey pointed me to the solution I used in the model. Stan Stubbe at Environment Canada was helpful in providing data. Discussions with Stephanie and Markus Kienast were helpful, especially in the last days of writing. Thanks to Greg Cowie, Lou Hobson and Graham Shimmield for providing data. And thanks to Roger François for his early involvement in the project.

Very rarely, but every once in a while, I was not in the lab or in front of the computer. Thanks to the many friends who have made my experiences in British Columbia fantastic! I am grateful to my family for their support while I've been so far away and to William for ... refraining from tearing me limb from limb with his terrible sharp teeth and vicious, slashing claws!

Chapter 1

Physical, ecological and environmental setting

1.1 Introduction

An improved understanding of primary production and particle flux in the ocean requires the construction of reliable budgets of biogenous elements. Indeed, much work has focussed on descriptions of carbon and nutrient cycling for both open ocean (Bishop, 1989; Siegenthaler and Sarmiento, 1993; Michaels et al., 1994; Emerson et al., 1995) and coastal regions (Burrell, 1988; Wassmann, 1991; Smith and Hollibaugh, 1993; Liu et al., 2000). Budgets for carbon are of special interest because of the role that the oceans play in modulating atmospheric CO_2 concentration (Siegenthaler and Sarmiento, 1993). However, descriptions for coastal regions are complicated because at the coastal boundary continental inputs (Berner, 1989; Smith and Hollibaugh, 1993; Liu et al., 2000) and turbulent processes causing sediment resuspension and redistribution (Håkanson et al., 1989) are significant but difficult to quantify. The coastlines are furthermore marked by their heterogeneity, so that generalisations of biogeochemical processes are difficult to make (Liu et al., 2000). Nevertheless, a description of the fluxes occurring at the oceanic boundary is crucial to our understanding of carbon and nutrient cycling on a global scale, as the ocean margins account for $\sim$20% of global ocean primary production (Walsh, 1988; Liu et al., 2000) and most of the organic carbon burial in marine sediments (Berner, 1982; Hedges and Keil, 1995; Middleburg, 1997).

Large, fast-sinking particles make up a small fraction of the particulate matter in sea

water, but they are the primary vehicle by which material is transported through the water column (McCave, 1975). Therefore, an important component of our understanding of element cycling is a description of large particle sinking and decay. Combined with knowledge of the export flux of material from surface waters (Dugdale and Goering, 1967; Eppley and Petersen, 1979; Boyd and Newton, 1995), decay rates can then be used to infer, for example, the vertical distribution of oxygen and nutrients (e.g.; Suess, 1980; Martin et al., 1987) and the effectiveness of carbon delivery to the deep ocean and sediments (Suess and Müller, 1980; Hargrave et al., 1994; Hedges, 1992). To this end, sediment-trap fluxes are often appropriate for estimates of vertical flux and particulate decay (e.g.; Bishop, 1989), but in coastal waters a number of processes can contribute excess material to deep sediment traps rendering the information they collected difficult to interpret.

Fjords are semi-enclosed, overdeepened coastal features that have long been recognised as accessible locations where biological and geochemical processes relevant to oceanic systems can be studied (e.g.; Skei, 1983). Studies in fjords have greatly contributed to our understanding of the ecology and physiology of phytoplankton (e.g.; Sakshaug and Myklestad, 1973; Takahashi et al., 1977, 1978; Hobson, 1981; Parsons et al., 1983; Sakshaug and Olsen, 1986; McQuoid and Hobson, 1995; Kukert and Riebesell, 1998) and zooplankton (Huntley and Hobson, 1978; Takahashi and Hoskins, 1978; Koeller et al., 1979; Dagg et al., 1989; Buck and Newton, 1995), and the factors that control plankton community development have been tested using the environment of a fjordal basin (Ross et al., 1993). Links between the plankton community and sedimentation have been investigated in a number of fjords (e.g.; Wassmann, 1984; Burrell, 1988; Sancetta and Calvert, 1988; Sancetta, 1989c; Wassmann, 1991; Overnell et al., 1995), and models of diatom aggregation have here been explored (Kiørboe et al., 1994, 1996; Hansen and Kiørboe, 1995). Measurements of biochemical markers for marine and terrigenous organic matter

collecting on the continental margins have been made in this environment (Hedges et al., 1988a, 1988b; Cowie and Hedges, 1992) and, as analogs of anoxic basins, the redox chemistry within fjords has been studied in great detail (e.g.; Richards, 1965; Emerson, 1980; Skei, 1983; Smethie, 1987; McKee and Skei, 1999).

This thesis reports a multi-year time series of primary production and sediment-trap flux collected during the 1980s in Saanich and Jervis Inlets, two fjords of southern British Columbia, Canada. In this chapter, I provide physical and ecological descriptions of the fjords and show environmental time series from the 1980s, providing a backdrop for subsequent chapters. Chapter 2 reports the primary production results and discusses causes of anoxia in Saanich Inlet. Chapter 3 presents the sediment-trap data, discusses the relationship between primary production and water-column flux and compares sediment-trap fluxes with bottom sediment accumulation rates. In chapter 4, a balance equation is used to determine rates of water-column remineralisation of the biogenous fluxes and describes the causes of observed increases in flux with depth in both fjords. Chapter 5 provides a summary of conclusions.

1.2 Saanich and Jervis Inlets

1.2.1 Physical descriptions

Saanich and Jervis Inlets of southern British Columbia (Figures 1.1 through 1.3) are contrasting fjords contiguous with the southern Strait of Georgia. Jervis Inlet is a long (89 km), deep-silled (240 m) fjord with a maximum depth of 730 m. Moderate fresh-water input at the head of Jervis Inlet (annual mean of 180 m^3 s^{-1}; Pickard, 1961) drives weak estuarine circulation with a net movement of surface waters seaward and replacement flow at depth (Pickard, 1961; Lazier, 1963). Jervis Inlet is within the coastal western hemlock (CWH) biogeoclimatic zone that extends throughout most of coastal BC (Pojar et al.,

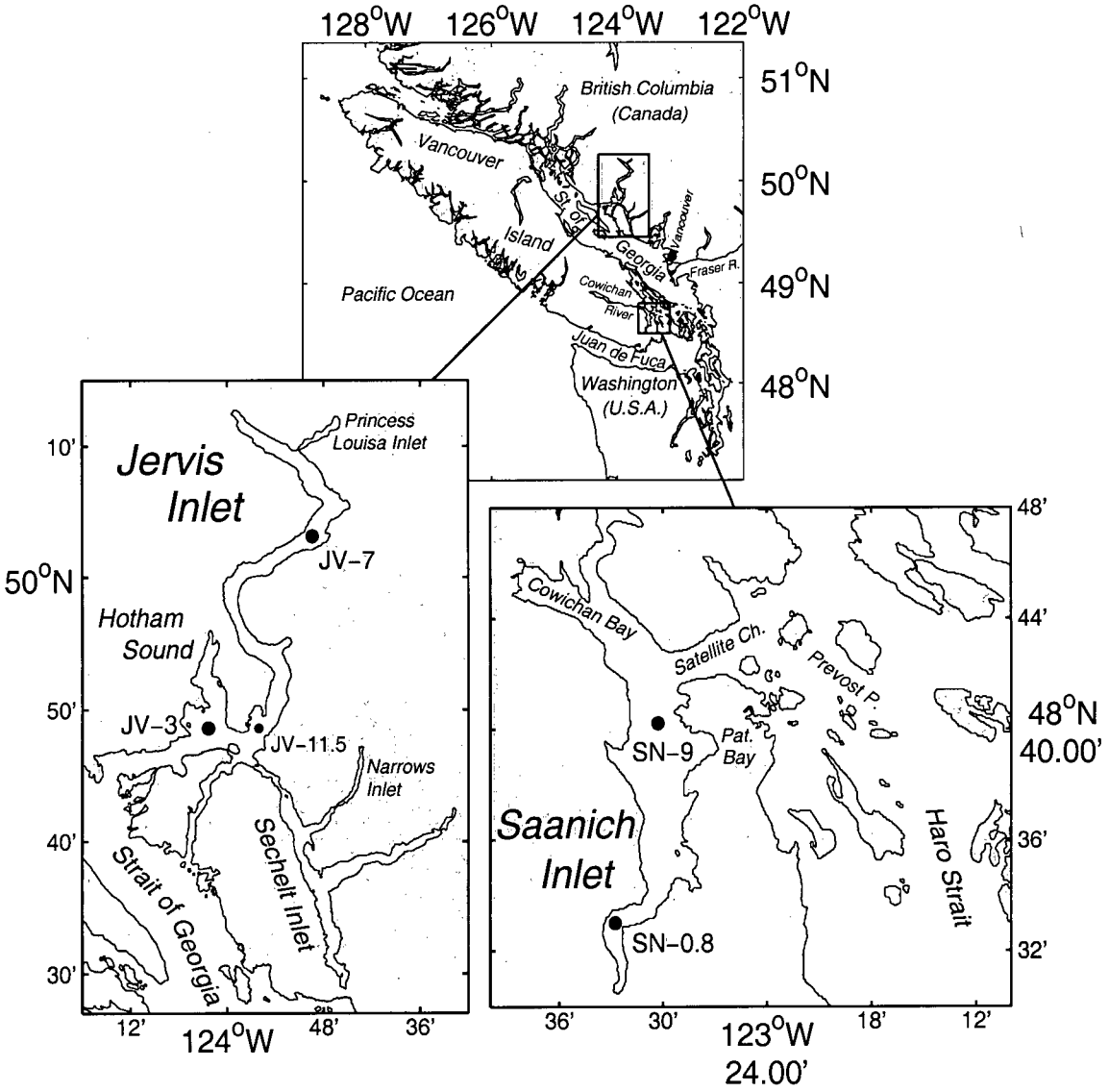

Figure 1.1: Sampling stations in Saanich and Jervis Inlets. The Cowichan River flows into Cowichan Bay.

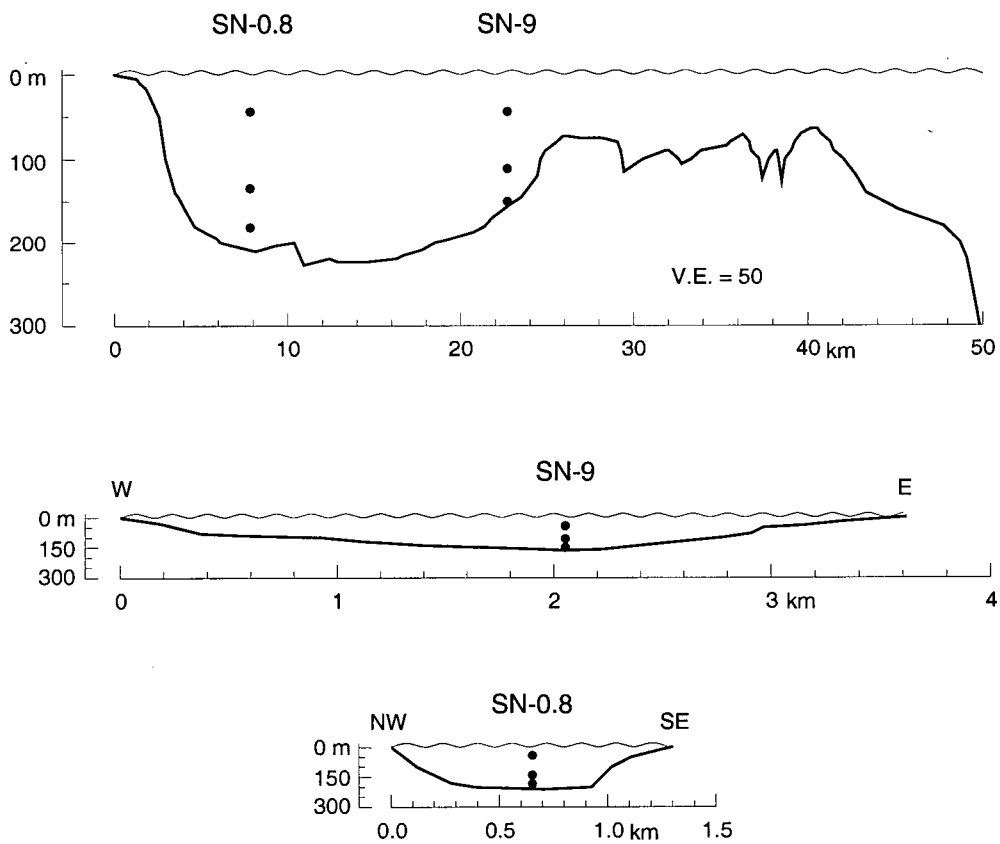

Figure 1.2: Longitudinal (vertical exaggeration = 50) and transverse (to scale) cross-sections of Saanich Inlet showing mooring locations and sediment-trap depths. Sill and maximum depths of Saanich Inlet are 70 m and 235 m, respectively.

1991). The CWH zone is characterised as cool and mountainous with heavy precipitation in the fall and winter (Figure 1.11). Anoxia is not known to occur in Jervis Inlet (Lazier, 1963; Smethie, 1987; Figures 1.6 and 1.7).

Located on southern Vancouver Island, Saanich Inlet (Figures 1.1 and 1.2) is 24 km long, has a maximum depth of 235 m and a broad, shallow (70-80 m) sill that runs the length of the eastern branch of Satellite Channel. Saanich Inlet is in the coastal Douglas-fir (CDF) zone, a low-elevation region along the southeastern coast of Vancouver

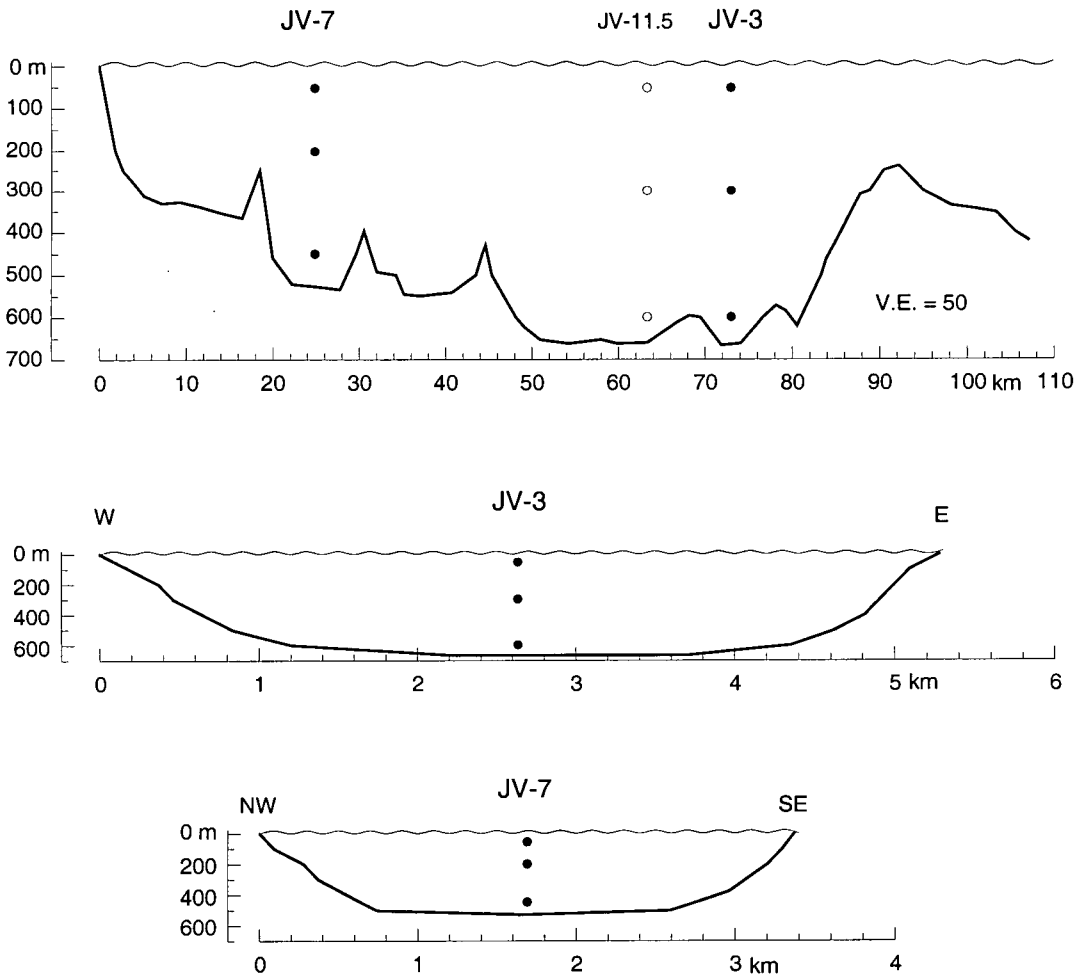

Figure 1.3: Longitudinal (vertical exaggeration = 50) and transverse (to scale) cross-sections of Jervis Inlet showing mooring locations and sediment-trap depths. The mooring at the mouth of Jervis Inlet was moved from JV-11.5 to JV-3 early in the time-series (see Table 3.1 dates of deployment). Sill and maximum depths of Jervis Inlet are 240 m and 730 m, respectively. This sill depth is significantly shallower than has been reported by others, including Timothy and Soon (2001), who used a value reported by Pickard (1961). Pickard's value of 385 m refers to the depth of the region where surface water properties are no longer affected by the outflow from Jervis Inlet, a location somewhat inside the morphological sill.

Island and including many islands within the southern Strait of Georgia (Nuszdorfer et al., 1991). The CDF zone is within the rainshadow of Vancouver Island and the Olympic mountains, and is drier and warmer than the CWH zone surrounding Jervis Inlet. Runoff from the Goldstream River (Figure 1.13) at the head of Saanich Inlet is very small (annual mean ≤ 2 m^3 s^{-1}; Stucchi and Whitney, 1997) and the largest sources of fresh water, the Cowichan and Fraser Rivers (Figure 1.1), are located seaward of the fjord (Herlinveaux, 1962). Precipitation in coastal southern British Columbia tends to be highest in the fall and winter. Thus, runoff from the Cowichan River peaks in the winter while that of the Fraser River, the predominant source of freshwater to the Strait of Georgia, is highest in June when the melt from ice and snow peaks. These external sources of freshwater cause irregular surface currents and weak or absent estuarine flow within Saanich Inlet (Herlinveaux, 1962; Stucchi and Whitney, 1997). A characteristic relatively unique among British Columbia fjords is the periodic development of anoxia in the bottom waters of Saanich Inlet (Richards, 1965; Anderson and Devol, 1978; Cowie et al., 1992; Figures 1.4 and 1.5); hydrogen sulphide periodically extends to 50-80 m off the bottom in the central basin of Saanich Inlet (Richards, 1965).

Generally, neither inlet exhibits an upper mixed layer. Instead, the steepest density gradient occurs at the surface in Saanich Inlet (Herlinveaux, 1962) and Jervis Inlet (Pickard, 1961) and is larger in Jervis Inlet (Sancetta, 1989a). Deepwater renewal to both fjords occurs during the summer or fall when upwelling along the coastal rim of the northeast Pacific Ocean brings dense, nutrient-rich waters through Juan de Fuca Strait and into the Strait of Georgia. Deepwater renewal appears to occur most years in Saanich Inlet (Anderson and Devol, 1973; Figures 1.4 and 1.5), but renewals occur every several years in Jervis Inlet (Lazier, 1963; Pickard, 1975; Figures 1.6 and 1.7).

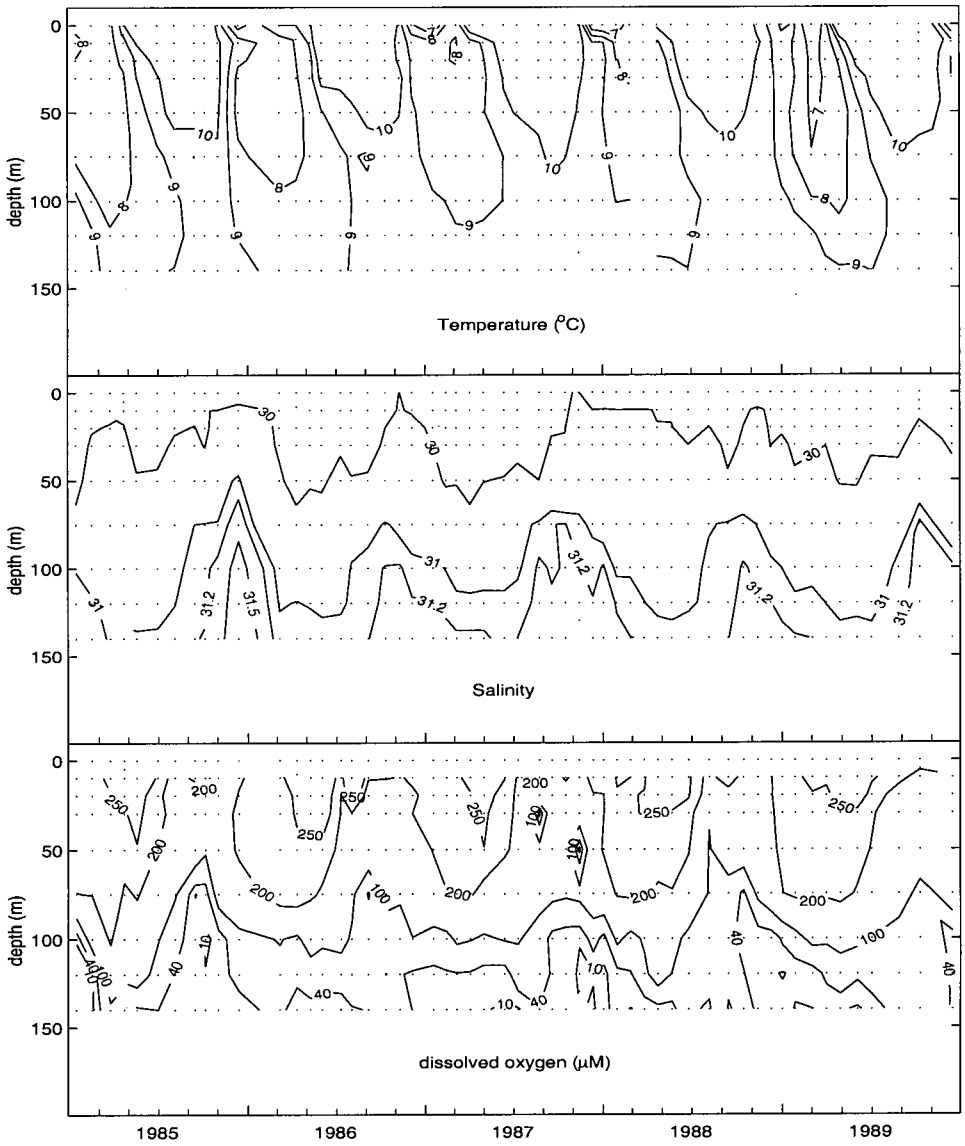

Figure 1.4: Temperature, salinity and dissolved oxygen at station SN-9. Greater detail of the temperature and salinity structure of the upper 40 m is given in Figure 2.1.

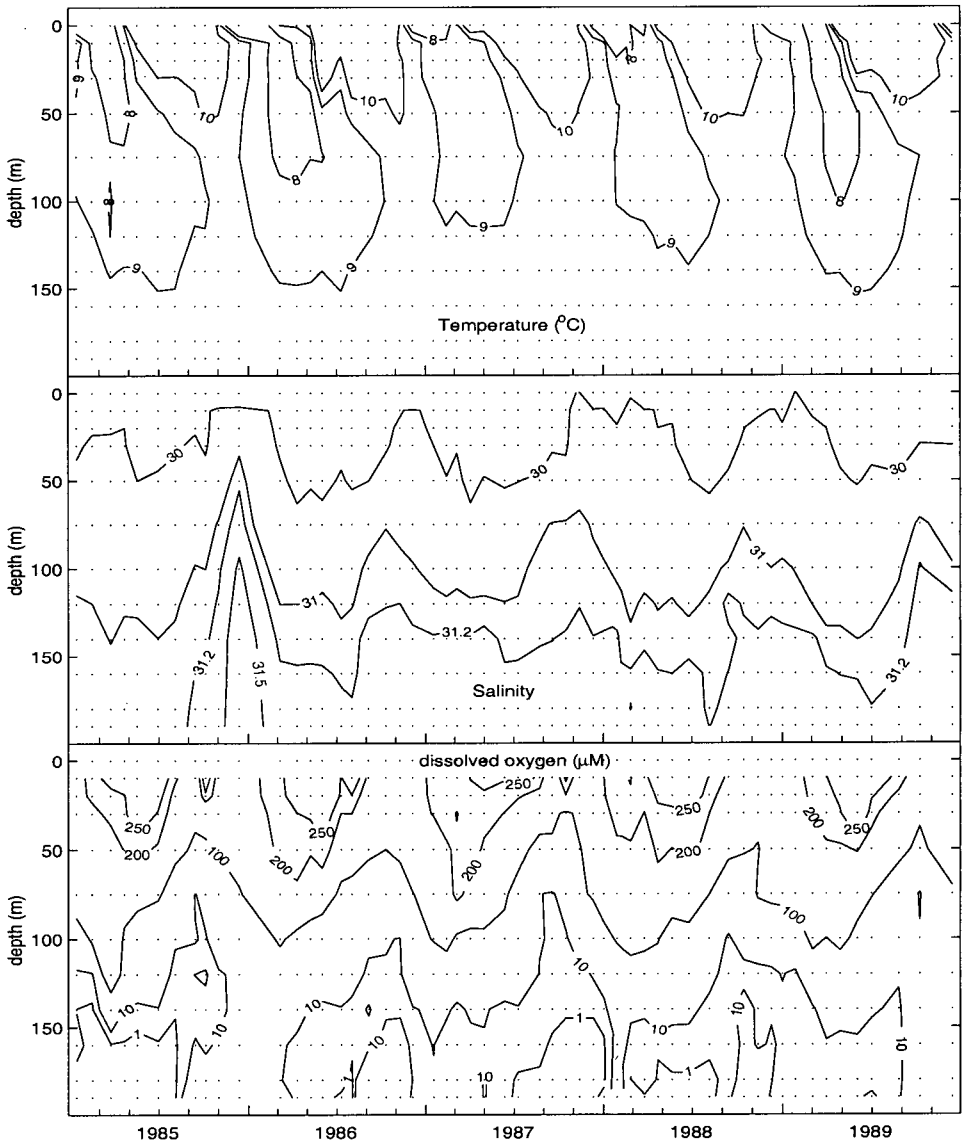

Figure 1.5: Temperature, salinity and dissolved oxygen at station SN-0.8. Zero dissolved oxygen concentrations were measured in waters inside the 1 μM contour. Greater detail of the temperature and salinity structure of the upper 40 m is given in Figure 2.2.

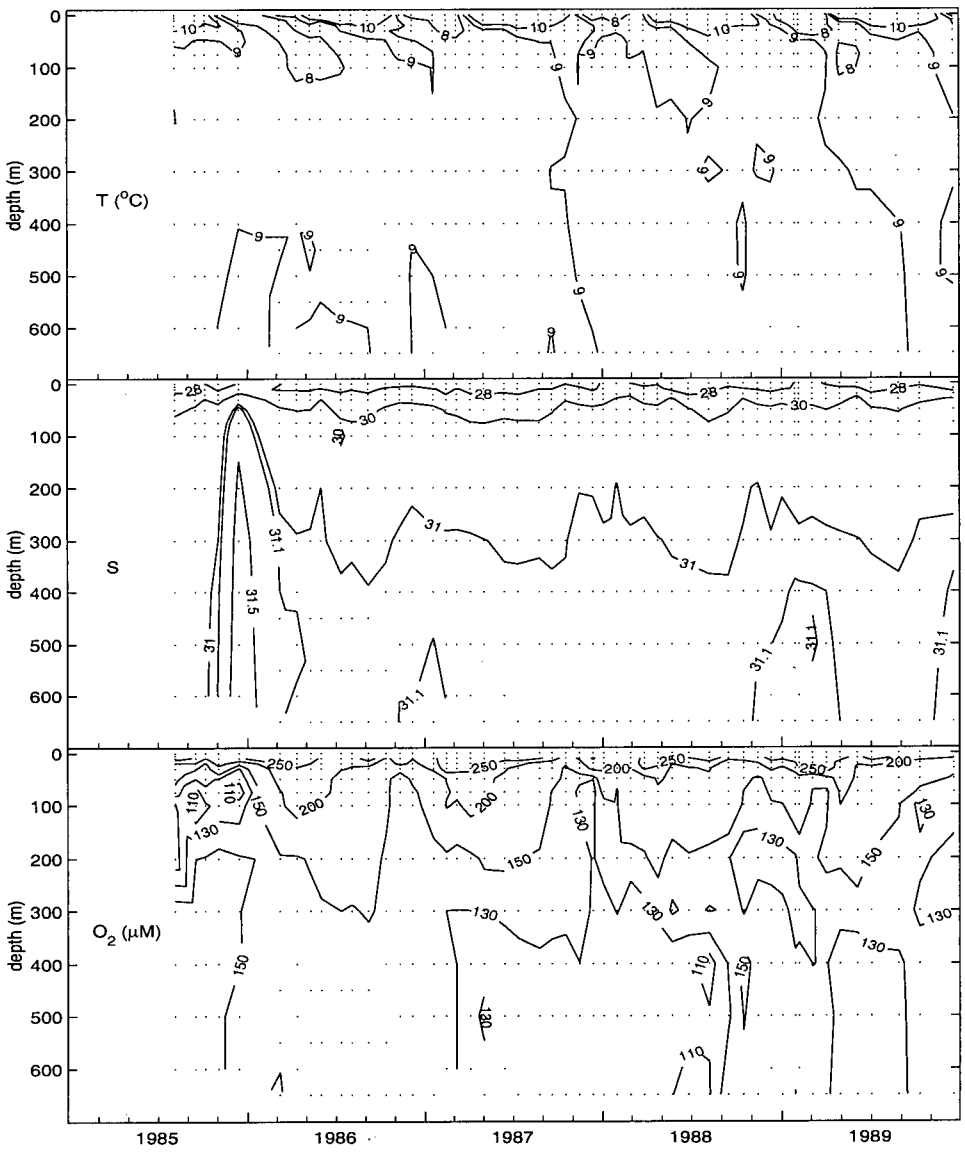

Figure 1.6: Temperature, salinity and dissolved oxygen at station JV-3. Greater detail of the temperature and salinity structure of the upper 40 m is given in Figure 2.3.

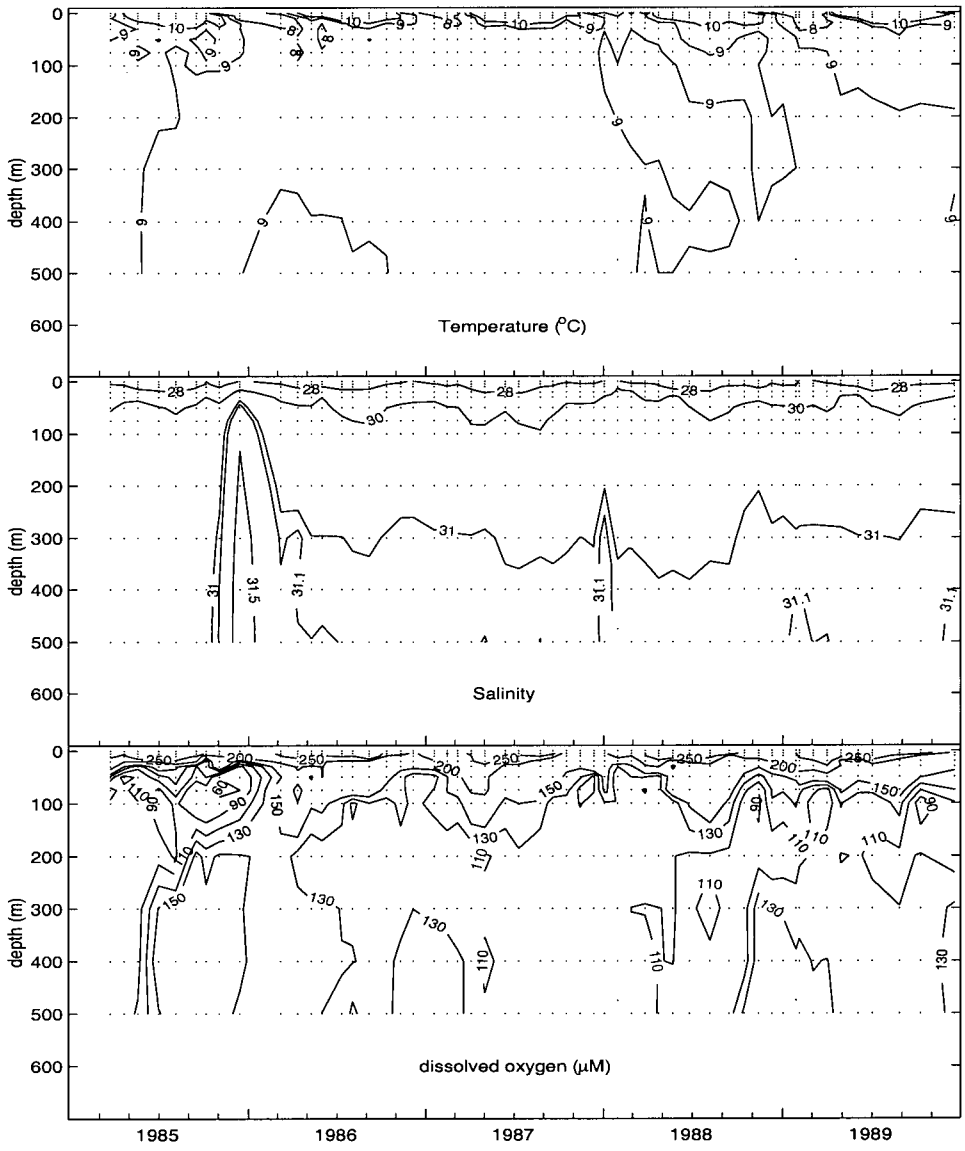

Figure 1.7: Temperature, salinity and dissolved oxygen at station JV-7. Greater detail of the temperature and salinity structure of the upper 40 m is given in Figure 2.4.

1.2.2 Plankton ecology

Harrison et al. (1983) provide a thorough review of plankton ecology for the Strait of Georgia and contiguous waters, for which reports from Saanich Inlet are significant. From what is known about plankton dynamics in Jervis Inlet (Stockner and Cliff, 1975; Parsons et al., 1984b; Cochlan et al., 1986; Sancetta, 1989a, 1989b, 1989c), they appear similar to the descriptions of Harrison et al. (1983). Further insight into Jervis Inlet is provided by Haigh et al. (1992) and Taylor et al. (1994) who present a two-year study of phytoplankton ecology in a connected fjord, Sechelt Inlet (Figure 1.1). Similarly, a one-year study of diatom populations outside but near Saanich Inlet (Hobson and McQuoid, 1997) is relevant.

The phytoplankton succession typical of coastal, temperate seas (Margarlef, 1958; Guillard and Kilham, 1977) is observed in the southern Strait of Georgia (Harrison et al., 1983; Haigh et al., 1992) with some exceptions in Saanich and Jervis Inlets (Sancetta, 1989a). Thus, diatoms contribute most of the yearly primary production with occasionally significant growth of dinoflagellates and nanoflagellates, while diatom-predominance is greater in Saanich Inlet than in Jervis Inlet (Sancetta, 1989a). During much of the fall and winter in Saanich Inlet, light limits photosynthesis (Takahashi et al., 1978) and nanoflagellates are the predominant phytoplankton (Takahashi et al., 1978; Smith and Hobson, 1994). Although winter conditions may be similar in Jervis Inlet, sampling has been less frequent there. In and near both inlets, the productive season begins around April with the blooming of *Thalassiosira* spp., while blooms of *Skeletonema costatum* and small *Chaetoceros* species occur concomitantly or shortly thereafter (Stockner and Cliff, 1975; Takahashi et al., 1977; Hobson, 1981, 1983; Sancetta, 1989a, 1989b, 1989c; Haigh et al., 1992; Hobson and McQuoid, 1997). Through frequent sampling, Takahashi et al. (1977) found the spring bloom in Saanich Inlet to last for about two weeks and,

throughout the summer and fall, various other diatom and flagellate blooms occurred. They showed that these blooms were always preceded by high surface nitrate and silicic acid concentrations and later Parsons et al. (1983) suggested that they were caused by increased mixing across the broad sill during spring tides leading to greater influxes of nutrients. Hobson (1985) found periods of the summer when nutrients were severely depleted in Saanich Inlet and flagellates predominated. Similar flagellate-predominance was observed during nutrient-deplete, summertime conditions in Sechelt Inlet (Haigh et al., 1992; Taylor et al., 1994), a branch of the Jervis Inlet system (Figure 1.1).

The zooplankton of these waters can have a significant impact on phytoplankton dynamics. Their populations sometimes comprise a large amount of surface layer biomass and can lead to mass export of the phytoplankton population (Takahashi and Hoskins, 1978; Koeller et al., 1979; Harrison et al., 1983; Sancetta, 1989a, 1989b, 1989c). Calanoid copepods such as *Pseudocalanus* spp., *Calanus pacificus* and *Neocalanus plumchrus* have the largest effect on the phytoplankton of waters contiguous with the Strait of Georgia (Harrison et al., 1983). Their greatest grazing pressure occurs at or shortly after the spring bloom, when *Calanus pacificus* and *Neocalanus plumchrus* have returned to surface waters from depth in their ontogenic cycle. In the past decade, it appears that the timing of this cycle has shifted to about one month earlier than historically reported, but when this shift occurred relative to the 1980s when this experiment occurred is unclear (Bornhold, 2000). Medusoid zooplankton have been reported to penetrate into Saanich Inlet and significantly impact phytoplankton nutrient dynamics (Huntley and Hobson, 1978).

1.3 Environmental setting

The time series reported in this thesis began in 1983 and ended in 1989. Environmental data from this period are presented in Figures 1.9 through 1.14 in order to put the primary production and sediment-trap time series in context. A weak El Niño occurred in 1986/87, and a larger El Niño occurred in 1982/83 shortly before the time series began (Figure 1.9). There does not appear to have been a strong atmospheric response to these El Niño events; however, the Fraser River freshet was perturbed from the decadal average in 1982 and 1986. Where available, the environmental data go back to 1980 in order to include the earlier El Niño and to test for teleconnections between the Equatorial Pacific and southern BC.

Temperature and precipitation data (Figures 1.10 and 1.11) were collected at Victoria Airport, Merry Island and Malibu Rapids (Figure 1.8), and sunshine measurements (Figure 1.12) were made at Victoria Airport and Merry Island (Environment Canada). The sunshine data were collected using Campbell-Stokes Sunshine Recorders to measure cloud opacity. These instruments record the number of hours per day that light intensity is above a threshold value and are reported in units of 'actual sunlight hours', ranging between zero and the number of hours between sunrise and sunset on a given day. Efforts to convert 'actual sunlight hours' into irradiance ($\mu E/m^2/s$) or photosynthetically available radiation (PAR; $\mu E/m^2/s$ of wavelengths between ~400-700 nm) are generally unsuccessful because the threshold value, determined as the ability to burn chemically coated cardboard, is affected by atmospheric humidity. Nevertheless, Figure 1.12 provides a subjective record of seasonal variability in the amount of sunshine reaching Saanich Inlet and a region near the mouth of Jervis Inlet. Sunshine at Victoria Airport and Merry Island were similar throughout the 1980s, but, because precipitation was significantly

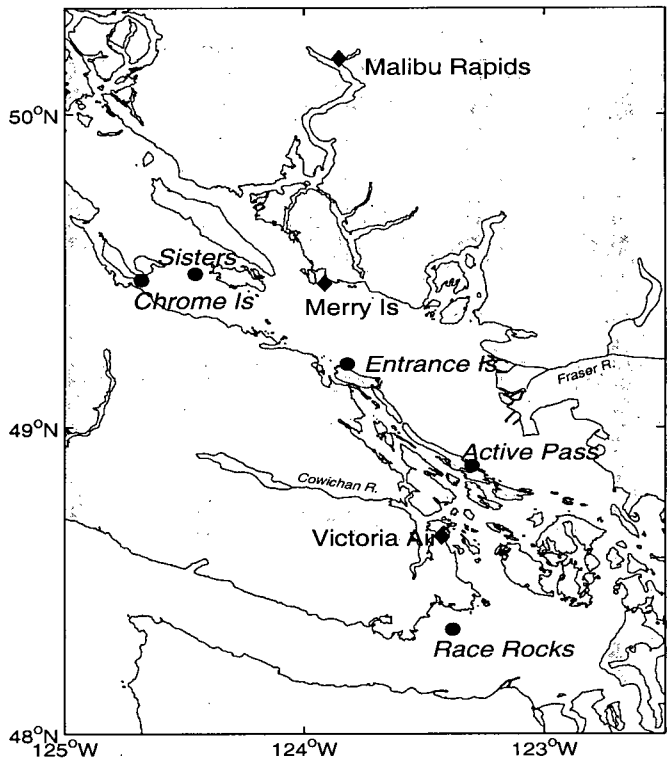

Figure 1.8: Environmental (diamonds) and lighthouse (circles) stations. Temperature, precipitation and sunshine (Figures 1.10 through 1.12) were collected daily at the environmental stations; sea surface salinity (Figure 1.14) was obtained daily at the lighthouse stations.

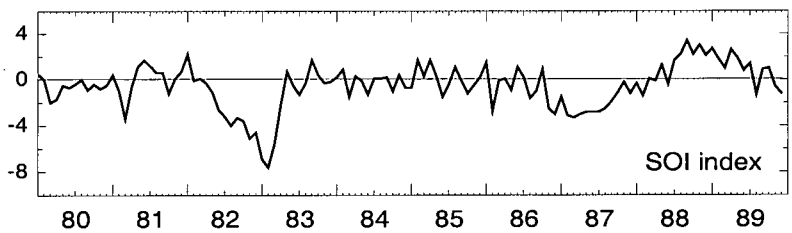

Figure 1.9: The Southern Oscillation Index. The SOI is the atmospheric sea level pressure anomaly between Darwin, Australia, and Tahiti. El Niño events occur when the pressure anomaly is negative, La Niñas when it is positive. (Source: http://www.cgd.ucar.edu/cas/catalog/climind/soi.html.)

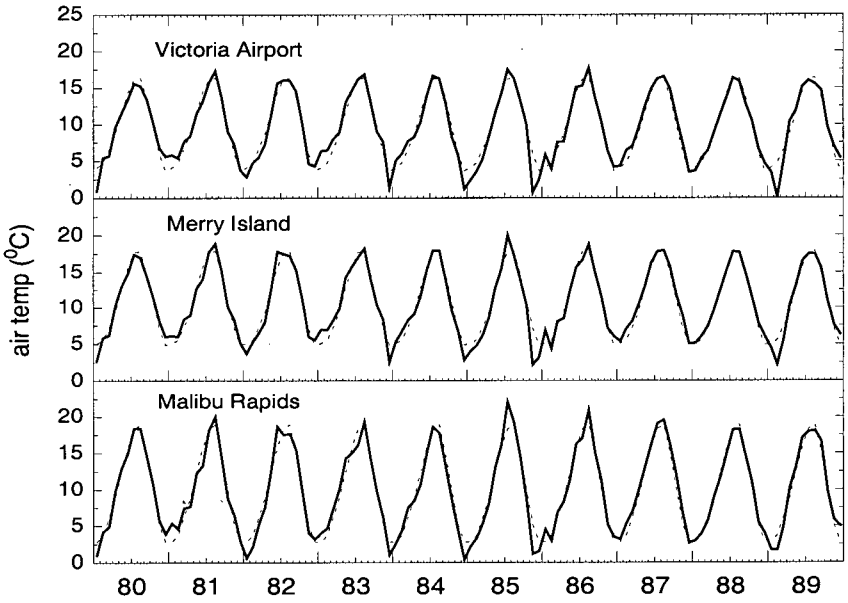

Figure 1.10: Atmospheric temperature at weather stations near Saanich and Jervis Inlets. Dashed lines are the decadal means.

higher at Malibu Rapids (Figure 1.11) where sunshine measurements are not made, irradiance was certainly lower towards the head of Jervis Inlet. There is no clear evidence of an El Niño effect on temperature, precipitation or sunshine in the southern Strait of Georgia.

The Cowichan and Fraser Rivers are the major sources of fresh water to the region of Saanich Inlet, and both are continually monitored by Environment Canada (Figure 1.13). The Goldstream River at the head of Saanich Inlet has a smaller effect on Saanich Inlet due to its low flow, and is not continually monitored. However, data from 1977 and 1978 exist and are presented in Figure 1.13. The Skwawka and Hunaechin Rivers flow into the head of Jervis Inlet, but Environment Canada has no record of their flow. Adjacent to and east of the Skwawka and Hunaechin watersheds is the the larger, glaciated watershed of the Elaho River. The Elaho is a monitored river, and the record is given in Figure 1.13 as a proxy for flow into the head of Jervis Inlet. Although the Jervis Inlet watershed has only minor glaciers, it is influenced by the spring freshet (Lazier, 1963; Pickard,

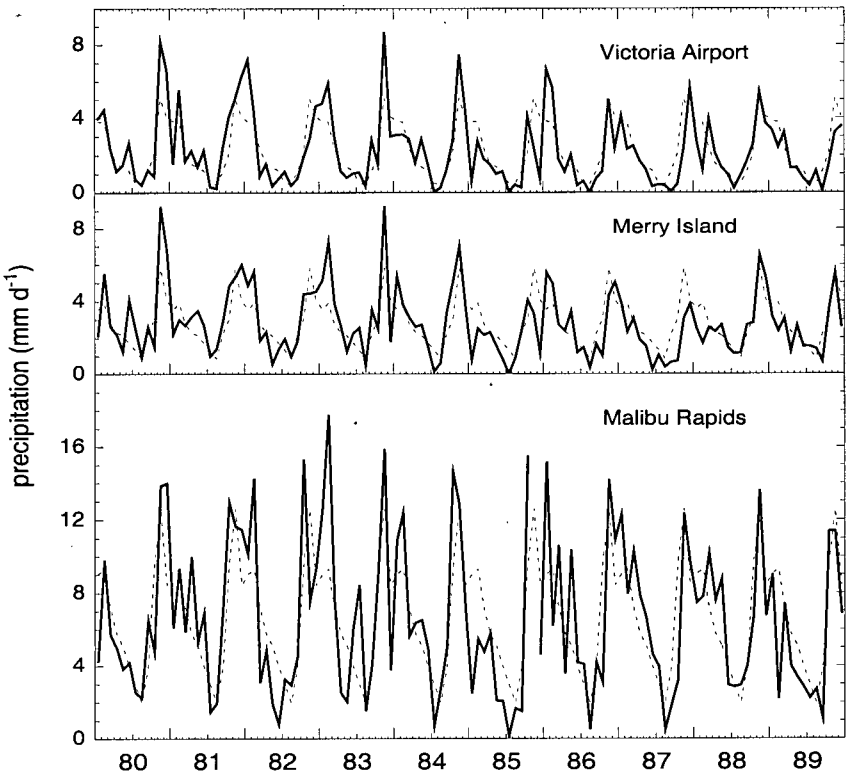

Figure 1.11: Total precipitation at weather stations. Dashed lines are the decadal means.

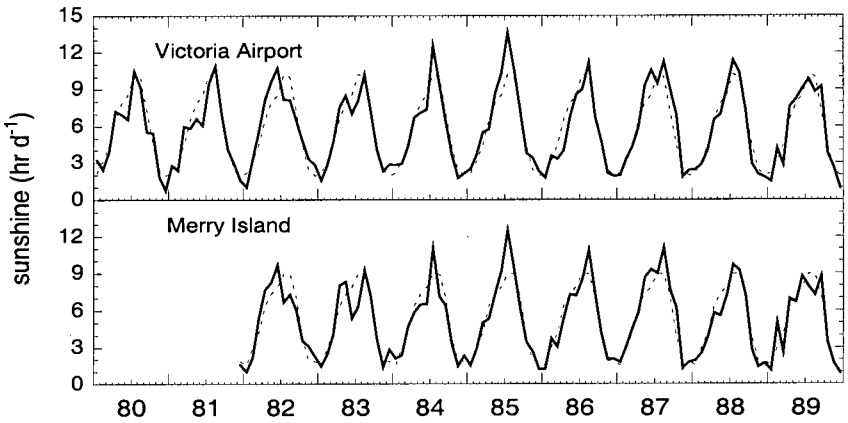

Figure 1.12: Hours of sunshine at weather stations. Campbell-Stokes Sunshine Recorders were used to measure the number of hours per day that light intensity was above a threshold value (cloud opacity). Dashed lines are the decadal means.

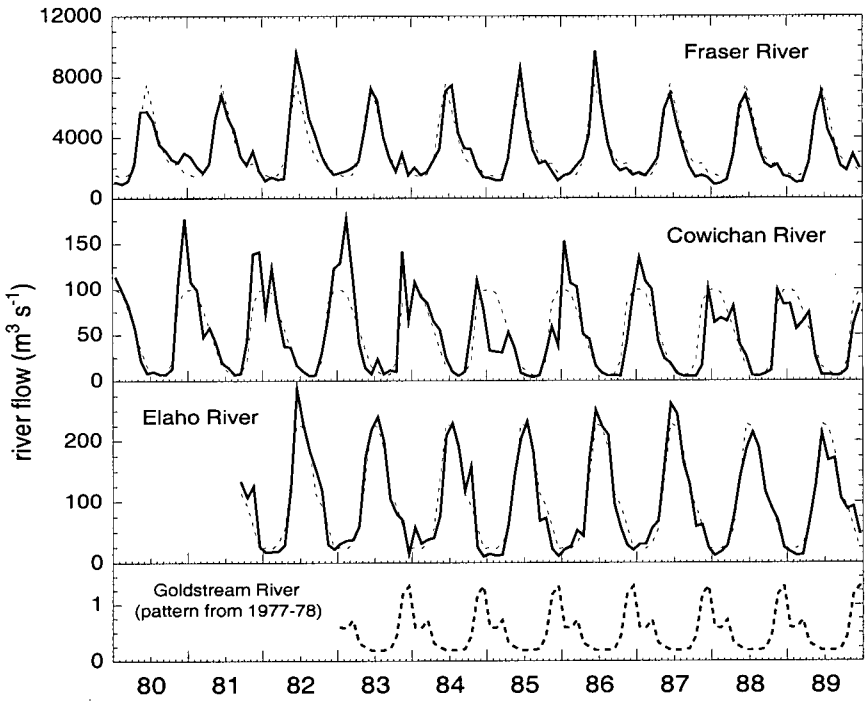

Figure 1.13: River flow from the Fraser, Elaho, Cowichan and Goldstream Rivers. The Elaho is included as an analog for the Skwawka and Hunaechin Rivers (un-metered) that flow into the head of Jervis Inlet. Monthly flows (heavy line) are given, as are the averages for 1980-1989 (dashed lines). The Goldstream River drains into the head of Saanich Inlet and was metered during 1977 and 1978. Average flow for those years is shown.

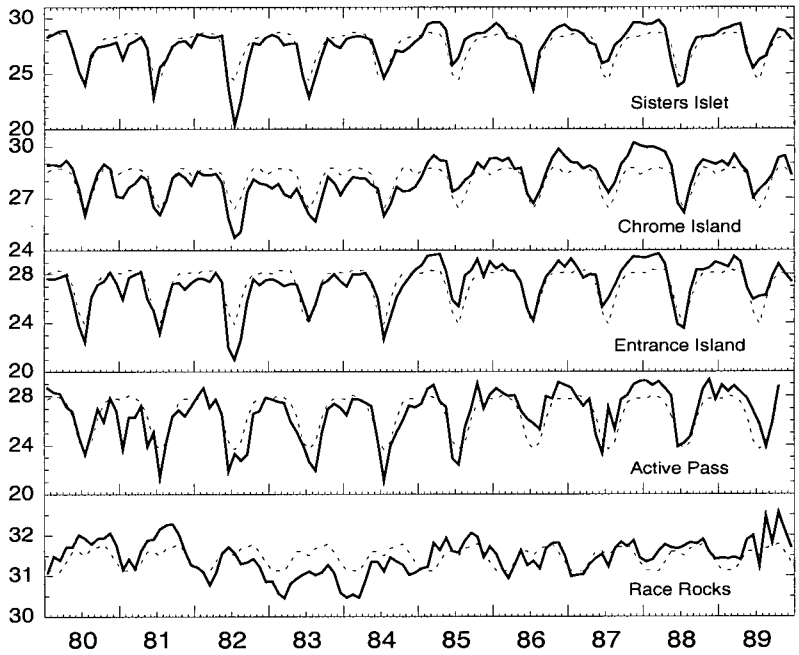

Figure 1.14: Surface salinity measured daily at lighthouses throughout the southern Strait of Georgia. Monthly averages are plotted, and the dashed lines are the decadal means.

1961) due to melting snow from surrounding mountain peaks reaching 2000 m elevation. Therefore, the seasonal pattern (dominated by the freshet) and interannual variability may have been similar for the two watersheds.

In the summers of 1982 and 1986, the peak of the Fraser River freshet was anomalously high, and in 1982 the Elaho freshet was large. In chapter 2 it is postulated that the 1986 freshet may have affected primary production in Saanich and Jervis Inlets, but it is unlikely the atypical riverflows of the summers of 1982 and 1986 were related to El Niño events. The freshet is the result of melting of snow and ice and therefore is controlled by precipitation of the preceding winter and by spring and summer temperatures. Because the large freshets occurred as the 1982/83 and 1986/87 El Niños were beginning, it is doubtful that the 1982 and 1986 freshets were somehow a response to El Niño.

The majority of the fresh water reaching the Strait of Georgia is delivered by the Fraser River, and the summer freshet results in a surface brackish layer of 5-10 m thickness extending over the southern and central portions of the Strait of Georgia (LeBlond et al., 1994). Surface salinity collected daily at lighthouse stations throughout the southern Strait of Georgia and Juan de Fuca (Figures 1.8 and 1.14) show the effect of the Fraser River freshet as low salinities around June and July. The large freshet of 1982 caused low surface salinities at lighthouse stations throughout the southern Strait of Georgia, while effects of the 1986 freshet on surface salinity are less evident (Figure 1.14). At Race Rocks in Juan de Fuca, high summertime salinities (Figure 1.14) are caused by wind-driven upwelling and greater mixing of intermediate Pacific waters due to enhanced estuarine exchange during the Fraser River freshet.

Chapter 2

Primary production in Saanich and Jervis Inlets: what causes high production in Saanich Inlet?

2.1 Introduction

The main processes of oxygen consumption in aquatic basins are by the heterotrophic oxidation of organic matter and through bacterially mediated oxidation of reduced chemical species (e.g.; HS^-, NH_4^+, CH_4, Fe^{2+} and Mn^{2+}) that accumulate due to organic organic matter degradation in low-oxygen regions and then mix or diffuse into oxygen-replete waters. The advective supply of oxygen to the deep waters of silled fjords such as Saanich and Jervis Inlets is limited to periodic renewal events so that, where oxygen consumption exceeds the diffusive supply and the period between renewals is sufficiently long, anoxia can result.

Of the many deep- and shallow-silled fjords of BC, only a few are known to develop severe anoxia and, compared with these, renewal of the bottom waters in Saanich Inlet (Anderson and Devol, 1973) is regular and relatively vigorous. Narrows and Princess Louisa Inlets (Figure 1.1), smaller fjords within the Jervis Inlet system, are separated from the Strait of Georgia by multiple sills and deep-water renewal tends to be irregular and weak (Lazier, 1963; Pickard, 1975). In Nitinat Lake, a true fjord on the southwest coast of Vancouver Island where the waters are permanently anoxic below $\sim$30 m, renewal to depth is severely restricted by a very shallow and protracted sill (Northcote et al., 1964; Richards, 1965). Effingham Inlet, located on the central west coast of Vancouver Island,

has only recently been discovered to be periodically anoxic (e.g.; Baumgartner et al., in review) and the dynamics of deep-water renewal have yet to be described. However, mixing along the approaching channel of approximately 25 km length and a set of sills leading to the inner basin of Effingham Inlet reduce the potential for deep-water renewal. Although verification is needed that Muchalat Inlet on the west coast of Vancouver Island develops strong bottom-water anoxia (Pickard, 1963), a long channel and several sills lead to this fjord. The characteristics of deep-water renewal and advective oxygen supply, therefore, distinguishes Saanich Inlet from other anoxic BC fjords.

Local primary production is an important factor that can lead to anoxic bottom waters (Richards, 1965; Calvert and Pedersen, 1992) and, indeed, conditions in Saanich Inlet are uniquely suited for phytoplankton growth. Surface stratification and relatively low vertical mixing due to weak winds, tidal currents and estuarine circulation (Stucchi and Whitney, 1997) create stable conditions for phytoplankton growth, and surface nutrient concentrations outside the sill are high year-round (Lewis, 1978; Mackas and Harrison, 1997). Intrusions of nutrient-rich, surface waters into Saanich Inlet were seen to cause phytoplankton blooms (Takahashi et al., 1977) in phase with the fortnightly, spring-neap tidal cycle (Parsons et al., 1983), and Hobson and McQuoid (in press) observed that increases in phytoplankton biomass in Saanich Inlet were related to tidally-modulated nutrient intrusions. Herlinveaux (1962) has postulated that benthic and pelagic phytoplankton are ultimately responsible for deep-water anoxia in Saanich Inlet, while Hobson's (1983) test of the relationship between phytoplankton biomass, bacterial metabolism and deep-water oxygen content was complicated by deep-water replacement during that study.

This chapter presents the primary production time-series from Saanich and Jervis Inlets. Primary production was significantly higher in Saanich Inlet than in Jervis Inlet or the majority of the Strait of Georgia, supporting the possibility that a large delivery of organic matter to the deep waters is partly responsible for the anoxia in Saanich Inlet.

Also considered are the possibilities that weak estuarine circulation, leading to particle-retention within the fjord, and low rates of vertical mixing in Saanich Inlet stimulate deep-water anoxia.

2.2 Methods

From August, 1985 to October, 1989, primary production was measured at each station (SN-9 and SN-0.8 in Saanich Inlet; JV-11.5 or JV-3, and JV-7 in Jervis Inlet) when the sediment-trap moorings were serviced. On station, subsurface light was determined using a LI-COR 185B quantum meter. Water samples were collected from depths corresponding to 56, 32, 18, 11 and 7% surface irradiance and carbon fixation was determined by the uptake of ^{14}C following the method and equation, including dark-bottle subtraction, of Parsons et al. (1984a). Unscreened seawater was transferred to two 125 mL borosilicate bottles and about 5 μCi of $NaH^{14}CO_3$ were added. One bottle from each depth was wrapped with neutral density screening to mimic *in situ* irradiance and the dark bottle was wrapped with electrical tape. Both were placed in a Plexiglas incubator thermally regulated by flowing surface seawater. After approximately 2 h, cells were collected by filtration with applied pressure < 12 cm Hg onto Millipore HA filters, rinsed with filtered seawater and placed in Aquasol II for analysis of radioactivity by scintillation spectrometry. The incubations may have occurred at any time during the day, depending on when stations were visited.

The hourly rates of ^{14}C-uptake thus obtained can be converted to daily rates of primary production by assuming that carbon assimilation is proportional to photosynthetically available radiation (PAR) and scaling the incubation results by the ratio of total, daily PAR to PAR integrated throughout the incubation (e.g., Perry et al., 1989; Clifford et al., 1992). PAR was not measured during the experiment, so it was assumed

that PAR throughout the day follows the first-order sine function. The incubation results were then appropriately scaled knowing the times of the beginning and end of each incubation relative to sunrise and sunset. Platt et al. (1990) showed that the first-order sine function provides a good description of the curve for daily irradiance when daylength is $<$ 20 h; at the latitude of southern British Columbia, maximum daylength is approximately 16 h. One assumption of this conversion is that the fraction of PAR attenuated by clouds during the incubation was similar to the attenuation throughout the day. Although this assumption may lead to errors in the primary production estimates for any given day, it should not result in systematically positive or negative errors. If cloud attenuation is constant throughout the day, this sine conversion will accurately estimate the ratio of daily PAR to incubation-period PAR.

Areal estimates of primary production were obtained by trapezoidal integration over depth of the carbon assimilation profiles. During this procedure, the measurement of ^{14}C uptake at 56% surface irradiance was used as the rate of carbon assimilation from that depth to the surface. Also, rates of ^{14}C-uptake were extrapolated from 7 to 1% surface irradiance by assuming that the rates measured at 7% surface irradiance decreased with depth proportionally to light. The extinction coefficient for light was approximated as the slope of the relationship between ln(PAR) and depth as measured prior to each incubation. These shallow and deep extrapolations were performed to account for the carbon assimilation that likely was occurring above the depth of 56% surface irradiance and below the depth of 7% surface irradiance. On average, the shallow and deep extrapolations are 38 and 12%, respectively, of the primary-production estimates integrated between the depths for which ^{14}C-uptake was measured (from 56 to 7% surface irradiance). Deep chlorophyll maxima between the depths of 7 and 1% surface irradiance are common in these waters, but they should not have caused the deep extrapolations to

be large under-estimates because the primary production associated with them is typically low (e.g., Clifford et al., 1991; Harrison et al., 1991). The deep extrapolations may be over-estimates in winter, as Takahashi et al. (1978) have shown that the wintertime compensation depth in Saanich Inlet is less than the depth of 1% surface irradiance. Nevertheless, the deep extrapolation has been applied to the entire time-series to maintain consistency. For the data collected between November and February, the deep extrapolations are on average 11% of the ^{14}C-uptake profiles integrated from the surface to the depth of 7% surface irradiance. Because they are relatively low, the estimates of wintertime primary production have little effect on yearly estimates.

Temperature and salinity were measured throughout the water column using a Guildline 8705 CTD when each station was visited. Beginning January, 1988 and for the remaining two years of the program, samples for nutrient analyses (nitrate + nitrite, orthophosphate and silicic acid {Parsons et al., 1984a}) were collected.

2.3 Results

2.3.1 Salinity and temperature

Contour plots of nitrate concentration, temperature and salinity are shown in Figures 2.1 through 2.4, and these data are compressed into average "summer" and "winter" profiles in Figure 2.5. The primary production results presented in Figures 2.1 through 2.4 are discussed in the next section.

In Saanich Inlet, low surface salinities occurred in the fall and winter (Figures 2.1, 2.2 and 2.5) when local precipitation (Figure 1.11) was highest. Low surface salinity anomalies recorded at one station were not always observed at the other (Figures 2.1 and 2.2), suggesting spatial heterogeneity of the surface water masses of Saanich Inlet, a feature that was likely caused by tidally-modulated intrusions of water from the Cowichan and

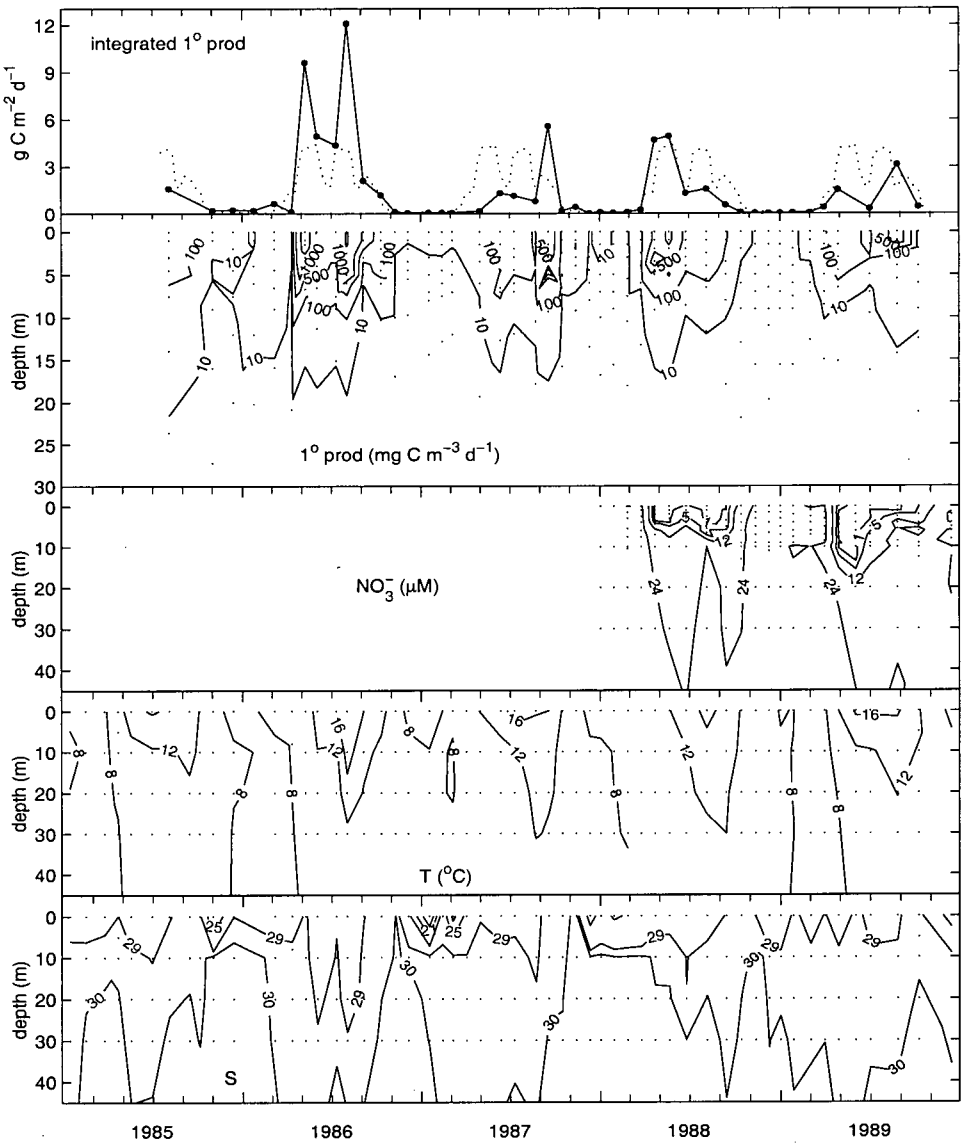

Figure 2.1: Depth-integrated primary production at station SN-9 in Saanich Inlet (top panel) from August, 1985 to October, 1989. The dotted line is the smoothed curve of daily averages from Figure 2.8, repeated annually. The plots below show volumetric primary production (isopleths at 10, 100, 500, 1000 and 2000 mg C m^{-3} d^{-1}), nitrate concentration (isopleths at 24, 12, 5 and 1 μM), temperature (isopleths at 8, 12 and 16°C) and salinity (highest isopleth at 30, the next at 29 and others decreasing by four). Points in the contour plots are sampling locations.

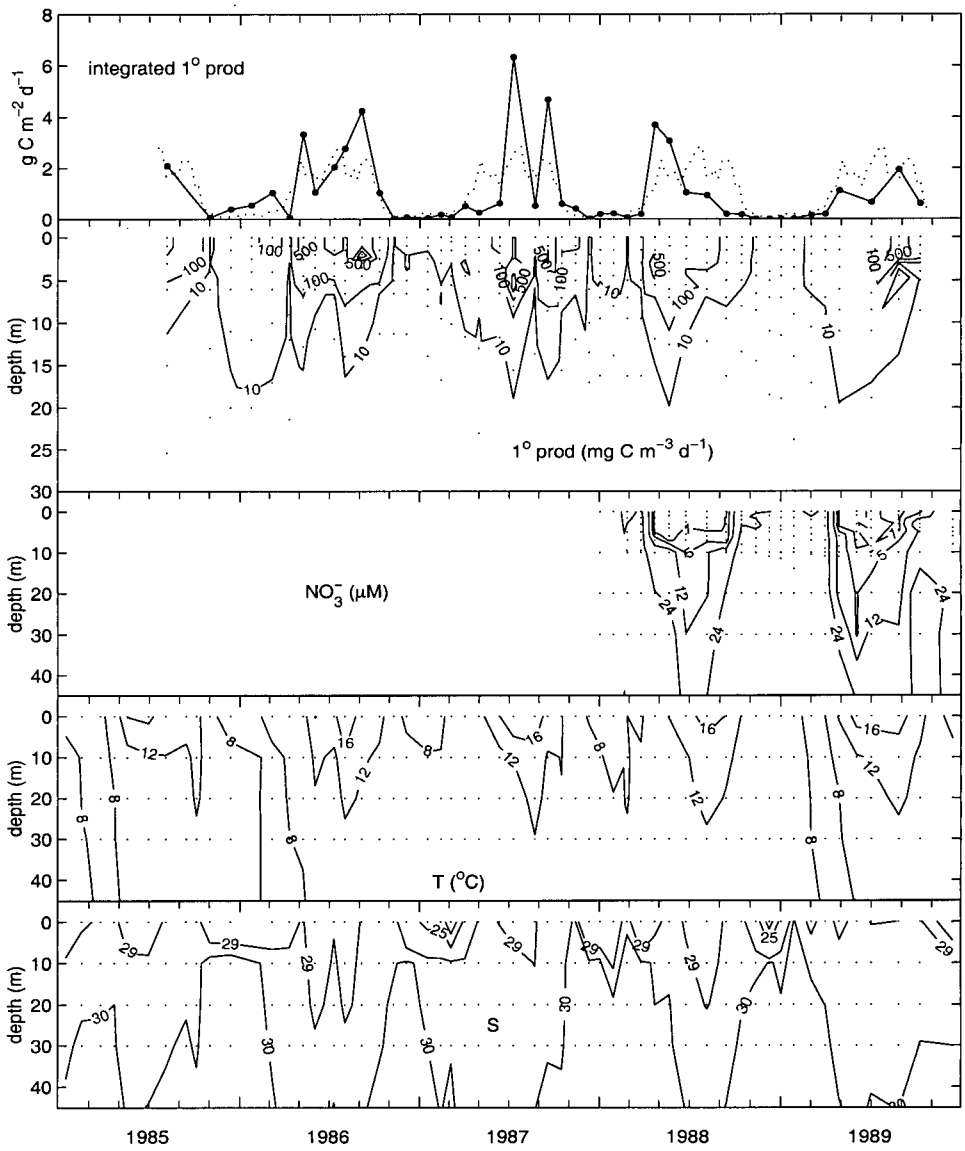

Figure 2.2: Depth-integrated primary production at station SN-0.8 in Saanich Inlet (top panel) from August, 1985 to October, 1989. The dotted line is the smoothed curve of Figure 2.8, repeated annually. The plots below show volumetric primary production (isopleths at 10, 100, 500, 1000 and 1500 mg C m^{-3} d^{-1}), nitrate concentration (isopleths at 24, 12, 5 and 1 μM), temperature (isopleths at 8, 12 and 16°C) and salinity (highest isopleth at 30, the next at 29 and others decreasing by four). Points in the contour plots are sampling locations.

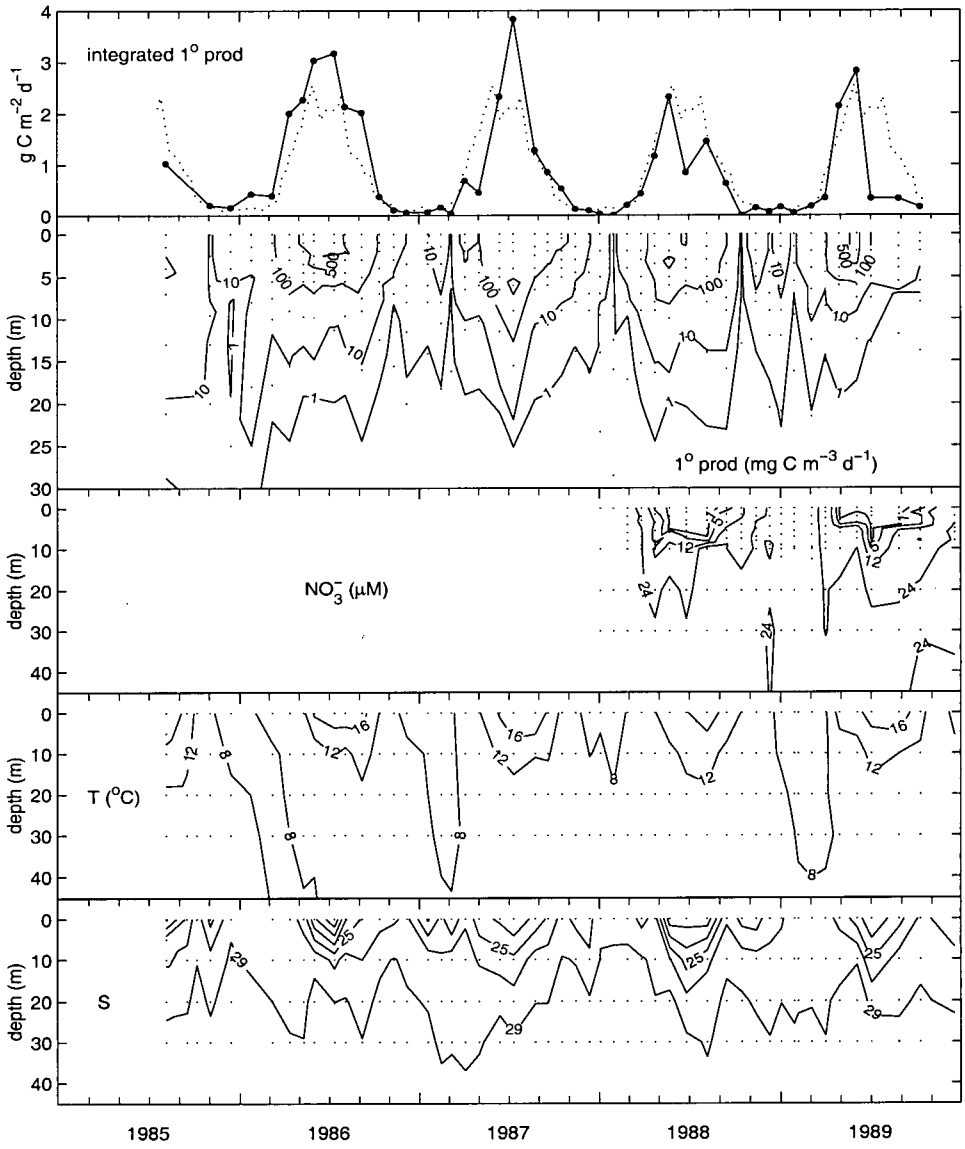

Figure 2.3: Depth-integrated primary production at station JV-3 in Jervis Inlet (top panel) from August, 1985 to October, 1989. The dotted line is the smoothed curve of Figure 2.8, repeated annually. The plots below show volumetric primary production (isopleths at 1, 10, 100 and 500 mg C m^{-3} d^{-1}), nitrate concentration (isopleths at 24, 12, 5 and 1 μM), temperature (isopleths at 8, 12 and 16°C) and salinity (highest isopleth at 29, others decreasing by two). Points in the contour plots are sampling locations.

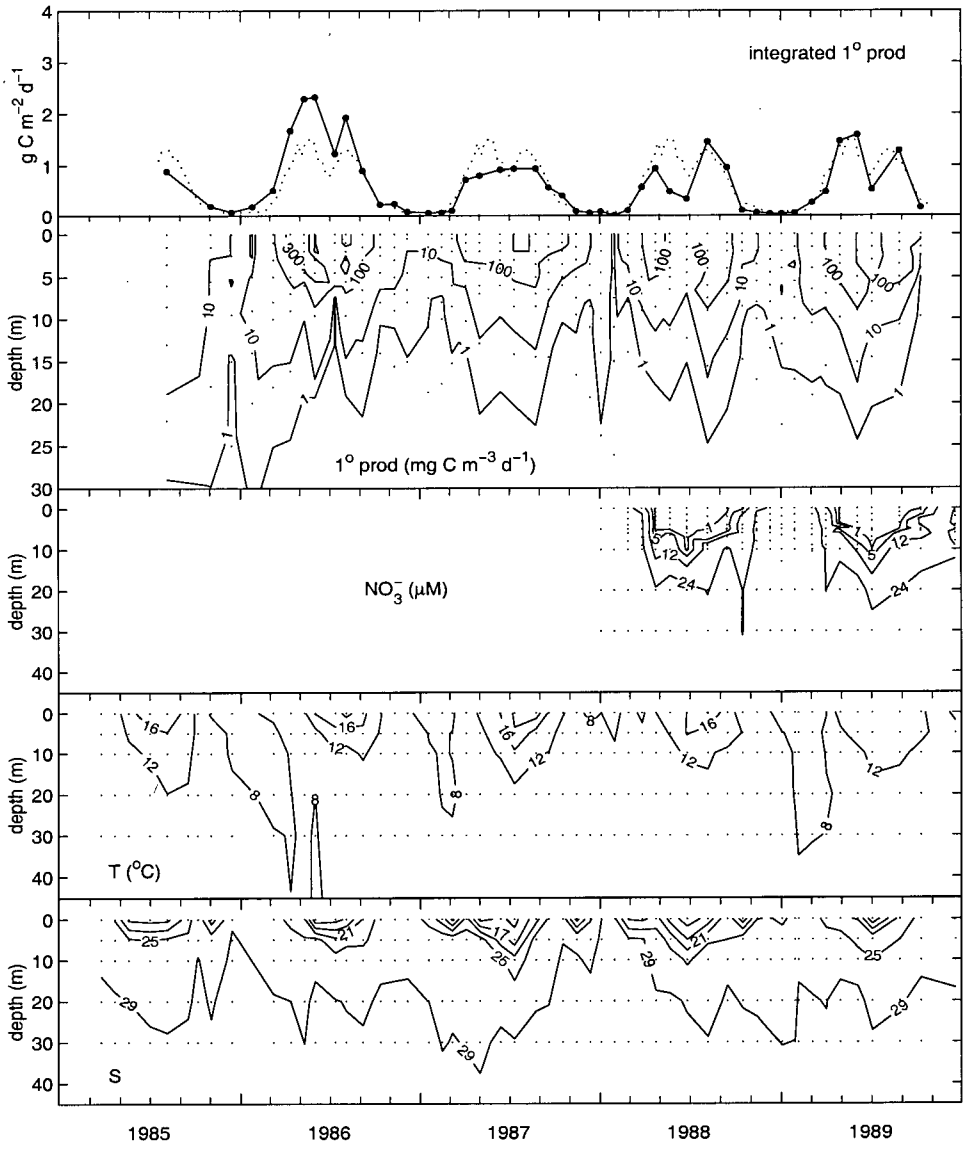

Figure 2.4: Depth-integrated primary production at station JV-7 in Jervis Inlet (top panel) from August, 1985 to October, 1989. The dotted line is the smoothed curve of Figure 2.8, repeated annually. The plots below show volumetric primary production (isopleths at 1, 10, 100 and 300 mg C m^{-3} d^{-1}), nitrate concentration (isopleths at 24, 12, 5 and 1 μM), temperature (isopleths at 8, 12, 16 and 20°C) and salinity (highest isopleth at 29, others decreasing by four). Points in the contour plots are sampling locations.

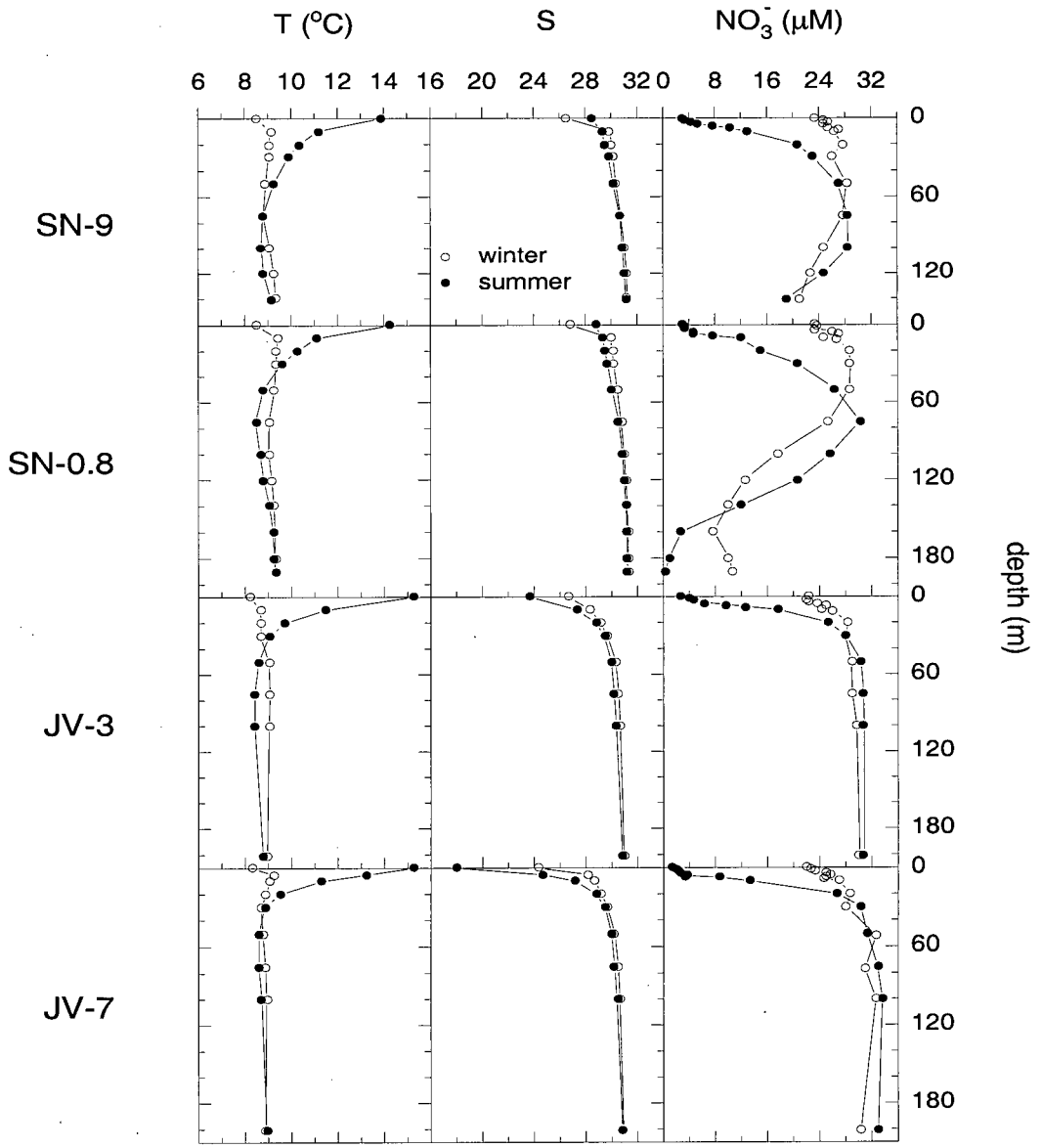

Figure 2.5: Temperature, salinity and nitrate concentrations during the study. Each row of figures presents data from a different station. Profiles were created by averaging measurements collected from October to March ("winter"; open circles) and April to September ("summer"; solid circles). T and S were measured throughout the study, while nitrate was measured in 1988 and 1989 only. In Saanich Inlet, the deepest sampling depths were about 20 m from the bottom (165 m at SN-9 and 210 m at SN-0.8). Water depths are 660 m at JV-3 and 530 m at JV-7, but water properties changed little below 200 m at these stations.

Fraser Rivers (Herlinveaux, 1962). There was little discernible along-inlet salinity gradient in Saanich Inlet as would be expected if typical estuarine circulation were occurring. In Jervis Inlet, decreases in surface salinity caused by fall, winter and spring precipitation were superimposed on a yearly cycle of surface salinity dominated by the freshet, causing lowest surface salinities in June and July (Figures 2.3, 2.4 and 2.5). Also, in contrast to Saanich Inlet, the surface salinity pattern in Jervis Inlet was indicative of estuarine flow. Surface salinity increased seaward from JV-7 to JV-3, while the depth of the pycnocline remained similar at both stations (Figures 2.3, 2.4 and 2.5). This salinity structure is characteristic of estuarine flow where entrainment of mid-depth waters moving landward causes the surface layer to gain salt and velocity as it flows seaward. No upper mixed layer exists in Saanich Inlet (Herlinveaux, 1962) or Jervis Inlet (Pickard, 1961). Instead, the pycnocline (closely represented by the halocline) intersected the surface in both inlets and was steepest in Jervis Inlet (Figure 2.5).

The vertical temperature structure of both inlets (Figures 2.1 through 2.5) reflected seasonal heating. Maximum surface temperatures were usually in July and August, but in some years were in June (Figures 2.1 through 2.4). In Jervis Inlet, maximum surface temperatures lagged the freshet by one or two months. In the fall and winter, surface cooling destroyed the seasonal thermocline.

2.3.2 Nutrient concentrations and uptake

Of the measured nutrients, nitrate most frequently dropped below detectable concentrations. Beginning late April to early May and continuing until the early fall, surface nitrate concentrations were always below 5 μM at each station and concentrations less than 1 μM occurred during most of this period (Figures 2.1 through 2.5). Of the four stations, nitrate depletion ($< 1\mu$M NO_3^-) was most common at JV-7 (Figure 2.4). In Saanich Inlet, surface nitrate replenishments at SN-9 were detected on June 27, 1988,

July 4, 1989 and August 28, 1989. At SN-0.8, replenishment was observed on July 4, 1989. When these nutrient replenishments occurred, primary production was relatively low, except on August 28, 1989 at SN-9. Similar lags between nutrient supply and phytoplankton production or biomass were found by Takahashi et al. (1977) and Parsons et al. (1983).

Low nitrate concentrations in the deep waters of Saanich Inlet (Figure 2.5) were caused by nitrate reduction in the oxygen-depleted basin. The slight increase in winter nitrate concentrations near the bottom at station SN-0.8 was most likely caused by up-inlet penetration of dense, nitrate-rich waters.

The nutrient assimilation ratios are estimated as the slopes of nutrient-nutrient plots (Corner and Davies, 1971) for samples from waters collected at $\leq$ 50 m (Figure 2.6). The nitrate:phosphate (N:P) assimilation ratios were 13.6 - 14.2 in Saanich Inlet and 12.7 - 13.1 in Jervis Inlet, compared with 12.5 as found by Smethie (1987) in Jervis Inlet. These assimilation ratios are only slightly lower than the global average of 15 - 16 for the N:P concentration ratio in seawater (Redfield, 1963; Takahashi et al., 1985). The silicic acid:nitrate (Si:N) assimilation ratios were between 1.51 and 1.56 at stations SN-9, SN-0.8 and JV-3, but at station JV-7 the ratio was 1.22, implying that toward the head of Jervis Inlet diatoms were either more weakly silicified or they made a somewhat smaller contribution to the phytoplankton community. These Si:N assimilation ratios are high, even for phytoplankton communities composed entirely of diatoms. Brzezinski (1985) found that the ratio of the contents of Si and N for various diatoms grown in the laboratory ranged between 0.8 and 1.4, but much higher Si:C (and, assuming a less variable C:N assimilation ratio, Si:N) assimilation ratios have been measured in the Southern Ocean (Quéguiner et al., 1997).

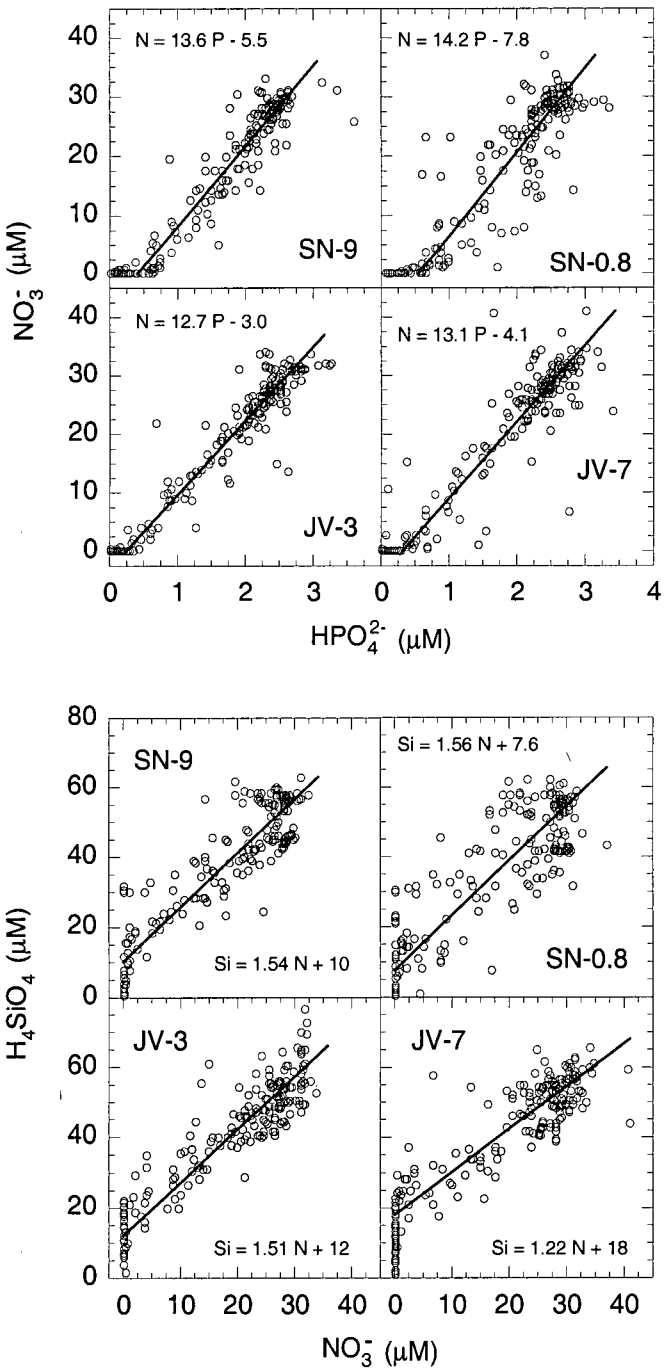

Figure 2.6: N:P and Si:N uptake ratios, taken as the slopes of the regression lines through points representing samples from waters $\leq$ 50 m and excluding those with nutrient concentrations less than the detection limit. The 95% confidence intervals of the slopes (in percent of the slope value) are: $\pm$ 5.1 - 7.2% for N:P, and $\pm$ 7.0 - 8.7% for Si:N. 95% confidence intervals for the intercepts (in μM) are: $\pm$ 1.4 - 2.2 μM for N:P, and $\pm$ 2.4 - 3.2 μM for Si:N.

2.3.3 Estimates of primary production

Volumetric and areal estimates of primary production are shown in Figures 2.1 through 2.4 along with contour plots of nitrate, temperature and salinity in the upper 45 m so that comparison can be made between phytoplankton growth and the hydrographic and nutrient conditions. The primary production results are summarized in Figures 2.7 (mean vertical profiles) and 2.8 (smoothing of the areal values to describe production throughout the year). The sampling depths for ^{14}C incubations were predicated by *in situ* light intensity and the deepest points in panel 2 of Figures 2.1 to 2.4 are the extrapolated depths of 1% surface irradiance (see section 2.2). On average, the depth of 1% surface irradiance was at 12 to 15 m during the summer and 16 to 20 m in winter (Figure 2.7). Generally, the highest rates of carbon fixation occurred at the depth of 56% surface irradiance, but some subsurface maxima were observed (Figures 2.1 through 2.4 and Figure 2.7). However, because surface primary production was not measured, subsurface maxima occurring above the depth of 32% surface irradiance (the second measurement in the depth profiles) would have been undetected.

Excluding the 89-day interval separating the first (7-9 August, 1985) and second (4-5 November, 1985) cruises, the sampling interval was between 21 and 55 days, with an average of 32 days. In Saanich Inlet, changes in phytoplankton biomass fluctuate more frequently than this interval (Takahashi et al., 1977; Hobson and McQuoid, in press) and the same is likely true for Jervis Inlet. Because the sampling frequency may have missed important periods of high or low primary production, this time-series is not ideally suited for a comparison of primary production between years. However, 45 to 47 profiles of ^{14}C-uptake were made at each station. Assuming the sampling was random with respect to short-term fluctuations, these data provide a means to describe average primary production throughout the four-year period of the study (Figure 2.8 and

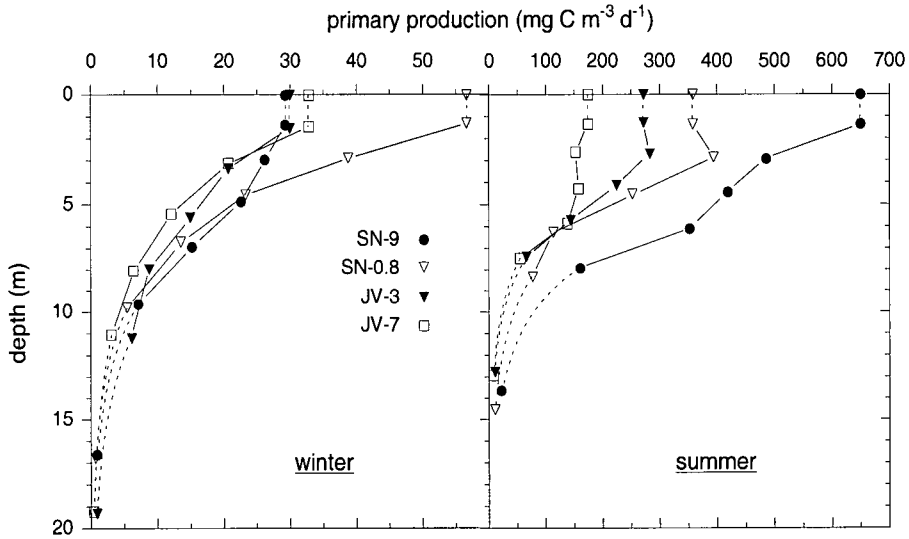

Figure 2.7: Vertical profiles of primary production during October to March ("winter") and April to September ("summer"). The plotted depths and rates of carbon uptake are the averages of all measurements taken within each time period (Figures 2.1 to 2.4; n = 21-24 for each profile); surface and deepest (1% surface irradiance) points are extrapolations. As these plotted depths are the average depths of 56, 32, 18, 11 and 7% surface irradiance, they can be used to estimate extinction coefficients of light at each station (section 2.4.2). In the winter, the extinction coefficients were: 0.23 m^{-1} (JV-7) < 0.24 m^{-1} (JV-3) < 0.28 m^{-1} (SN-0.8) < 0.30 m^{-1} (SN-9). In the summer, the coefficients were: 0.34 m^{-1} (SN-9) < 0.35 m^{-1} (SN-0.8) < 0.36 m^{-1} (JV-3 and JV-7).

Table 2.1). By averaging the yearly estimates at the two stations in each fjord, primary production in Saanich Inlet (1.3 g C m^{-2} day^{-1}) was approximately 1.7 times higher than in Jervis Inlet (0.78 g C m^{-2} day^{-1}). Average primary production for the entire Strait of Georgia has been estimated to be 280 g C m^{-2} y^{-1}, or 0.77 g C m^{-2} d^{-1} (Harrison et al., 1983, using data of Stockner et al., 1979). Thus, Saanich Inlet appears to be significantly more productive than other local waters.

Table 2.1 includes other published reports of primary production from Saanich and Jervis Inlets and, in general, there is good agreement with the results from this study. However, except for those of Takahashi et al. (1975) and Takahashi and Hoskins (1978),

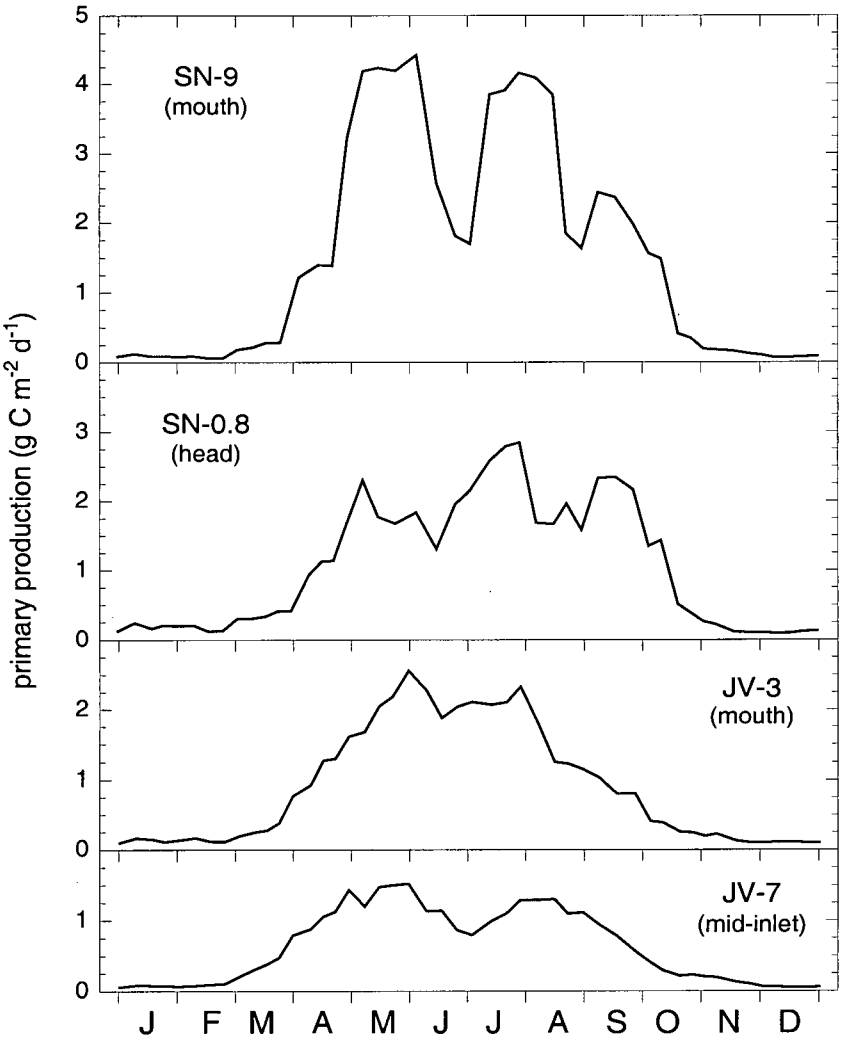

Figure 2.8: Averages of daily primary production. The estimates of Figures 2.1 to 2.4 were arranged by calendar day and a five-point running average was used to smooth the time-series. For each 31-day period, there are approximately five estimates of daily primary production.

location/source	annual avg	monthly averages											
		Jan	Feb	Mar	Apr	May	Jun	Jul	Aug	Sep	Oct	Nov	Dec
		(all values: g C m^{-2} d^{-1})											
Figure 6													
SN-9	**1.6**	0.097	0.079	0.31	1.6	4.1	2.9	3.4	3.1	2.2	0.89	0.16	0.078
SN-0.8	**1.1**	0.20	0.17	0.34	1.1	1.9	1.7	2.6	1.8	2.2	0.88	0.16	0.11
JV-3	**0.92**	0.14	0.14	0.32	1.1	2.0	2.2	2.1	1.5	0.91	0.33	0.16	0.11
JV-7	**0.64**	0.075	0.093	0.38	1.0	1.4	1.1	1.0	1.2	0.81	0.29	0.15	0.057
Saanich Inlet													
Takahashi et al. (1975)[1]						2.1							
Takahashi and Hoskins (1978)[2]		0.061	0.080										0.053
Parsons et al. (1983)[3]							1.8						
Parsons et al. (1983)[4]							4.0						
Parsons et al. (1983)[5]							1.6						
Jervis Inlet													
Stockner and Cliff (1975)[6]				0.31		2.8		1.1	3.1	0.77			
Stockner and Cliff (1975)[7]				0.29		2.1		1.7	0.83	1.5			
Parsons et al. (1984b)[8]							1.8						
Cochlan et al. (1986)[9]							0.74						
Cochlan et al. (1986)[10]							1.8						

[1] Patricia Bay; n = 15
[2] mouth; n = 2-4 $month^{-1}$
[3] Prevost Passage; n = 3
[4] Satellite Channel; n = 5
[5] mouth; n = 3
[6] northern Hotham Sound; n = 1 $month^{-1}$
[7] southern Hotham Sound; n = 1 $month^{-1}$
[8] various stations near mouth; n = 6
[9] ~11 km up-inlet from JV-3; n = 1
[10] ~11 km seaward of JV-3; n = 1

Table 2.1: Annual and monthly estimates of primary production at each station derived by integrating the curves of Figure 6 over the appropriate time intervals. The annual averages are based on 45-47 profiles of primary production measured at each station, while each monthly estimate represents the results of approximately four profiles. For comparison, other estimates of primary production in Saanich and Jervis Inlets are given. Where only hourly estimates of primary production were available (Takahashi et al., 1975; Cochlan et al., 1986), we converted to daily rates using a best approximation of their incubation periods and the model of daily sunshine described in section 2.2.

	primary production ($g\ C\ m^{-2}\ d^{-1}$)		
Period	head (SN-0.8)	central basin	mouth (SN-9)
08 Jan - 13 Aug	1.2	0.95	2.0
31 Mar - 30 Sep	1.8	2.2	2.9

Table 2.2: Comparison of the curves of Figure 2.8 for Saanich Inlet with estimates of primary production made by L. A. Hobson (Department of Biology, University of Victoria, Victoria, BC, pers. comm.) in the central basin several km south of SN-9. Hobson's sampling interval was, on average, 18 days. His estimates are based on *in situ* 24 h ^{14}C incubations usually carried out at the depths of 0, 1, 2, 3, 4, 5, 6 and 7 m. His 08 Jan - 13 Aug ($n = 12$) and 31 Mar - 30 Sep ($n = 11$) estimates are from 1975 and 1976, respectively, while the estimates for stations SN-0.8 and SN-9 are from integrating the curves of Figure 2.8 over the appropriate time periods (08 Jan - 13 Aug and 31 Mar - 30 Sep). Hobson's estimates are his revisions of those presented in Harrison et al. (1983).

all of the estimates of primary production in Table 2.1 are the result of << 24-hour ^{14}C incubations and therefore do not account for autotrophic respiration at night which can consume a significant fraction of gross carbon assimilation (Langdon, 1993; Sakshaug, 1993). For instance, by comparing 24-h and shorter ^{14}C incubations made throughout the year, Perry et al. (1989) estimated that 20% of daytime net primary production was respired at night by the phytoplankton communities off the continental shelf and slope of Washington State. The thorough investigation carried out in the center of Saanich Inlet during 1975 and 1976 (L. A. Hobson, Department of Biology, University of Victoria, Victoria, BC, pers. comm.) is therefore a pertinent comparison because his results (Table 2.2) are based on 24 h ^{14}C incubations and therefore should account for respiration at night. Considering year-to-year variability and spatial heterogeneity, Hobson's estimates for the center of Saanich Inlet and those from SN-0.8 are similar, while the mouth of Saanich Inlet (SN-9) appears to be significantly more productive (Table 2.2).

Other work has found similar along-inlet gradients in phytoplankton biomass (Hobson and McQuoid, in press) and sinking particle flux (Sancetta and Calvert, 1988; Chapter 3). The winter estimates of primary production at stations SN-9 and SN-0.8, however, are significantly higher than those made by Takahashi and Hoskins (1978) using 24 h ^{14}C incubations. This discrepancy is unlikely the result of our deep extrapolations (see section 2.2) because the differences are too large, but may be due to their methodological consideration of autotrophic respiration at night. Assigning the difference in our winter estimates to respiration at night, up to 60% of the carbon assimilated during the day may have been respired at night by phytoplankton. It is also possible that the estimates of Takahashi and Hoskins (1978) are low due to grazing by the large microzooplankton populations during the 24 h incubations. Because the winter values are small, uncertainty in them has little effect on average yearly primary production.

Stockner et al. (1979) present a map of primary production for the Strait of Georgia and connecting waters. Their classification of the mouth of Jervis Inlet (JV-3) agrees with the estimate presented here, while their estimates for the upper reaches of the fjord (JV-7) may be too low. They classify the body and head of Saanich Inlet as a region with rates of primary production between 300 and 400 g C m^{-2} y^{-1}. The results from SN-0.8 located within this area place it at the top of that range. However, their designation of primary production at the mouth of Saanich Inlet and in Satellite Channel (200 to 300 g C m^{-2} y^{-1}) is half the value of the estimate at station SN-9. The results of Parsons et al. (1983, see our Table 1) suggest that Satellite Channel might also be considered a region with rates > 400 g C m^{-2} y^{-1}.

2.4 Discussion

2.4.1 Temporal pattern of primary production

Seasonal variability

At each station, daily primary production began to increase around April and by late September or October decreased to near-winter levels (Figures 2.1 through 2.4 and Figure 2.8), reflecting the availability of light with the exception of notable decreases occurring near the summer solstice. Except at station SN-0.8, the lull in production in early summer is especially noticeable in the curves of Figure 2.8, but it is also apparent for at least one year at all of the stations (Figures 2.1 through 2.4). Although these lulls may have been due to sampling artifacts, early to mid-summer minima in primary production or phytoplankton biomass are commonly observed in waters contiguous with the Strait of Georgia (e.g., Gilmartin, 1964; Huntley and Hobson, 1978; Stockner et al., 1979; Harrison et al., 1983; Hobson, 1983; Haigh et al., 1992) and may be related to the transition from the blooms of several diatom species in the spring (*Thalassiosira* spp., *Skeletonema costatum* and *Chaetoceros* spp.) to summer phytoplankton assemblages. This transition may be facilitated by a number of factors, including decreased upward mixing of subsurface nutrients due to stratification caused by surface-water warming and weak winds, variations in grazing pressure (Harrison et al., 1983; Bornhold, 2000) and photoinhibition (Takahashi et al., 1973; Harrison et al., 1983). Warm water may further enhance nutrient limitation by causing greater photosynthetic nutrient demands (Hobson, 1981). Aggregate formation (e.g.; Kiørboe et al., 1994; see also Kiørboe et al., 1996) at the end of the spring bloom and the summertime freshet may also influence primary production throughout the Strait of Georgia at this time of year. Sancetta (1989a) found that, in the spring and fall, many of the diatom frustules caught by the sediment traps deployed

at each station during the experiment were intact, while during July and August they were mostly fragmented, suggesting that grazing may have been the cause of the early summer minima in production. Low phytoplankton biomass was likely associated with these mid-summer lulls, which probably occurred when chlorophyll-normalised rates of photosynthesis were maximum (Hobson, 1981).

A somewhat surprising feature of this time-series is the lack of a pronounced spring-time peak in production. For a station in the Strait of Georgia, Parsons (1979) shows a large peak in primary production in March, and similar peaks have been observed in Boca de Quadra, southeast Alaska (Burrell, 1983) and Balsfjorden, northern Norway (Hopkins, 1981). However, the production cycles of Figures 2.1 through 2.4 and Figure 2.8 show little evidence for a spring bloom more productive than subsequent months. The lack of this signal may be the result of the long period between sampling (~32 days). Assuming a winter-accumulated nitrate concentration of 30 μM in the upper 10 m, complete utilisation would result in approximately 20 to 30 g C m^{-2} of production which in these waters can be realised in 2 to 10 days. Thus, the sampling may have missed the growth associated with the consumption of winter-accumulated nutrients. This analysis also demonstrates that, in productive waters with a shallow euphotic zone, the portion of yearly primary production occurring as a result of winter-accumulated nutrients is minimal compared with the production driven by nutrients mixed into and regenerated within the euphotic zone; less than 10% of yearly primary production in Saanich and Jervis Inlets is generated by winter-accumulated nutrients. Similar seasonal patterns occur in some shallow fjords and polls of western Norway. Although Korsfjord and Kviturdvikpoll show highest rates of primary production during the spring, Nordåsvann and Vågsbøpoll do not (Wassmann, 1991). Also, a model based on chlorophyll *a* concentrations, light availability and temperature does not predict peaks in primary production in the spring for fjords and the coast of western Sweden near Norway (Soderöström, 1996).

Interannual variability

Because of the long period (~32 day) between sampling, year-to-year variability in this time-series is not emphasised. Nevertheless, during the El Niño year of 1986 (Figures 2.1 through 2.4), primary production was 1.8, 1.3, 1.5 and 1.5 times higher than the annual averages (Table 2.1) at stations SN-9, SN-0.8, JV-3 and JV-7, respectively. Also in 1986, the Fraser River freshet was delayed and the June peak was amplified. Compared to the averages for 1987-1989, flow of the Fraser River at the beginning of the freshet in May, 1986, was about 25% reduced, in June and July at the peak of the freshet was approximately 30% greater and total flow for the year of 1986 was 12% greater.

The Fraser River freshet has a significant impact on the physical and biological oceanography of the Strait of Georgia (Harrison et al., 1983; LeBlond et al., 1994) and Saanich Inlet (Herlinveaux, 1962; Stucchi and Whitney, 1997). Estuarine exchange between the Strait of Georgia and the northeast Pacific Ocean is driven by the Fraser River and occurs primarily through Juan de Fuca Strait (Griffin and LeBlond, 1990). As well as wind-induced upwelling occurring at the seaward end of Juan de Fuca Strait during the summer and fall (Mackas et al., 1987), modelling and data show that the estuarine circulation within Juan de Fuca Strait also forces upwelling (Masson and Cummins, 1999). Intense mixing caused by strong tidal currents and estuarine exchange through Juan de Fuca and Haro Straits (eg; Pawlowicz and Farmer, 1998) maintains high surface nutrient concentrations year-round throughout the southern Strait of Georgia (Mackas and Harrison, 1997). Perhaps, from the delay of the Fraser River freshet later into the summer when nutrients normally would be most limiting to phytoplankton in the southern Strait of Georgia, increased estuarine flow in June and July of 1986 provided a greater supply of nutrients to surface waters by enhancing upwelling and mixing at this time of year. Although the effect on Jervis Inlet is less certain, it is possible that the imprint

of Fraser River discharge on the density structure of waters of the Strait of Georgia affects exchange with Jervis Inlet and therefore has an influence on the phytoplankton populations within the fjord. It is possible that the freshet from the various rivers (all un-metered) entering Jervis Inlet was also anomalous in 1986.

2.4.2 Geographic pattern of primary production

Primary production in Saanich Inlet was significantly higher than in Jervis Inlet and the seaward stations of both fjords were more productive than their landward counterparts (Table 2.1). This pattern was reflected in the flux recorded by the sediment traps moored at 50 m at each station during the study (Chapter 3). Of the sediment-trap material, biogenic silica (BSi) is a good tracer of local primary production (Sancetta and Calvert, 1988; Sancetta, 1989a) as diatoms are its principal source. Organic carbon (OC) is not as good a tracer of primary production due to the presence of terrestrial OC and the high degree of recycling of OC in surface and sub-surface waters (Sancetta and Calvert, 1988; Timothy and Pond, 1997; Chapters 3 and 4). The measured flux of OC might also be affected by live zooplankton entering the traps; swimmers would more likely modify measured fluxes of OC than those of BSi.

Annually averaged, the fluxes of BSi to the 50 m traps (g BSi m^{-2} d^{-1}) were: 1.8, 0.67, 0.46 and 0.31 at SN-9, SN-0.8, JV-3 and JV-7, respectively (Chapter 3). Other than at station SN-9 where material washing into Saanich Inlet or resuspended off the sill may have reached the 50 m traps (Sancetta and Calvert, 1988; Sancetta, 1989a; Chapter 3), the molar ratio of the 50 m BSi flux to local primary production (each averaged over the entire study period) was similar at each station, ranging between 0.087 and 0.11. Assuming that the average Si:C ratio of cultured marine diatoms (0.13±0.04, Brzezinski, 1985) can be applied to the diatoms of Saanich and Jervis Inlets, more than half of assimilated Si sank out of the euphotic zone and was caught in the 50 m traps.

This large BSi flux supports the supposition that diatoms were the predominant primary producers in these fjords in spring and summer when most of the growth occurred, even though flagellates are present throughout the year and can be abundant or predominant during periods of the summer, fall and winter (e.g.; Harrison et al., 1983 and references therein). The large BSi flux also implies that much of the Si deposited as diatom frustules was neither recycled in the euphotic zone nor dissolved in waters less than 50 m deep.

The recycling of organic carbon in surface waters appears to have been much greater than that of BSi, as was its spatial and temporal variability (Sancetta and Calvert, 1988; Chapter 3). The ratios of the 50 m OC flux to primary production at each station (each averaged over the entire study) ranged between 0.10 and 0.16 (see Chapter 3). These low export ratios, especially considering that terrestrial OC is included in the sediment-trap fluxes, may have been due to the degradation of OC within the sediment traps. Kumar et al. (1996) found that as much as 70% of particulate organic carbon caught by sediment traps was released into solution during deployment, even when the deployments were short. The factors affecting the OC fluxes will be discussed further in Chapter 3.

The spatial pattern of primary production may have been the result of the distribution of nutrient supply to surface waters throughout the southern Strait of Georgia. Due to upwelling into Juan de Fuca Strait and mixing in Juan de Fuca and Haro Straits as discussed above, surface waters with year-round nitrate concentrations in excess of 10 μM reach into Satellite Channel at the mouth of Saanich Inlet but do not extend as far north as the entrance to Jervis Inlet (Mackas and Harrison, 1997). Waters above the sill in Saanich Inlet are in exchange with those of Satellite Channel both tidally and through isopycnal mixing (Herlinveaux, 1962; Hobson, 1985; Stucchi and Whitney, 1997), and Hobson (1985) showed that lateral mixing at depths of 5-20 m, then vertical mixing to the surface, was a major source of nutrients to the phytoplankton in Saanich Inlet. The surface stratification and generally weak winds and tides of Saanich Inlet (Herlinveaux,

1962; Stucchi and Whitney, 1997) are furthermore conducive to phytoplankton growth, and intrusions of nutrient- and phytoplankton-laden waters into the inlet during spring tides result in high chlorophyll biomass throughout much of the inlet, but especially towards the mouth (Takahashi, 1977; Parsons et al., 1983; Hobson and McQuoid, in press).

Although the biological front at the mouth of Saanich Inlet is well documented (Parsons et al., 1983; Hobson and McQuoid, in press), there is less evidence that tidal mixing through constrictions in the vicinity of the mouth of Jervis Inlet (JV-3) causes heightened primary production. Cochlan et al. (1986) found no evidence of a biological front at the mouth of Jervis Inlet, while Parsons et al. (1984b) did observe high chlorophyll *a* concentrations and high rates of primary production ~6 km southeast of JV-3. They ascribed the heightened biological activity to enhanced nutrient supply by intense mixing through Skookumchuk Narrows at the mouth of Sechelt Inlet (Figure 1.1). The finding that primary production at the mouths of Saanich and Jervis Inlets was approximately 1.4 times greater than at the inland stations is surprising considering the relative weakness of the front at the mouth of Jervis Inlet. However, unpublished work by Ann Gargett (Old Dominion University, Norfolk, VA, pers. comm.) suggests an efficient supply of surface nutrients throughout the length of Saanich Inlet during transitions from neap to spring tides. During neap tides, water from the Cowichan and Fraser Rivers causes low surface salinity of Satellite Channel and Saanich Inlet. Intensified mixing during spring tides increases surface salinity in Satellite Channel and a density-driven surface outflow from Saanich Inlet results. This outflow is accompanied by rapid, sub-surface inflow, providing much of the length of Saanich Inlet with a new supply of nutrients.

Other evidence that nutrients were supplied to the phytoplankton of Saanich Inlet laterally from Satellite Channel is the high nitrate to phosphate (N:P) ratios at mid-depths

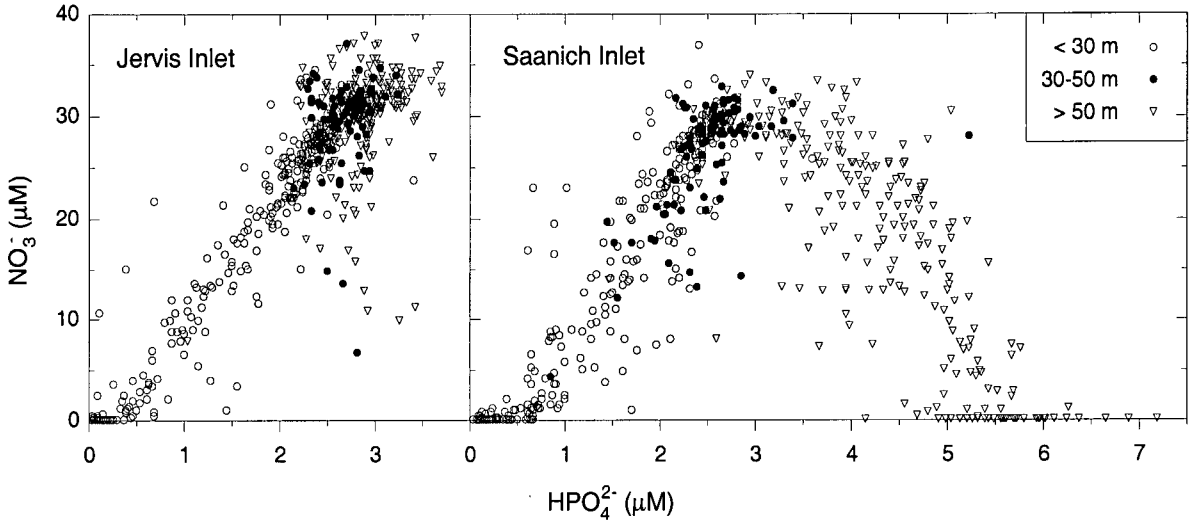

Figure 2.9: Nitrate versus phosphate in both inlets. The average N:P ratio at 30-50 m was 10.7 in Saanich Inlet and 11.4 in Jervis Inlet. Most of the samples from 30-50 m in Saanich Inlet with PO_4^{3-} concentrations greater than 3 μM and low N:P ratios were collected in the summer and fall during deep-water renewals. Otherwise, the N:P ratios at 30-50 m in Saanich Inlet suggest little mixing between deep and mid-depth waters.

of the inlet (Figure 2.9). When oxygen depletion and subsequent nitrate reduction (Figure 2.5) occurred in the deep waters of Saanich Inlet, N:P ratios decreased substantially (Figure 2.9). If vertical mixing between deep and shallow waters were a significant source of nutrients to the phytoplankton, then, assuming a significant fraction of nitrate reduction were to completion (yielding N_2 gas), low N:P ratios would have been found at intermediate depths (~30-50 m). Although some mixing into shallower regions did occur during deep-water renewal (see caption to Figure 2.9), for most of the year there is little evidence that deep nutrients mixed upward. Finding that $\delta^{15}N$ of the sediment-trap material caught in Saanich Inlet was similar to that from Jervis Inlet, Calvert et al. (2001) have come to the same conclusion; mixing of nitrate from the deep waters of Saanich Inlet (where nitrate reduction would cause the remaining nitrate to be isotopically heavy) into the euphotic zone must have been small compared with the lateral nutrient supply from outside the fjord. Also, Ward et al. (1989) showed that upward methane fluxes across

30 m depth in Saanich Inlet were too small to balance the evasive flux to the atmosphere and Lilley et al. (1982) concluded that lateral exchange between Saanich Inlet, Satellite Channel and the Strait of Georgia, combined with the isolation of the deepwater methane of Saanich Inlet, caused regional similarity in methane profiles at depths above the sill.

Thus, enhanced primary production at SN-0.8 relative to JV-7 may have been the result of a greater landward nutrient flux in Saanich Inlet and could explain the similarity in the seaward:landward ratios of primary production between the fjords despite the productive biological front at the mouth of Saanich Inlet. Indeed, of the four stations, surface nitrate depletion during the growing seasons was most severe at JV-7 (Figures 2.1 through 2.4) and it appears that at JV-7 diatoms were a smaller fraction of the phytoplankton compared with the other stations (Figure 2.6). A higher relative abundance of flagellates at the landward station in Jervis Inlet may have been a response to a lower nutrient supply.

It should be noted that variations in light attenuation due to riverine silt is an unlikely cause of the observed geographic pattern of primary production. Within Howe Sound south of the Jervis Inlet system, primary production is affected by the turbidity caused by riverine silt and clay (Stockner et al., 1977; Parsons et al., 1981), raising the possibility that the more glacially influenced riverwater of Jervis Inlet may contain sufficient silt to affect light transmission, especially at station JV-7. However, a comparison of average winter and summer extinction coefficients at each station is not consistent with this possibility (Figure 2.7). Indeed, Captain Vancouver (1798, from Pickard {1961}) observed silty waters in some of the British Columbian fjords, but not in Jervis Inlet and, during the cruises of this experiment, silt was not noticed in the surface waters of Saanich or Jervis Inlet (Maureen Soon, UBC, pers. comm.).

2.4.3 Bottom-water oxygen in Saanich and Jervis Inlets

The oxygen dynamics of fjords are affected by factors including fjord morphology (e.g.; sill and fjord dimensions), water circulation and mixing, the frequency and oxygen supply of deep-water renewal and the delivery of autochthonous and allochthonous organic matter to the deep waters. Of the BC fjords, Saanich Inlet is unique, as the other anoxic basins are severely restricted by their sills from deep-water renewals (section 2.1). The results of this chapter show that primary production and export flux were high during the study in Saanich Inlet and the principal cause has been argued to be the fertility of adjoining waters. The weakness of estuarine flow may have further enhanced particle flux to bottom waters. Advection is recognised as an important factor in the transport of particles into and out of fjords (e.g.; Sakshaug and Myklestad, 1973; Lewis and Thomas, 1986; Wassmann, 1996) and Gilmartin (1964) estimated that 25% of local community production was lost from a nearby fjord (Indian Arm) due to estuarine circulation. Such losses from Saanich Inlet would be minimal and, although the source of the very high sediment-trap fluxes at 50 m at station SN-9 is uncertain (whether resuspended off the sill or washed into the fjord; see Chapter 3), it is possible that because of the unusual circulation there was a net flux of organic material into Saanich Inlet. These sources of organic matter to the deep waters are likely to result in an unusually large oxygen demand behind the sill of Saanich Inlet. Also, low rates of vertical mixing will exacerbate oxygen depletion in deep basins. Although some evidence exists that mixing rates in Saanich Inlet are not anomalous (Smethie, 1981), weak estuarine circulation, winds and tides provide little energy to mix the deep waters of Saanich Inlet (Ann Gargett, Old Dominion University, Norfolk, VA, pers. comm.). Indeed, DeYoung and Pond (1988) found vertical eddy diffusion is about an order of magnitude lower in Saanich Inlet than in Indian Arm.

In Jervis Inlet, bottom waters remain oxygenated despite infrequent ($<$ one year^{-1})

deep-water renewals. Primary production was not exceptionally high in Jervis Inlet and the estuarine flow, albeit weak, would carry a portion of surface biomass out of the fjord. The deep (385 m) sill must also play an important role in the oxygen balance of the deep waters of Jervis Inlet, as much of the sinking organic matter will be oxidised before bottom waters are reached.

2.5 Conclusions

A four-year time-series of monthly primary-production determinations in Saanich and Jervis Inlets, British Columbia, Canada shows that Saanich Inlet was significantly more productive than Jervis Inlet or the Strait of Georgia, while the landward stations within each fjord were less productive than those seaward. Surface nutrient-supply from outside the fjords was likely higher to Saanich Inlet and may have controlled the differences in primary production between stations. Fluxes of biogenic silica at 50 m reflected the geographical pattern of primary production and the oxygen demand caused by the settling flux of organic matter probably contributed significantly to the periodic, deep-water anoxia of Saanich Inlet. Retainment of organic particles due to weak estuarine exchange and low rates of vertical mixing in Saanich Inlet would have further induced anoxia.

Chapter 3

Sources and patterns of settling fluxes in Saanich and Jervis Inlets

3.1 Introduction

Coastal oceans constitute approximately 10% of the area of the global oceans, yet these margins account for ~20% of global ocean primary production (Walsh, 1988; Liu et al., 2000) and most of the organic carbon burial in marine sediments (Berner, 1982; Hedges and Keil, 1995; Middleburg, 1997). Fluvial delivery (Meybeck, 1982) is the principal source of organic matter to coastal waters and sediments (Berner, 1989; Hedges and Keil, 1995; Liu, 2000). However, much of the primary production of these nutrient-replete boundaries is by diatoms (Nelson et al., 1995) and, because of their high growth rates and unique physiological adaptations to turbulent and nutrient-rich waters (Smetacek, 1985), diatoms are also important vectors of carbon flux in coastal settings (e.g.; Pitcher, 1986; Sancetta and Calvert, 1988; Sancetta, 1989a, 1989b, 1989c; Waite et. al., 1992; Conley and Malone, 1992; Kiørboe et al., 1994; Kiørboe et al., 1996; Tiselius and Kuylenstierna, 1996; Del Amo et al., 1997; Pike and Kemp, 1999). The relatively shallow waters of continental margins and the high rates of sediment accumulation and burial furthermore result in short diagenetic residence times and enhanced organic matter preservation (Middleburg, 1997). Thus, these factors (large terrestrial and marine inputs, enhanced preservation) result in the disproportionate amount of organic matter burial in coastal marine regions. However, although coastal regions play an important role in global carbon fluxes, they are characteristically heterogeneous and generalisations of biogeochemical processes

are difficult to make (Smith and Hollibaugh, 1993; Liu et al., 2000).

Glacially-carved fjords are unique coastal features that are typically over-deepened and hydrographically restricted by sills (Syvitski et al., 1987; Burrell, 1988; Wassmann, 1991; Wassmann et al., 1996). Fjords are catchment basins for high-latitude mountainous regions and collect a disproportionate amount of weathered products delivered from land to the sea; as much as one quarter of the fluvial sediment entering the sea in the past 100,000 years is trapped in fjord basins (Syvitski et al., 1987). Furthermore, fjords are semi-enclosed mesocosms mimicking ocean basins (Skei, 1983; Burrell, 1988) and have long been recognised as accessible locations where physical, biological and geochemical processes relevant to oceanic systems can be studied.

In this chapter, I examine a unique time-series of particle fluxes in two British Columbian fjords in an attempt to gain further understanding of the physical and ecological processes leading to water-column sedimentation and, ultimately, bottom sediment burial. Sediment traps were moored at stations in Saanich Inlet and Jervis Inlet, two contrasting fjords of British Columbia, Canada, for about five years during the 1980s; some of the information on the time series has been published. The 1983-84 sediment-trap fluxes from Saanich Inlet were used to aid interpretation of the geochemistry of the bottom sediments (François, 1987; 1988), and the fluxes at 50 m from a 1985 station were included in a study of marine and terrigenous biomarkers in Saanich Inlet (Cowie et al., 1992). Fluxes of total dry weight, carbon, biogenous silica and diatom valves from Saanich Inlet during 1985 have been described (Sancetta and Calvert, 1988), as well as diatom valve flux in relation to atmospheric conditions for both inlets from 1985 to 1987 (Sancetta, 1989a; 1989c). Sancetta (1989b) reported fecal pellet flux for 1986 at the landward station in each fjord. Based on microscopic examination of the sediment-trap samples, Sancetta's observations provide a very useful descriptive foundation for this work. Primary production for most of the time-series has also been reported (Chapter

2; Timothy and Soon, 2001).

The total mass, biogenic silica, organic carbon, nitrogen and aluminium fluxes are presented and discussed in this chapter. A relationship between $\delta^{13}C$ and biogenic silica content is used to separate marine and terrestrial organic carbon in a way that allows estimates of the relative contribution of diatoms to the sinking flux of marine organic matter. Export ratios for organic carbon and biogenic silica are computed using the primary production results of Chapter 2 and the sediment trap fluxes. Finally, the sediment-trap fluxes are compared to mass accumulation rates of the bottom sediments, allowing a top (primary production) to bottom (sediment accumulation) description of the organic carbon and biogenic silica fluxes in two fjords with differing redox conditions.

3.2 Materials and methods

3.2.1 Field design and sample preparation

The sediment-trap study began in the fall and winter of 1983-84 in Saanich Inlet and expanded into Jervis Inlet in spring-summer of 1985 (Figures 1.1, 1.2 and 1.3, and Table 3.1). The initial mooring site (JV-11.5) at the mouth of Jervis Inlet was in an active shipping lane, so the mooring was moved to station JV-3 after several deployments. Throughout this work, the data collected from JV-11.5 are treated with those collected at JV-3. Sediment traps were placed at three depths on each mooring and were serviced and redeployed approximately monthly.

The sediment traps were made from PVC cylinders with an inside diameter of 12.7 cm and a height of 48 cm (aspect ratio = 3.8). Baffle grids (1.5 cm square) were placed in the opening and toward the base of each trap in order to decrease mixing (Gardner, 1980a). Prior to deployment, traps were filled with seawater and 500 mL of a 30% brine solution were funneled to the bottom of the traps. The sediment traps were always

station	location	water depth (m)	trap depths (m)	sediment-trap time series (yymmdd)	1°-production time series (yymmdd)
	Saanich mouth		45	830809	850807
SN-9	48°40.2'N	165	110	to	to
	123°30.2'W		150	891215	891010
	Saanich head		50	840112	850809
SN-0.8	48°33.0'N	210	135	to	to
	123°32.7'W		180	891215	891010
	Jervis mid-inlet		50	850328	850808
JV-7	50°03.4'N	530	200	to	to
	123°48.9'W		450	891219	891011
	Jervis mouth		50	850808	850808
JV-11.5	49°48.6'N	660	300	to	to
	123°56.1'W		600	860128	860128
	Jervis mouth		50	860311	860311
JV-3	49°48.3'N	660	300	to	to
	124°02.4'W		600	890829	891011

Table 3.1: Station locations, sediment trap depths, and duration of the sediment-trap and primary-production time series.

deployed in pairs with 0.5% sodium azide (NaN_3) as a bactericide in one trap of each pair. NaN_3 inhibits aerobic but not anaerobic bacterial respiration and acts as a poison to zooplankton that may be attracted to material caught by traps. Upon retrieval, the trapped debris was filtered through 0.47 mm Nitex monofilament bolting cloth to remove large zooplankton and other swimmers and in the laboratory the sediment was washed free of salt by repetitive centrifugation with deionised water. The solid phase was freeze-dried, weighed and ground to a fine powder. From 1985 to 1987, the sample was split upon retrieval and analysed microscopically (Sancetta and Calvert, 1988; Sancetta, 1989a, 1989b, 1989c).

3.2.2 Laboratory analyses

Total carbon and nitrogen were determined by gas chromatography on a model 1106 Carlo-Erba CHN analyser with an analytical precision of ±1.3% for carbon and ±2% for nitrogen (Verardo et al., 1990). Inorganic carbon was determined with a Coulometrics Inc. CO_2 coulometer (precision ±2%) and converted to $CaCO_3$. Organic carbon (OC) was determined by subtracting inorganic carbon from total carbon.

Biogenic silica (BSi) was measured following the method and equations of Mortlock and Froelich (1989). The procedure involves extracting amorphous silica with 2 M Na_2CO_3 and then measuring the dissolved silicon concentration in the extract by molybdenum-blue spectrophotometry. Conversion from biogenic silicon (%Si) to biogenic silica ($\%SiO_2 \cdot nH_2O$) assumed biogenic silica contains 12% water by weight. The precision for replicates of in-house sediment standards with relatively high BSi content (> 10% BSi) was ±4%.

Aluminium (Al) and other metals (Ti, Fe, Ba and Zr) were measured by inductively-coupled plasma mass spectrometry (ICP-MS). Approximately 5 mg sediment were added to a ~0.5 mL cocktail of concentrated HNO_3, HCl and HF in 1.5 mL Teflon vials with screw caps. The vials were placed in larger Teflon 'bombs' and microwaved for 30 min at ~40 psi. The vials were then placed on a hotplate, with their caps removed, until dryness. ~0.5 mL 2 N HNO_3 was weighed and added to the residue and after a second 30 min, 40 psi microwave digestion, the 2 N HNO_3 solution was diluted ~400-fold with 0.1 N HNO_3 using a precision balance. Further dilutions were performed by volume. Al, Ti, Ba, Fe and Zr were analysed on a VG Elemental 'PlasmaQuad Turbo Plus' ICP-MS equipped with an SX300 quadrupole mass analyser and Galileo 4870-V channel electron multiplier. Liquid argon served as nebuliser, auxiliary and cooling gases. External standards were used to determine metal concentrations in the diluted samples. The ICP-MS was de-tuned

so that the response was linear to 100 ppb Al in order to minimise required dilutions. Indium and scandium were used as internal standards to correct for plasma instabilities and sensitivity changes during the analyses. A number of in-house (bottom sediments from Saanich and Jervis Inlets) and certified sediment (MESS-2) standards were digested and analysed with the sediment-trap samples; the accuracy of the Al analyses on these standards was 3% or better, while the precision was ±6% or better.

The isotopic composition of organic carbon was determined on decarbonated (10% HCl) subsamples using a VG PRISM isotope ratio mass spectrometer, with a Carlo Erba CHN analyser fitted in-line as a gas preparation device. Values are reported in δ notation relative to the PDB reference: $\delta^{13}C = 1000\ ([^{13}C{:}^{12}C]_{sample}/[^{13}C{:}^{12}C]_{PDB} - 1)$. The precision was $\pm 0.2^{0}/_{00}$.

3.2.3 Effect of preservative treatments

To test the effectiveness of sodium azide as a preservative, fluxes measured by the sediment traps with and without NaN_3 from all depths at each station were averaged. Fluxes were considered instead of percentages because variable preservation of one constituent could affect the content of another constituent. For the total mass, OC and N fluxes, there was no clear preservative effect for NaN_3 (Table 3.2). Therefore, in order to reduce the number of analyses, BSi and Al were measured on sediments collected from the NaN_3-treated traps and $\delta^{13}C$ was measured on samples from the 'brine only' traps. A number of cross-analyses found little or no effect of preservative treatment on BSi fluxes (Table 3.2). Where analyses were performed on samples from each trap in a pair, the values presented in this chapter are the average of the two treatments.

$CaCO_3$ fluxes were 16 to 28% greater for the sediment traps treated with NaN_3 (Table 3.2). CO_3^{2-} is undersaturated with respect to $CaCO_3$ in coastal waters, but NaN_3 buffers $CaCO_3$ dissolution (Knauer and Asper, 1989); Timothy and Pond (1997) also

	SN-9	SN-0.8	JV-3	JV-7
		mass flux (g m^{-2} d^{-1})		
brine	9.66	2.16	1.62	1.27
brine + NaN_3	9.74	2.19	1.66	1.31
%Δ (n)	0.79 (173)	1.3 (189)	2.2 (122)	3.3 (144)
		OC flux (mg m^{-2} d^{-1})		
brine	468	176	144	130
brine + NaN_3	457	173	140	135
%Δ (n)	-2.4 (173)	-1.5 (189)	-2.7 (122)	4.0 (144)
		N flux (mg m^{-2} d^{-1})		
brine	57.6	22.7	16.8	15.7
brine + NaN_3	55.2	22.2	16.4	16.3
%Δ (n)	-4.2 (173)	-2.2 (189)	-2.4 (122)	3.9 (144)
		$CaCO_3$ flux (mg m^{-2} d^{-1})		
brine	66.3	36.0	22.8	19.1
brine + NaN_3	78.9	45.4	30.4	26.6
%Δ (n)	16 (173)	21 (189)	25 (122)	28 (144)
		BSi flux (mg m^{-2} d^{-1})		
brine	2750	1450	703	668
brine + NaN_3	2840	1400	686	677
%Δ (n)	3.4 (9)	-3.5 (7)	-2.4 (13)	1.5 (6)

Table 3.2: Average fluxes to both sets of traps (with and without NaN_3) in each deployment-pair. Negative differences occur where fluxes to NaN_3-treated traps were smaller than fluxes to traps without NaN_3.

found that $CaCO_3$ was higher in sediments from NaN_3-treated traps in a shorter experiment in Sechelt Inlet (Figure 1.1). Because of the NaN_3 effect on $CaCO_3$ preservation, the lack of an effect on organic preservation cannot be attributed to outwash of the preservative during each deployment. Although these results might therefore suggest that sodium azide is an ineffective bactericide, Lee et al. (1992) found it to be a better preservative than brine alone, though not as good a bactericide as other preservatives. Other possible explanations for the lack of a preservative effect on the organics include: OM loss was minimal in both treatments or the organic degradation was not aerobic; cell lysis and other physical processes affected solubilisation of the most labile organics while the sediment traps were moored; the treatment of samples after they were retrieved (rinsing and centrifugation) removed the labile organics that may have been preserved differently in the traps.

3.2.4 Linear regressions

All linear regressions are model II (functional) geometric mean regressions (GMR), also known as the reduced major axis regression. The 95% confidence intervals of the slopes and intercepts are calculated according to Ricker (1984). Functional regressions are preferred over the more commonly applied model I (predictive) regression when describing relationships of field data such as reported here (Ricker, 1973, 1984; Mark and Church, 1977; Laws and Archie, 1981; Sokal and Rohlf, 1995). A property of the GMR line that makes it better for describing the relationship between two variables with similar degrees of natural variability is that, when y is plotted against x, the slope is the inverse of the line obtained when x is plotted against y. For practical purposes, it is useful to know that the slope of the GMR line (m_{II}) can be calculated from the slope of the model I regression (m_I): $m_{II} = m_I / |r|$, where r is the correlation coefficient. Thus, the slope of the GMR line is always steeper than the slope of the model I regression line; the

importance of choosing the proper regression increases as the correlation between two variables decreases.

Although the use of GMR is strongly advised for the description of naturally varying data (references above), there remains controversy about the application of model II regression for predictive purposes. Ricker (1973, 1975, 1984) recommends that, in some cases where there is natural variability in a data set, GM regression should be used for both description and prediction, while Sokal and Rohlf (1995, p. 543) discourage the use of model II regressions for any predictive purpose. In the one case where regression is used for predictive purposes (Figures 3.19 and 3.20), the GMR is used.

3.3 Results

3.3.1 Components of the mass flux

To satisfy the mass balance of the total flux, factors to convert organic carbon (OC) to total organic matter and Al to total lithogenic material are estimated. Following Timothy (1994) and Timothy and Pond (1997), the OM:OC ratio is approximated by assuming a molar OC:P ratio of 106:1 (Redfield et al., 1963) and writing the model organic molecule as: $(CH_2O)_{106}(NH_3)_x(H_3PO_4)$, where x = 106 N:OC. For the range of OC:N ratios observed during the study (7.1 to 15; Figure 3.1), the OM:OC ratio was 2.67 to 2.78. The use of 106:1 for the OC:P ratio is an overestimate of the amount of phosphorus in the sediment-trap samples (unpublished data), but these estimates are not sensitive to the OC:P ratio.

Figure 3.2 shows the relationship between Al and total lithogenic material (LM). According to these plots, the lithogenic flux was 8.5 - 10% Al. The tendency for negative intercepts on the Al axes of Figure 3.2, especially at station SN-0.8, may be caused by the presence of quartz in the samples. Gucluer and Gross (1964) reported quartz in the

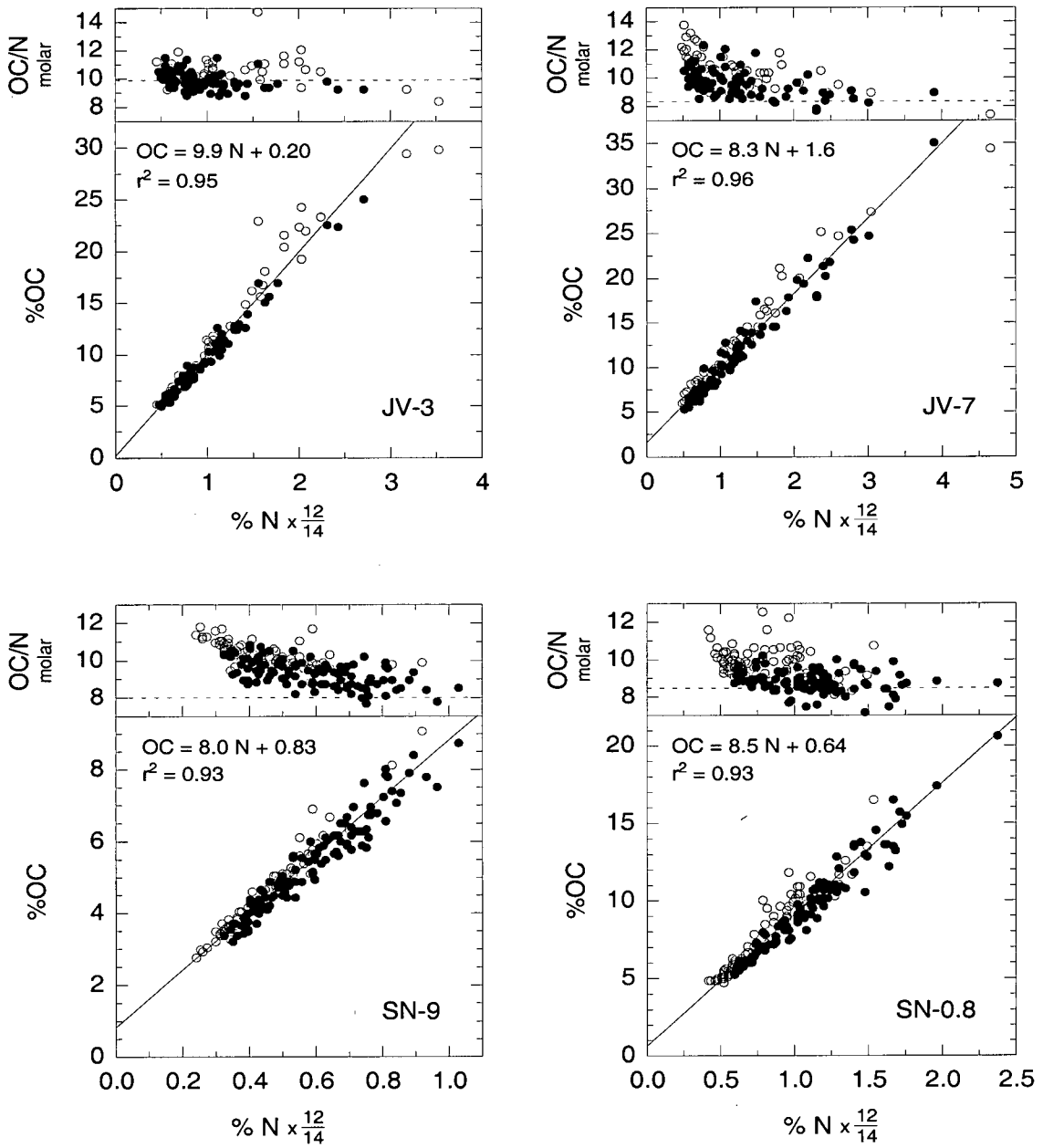

Figure 3.1: OC versus N for the entire data set, showing the range in OC:N ratios caught in the traps. Dashed lines in the upper panels are the slopes of the regression lines of the lower figures. Filled circles are summer data, open circles winter data. By multiplying weight percent N by 12/14, the slope of the regression line gives the mean molar ratio.

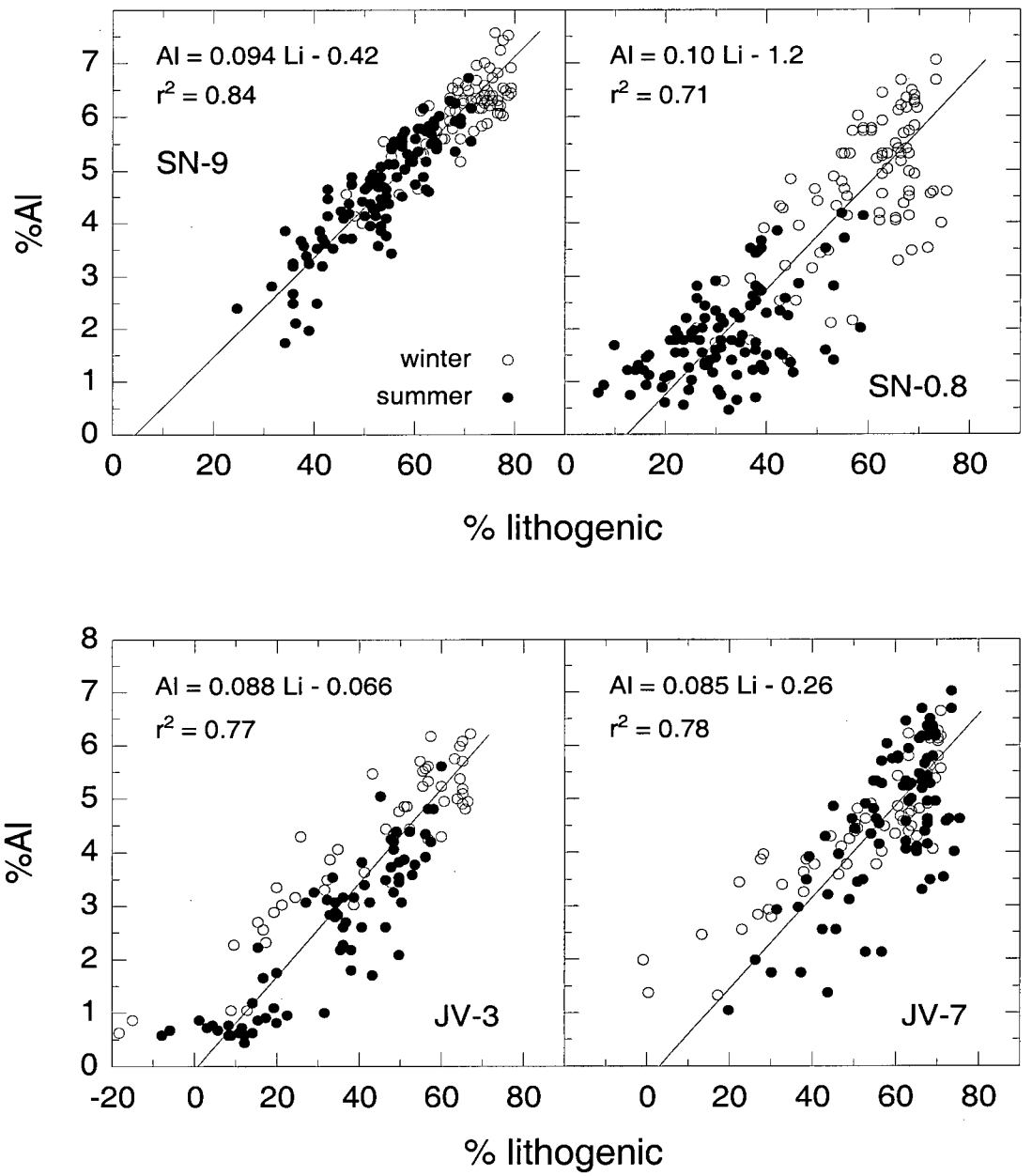

Figure 3.2: Al versus lithogenic material at each station. The lithogenic percentage is calculated as 100 - %BSi - (OM:OC) %OC - $\%CaCO_3$. The slopes are interpreted as being the average Al content of the settling aluminosilicates.

sands and fine laminae of the bottom sediments of Saanich Inlet and X-ray diffraction analyses (unpublished) indicate the presence of quartz in both sediment-trap and bottom sediments of Saanich and Jervis Inlets.

$CaCO_3$ made only small contributions to the sediment-trap material (on average 2% of the mass flux at stations JV-3, JV-7 and SN-0.8, and 0.8% of the mass flux at station SN-9), as foraminifera and coccolithophorids are rare in waters connecting to the Strait of Georgia. Other sources of $CaCO_3$ may have been resuspended fragments of mollusk shells, eroded limestone exposures within the watersheds and, in Saanich Inlet, a cement plant at mid-fjord on the west side (Gucluer and Gross, 1964). Higher carbonate fluxes to the deep trap at SN-0.8 (average of 2.2% and occasionally surpassing 4% of the mass flux) might have been the result of sediment transport from the area of the cement plant.

3.3.2 Fluxes at the head of Saanich Inlet (station SN-0.8)

The magnitude and the character of the settling fluxes at the two stations in Saanich Inlet differred dramatically, as the sediment traps at station SN-9 were in a nepheloid region or depocenter affected by resuspended sediments most likely originating from the broad sill at the mouth of the inlet (Figure 1.1). Therefore, discussed first are the settling fluxes measured at station SN-0.8 toward the head of Saanich Inlet where the influence of the autochthonous phytoplankton was more apparent. At station SN-0.8, interannual variability of the mass, BSi, OC and Al fluxes was small during the study (Figures 3.3 through 3.6), so when referring to the entire time series, most of the attention will be given to seasonal patterns and depth variations of fluxes (Figures 3.7 and 3.8, and Table 3.3).

Biogenic fluxes

Mass fluxes to 50 m at station SN-0.8 (Figures 3.3 and 3.7; Table 3.3) were highest in the spring, decreased in the summer and were low in the fall and winter. Of the primary

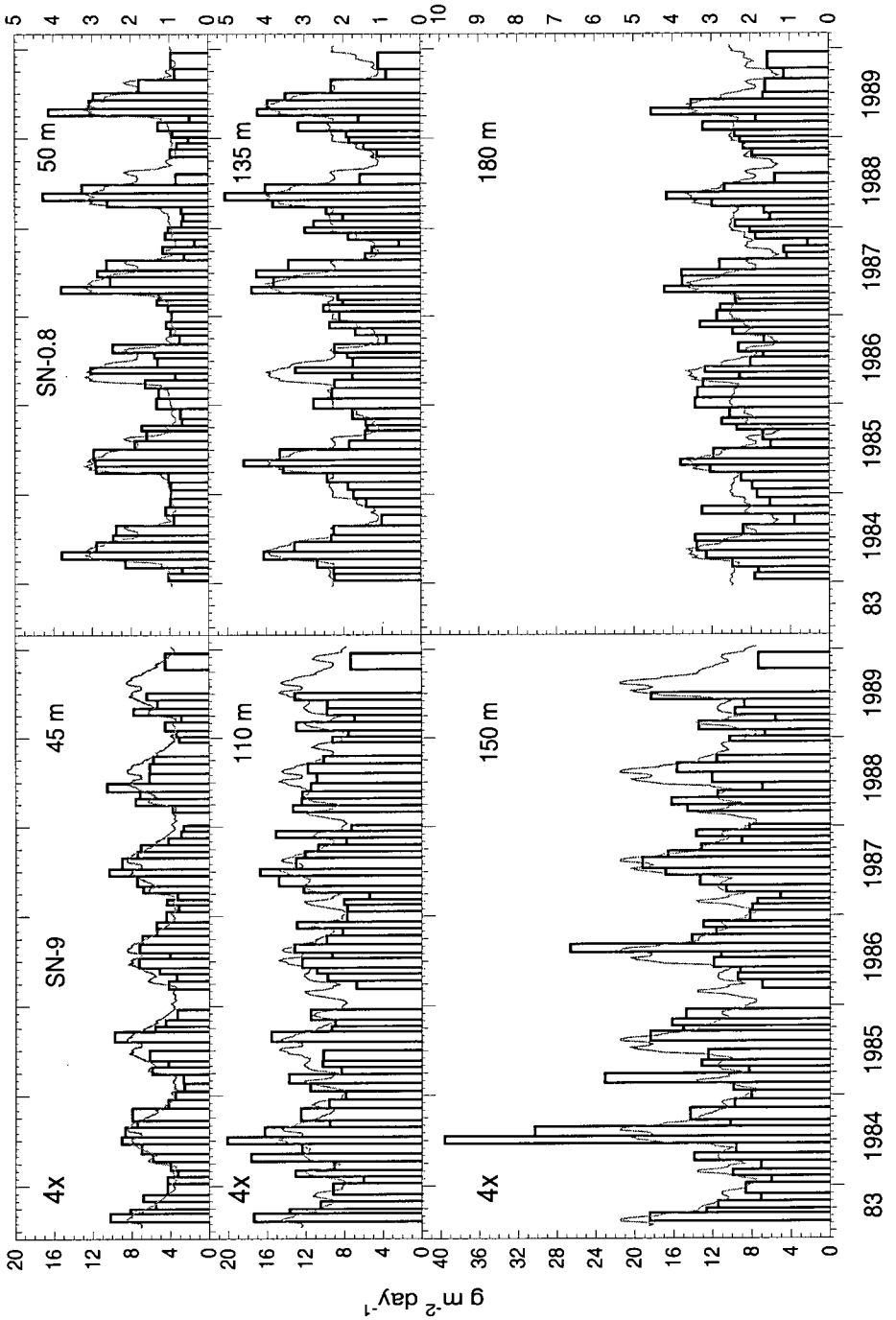

Figure 3.3: Total mass fluxes in Saanich Inlet. The gray lines are the curves of Figure 3.7, repeated annually. Pooling both stations and all depths, lost samples represented 9% of the time series and on 1% of the collected samples not all laboratory analyses were performed. Missing data can be inferred from gaps in the bar graphs. Note that the range of the ordinate is four times larger for station SN-9 than for station SN-0.8.

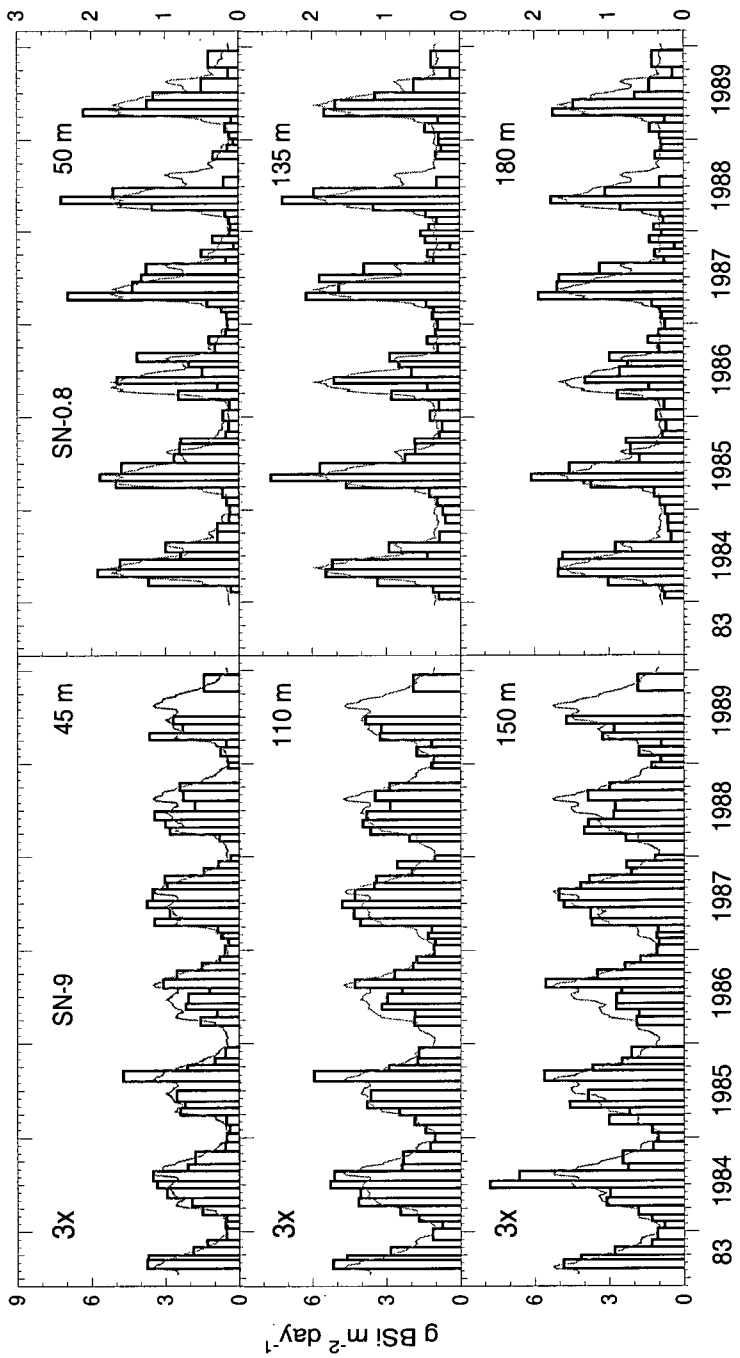

Figure 3.4: Biogenic silica fluxes in Saanich Inlet. The gray lines are the curves of Figure 3.7, repeated annually. Note the difference in the scale of the y-axes for the two stations.

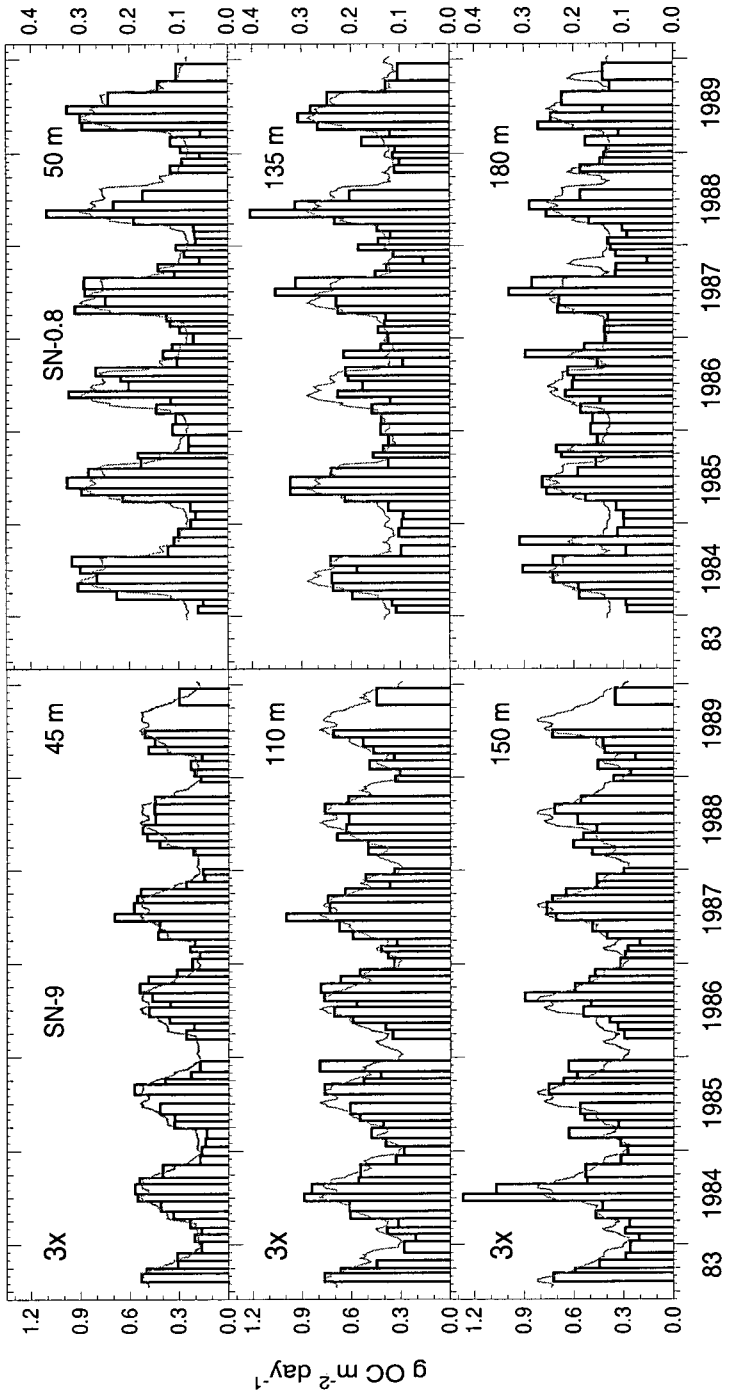

Figure 3.5: Organic carbon fluxes in Saanich Inlet. The gray lines are the curves of Figure 3.7, repeated annually. There is a three-fold scale change between stations for the OC flux.

components, this pattern resembled most closely that of BSi (Figures 3.4 and 3.7). The main source of amorphous silica to Saanich and Jervis Inlets is diatom frustules, with minor contributions made by silicoflagellates (Sancetta and Calvert, 1988; Sancetta, 1989a), while organic matter can have terrigenous and other marine (e.g.; flagellates and zooplankton) sources. Even with the terrestrial contributions (section 2.4.1), OC fluxes at 50 m showed a similar seasonal pattern to those of BSi (Figures 3.5 and 3.7) and both roughly reflected the yearly cycle of primary production (Figure 3.7) by increasing in March-April and decreasing in September-October. Although the deployment period ($\sim$1 month) was too long to measure changes in plankton dynamics shorter than seasons (e.g.; Deuser, 1996), the averaged curves of Figure 3.7 show a pronounced June-July drop in the flux of BSi, followed by a small rebound in August. The early summer drop in BSi fluxes occurred while OC fluxes decreased slightly but remained near peak levels, supporting the possibility that, due to limited nutrient supply, flagellates played an increasingly important role in the ecology of the plankton after the spring bloom towards the head of Saanich Inlet (Takahashi et al., 1977; Hobson, 1981; Parsons et al., 1983; François, 1987; Sancetta and Calvert, 1988; Hobson and McQuoid, in press; Timothy and Soon, 2001).

Winter fluxes of BSi to 50 m at station SN-0.8 were a factor of 10 smaller than their spring peaks, while the contribution of BSi to the mass flux fell from a maximum of more than 50% to about 15% in the winter (Figures 3.4, 3.7 and 3.8). Seasonal variations in OC fluxes were smaller; the winter fluxes were about 30% of the spring and summer maxima (Figures 3.5 and 3.7). The proportion of OC in the settling flux peaked in the summer at about 15% in the upper traps, and dropped to 8% in the winter and early spring (Figure 3.8). OC contents were low in the spring when fluxes of organic matter were highest at station SN-0.8, the result of dilution by BSi.

Changes in flux with depth were minimal for BSi and OC at station SN-0.8. In

the fall and winter, both tended to increased with depth, especially from the shallow (50 m) to the mid-depth (135 m) traps (Figure 3.7). In the spring and summer, OC decreased slightly with depth, as did BSi in the summer. However, springtime fluxes of BSi were highest to the mid-depth traps (Figure 3.7). As at the other stations, the mass flux generally increased with depth at station SN-0.8, largely due to increasing fluxes of lithogenic material in deep waters. Thus, while at 50 m the mass flux was determined mostly by BSi and OC fluxes, at depth the mass flux was more heavily influence by lithogenic debris (Figure 3.7). Contents of BSi and OC in the settling material usually decreased with depth at station SN-0.8 (Figure 3.8).

Aluminium fluxes

With a remarkably regular pattern and unlike at any other station, Al fluxes at station SN-0.8 were high in the winter and low in the summer (Figures 3.6 and 3.7, and Table 3.3). This seasonality occurred at all depths, while Al fluxes increased by a factor of two from 50 m to 135 m and were nearly the same at 135 m and 180 m. As the Al flux showed an opposite seasonal trend to the mass flux, the contribution to the mass flux by aluminosilicates was particularly high in the winter. The proportion of aluminosilicates in the sinking particles at station SN-0.8 was 10-20% in the spring and summer and rose to more than 50% in the winter (Figure 3.8).

The pronounced seasonality of the Al flux at the head of Saanich Inlet followed that of local rainfall and flows from the Cowichan and Goldstream Rivers, and effectively rules out the Fraser River as a potential source of lithogenic particulate matter at station SN-0.8 because flow from the Fraser River peaks during the June freshet. The sources of Al to Saanich Inlet are discussed in section 3.4.4.

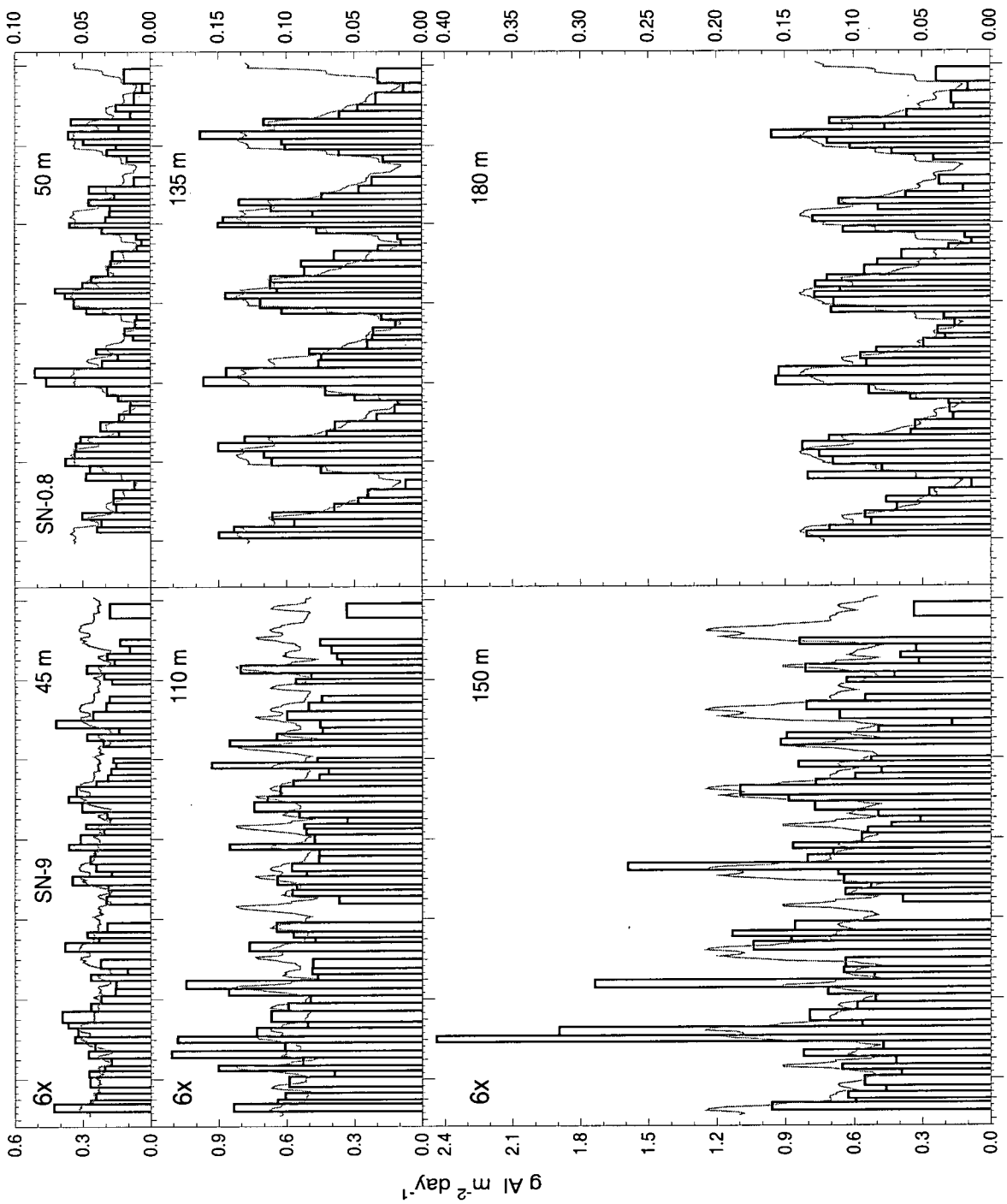

Figure 3.6: Aluminium fluxes in Saanich Inlet. The gray lines are the curves of Figure 3.7, repeated annually. There is a six-fold scale change between stations for the aluminium flux.

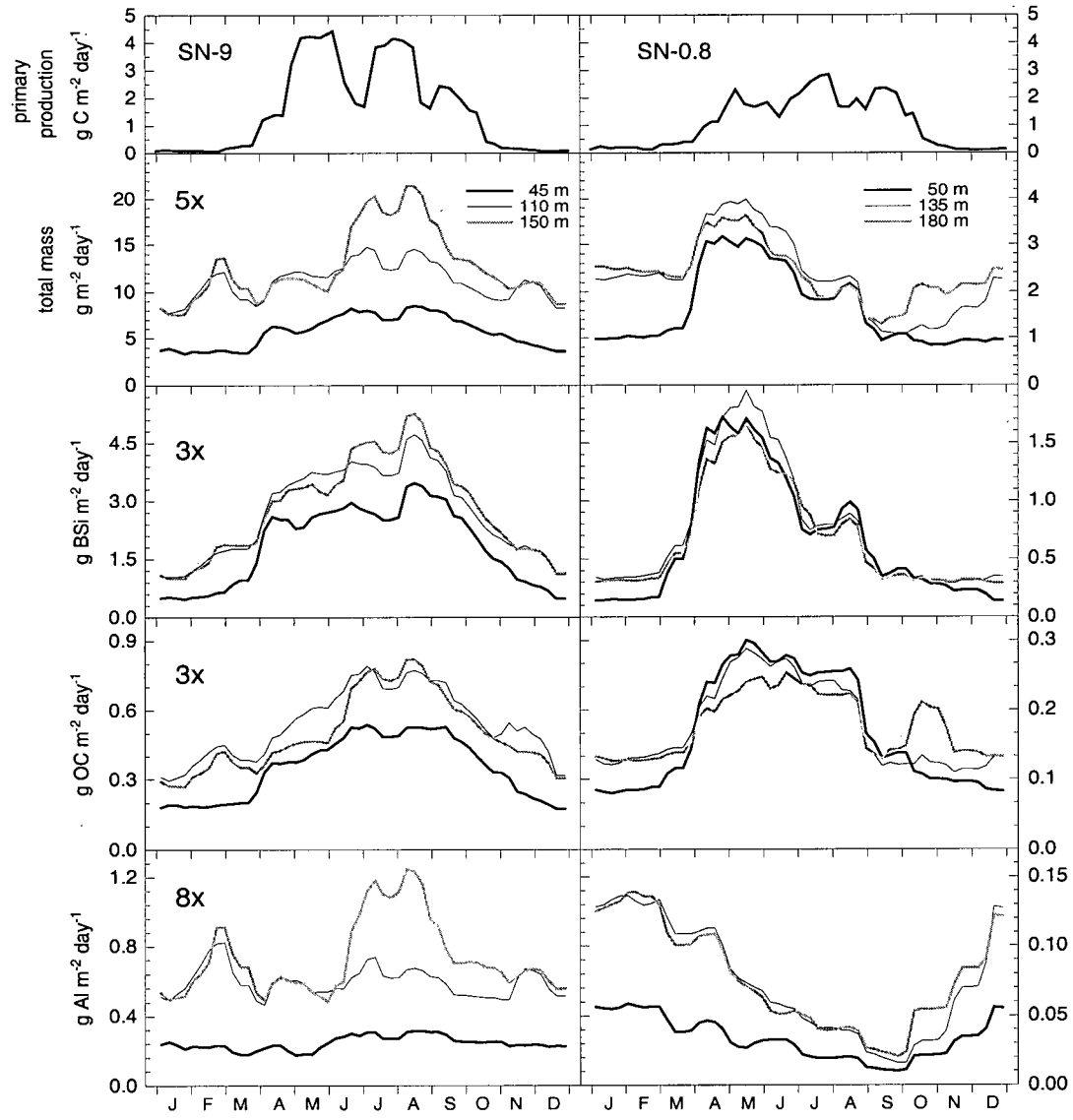

Figure 3.7: Seasonally-averaged sediment-trap fluxes (total mass, BSi, OC and Al) in Saanich Inlet. The seasonal pattern of primary production (Figure 2.8) at each station is included for comparison. The curves describing the fluxes at different depths were made by giving each day during the time series (Figures 3.3 through 3.6) the flux value measured on that day. The series was then sorted by julian day and a seven-day smoothing was applied. Note the difference in scale between stations.

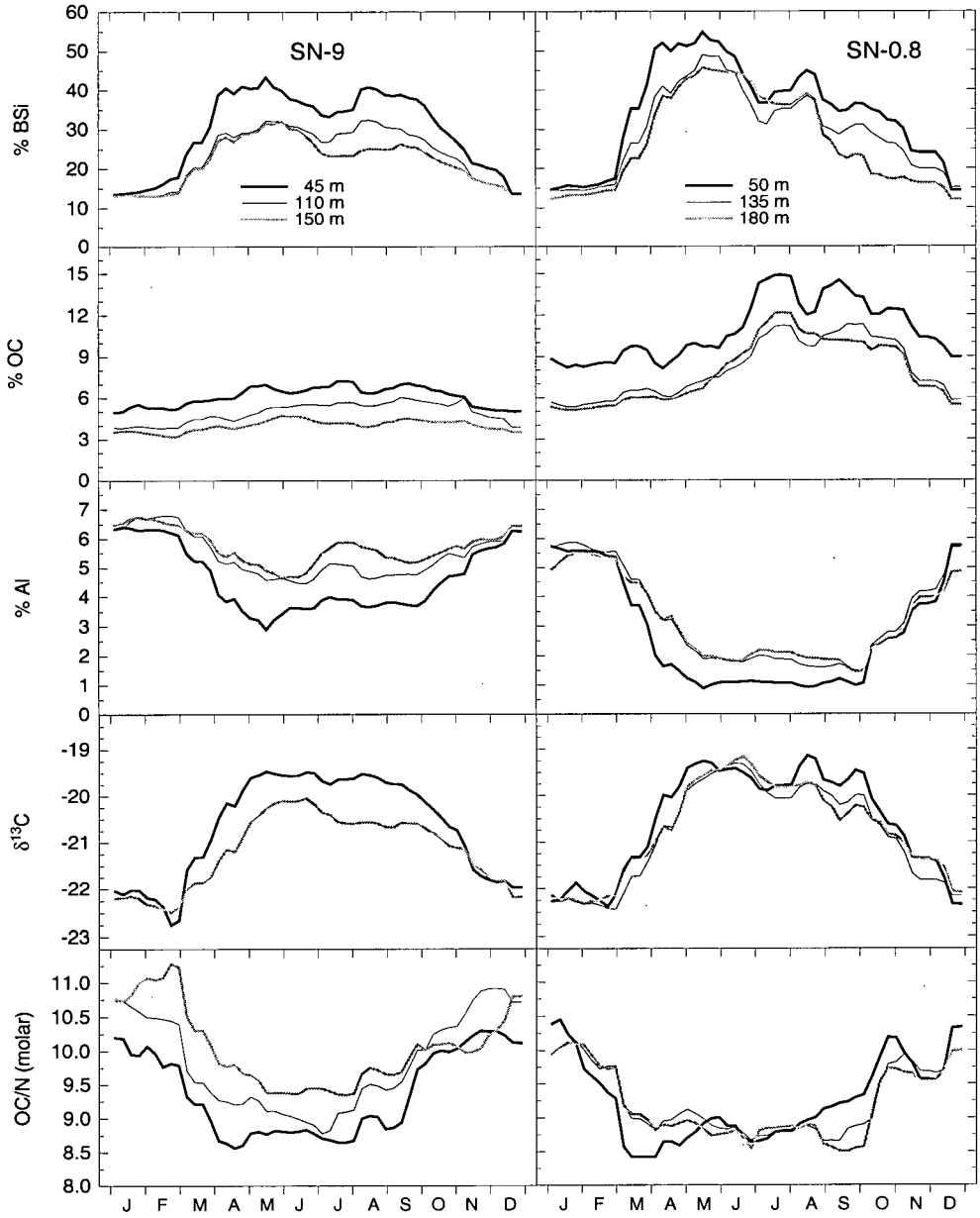

Figure 3.8: Seasonally-averaged compositional characteristics of settling fluxes in Saanich Inlet. The curves were created as described for Figure 3.7. $\delta^{13}C$ and OC/N are flux-weighted averages. Multiplication of %OC and %Al by 2.7 and 9.2, respectively, give estimates of %OM and % aluminosilicates (section 3.3.1).

	SN-9					SN-0.8				
	sp	su	au	wi	**annual**	sp	su	au	wi	**annual**
					mass flux (g m^{-2} d^{-1})					
z_1	6.12	7.80	5.19	3.59	**5.67**	2.75	1.79	0.936	1.04	**1.63**
z_2	11.3	13.4	10.1	9.50	**11.1**	3.51	2.11	1.41	2.31	**2.33**
z_3	11.0	18.7	11.5	9.81	**12.7**	3.19	1.95	2.00	2.45	**2.40**
					BSi flux (mg m^{-2} d^{-1})					
z_1	2400	2940	1420	608	**1840**	1430	757	284	208	**669**
z_2	3310	4030	2110	1360	**2700**	1530	756	324	390	**750**
z_3	3090	4500	2240	1380	**2800**	1320	736	324	351	**680**
					OC flux (mg m^{-2} d^{-1})					
z_1	385	517	312	189	**351**	250	228	106	89.9	**168**
z_2	551	737	518	366	**543**	244	211	121	132	**177**
z_3	451	744	468	330	**498**	215	204	162	131	**178**
					Al flux (mg m^{-2} d^{-1})					
z_1	220	296	240	220	**244**	35.7	18.9	26.1	53.7	**33.6**
z_2	560	646	556	626	**597**	86.2	37.7	48.6	128	**75.1**
z_3	576	1060	659	649	**735**	81.8	39.1	62.1	126	**77.3**
					δ^{13}C					
z_1	-19.8	-19.6	-20.7	-22.0	**-20.2**	-19.6	-19.5	-20.6	-21.9	**-20.0**
z_2						-20.0	-19.9	-21.1	-22.2	**-20.5**
z_3	-20.6	-20.5	-21.2	-22.2	**-21.0**	-19.9	-19.7	-20.9	-22.0	**-20.5**
					OC/N (molar)					
z_1	8.77	8.82	10.0	9.83	**9.29**	8.73	8.90	9.71	9.58	**9.20**
z_2	9.18	9.21	10.5	10.4	**9.73**	8.94	8.76	9.45	9.74	**9.16**
z_3	9.60	9.54	10.1	10.8	**9.97**	8.85	8.75	9.32	9.76	**9.09**

Table 3.3: Fluxes in Saanich Inlet at each sediment-trap depth (z_1, z_2 and z_3; see Table 3.1 for depths of traps). Values were obtained by averaging the curves of Figure 3.7 over each seasonal period. δ^{13}C and OC/N were flux-weighted. sp = spring, su = summer, au = autumn and wi = winter.

3.3.3 Fluxes at the mouth of Saanich Inlet (station SN-9)

Compared to those at station SN-0.8, The settling fluxes at station SN-9 inside the sill of Saanich Inlet were many times larger (Figures 3.3 through 3.7; Table 3.3) and the trapped material was rich in Al, depleted in BSi and especially OC-poor (Figure 3.8). Fluxes of biogenic silica and organic carbon generally followed autochthonous primary production (high in spring and summer, decreasing in fall and winter; Figures 3.4, 3.5 and 3.7), but the Al fluxes show that resuspension was significant throughout the water column and especially at the deep traps when replacement waters flowed over the sill and into the fjord basin in the summer and fall (Chapter 4). Year-round, fluxes of BSi and OC increased significantly from 45 m to 110 m. From 110 m to 150 m, however, changes with depth were less pronounced (Figure 3.7); on average, BSi fluxes increased slightly, and OC fluxes decreased between these depth intervals (Table 3.3). Aluminium and mass fluxes increased ~two-fold from shallow to mid-depth traps, but changed little between 110 m and 150 m, except during renewal periods when peaks in Al and mass fluxes were recorded at 150 m (Figure 3.7 and Table 3.3). Thus, it appears that turbulence across the sill (approximately 70 m) regularly delivered sediment to the water column at station SN-9 such that fluxes at 110 m and 150 m were similar while, during renewal events, fluxes to the deep traps were most affected. %BSi and %OC decreased with depth year-round at station SN-9 while %Al increased with depth, a sign of water column organic remineralisation and a preponderance of resuspended, reworked sediments in deep sediment traps.

Deepwater renewal often overlapped with the period of high primary production at station SN-9 and, therefore, resuspended fluxes of BSi and OC clouded the sediment-trap signal of surface ecology. The resuspended fluxes tended to peak during the second half of the production season, broadening the biogenic flux maxima into the late summer and

fall. Upward transmission of the resuspension signal was common and examples of the effect on BSi and OC fluxes are the summer-fall periods of 1984, 1985 and 1986. During one or more deployments within this period of each year, Al fluxes were especially high at 150 m and decreased upward (Figure 3.6). The BSi and OC fluxes (Figures 3.4 and 3.5) behaved similarly, but their resuspension signals were nearly lost within the seasonal cycle of surface export delivered to the mid-depth and shallow traps. Despite the combined and large influences of both local production and resuspension, the yearly cycles of BSi and OC fluxes (Figures 3.4 and 3.5) were very regular at all depths throughout the time series at station SN-9. Thus, without recognising the extent of resuspension at this location, the BSi and OC flux patterns could be interpreted as primary production signals. Chapter 4 provides a more detailed description of the resuspended fluxes in Saanich and Jervis Inlets.

3.3.4 Fluxes in Jervis Inlet

The nature of the settling fluxes at the two mooring sites in Jervis Inlet (JV-3 and JV-7) were sufficiently similar that they are discussed together.

Biogenic fluxes

As in Saanich Inlet, mass, BSi and OC fluxes to the 50 m sediment traps in Jervis Inlet followed local primary production, increasing in March-April and decreasing in September-October (Figures 3.9, 3.10, 3.11 and 3.13). BSi fluxes varied by a factor of $\sim$20 at the 50 m traps in Jervis Inlet, while OC fluxes at stations JV-3 and JV-7 varied by factors of $\sim$3 and $\sim$5, respectively (Figure 3.13). Again, the smaller seasonal variations in OC flux (compared with BSi fluxes) were due to the wintertime presence of terrestial OC (see section 3.4.2) and to the likelihood that flagellates were larger contributors to the marine OC flux in the winter.

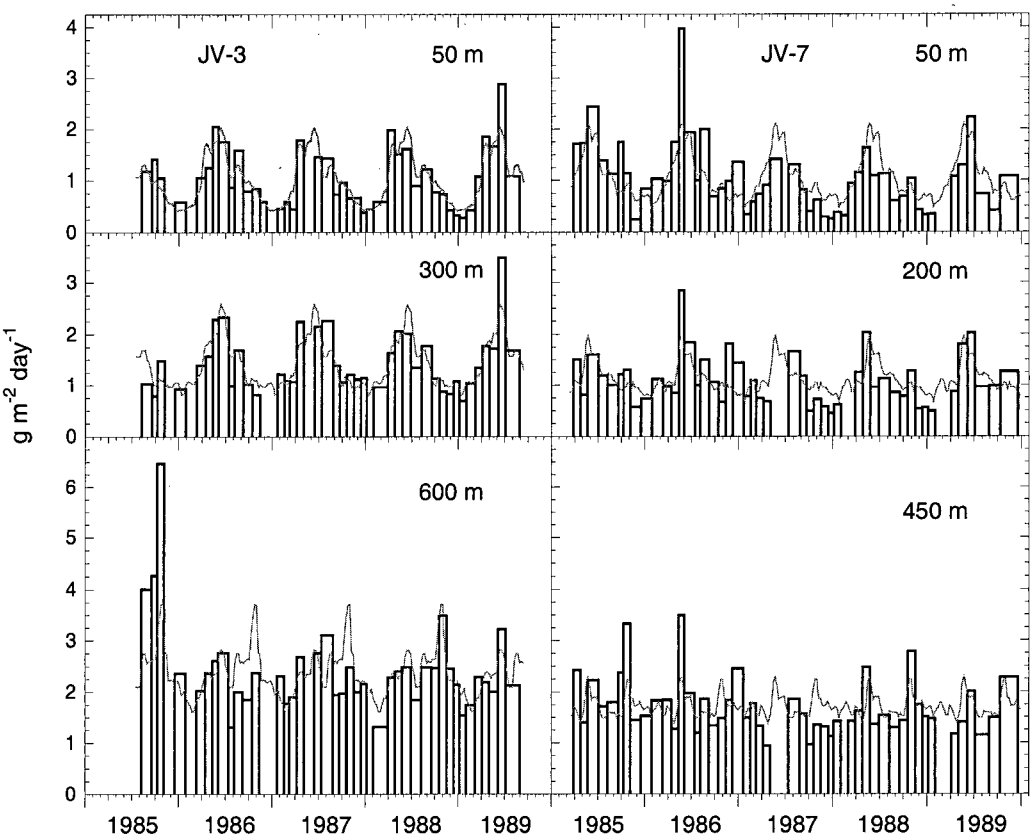

Figure 3.9: Total mass fluxes in Jervis Inlet. The gray lines are the curves of Figure 3.13, repeated annually. Pooling both stations and all depths, lost samples from all or part of a mooring represented 11% of the time series in Jervis Inlet and all analyses were performed on all collected samples. Missing data can be inferred from gaps in these bar graphs.

At both stations in Jervis Inlet, biogenic silica, organic matter and lithogenic debris all comprised >50% of the mass flux at certain times and depths (Figure 3.14). Organic matter often comprised a significant fraction of the settling debris at 50 m, but the seasonal pattern of OC content did not follow the pattern of OC flux (Figures 3.13 and 3.14). In fact, at station JV-3, OC content was inversely related to OC flux at the 50 m traps. The Al fluxes at this location were very low year-round (Figure 3.12), as were the BSi fluxes in the winter. Thus, in the fall and winter, organic matter remained the

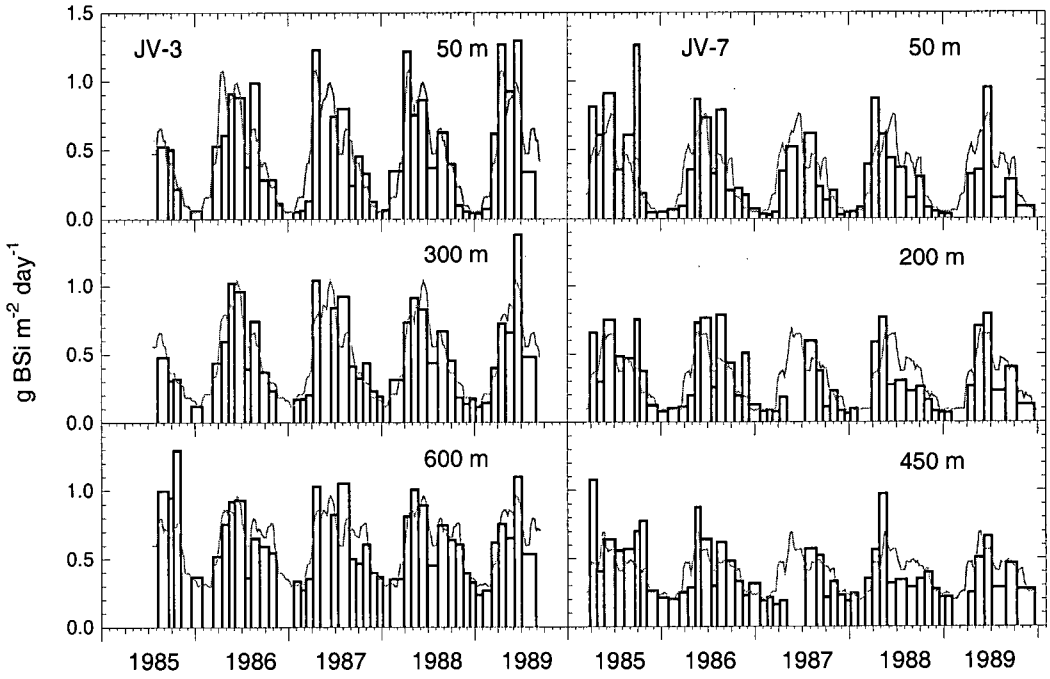

Figure 3.10: Biogenic silica fluxes in Jervis Inlet. The gray lines are the curves of Figure 3.13, repeated annually.

dominant constituent of the mass flux even though OM fluxes were minimal. Indeed, wintertime mass fluxes at the shallow traps of station JV-3 were the lowest of the time series (Tables 3.3 and 3.4), reflecting the small lithogenic and diatomaceous contributions.

In general, the magnitude of the BSi fluxes was similar from year to year and the seasonality was clear at all depths (Figure 3.10). Although spring and summer fluxes were relatively constant with depth, in the autumn and winter BSi fluxes increased with depth (Figure 3.13), possibly due to resuspension of BSi-rich sediments. During spring and summer, there were periods when fluxes of biogenic silica decreased and then rebounded (Figure 3.10). These fluctuations lagged the early-summer lulls in primary production (Chapter 2) by about two to four weeks (Figure 3.13). If the summertime drops in the two time series are not caused by sample biasing and are not an artifact

of the averaging schemes, then this lag implies that the early-summer lull in production resulted in a decrease in the BSi flux (and OC flux; see Figure 3.13) several weeks later. Sancetta (1989a) found evidence of increased grazing in July and August in Saanich and Jervis Inlets, while Sancetta (1989b) showed that fecal pellets and BSi fluxes were reduced at this time; if grazing was the cause of the mid-summer production lulls, it may have resulted in smaller fluxes of BSi to the sediment traps. Fecal pellets are important vectors of downward transport, but grazing can decrease the amount of material exported from the euphotic zone as fecal pellets are largely decomposed in the water column (Smetacek, 1980b; Jumars et al., 1989; Sancetta, 1989b; Noji et al., 1991) and grazing by zooplankton (e.g.; Harrison et al., 1983; Bornhold, 2000) and heterotrophic dinoflagellates (Jacobson and Anderson, 1986; Buck and Newton, 1995; Tiselius and Kuylenstierna, 1996) can control diatom growth, biomass and, ultimately, export flux.

The seasonality of the OC fluxes dampened significantly with depth (Figures 3.11 and 3.13; Table 3.4). Although for most depth intervals in Jervis Inlet OC fluxes remained relatively constant, from 50 m to 200 m at station JV-7, the summertime OC fluxes decreased substantially, while at 450 m the seasonal cycle was absent (Figures 3.11 and 3.13). In 1985 and 1986 at station JV-7, the spring and summer fluxes of OC at 50 m were significantly higher than the seasonal mean, although the deeper OC fluxes were similar to other years (Figure 3.11). Primary production was also high in 1986 (section 2.4.1), but the high OC fluxes at 50 m were not accompanied by BSi (Figures 3.10). The high OC fluxes, therefore, may have been caused by the deposition of non-diatomaceous phytoplankton caught at 50 m and largely remineralised or laterally transported before sinking to the depth of 200 m. If lateral transport were to have caused these changes in flux between 50 m and 200 m, then the horizontal gradients in the export flux must have been very large (e.g.; Siegel and Deuser, 1997; Timothy and Pond, 1997). Because high primary production in 1986 was recognised at the other stations, it is likely the

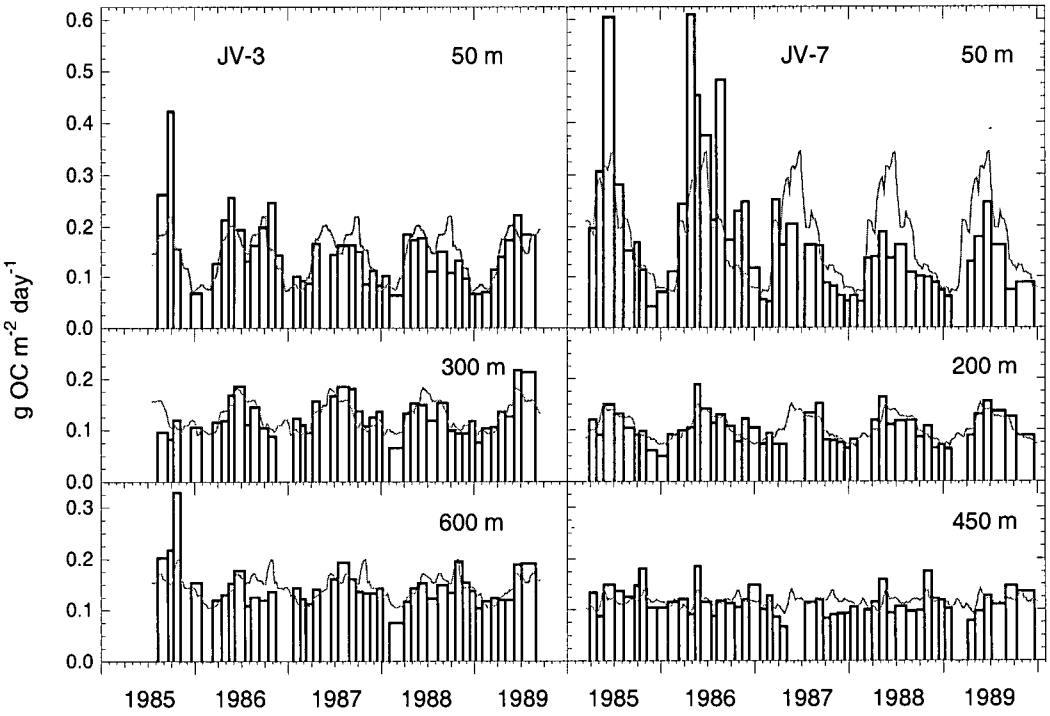

Figure 3.11: Organic carbon fluxes in Jervis Inlet. The gray lines are the curves of Figure 3.13, repeated annually.

production signal of 1986 was a regional event and horizontal gradients in the export flux were not significantly different than in other years. Lateral transport, therefore, probably did not cause the large depth changes in OC fluxes between 50 m and 200 m. Figure 2.6 suggests that flagellates were relatively more abundant at station JV-7 than at the other mooring sites; thus, blooms of phytoplankton other than diatoms could explain the OC fluxes to the shallow traps in 1985 and 1986. However, another possibility for the high OC fluxes is that 'swimmers' were attracted to the 50 m sediment traps during the summers of 1985 and 1986. Blooms of pelagic polychaetes were sometimes observed during the experiment and they were occasionally caught within the grids of the sediment traps. Perhaps the high OC fluxes were in fact polychaete remains. Correlations between residuals of primary production and of sediment-trap flux have been determined and it was

found that at all stations, BSi flux residuals were not strongly correlated with the production residuals. At stations SN-9, SN-0.8 and JV-7, OC flux residuals and production residuals also were not significantly correlated but, at station JV-7, there was a positive relationship between these residuals (Figure 3.15), lending support to the possibility that the high 50 m OC fluxes of 1985 and 1986 were the result of flagellate blooms.

Aluminium fluxes

At both stations in Jervis Inlet, Al flux (Figures 3.12 and 3.13) and Al content (Figure 3.14) increased with depth. Al fluxes showed little seasonality, except that Al associated with turbulent resuspension during deepwater renewals in the fall was caught in the deeper traps (Chapter 4). 50-m Al fluxes were smallest at station JV-3, as the mooring was within a large basin and was farther from riverine sources than station JV-7 (Figures 1.1 and 1.3). Al fluxes in Jervis Inlet were a good tracer of 'additional' fluxes, which are discussed in more detail in Chapter 4.

The high Al fluxes in the fall of 1985 and recorded for station JV-3 (Figure 3.12) occurred when the traps at the mouth of Jervis Inlet were moored at station JV-11.5 (Figures 1.1 and 1.3; Table 3.1). At 50 m and 300 m, the total flux did not deviate substantially from the seasonal averages but, at 600 m, the traps at station JV-11.5 collected a large amount of Al-rich material (Figures 3.9 and 3.12). Although there was a deepwater renewal occurring at the time (Chapter 4) and similarly high fluxes might have been recorded at station JV-3, the high fluxes at 600 m at station JV-11.5 may have been caused by localised slumping or resuspension and, therefore, may not represent the fluxes that were occurring at station JV-3.

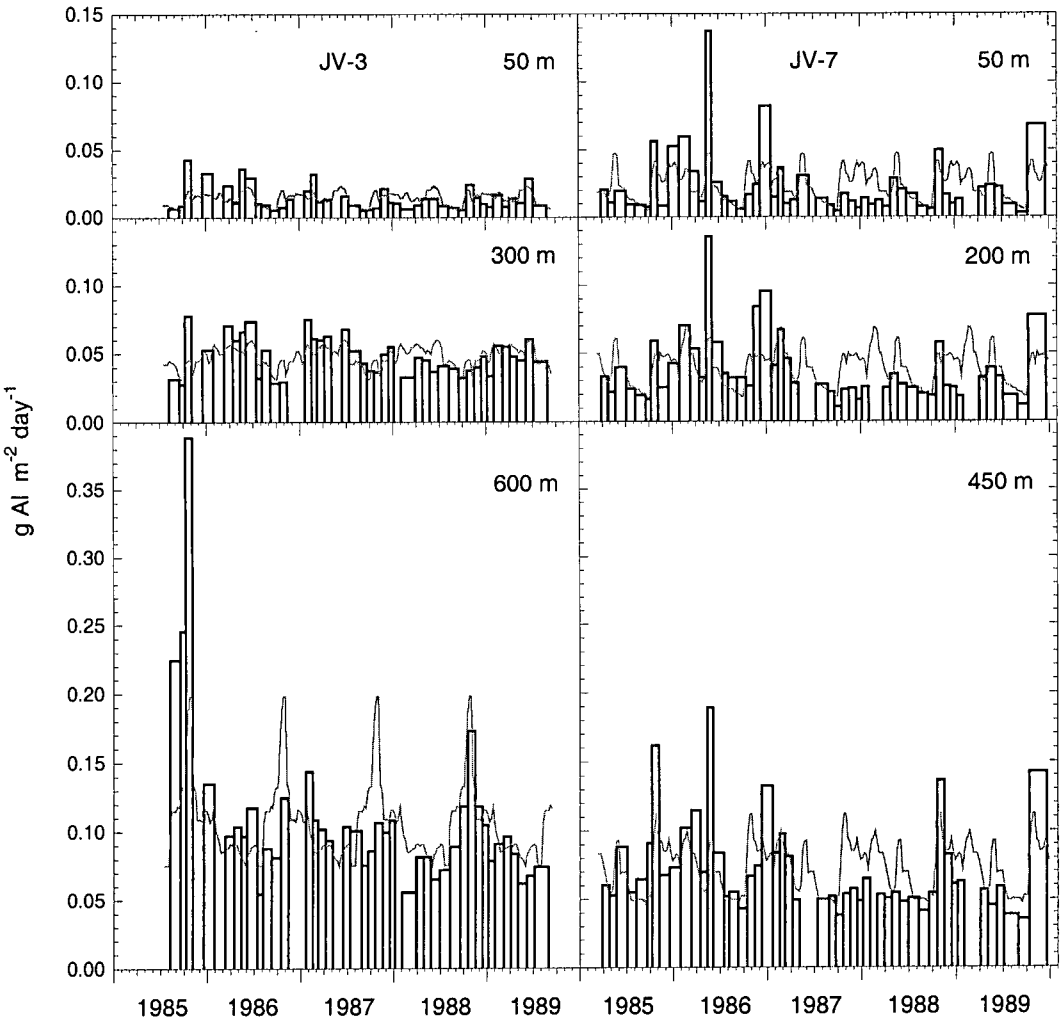

Figure 3.12: Aluminium fluxes in Jervis Inlet. The gray lines are the curves of Figure 3.13, repeated annually.

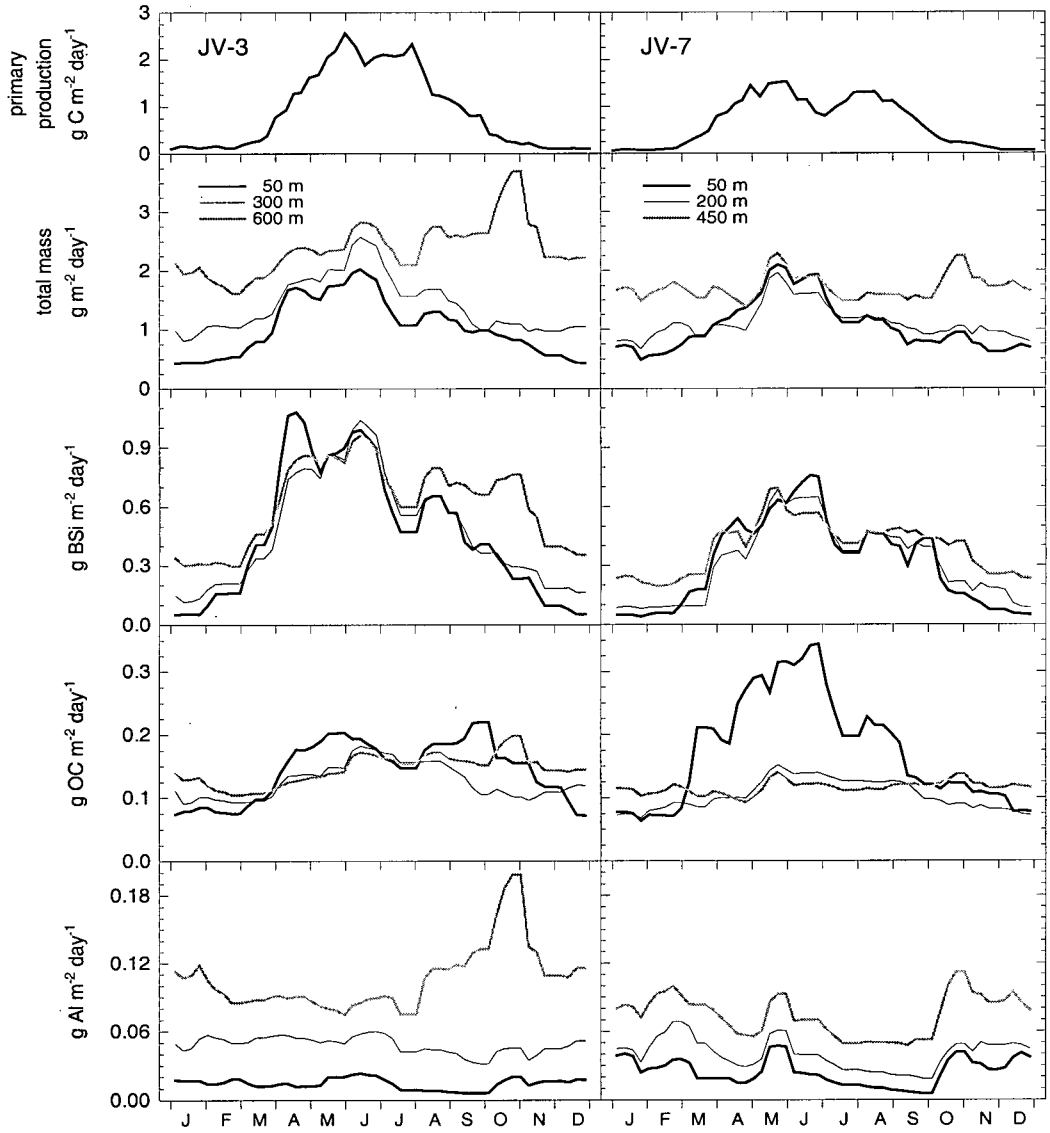

Figure 3.13: Seasonally-averaged sediment-trap fluxes (total mass, BSi, OC and Al) in Jervis Inlet. The seasonal pattern of primary production (Figure 2.8) at each station is included for comparison. The curves describing the fluxes at different depths were made by giving each day during the time series (Figures 3.9 through 3.12) the flux value measured on that day. The series was then sorted by julian day and a seven-day smoothing was applied.

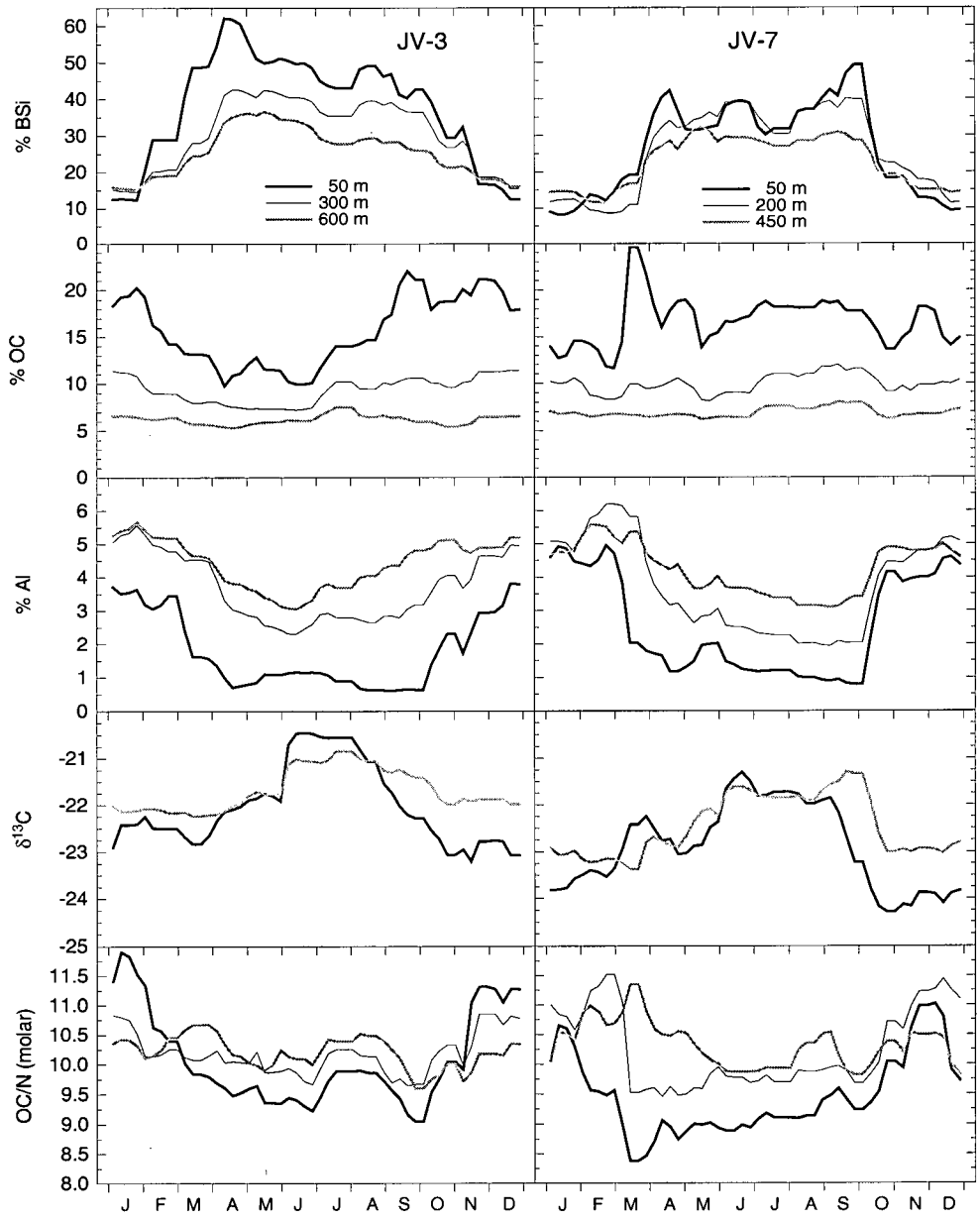

Figure 3.14: Seasonally-averaged compositional characteristics of settling fluxes in Jervis Inlet. The curves were created as described for Figure 3.13. $\delta^{13}C$ and OC/N are flux-weighted averages. Multiplication of %OC and %Al by 2.7 and 8.7, respectively, give estimates of %OM and % aluminosilicates (section 3.3.1).

	JV-3					JV-7				
	sp	su	au	wi	**annual**	sp	su	au	wi	**annual**
					mass flux ($g\ m^{-2}\ d^{-1}$)					
z_1	1.61	1.27	0.743	0.521	**1.04**	1.56	1.21	0.762	0.688	**1.05**
z_2	1.90	1.71	1.03	1.02	**1.42**	1.37	1.24	0.955	0.894	**1.11**
z_3	2.36	2.49	2.77	1.90	**2.38**	1.78	1.61	1.83	1.66	**1.72**
					BSi flux ($mg\ m^{-2}\ d^{-1}$)					
z_1	875	598	224	147	**460**	535	450	181	78.1	**311**
z_2	769	647	273	196	**471**	474	456	231	90.3	**313**
z_3	800	725	580	337	**611**	519	472	349	227	**392**
					OC flux ($mg\ m^{-2}\ d^{-1}$)					
z_1	174	173	150	80.6	**144**	268	222	110	93.3	**173**
z_2	141	157	107	99.5	**126**	120	127	87.8	80.3	**104**
z_3	136	162	161	121	**145**	113	116	122	111	**116**
					Al flux ($mg\ m^{-2}\ d^{-1}$)					
z_1	16.3	10.8	14.5	16.0	**14.4**	25.8	12.5	27.1	31.9	**24.3**
z_2	54.1	46.0	41.4	51.2	**48.2**	41.7	26.8	40.4	51.7	**40.2**
z_3	85.3	99.0	141	100	**107**	71.7	53.3	85.5	85.4	**74.0**
					$\delta^{13}C$					
z_1	-21.7	-21.0	-22.5	-22.5	**-21.8**	-22.4	-21.6	-23.7	-23.2	**-22.5**
z_2										
z_3	-21.7	-21.0	-21.8	-22.1	**-21.6**	-22.3	-21.7	-22.6	-23.1	**-22.4**
					OC/N (molar)					
z_1	9.53	9.66	10.2	11.0	**10.1**	8.83	9.19	10.1	9.52	**9.36**
z_2	10.0	10.0	10.3	10.4	**10.2**	9.63	9.82	10.5	10.9	**10.2**
z_3	10.2	10.3	9.93	10.4	**10.2**	10.3	10.1	10.2	10.6	**10.3**

Table 3.4: Fluxes in Jervis Inlet at each sediment-trap depth (z_1, z_2 and z_3; see Table 3.1 for depths of traps). Values were obtained by averaging the curves of Figure 3.7 over each seasonal period. $\delta^{13}C$ and OC/N were flux-weighted. sp = spring, su = summer, au = autumn and wi = winter.

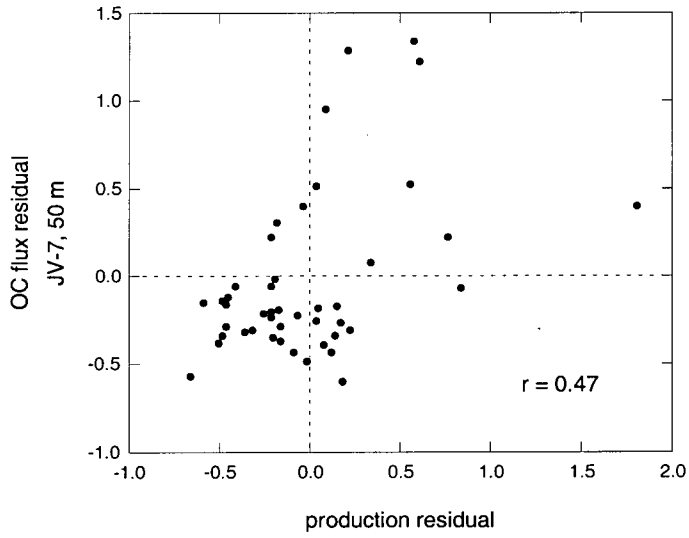

Figure 3.15: Production and 50 m OC flux residuals at station JV-7. Production residuals are the average of the production measurements at the beginning and end of each deployment minus the average for the deployment period from the curve of Figure 2.8. Flux residuals are values of Figure 3.11 minus the appropriate portion of the curve of Figure 3.13. Residuals are normalised to the mean production or OC fluxes for each deployment period.

3.4 Discussion

3.4.1 OC-BSi relationships

Figure 3.16 shows settling fluxes of organic carbon plotted against fluxes of BSi. The data are separated into 'summer' and 'winter' regimes. For the landward stations (SN-0.8 and JV-7) in 1986, Sancetta (1989b) found that fecal pellets in the traps deployed between April and September were pale green, while the pellets trapped between October and March were brown. She suggested the reason was not only changes in the zooplankton community, but also a shift from organic-rich to detrital sources of energy for the grazers. These time intervals (April-September, October-March) were used for the seasonal separation of the data in Figure 3.16.

The slopes of Figure 3.16 are interpreted as average ratios of the diatomaceous OC and

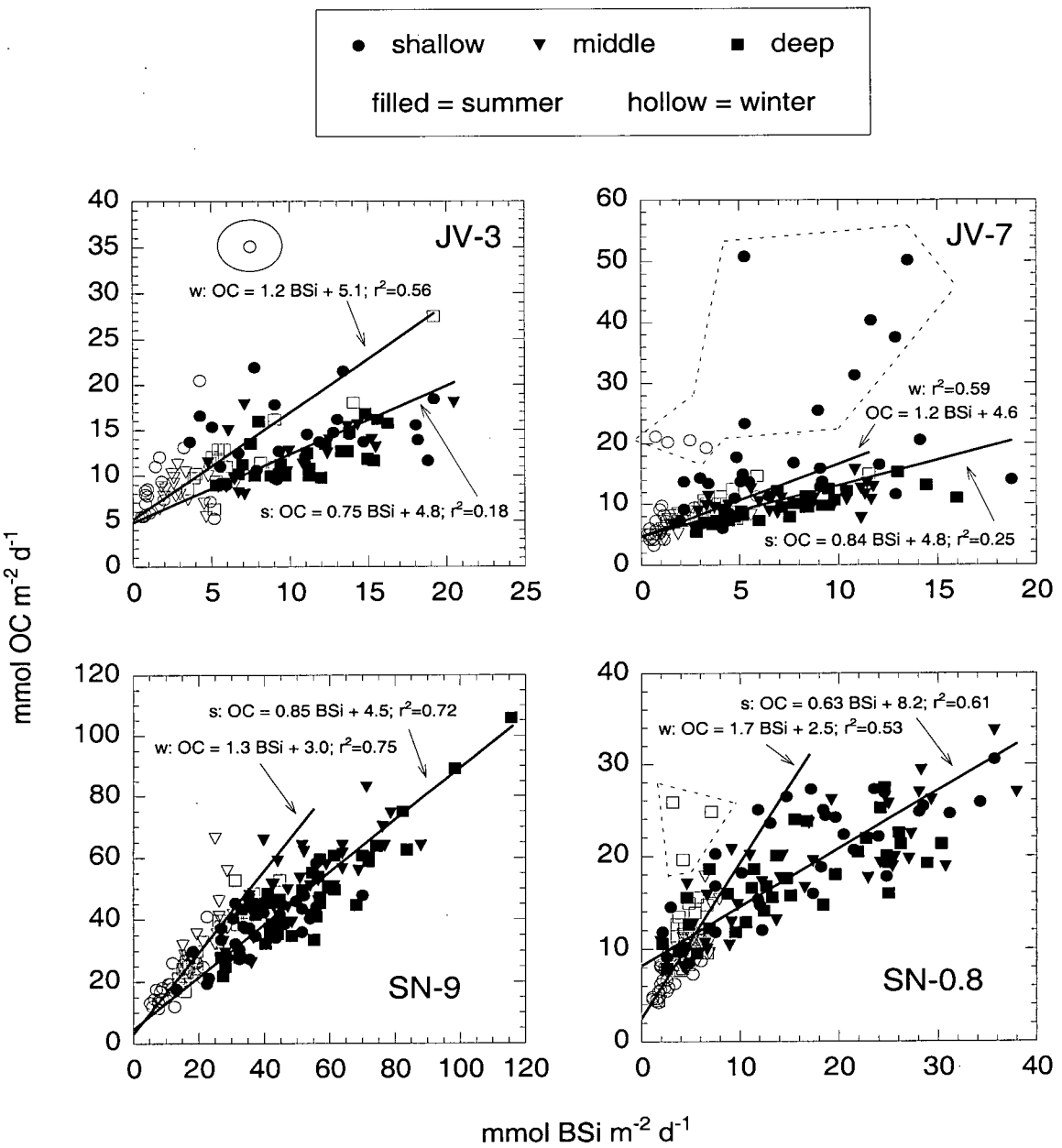

Figure 3.16: OC fluxes versus BSi fluxes. Data from summer (s) and winter (w) were separated. Points within dotted regions were not included in regressions.

BSi (OC_d:BSi ratios) for the material reaching the sediment traps. These molar ratios (approximately 1) are much lower than the OC_d:BSi ratio of about 7.7 for living diatoms (Brzezinski, 1985) and are indicative of intensive recycling of diatomaceous carbon relative to BSi. Glycine and serine are concentrated in the cell walls of diatoms (Hecky et al., 1973), and studies (Burdige and Martens, 1988; Cowie and Hedges, 1992) have shown these amino acids to have a longer residence time in the marine environment than intracellular amino acids, suggesting preferential preservation of the cell wall proteins. Not only will zooplankton grazing and cell lysis cause preferential loss of OC relative to BSi, dinoflagellates that phagocytise (Buck and Newton, 1995; Tiselius and Kuylenstierna, 1996) or extracellularly digest (Jacobson and Anderson, 1986) diatom chains while leaving the frustules intact also provide an efficient means to produce low OC_d:BSi ratios in sinking material. The intercepts of Figure 3.16 indicate that a significant portion of the settling organic material in Saanich and Jervis Inlets was non-diatomaceous. The non-diatomaceous OC would have been composed of both terrestrial OC and marine OC from sources such as nanoflagellates, dinoflagellates, heterotrophic plankton including bacteria, and transparent exopolymer particles (TEP; Alldredge et al., 1993).

3.4.2 Marine and terrigenous OC fluxes

Figures 3.17 and 3.18 show the time series of $\delta^{13}C$ at each station during the study (only at SN-0.8 were the mid-depth samples analysed for $^{13}C/^{12}C$). The isotopic signatures, summarised in Figures 3.8 and 3.14, and in Tables 3.3 and 3.4, were heavy in spring and summer and light in autumn and winter. In their seminal work, Sackett and Thompson (1963) noted that terrestrial plants are enriched in ^{12}C (isotopically light or $\delta^{13}C$ values that are more negative) when compared to marine plants, and suggested that the progressively heavier isotopic composition of sediments away from the mouth of the Mississippi River is the result of a decreasing presence of terrigenous OM. Although these data have

since been reinterpreted based on contributions to marine sediments by degraded, isotopically heavy, terrestrial C_4 grasses (Goñi et al., 1997; Goñi et al., 1998), in the Pacific Northwest, C_4 plants are rare (Teeri and Stowe, 1976). Indeed, changes in particulate $\delta^{13}C$ due to variable proportions of marine and terrestrial organics are consistent with the trends of marine and terrestrial biomarkers in Saanich Inlet (Cowie et al., 1992) and the Washington margin (Prahl et al., 1994). However, marine and terrestrial organic $\delta^{13}C$ endmembers vary regionally (Prahl et al., 1994), so that $\delta^{13}C$ endmembers appropriate for Saanich and Jervis Inlets should be determined if the $\delta^{13}C$ data are to be used to separate terrestrial from marine organics.

Cowie (unpublished) has measured $\delta^{13}C$ on soils collected from the banks of Saanich Inlet and Jervis Inlet. From his data, a best estimate for the organic matter of soils is -25.1$^0/_{00}$ in Saanich Inlet and -26.5$^0/_{00}$ in Jervis Inlet. These values are within the general range expected for terrestrial C_3 plants (Deines, 1980) and are saddled by the terrestrial $\delta^{13}C$ endmember (-25.7$^0/_{00}$) used by Prahl et al. (1994) to describe Columbia River basin sediments. The different endmembers observed for the fjords might be explained by the biogeoclimatic zones they occupy. Jervis Inlet is located in the coastal western hemlock (CWH) zone which covers most of the coast of British Columbia, penetrating into Alaska to the north and along the coasts of Washington and Oregon to the south (Pojar et al., 1991). The CWH zone is the rainiest biogeoclimatic zone of British Columbia with a cool, mesothermal climate where nutrient leaching from the mineral soils is rapid (Pojar et al., 1991). Saanich Inlet and portions of the Cowichan River watershed are located in the coastal Douglas-fir (CDF) zone, a stretch of low-elevation terrain covering the southeastern coast of Vancouver Island and many islands of the southern Strait of Georgia (Nuszdorfer et al., 1991). The CDF zone is in the rainshadow of Vancouver Island and the Olympic mountains, and is warmer and drier than the CWH zone (Nuszdorfer et al., 1991). Given the differences in the biogeoclimatic zones of these fjords, it is reasonable

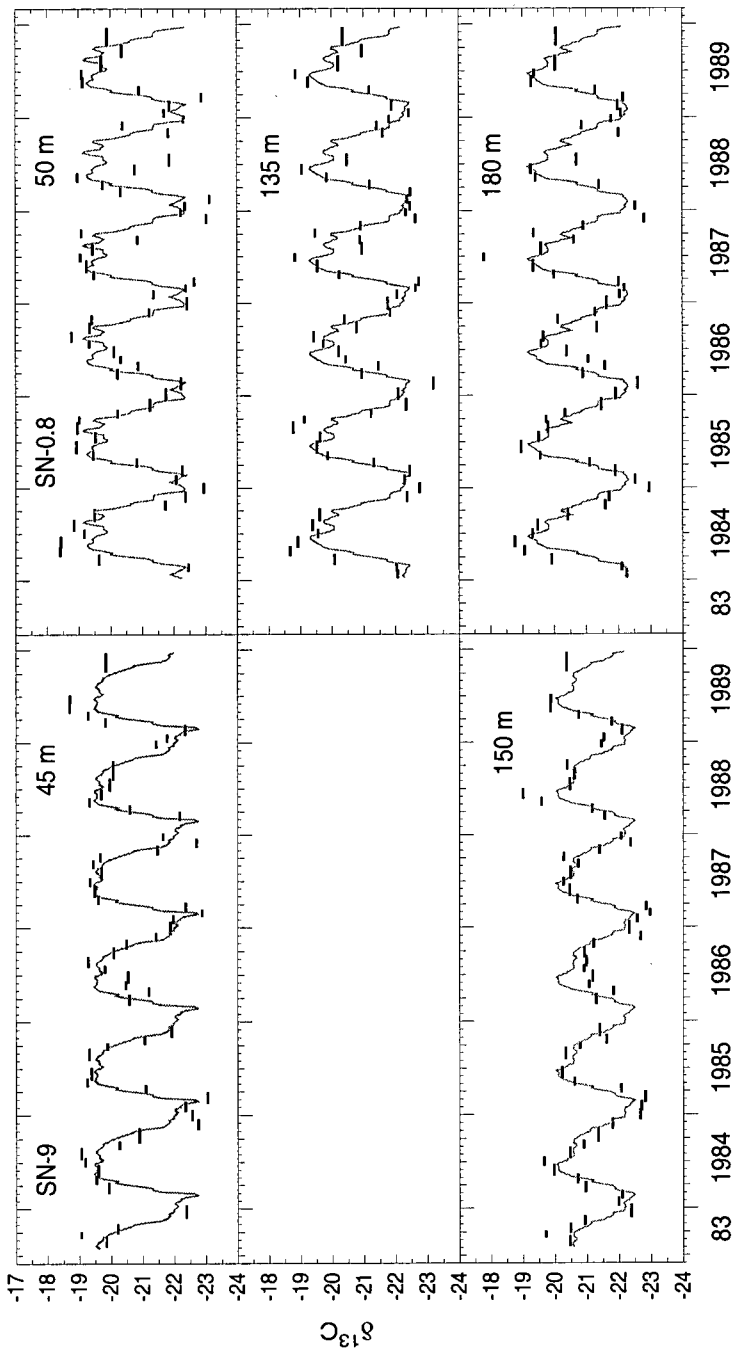

Figure 3.17: $\delta^{13}C$ of the trapped organic matter of Saanich Inlet. Carbon isotopes were not measured on sediments trapped at mid-depth at station SN-9. The gray lines are the curves of Figure 3.8, repeated annually.

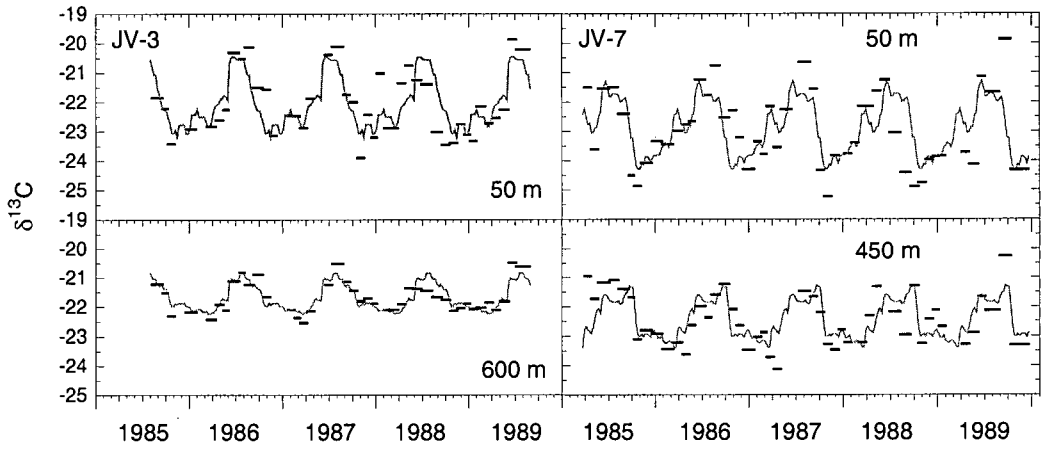

Figure 3.18: δ^{13}C of the trapped organic matter of Jervis Inlet. Carbon isotopes were not measured on samples collected at the mid-depth traps. The gray lines are the curves of Figure 3.14, repeated annually.

to expect that the residence time of the OM in the soils surrounding Saanich Inlet is longer than that for the OM of Jervis Inlet soils. The potential of a longer soil residence time and the warmer temperatures of the CDF zone may promote a greater degree of OM recycling within the Saanich Inlet/Cowichan Valley watershed, resulting in heavier terrestrial δ^{13}C as ^{12}C is preferentially respired.

δ^{13}C of marine OC varies significantly, but a median value at temperate latitudes is about -20$^0/_{00}$ (Deines, 1980). During photoautotrophic carbon fixation, the resulting isotopic composition of the phytoplankton is affected by δ^{13}C of the dissolved inorganic carbon pool and a number of physiological and environmental factors that affect biological fractionation (for a summary, see Kukert and Riebesell, 1998). Indeed, Hedges et al. (1988a) measured δ^{13}C on plankton tows from Dabob Bay and found values ranging between -26.0$^0/_{00}$ and -19.5$^0/_{00}$, Kukert and Riebesell (1998) found that δ^{13}C of suspended POC increased from -25$^0/_{00}$ to -20$^0/_{00}$ throughout the spring bloom of predominantly *Skeletonema costatum* in the Norwegian fjord Lindåspollene, and Rau et al. (2001)

attributed fluctuations in $\delta^{13}C$ of particulate OC between about -28$^0/_{00}$ and -16$^0/_{00}$ in Monterey Bay, California to variable photosynthetic ^{13}C fractionation. For the sediment-trap samples from Saanich and Jervis Inlets, the correlations between $\delta^{13}C$ and BSi content (Figure 3.19) were used to estimate the marine $\delta^{13}C$ endmembers of -17.3$^0/_{00}$ for Saanich Inlet, and -19.6$^0/_{00}$ in Jervis Inlet (Appendix A). During carbon assimilation, phytoplankton fractionate ^{12}C from ^{13}C less effectively (becoming isotopically heavier) as growth rate increases and $[CO_2]_{aq}$ decreases (Laws et al., 1995; Bidigare et al., 1997; Burkhardt et al., 1999; Tortell et al., 2000). Furthermore, diatoms are isotopically heavier than other phytoplankton (Fry and Wainright, 1991; Pancost et al., 1997; Kukert and Riebesell, 1998; Reinfelder et al., 2000), as are large cells when compared to small cells (Pancost et al., 1997; Popp et al., 1998). Thus, when the phytoplankton of Saanich Inlet are compared to those of Jervis Inlet, higher growth rates (as inferred from higher nutrient supply and primary production {Chapter 2; Timothy and Soon, 2001}), a greater predominance of diatoms (Sancetta, 1989a; 1989b; Chapter 2; Timothy and Soon, 2001) and larger diatoms (Sancetta, 1989a) could explain the heavier marine $\delta^{13}C$ endmember in Saanich Inlet.

The large difference between these marine $\delta^{13}C$ endmembers for Saanich and Jervis Inlets (-19.6$^0/_{00}$ to -17.3$^0/_{00}$) and $\delta^{13}C$ of the net tow samples from Dabob Bay (-26.0$^0/_{00}$ to -19.5$^0/_{00}$; Hedges et al., 1988a) and of filtered POC of Lindåspollene (-25$^0/_{00}$ to -20$^0/_{00}$; Kukert and Riebesell, 1998) must be addressed, as it is difficult to invoke large regional differences in plankton $\delta^{13}C$ for these similar environments. The size-fractionated samples of Hedges et al. (> 64 μm) and Kukert and Riebesell (< 20 μm and > 20 μm) represent suspended material, while this study sampled the sinking material. Kukert and Riebesell (1998) found the > 20 μm size fraction (predominately diatoms) to be several per mil heavier than the < 20 μm size fraction (mostly flagellates) and, furthermore, they found heaviest values when particulate OC concentrations (i.e.; *Skeletonema* biomass)

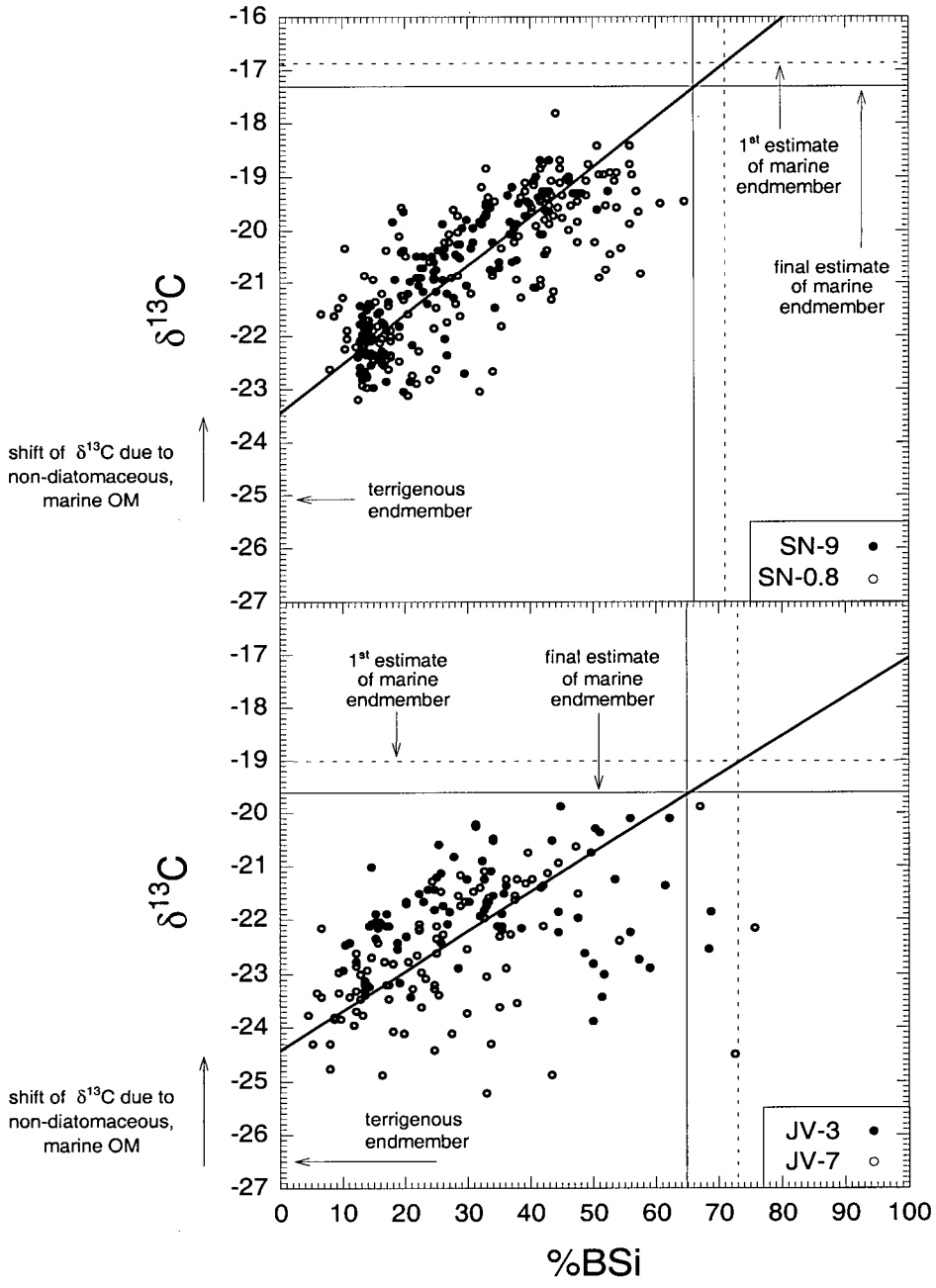

Figure 3.19: $\delta^{13}C$ versus %BSi in Saanich and Jervis Inlets. With estimates of the terrigenous $\delta^{13}C$ endmembers, these correlations are used to find the marine $\delta^{13}C$ endmember in each fjord. The equations of the regressions and the way they are used in this exercise is explained in Appendix A.

	terrigenous OC % of total OC at shallow trap				
	sp	su	au	wi	**annual**
SN-9	32	30	43	61	**37**
SN-0.8	29	28	42	59	**35**
JV-3	31	20	43	43	**32**
JV-7	40	29	59	53	**41**

Table 3.5: Terrigenous OC in Saanich and Jervis Inlet. These estimates were made using $\delta^{13}C$ of Tables 3.3 and 3.4, and the marine and terrigenous $\delta^{13}C$ endmembers of -17.3$^0/_{00}$ and -25.1$^0/_{00}$ in Saanich Inlet, and -19.6$^0/_{00}$ and -26.5$^0/_{00}$ in Jervis Inlet.

were highest. The isotopically heavy values associated with the large size fraction at the peak and end of the bloom (-21$^0/_{00}$ to -20$^0/_{00}$; Kukert and Riebesell, 1998) are the most likely signals to be transmitted to the settling flux, significantly decreasing the apparent discrepancy between the marine $\delta^{13}C$ endmembers identified here (Table A.1) and the time-course of particulate OC $\delta^{13}C$ in Lindåspollene. The sediment-trap samples also represent material that was likely recycled to some degree, and therefore potentially fractionated towards heavier values, as ^{13}C accumulates in higher trophic levels (DeNiro and Epstein, 1978; Wada et al., 1987). Finally, just as terrigenous organic debris contributes to the settling fluxes in coastal environments, it is likely to be suspended throughout the water column so that the records of Kukert and Riebesell (1998) and Hedges et al. (1988a) may be somewhat lighter than if only marine OM had been sampled. The net tow samples from Dabob Bay did not contain microscopically visible vascular plant debris (Hedges et al., 1988a), but flocculated terrestrial humic substances (Sholkovitz, 1976) are likely present in all these fjords.

	total primary production (diatom production) mg C m^{-2} d^{-1}				
	sp	su	au	wi	**annual**
SN-9	2740 (2160)	2880 (2280)	609 (481)	119 (94)	**1580 (1250)**
SN-0.8	1390 (1100)	2160 (1710)	621 (491)	207 (164)	**1090 (861)**
JV-3	1600 (1120)	1650 (1160)	280 (196)	157 (110)	**921 (645)**
JV-7	1150 (805)	1060 (742)	233 (163)	128 (90)	**641 (449)**

Table 3.6: Total and diatom production at each station. Total production is from averaging Table 2.1 over each season. Diatom production is estimated as 79% and 70% of the total production in Saanich and Jervis Inlets, respectively (Table A.1).

The marine and terrestrial $\delta^{13}C$ endmembers have been used to estimate the terrigenous contributions to the settling OC in the shallow sediment traps (Table 3.5). Considering the various errors of the estimates, the annually-averaged terrigenous contributions were similar at each station (30-40%). In spring and summer, terrestrial OM comprised 20-40% of total OM, while in the fall and winter it was 40-60% of the total. Ancillary information from the exercise in Appendix A is the composition of the 'typical' marine sample from each fjord (Table A.1). In Saanich Inlet, this marine sample was 66% BSi, 27% diatomaceous OM and 7% non-diatomaceous OM. In Jervis Inlet, it was 65% BSi, 24% diatomaceous OM and 11% non-diatomaceous OM. Comparing the proportions of diatomaceous and non-diatomaceous OM, 79% of the marine organic matter was diatomaceous in Saanich Inlet and 70% in Jervis Inlet. These estimates are not significantly different (Table A.1), although they are consistent with the supposition that

diatoms were more prevalent in Saanich Inlet. This result supports the generality made by Nelson et al. (1995) that 75% of primary production in nutrient-replete waters is by diatoms, and allows estimates of diatomaceous carbon assimilation in Saanich and Jervis Inlets (Table 3.6). However, because translation from the settling flux of diatomaceous carbon to diatom primary production assumes similarity in the recycling of diatomaceous and non-diatomaceous marine organic matter, the estimates of diatom production of Table 3.6 should be viewed as rough approximations.

The exercise in Appendix A has been carried out for various sub-sets of the time series. When the entire data set (all four stations) or some portion of it (one or two stations) was separated by season ('winter' and 'summer' as defined section 3.4.1), $\delta^{13}C$ of the marine endmember was not different for the two periods because the correlation between $\delta^{13}C$ and BSi content was low. Different marine $\delta^{13}C$ endmembers at any two stations (e.g.; SN-9 and SN-0.8) were not observed for the same reason.

The OC:N ratio of marine phytoplankton of 6.6 (Fleming, 1940; Redfield et al., 1963) is a broad average that can be used over large spatial scales, but locally varies because of factors including species composition and nutrient availability (Parsons, 1961; Redfield et al., 1963; Sakshaug, 1977; Sakshaug et al., 1983; Sakshaug and Olsen, 1986; Sakshaug et al., 1989; Wong et al., 1999). Nevertheless, the OC:N ratio of marine OM tends to be lower than the OC:N ratio of terrestrial OM (e.g.; Hedges et al., 1986), and can sometimes be used as an indicator of marine and terrigenous OM fractions (e.g.; Hedges et al.,1988b; Prahl et al., 1994; Ruttenberg and Goñi, 1997). Indeed, the OC:N ratio of the settling material in Saanich and Jervis Inlets was high in the fall and winter and lower in the spring and summer (Figures 3.8 and 3.14), correlating with the relative abundance of marine and terrigenous OM based on $\delta^{13}C$ endmembers (Table 3.5). However, the poor correlation between $\delta^{13}C$ and OC/N (Figure 3.20), especially for Jervis Inlet, indicates that one or both of these compositional traits was affected by factors other than the

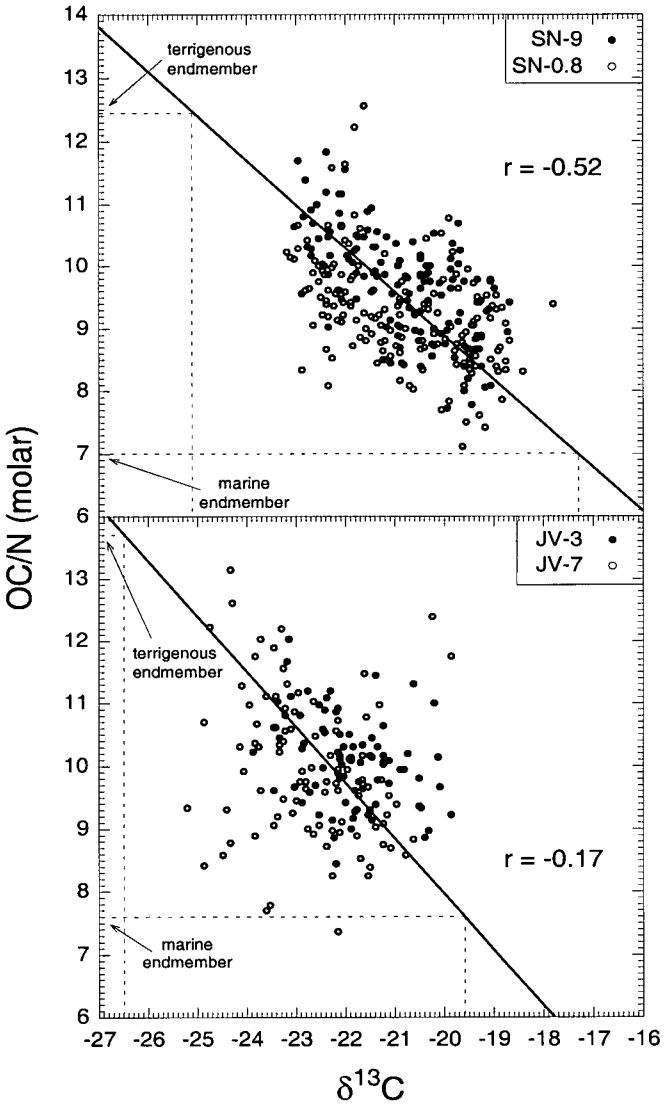

Figure 3.20: δ^{13}C versus OC/N in Saanich and Jervis Inlets. A point (OC/N = 14.7, δ^{13}C = -21.0) from Jervis Inlet is out of range and not included in the regression. The choice of Model I regression or Model II regression (used here) is crucial for descriptions of data with low r values. The common Model I regression ($|r|^{-1}$ less steep than these Model II regressions; section 3.2.4) would result in marine and terrigenous OC/N endmembers with little physical meaning and, statistically speaking, is interpreted as a lack of confidence in predicting OC/N endmembers from δ^{13}C endmembers.

marine:terrigenous OM ratio. Although the low correlation between $\delta^{13}C$ and %BSi in Jervis Inlet (Figure 3.19 and Appendix A) may have been caused by larger variability in the relative contributions of flagellates and other non-diatomaceous marine plankton to the settling flux than occurred in Saanich Inlet, it is also likely that the terrigenous and marine OC/N and $\delta^{13}C$ endmembers were not temporally constant.

The exercise to estimate $\delta^{13}C$ of the marine OM endmember (Figure 3.19 and Appendix A) could not be performed using a correlation between OC/N and %BSi because the OC:N ratio of terrigenous OM is not known. (In the exercise of Appendix A, a measure of $\delta^{13}C$ in the terrigenous OM fraction was required to estimate the marine $\delta^{13}C$ endmember.) However, using the $\delta^{13}C$ endmembers that have been described for each fjord (Figure 3.19), endmember values for the OC:N ratio of marine and terrigenous OM can be estimated (Figure 3.20). The overall agreement in the OC/N endmembers of Figure 3.20 with expected values (e.g.; Prahl et al., 1994) suggests that $\delta^{13}C$ and OC/N can be used as rough guides of marine and terrigenous OM in the sedimentary record of these fjords (e.g.; Tunnicliffe, 2000), while they should be used cautiously for sampling that represents short time periods. Figure 3.20 also demonstrates that these proxies of marine and terrigenous contributions are better suited for some environments (e.g.; Saanich Inlet) than others (e.g.; Jervis Inlet). Indeed, off the west coast of Vancouver Island, settling fluxes followed primary production and were highest in the spring and summer, but OC:N ratios of the sinking material were lowest in the winter (Peña et al., 1999). Peña et al. (1999) attributed this signal to inorganic nitrogen adsorbed onto clays, and to the possibility of reduced organic degradation caused by ballast-mediated, rapid sinking (e.g.; Ittekkot, 1993).

3.4.3 Export ratios of OC and BSi

The e-ratio (the ratio of the settling flux of an element to the photoautotrophic assimilation of that element; defined for organic carbon by Downs, 1989) is a measure of the degree of recycling and remineralisation that has occurred since the element was assimilated. In sections 3.3.2 through 3.3.4, OC and BSi fluxes are presented and, in section 3.4.2, terrigenous and marine OC are separated and estimates of the diatomaceous contribution to total primary production are made. From these data, Table 3.7 gives e-ratios for both total and marine OC. OC_{tot} e-ratios have less oceanographic significance than marine OC e-ratios, but they can be compared to other data sets where terrigenous OC has not been subtracted. The BSi e-ratios of Table 3.7 are relative to both total and diatom production. While (BSi flux/total production) has ecological and biogeochemical significance, (BSi flux/diatom production) is a better measure of the degree of recycling and dissolution of reactive silicon. Because the OC e-ratio is a C:C ratio, its hypothetical maximum is one. E-ratios for biogenic silica are Si:C molar ratios and the maximum is set by the assimilation of these elements by phytoplankton. Brzezinski (1985) found Si:C ratios of various species of laboratory diatoms ranging between 0.04 and 0.42. BSi:POC molar ratios as high as 1.75 in Antarctic surface waters were due to the presence of heavily silicified diatoms, and possibly to more rapid recycling of POC (Quéguiner et al., 1997).

For both OC and BSi, the annual e-ratios of Table 3.7 are flux weighted, so they most closely reflect the ratios of the spring and summer when fluxes were highest. The spring and summer OC_{mar} e-ratios of about 0.1 appear low when compared to the f-ratios that might be expected in these highly productive waters with large nutrient supply (Eppley and Peterson, 1979; Platt and Harrison, 1985; Harrison et al., 1987; Wassmann, 1991). The f-ratio is the ratio of new nutrient assimilation to total nutrient assimilation (*sensu*

	$\mathbf{OC_{tot}\ e\text{-}ratio} = \frac{OC_{tot}\ 50\ m\ flux}{tot\ prod}$ $(\mathbf{OC_{mar}\ e\text{-}ratio} = \frac{OC_{mar}\ 50\ m\ flux}{tot\ prod})$					$\mathbf{BSi\ e\text{-}ratio} = \frac{BSi\ 50\ m\ flux}{tot\ prod}$ $(\mathbf{BSi\ e\text{-}ratio} = \frac{BSi\ 50\ m\ flux}{diatom\ prod})$				
	C:C ratio					BSi:C molar ratio				
	sp	su	au	wi	**annual**	sp	su	au	wi	**annual**
SN-9	0.14	0.18	0.51	1.6	**0.22**	0.16	0.18	0.42	0.91	**0.21**
	(0.096)	(0.13)	(0.29)	(0.62)	**(0.14)**	(0.20)	(0.23)	(0.53)	(1.1)	**(0.26)**
SN-0.8	0.18	0.11	0.17	0.43	**0.15**	0.18	0.062	0.081	0.18	**0.11**
	(0.13)	(0.076)	(0.098)	(0.18)	**(0.10)**	(0.23)	(0.079)	(0.10)	(0.23)	**(0.14)**
JV-3	0.11	0.10	0.53	0.51	**0.16**	0.097	0.065	0.14	0.17	**0.089**
	(0.075)	(0.084)	(0.31)	(0.29)	**(0.11)**	(0.14)	(0.092)	(0.20)	(0.24)	**(0.13)**
JV-7	0.23	0.21	0.47	0.73	**0.27**	0.083	0.076	0.14	0.11	**0.086**
	(0.14)	(0.15)	(0.19)	(0.34)	**(0.16)**	(0.12)	(0.11)	(0.20)	(0.16)	**(0.12)**

Table 3.7: Export ratios of OC and BSi at 50 m at each station. 50 m fluxes are from Tables 3.3 and 3.4. Total and diatom production are from Table 3.6. While OC_{tot} e-ratios consider the total OC flux, OC_{mar} e-ratios subtract terrigenous OC contributions (Table 3.5). While the first values may be compared to other studies, values in parentheses are ecologically more meaningful.

Dugdale and Goering, 1967; Eppley and Peterson, 1979), and in steady state conditions is a predictor for the export of that nutrient in organic (dissolved and particulate) form. Therefore, for steady state and assuming lateral transport does not export significant amounts of organic material, f-ratios should be greater than e-ratios by the amount of dissolved and suspended matter that is exported, and by the amount of remineralisation occurring between the base of the euphotic zone and the depth of the sediment traps.

A number of factors can affect the amount of organic matter caught by sediment traps. DOC held interstitially within sinking particles can be a significant fraction of the total OC flux (Noji et al., 1999) and was not quantified in this experiment, and swimmers can unpredictably affect measured fluxes of organic matter (Lee et al., 1988; Karl and

Knauer, 1989; Michaels et al., 1990). Based on considerations of fluid flow (Hargrave and Burns, 1979; Lau, 1979; Gardner, 1980b; Butman et al., 1986; Hawley, 1988), variable trapping efficiency has been documented in controlled experiments (Hargrave and Burns, 1979; Gardner, 1980b; Gardner, 1985; Butman, 1986; Gardner and Zhang, 1997) and in the field (Gardner, 1980a; Blomqvist and Køfoed, 1981; Baker et al., 1988; Laws et al, 1989; Buesseler, 1991; Honjo et al., 1992; Gust et al., 1992; Gust et al., 1994; Nodder and Alexander, 1999; Buesseler et al., 2000; Yu et al., 2001). Although over-collection has been observed (e.g.; Buesseler et al., 1994), low trapping efficiency is more commonly observed. Poor trapping efficiency is especially common in surface waters, partly because the sinking debris is unconsolidated. As particulates sink, they are biologically and physically repackaged with the result that sinking rates tend to increase with depth. Syvitski et al. (1985) found that sinking rates increase with depth, and several authors have suggested trapping efficiency improves in deep waters at least partly because of the increased fall velocities and greater consolidation of the settling debris (Smetacek et al., 1978; Timothy and Pond, 1997; Yu et al., 2001).

Some of the explanations for the lack of a difference in measured fluxes of organic matter by the sediment traps with and without sodium azide as a preservative (section 3.2.3) involve the loss of labile organic matter between the time of interception and measurement in the laboratory. Iseki et al. (1980) described a sediment-trap experiment in Patricia Bay of Saanich Inlet. The absolute OC fluxes they reported for traps moored at 50 m (2 to 3 times lower than the fluxes collected at a similar season and depth and given in Table 3.3 for stations SN-0.8 and SN-9) are not comparable to the fluxes of this study because their experiment occurred in a relatively isolated portion of Saanich Inlet. However, Iseki et al. (1980) determined rate constants of decay for the OC collected at 50 m to be between 0.014 and 0.029 day^{-1}. They also derived an equation to correct for *in situ* loss knowing the rate constant of decay and the length of a deployment. Using their

rate constants for 50 m (0.014 0.029 day^{-1}) and their equation 6, measured OC fluxes should be multiplied by a factor of 1.2 to 1.5 to obtain the true flux caught by sediment traps moored for 30 days. Others have also shown organic matter to leach into the surrounding sediment-trap solution (Knauer et al., 1984; Karl et al., 1988) and Knauer et al. (1990) found that more than half of the organic nitrogen contained within sediment traps was dissolved. Furthermore, Kumar et al. (1996) found that as much as 70% of organic matter was rapidly lost during even short sediment trap deployments. Thus, the apparently low e-ratios for organic carbon (Table 3.7) are likely caused by the presence of interstitial DOM, low trapping efficiency and organic leaching after interception. Of these possibilities, trapping efficiency may not have been a serious problem, as it appears the majority of sinking diatom frustules was trapped (discussed below). To correct for possible OC leaching, multiplication of the spring and summer carbon fluxes by a factor of two to four (Knauer et al., 1990; Kumar et al., 1996) would make the OC e-ratios of Table 3.7 closer to the expected values for these highly productive fjords.

In light of these complications, it is difficult to interpret the higher e-ratios in the fall and winter for both marine and total OC (Table 3.7). They may reflect less OM recycling and remineralisation or better trapping efficiency due to a shift from unconsolidated diatom aggregates to a greater proportion of fecal pellets (Sancetta, 1989a, 1989b, 1989c). Lithogenic ballast in the fall and winter (Ittekkot, 1993) might facilitate decreased water-column remineralisation and increased trapping efficiency, although the flux of aluminosilicates was not notably seasonal, except at station SN-0.8 (Figures 3.6, 3.7, 3.12 and 3.13). Organic matter in fecal pellets might also be less likely leached while in the sediment traps or during rinsing and centrifugation after retrieval. It is also possible that a large proportion of resuspended OC reached the shallow traps during the fall and winter. The range of OC_{tot} e-ratios (0.24 to 0.55) presented by Wassmann (1990) for coastal waters of the north Atlantic including many fjords and bays is

generally higher than the spring and summer values from Saanich and Jervis Inlets, but similar to, or lower than, the autumn and winter values (Table 3.7).

The Si:C ratio (molar) for a suite of laboratory diatoms ranged between 0.04 and 0.42, with a mean of 0.13 $\pm$0.04 (Brzezinski, 1985). If this ratio is applicable to the diatoms of Saanich and Jervis Inlets, it appears that most of the silicon assimilated by diatoms was eventually trapped at 50 m, as the BSi e-ratios with respect to diatom production are very close to Brzezinski's average (Table 3.7). It should be noted, however, that Kumar et al. (1996) found 25% of biogenic silica was lost from sediment traps and Scharek et al. (1999) estimated 10-60% of captured biogenic silica dissolved in sediment traps. Thus, unlike the case for organic carbon, the BSi e-ratios appear high, but could be the result of the combined effects of minimal BSi recycling, heavily silicified diatoms (Si:C ratio $>$ 0.13) and the presence of a BSi-rich, resuspended fluxes reaching the shallow traps. This latter possibility seems especially likely in the fall and winter throughout the study area (except in the fall at station SN-0.8; Table 3.7) and year-round at station SN-9. The water-column fluxes at the mouth of Saanich Inlet were much higher than elsewhere (section 3.3.3) and were likely caused by sediment transport from the broad sill at the entrance to Saanich Inlet.

3.4.4 The riverine source of particulates to Saanich Inlet

One of the most interesting and certainly the most unexpected feature of this time series is the aluminium record from station SN-0.8 (Figure 3.6). Unlike at the other stations (SN-9, JV-3 and JV-7) where Al fluxes were largely affected by the physical processes leading to turbulent resuspension, at station SN-0.8 fluxes of Al appear to have been determined by the environmental factors that delivered Al to surface waters. Al fluxes peaked in the late fall and winter when local rainfall (Figure 1.11) and flow of the Cowichan and Goldstream Rivers (Figure 1.13) were highest; local runoff in the vicinity of station

SN-0.8 and/or the sediment load of the Cowichan River could have delivered the Al to the head of Saanich Inlet. The correlation (r = 0.72) between Cowichan River flow and 50 m Al flux at station SN-0.8 is better than the correlation (r = 0.49) between precipitation at Victoria Airport and the Al flux, but these correlations may be caused by coincidence of the seasonal cycle in each time series. Comparison of the residuals of each time series (Figure 3.21), however, suggests that the Cowichan River had a greater influence on the flux of aluminosilicates at the head of Saanich Inlet than did local runoff. Because daily riverflow is available, it was also possible to test whether a time lag occurred between Cowichan River flow and Al flux at the head of Saanich Inlet. As the residuals of Cowichan River flow were allowed to precede the flux residuals, the correlation did not improve, but it did remain constant for 4-6 days and decreased as the separation lengthened. Noting that the 30 day flux and riverflow averages (see caption to Figure 3.21) are not well suited to explore time-lags less than about one averaging period, or a month, one interpretation of these results is that sediments reach the head of Saanich Inlet within a week of discharge from the Cowichan River.

Aluminium appears to have been delivered from the surface at station SN-0.8 and the seasonal pattern of flux was nearly identical at each depth (Figures 3.6 and 3.7). However, Al fluxes increased by a factor of $\sim$2 between 50 m and 135 m and were similar at 135 m and 180 m (Table 3.3). The increase in flux with depth between 50 m and 135 m was probably not caused by turbulent resuspension, as no high-energy events (e.g., similar to the Al fluxes associated with deepwater renewals) were recorded. For a shorter time series from Sechelt Inlet, fluxes similarly increased with depth most dramatically from shallow to mid-depth traps, increasing less towards the bottom. Timothy (1994) and Timothy and Pond (1997) concluded that, although resuspension events were probably recorded, particle focusing in the U-shaped fjord (e.g., Wassmann, 1984) and increases in trapping efficiency with depth were largely responsible for observed changes in flux

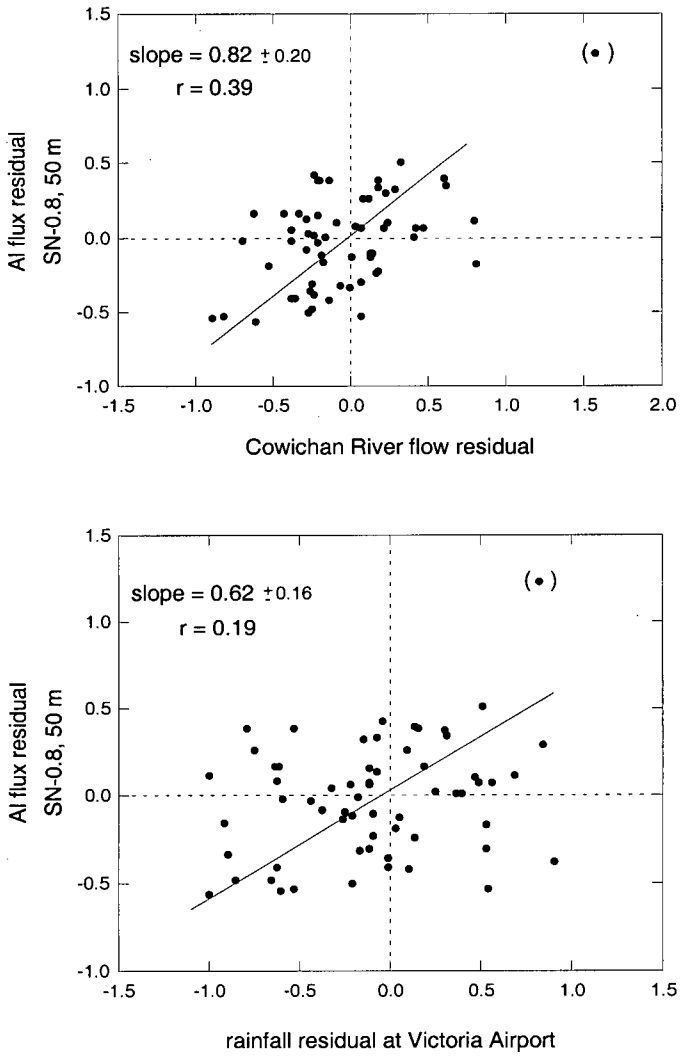

Figure 3.21: Residuals of 50 m Al flux from station SN-0.8 plotted against residuals of Cowichan River flow and residuals of rainfall at the Victoria Airport. Daily riverflow and rainfall data were used to create average values for time periods corresponding to the sediment trap deployment periods. Points in parentheses were not included in regressions.

with depth. At station SN-0.8, the channel width (Figure 1.2) is 1.3 times greater at 50 m than at 135 m and, therefore, particle focusing cannot have accounted for all of the Al flux changes between these depths. Although no data on currents exist from the study in Saanich and Jervis Inlets, current speed probably decreased with depth, and particles aggregate and consolidate as residence time (depth) increases. This flocculation will cause sinking rates to increase (e.g.; Syvitski et al., 1985) and therefore trapping efficiency to improve (Butman, 1986; Yu et al., 2001).

Fraser River flow peaks in the spring and summer (Figure 1.13) and thus cannot have been the source of aluminosilicates to station SN-0.8 at the head of Saanich Inlet. But, was sediment from the Fraser River plume deposited at station SN-9 inside the mouth of Saanich Inlet? Because the Cowichan and Fraser Rivers are both seaward of Saanich Inlet, the ratio of the concentrations of particulate matter from the rivers occurring in surface waters at the mouth of the fjord cannot vary within the fjord except by differential sinking of the particles from the two sources. As a plume leaves the mouth of a river, the particulate load decreases due to mixing with seawater and settling (Hill et al., 2000) and the size fractions of the particulates shift from predominantly coarse silts to fine silts and clays (e.g.; Syvitski et al, 1988). The Stokesian settling velocity of the particulate load of a plume, therefore, decreases as the distance from a river mouth increases; however, a number of studies (e.g.; Syvitski et al., 1985; Gibbs and Konwar, 1986; Kineke et al., 1986; Milligan, 1995; Sternberg et al., 1999; Hill et al., 2000) show that flocculation has a significant effect on predicted settling rates of the smallest size fractions. Nevertheless, it is reasonable to model the sinking rate of plume particles as either constant (e.g.; as found by Hill et al. {2000} for the Eel River plume) or as decreasing (e.g.; as found by Syvitski et al., {1985} for the Homathko River of Bute Inlet) with distance from the source. The Fraser River is farther from Saanich Inlet ($\sim$ 50 km) than is the Cowichan River ($\sim$ 14 km). At the mouth of Saanich Inlet, Fraser River sediments will be more fine-grained

with similar or smaller sinking rates than Cowichan River sediments and thus the Fraser River sediments will disperse throughout Saanich Inlet as well or better than Cowichan River sediments. Because a Fraser-River signal was not observed at station SN-0.8 where discharge of the Cowichan River appears to have affected Al fluxes, it is unlikely fine silt and clay from the Fraser River reached parts of Saanich Inlet seaward of station SN-0.8.

3.4.5 Deep water-column, sediment-interface and burial fluxes

Comparison of sediment-trap fluxes and bottom accumulation rates has been used to gain information on the processes that control sediment delivery to the seafloor and burial (e.g.; Dymond, 1984; Anderson et al., 1994) and also to judge the fidelity of sediment traps (e.g.; Dymond, 1984). This section uses estimates of mass accumulation rate (MAR) calculated from ^{210}Pb profiles to evaluate the accuracy of the sediment-trap fluxes and to address the causes and consequences of the depth-dependent fluxes in the two fjords. Because of the unique sedimentary environment at the mouth of Saanich Inlet, the high water column fluxes at station SN-9 are considered separately.

MAR from ^{210}Pb profiles

In the summer of 1988, sediment cores were extracted from each station using a Pedersen corer (Pedersen et al., 1985), and the top 25-30 cm were sampled at 1 cm intervals. OC, N and δ^{13}C were measured in the sediment samples as described in section 3.2.2. Al_2O_3, SiO_2 and other metals were measured by X-ray fluorescence (XRF) spectrometry. BSi was not measured on the core samples, but was estimated by subtracting lithogenic SiO_2 from total SiO_2. Lithogenic SiO_2 was calculated using the regression equation of Figure 3.22 and measured Al_2O_3 concentrations. The slope of the regression line of Figure 3.22 (3.4) is a best estimate of the Al_2O_3:SiO_2 ratio for the aluminosilicate fraction caught by the sediment traps and is within the range expected for upper continental

	SN-9	SN-0.8	JV-3	JV-7
	linear AR (cm yr^{-1})			
	1.5	0.60	0.60	0.27
	sediment composition			
% BSi	19.9	24.5	15.0	18.7
% OC	2.91	4.84	3.96	3.59
% N	0.292	0.461	0.400	0.266
% Al	6.73	5.03	6.38	6.84
δ^{13}**C**	-21.7	-21.9	-21.7	-22.9

Table 3.8: Compositional properties of the upper 25-30 cm of cores extracted at each station. (See Table 3.1 for station locations.)

crust (Taylor and McClennan, 1985). Linear sedimentation rates for the upper 25-30 cm were estimated from measures of excess ^{210}Pb and converted to depth-averaged mass accumulation rates (MAR) using measured porosity values and estimated dry bulk density (Shimmield, unpublished data). ^{210}Pb has a half life of 22.26 yr and is well suited for dating rapidly accumulating, laminated sediments such as those in Saanich Inlet. With more uncertainty, ^{210}Pb can be used to date bioturbated sediments if linear accumulation rates are sufficiently fast that excess ^{210}Pb accumulates below the bioturbated layer (Bruland, 1974; Skei and Paus, 1979; Skei, 1981; Crusius and Anderson, 1995), as is the case in Jervis Inlet. Linear accumulation rates and average sedimentary composition for the upper 25-30 cm of each core are given in Table 3.8, while within Table 3.9 are the mass accumulation rates (therein termed burial of the mass flux). The linear sedimentation rate at station JV-7 is half those of stations JV-3 and SN-0.8, but the porosity at station JV-7 was proportionally lower so that MAR at the three stations was similar.

Table 3.9 compares fluxes to the deep sediment traps, to the sediment-water interface

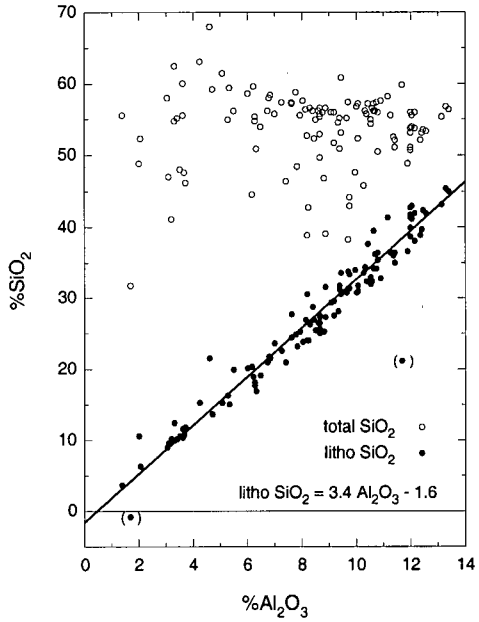

Figure 3.22: The Al_2O_3:SiO_2 ratio for the lithogenic debris in Saanich and Jervis Inlets using analyses on the sediment trap material. Al_2O_3 and SiO_2 were measured by XRF on 104 sediment-trap samples from Saanich Inlet and nine samples from Jervis Inlet (François, 1989). Biogenic silica has been measured on all samples. Open circles are total metal concentrations (XRF). Closed circles are lithogenic SiO_2 plotted against total Al_2O_3. Lithogenic SiO_2 is calculated as total SiO_2 minus biogenic SiO_2. Two points with parentheses were not included in the regression. The nine samples from Jervis Inlet fall close to the regression line.

and those representing permanent burial. The sediment-trap fluxes are the annual averages of Tables 3.3 and 3.4 and the burial fluxes are from multiplying the ^{210}Pb-derived MARs by the sediment concentration of each constituent (Table 3.8). The differences between interface and burial fluxes of Table 3.9 provides the percent of the interface flux that was remineralised. The flux of constituent j reaching the sediment-water interface was estimated using the focusing factor for the change in flux of Al between the depths of the deep sediment trap and the bottom sediments ($Al_{burial}/Al_{deep\ trap}$).

$$j_{interface} = \left(\frac{Al_{burial}}{Al_{deep\ trap}}\right) j_{deep\ trap}. \tag{3.1}$$

Equation 3.1 assumes Al behaves conservatively during diagenesis and that the material

causing the difference in flux between sediment traps and the sediment-water interface is compositionally similar. The first assumption is reasonable for these recently deposited sediments and the second is supported by work suggesting that resuspended material is "rebound" in nature (Walsh et al., 1988a) and is often similar in composition to the bulk material caught in deep traps (Bloesch, 1982; Walsh and Gardner, 1992; Timothy and Pond, 1997; Lampitt et al., 2000), so that debris transported laterally underneath the deep traps may have been compositionally similar to the sediments reaching the deep traps. If diagenetically old sediment with high Al content is a significant fraction of the material causing larger fluxes to the interface, however, Equation 3.1 will overestimate constituent fluxes to the interface.

For a station in the center of Saanich Inlet nine km south of SN-9 and using ^{210}Pb profiling in the manner described above, Bruland (1974) estimated a linear accumulation rate of 0.8 cm yr^{-1} and a MAR of 1,300 g m^{-2} yr^{-1}. Again from ^{210}Pb profiles, Sage (1994) measured a MAR of 2,600 g m^{-2} yr^{-1} two km south of SN-9. Thus a gradient exists in the MAR of bottom sediments in Saanich Inlet, from 1,900 to 2,600 g m^{-2} yr^{-1} at the mouth (Table 3.9; Sage, 1994), to 1,300 g m^{-2} yr^{-1} in the center of the fjord (Bruland, 1974) and 770 g m^{-2} yr^{-1} towards the head at station SN-0.8 (Table 3.9). Based on chlorophyll *a* concentrations (Hobson and McQuoid, in press), rates of primary production (Chapter 2; Timothy and Soon, 2001) and the sediment trap fluxes at stations SN-9 and SN-0.8, these decreasing MARs towards the head of Saanich Inlet can be explained by a gradient in primary production and the introduction of sediments into the fjord from the region of the sill.

At a station one km south of JV-3 and in waters slightly deeper (685 m versus 660 m at JV-3), Sage (1994) estimated a MAR of 1,500 g m^{-2} yr^{-1}, more than twice the value of 650 g m^{-2} yr^{-1} reported for JV-3 in Table 3.9. This difference may reflect inherent errors in ^{210}Pb dating, but may also be the result of heterogeneous sedimention rates near

the mouth of Jervis Inlet; the core extracted in somewhat deeper waters (Sage, 1994) may have been from a localised depocenter.

Stations SN-0.8, JV-3 and JV-7

Apart from station SN-9, the accumulation rate of Al was higher in the sediments than in the deep sediment traps by factors ranging from 1.1 to 1.7 (Table 3.9). Focusing in these U-shaped fjords (Wassmann, 1984; Timothy and Pond, 1997), as well as lateral transport of material from topographic rises and slumping of sediment off the side-walls (Hedges et al., 1988b; Cowie et al., 1992; Bornhold et al., 1994) is likely to have caused the Al flux increases from the deep sediment traps to the fjord floors. Noting that some increase in flux with depth is expected between the deep sediment traps and the seafloor, the magnitude of these focusing factors qualitatively suggests the deep sediment traps were accurately trapping the settling flux of Al. The largest increases in flux between the depths of the middle and deep sediment traps (Tables 3.3 and 3.4) were recorded at station JV-3. Therefore, the small focusing factor there (Table 3.9) needs explanation. Much of the difference in flux between 300 and 600 m at station JV-3 is the result of turbulent resuspension during deepwater renewals (Chapter 4). Otherwise, station JV-3 is in the largest basin of the four sediment-trap mooring sites. The shallowest part of the Jervis Inlet sill is at ~280 m and, apparently, during deepwater renewal a sediment plume propagates at depths principally below 300 m. Because station JV-3 is otherwise in a large basin, changes in flux with depth below 600 m may be small. The water-column fluxes at station SN-9 demonstrate the effects of a plume propagating from a sill. The largest increases in flux with depth occurred between the shallow (45 m) and mid-depth (110 m) traps, where the lip of the sill is located, but fluxes between the mid-depth (110 m) and deep (150 m) sediment traps changed little. Nevertheless, it may be that the small focusing factor at station JV-3 reflects error in the ^{210}Pb dating, as Sage (1994)

	SN-9	SN-0.8	JV-3	JV-7
	Al flux (mol m^{-2} yr^{-1})			
deep trap	9.94	1.05	1.44	1.00
interface	4.77	1.43	1.54	1.72
burial	4.77	1.43	1.54	1.72
focusing factor	0.48	1.4	1.1	1.7
	mass flux (g m^{-2} yr^{-1})			
deep trap	4650	875	870	628
interface	2230	1200	928	1080
burial (MAR)	1910	770	650	680
% loss	14	36	30	37
	BSi flux (mol m^{-2} yr^{-1})			
deep trap	15.2	3.69	3.31	2.12
interface	7.27	5.06	3.53	3.65
burial	5.65	2.80	1.45	1.89
% loss	22	45	59	48
	OC_{tot} flux (mol m^{-2} yr^{-1})			
deep trap	15.1	5.41	4.41	3.52
interface	7.26	7.42	4.70	6.06
burial	4.63	3.10	2.14	2.03
% loss	36	58	54	66
	OC_{mar} flux (mol m^{-2} yr^{-1})			
deep trap	8.05	3.21	3.11	2.09
interface	3.86	4.40	3.31	3.60
burial	2.03	1.28	1.49	1.07
% loss	47	71	55	70
	OC_{ter} flux (mol m^{-2} yr^{-1})			
deep trap	7.10	2.20	1.31	1.43
interface	3.40	3.02	1.39	2.46
burial	2.60	1.82	0.66	0.97
% loss	24	40	53	61
	N flux (mol m^{-2} yr^{-1})			
deep trap	1.53	0.595	0.432	0.341
interface	0.734	0.816	0.461	0.587
burial	0.398	0.253	0.186	0.129
% loss	46	69	60	78

Table 3.9: Deep sediment-trap (Tables 3.3 and 3.4), sediment-water interface (Equation 3.1) and burial (Shimmield, unpublished) fluxes. The focusing factor is of Equation 3.1. The percent lost is the fraction of the interface flux remineralised during diagenesis in the upper sediment core. Marine and terrestrial OC fluxes are estimated from $\delta^{13}C$ as for section 3.4.2.

obtained a MAR for a core collected near station JV-3 of more than twice the estimate in Table 3.9.

As much as 54 to 66% of the OC deposited at the sediment-water interface at stations SN-0.8, JV-3 and JV-7 was remineralised in the upper 30 cm of sediment, and 45 to 59% of the biogenic silica dissolved (Table 3.9); most of this loss probably occurred in the uppermost portion of the core (e.g.; Hedges et al., 1988b). These OC losses agree with other estimates made in Saanich Inlet (Cowie et al., 1992) and other fjords (Burrell, 1983). In Jervis Inlet, roughly equal fractions of the marine and terrigenous organic matter reaching the sediments were remineralised, while at station SN-0.8 significantly more of the marine OC was degraded (71%) than of the terrigenous OC (40%; Table 3.9). This difference between fjords may be due to a greater degree of water-column remineralisation of the most labile marine OM in Jervis Inlet due either to its greater depth, or the periodic anoxia in Saanich Inlet. However, anoxia does not appear to affect the decomposition of bulk OM, as similar amounts of the carbon flux to the interface are lost during sediment diagenesis. In Saanich Inlet, low oxygen conditions may indirectly effect opal preservation by decreasing the rate by which organic coatings are degraded (e.g.; Lewin, 1961; Bidle and Azam, 1999), but this factor does not appear to be significant; at station SN-0.8 45% of the biogenic silica dissolved, while in Jervis Inlet 48-59% was lost from the sediment.

Station SN-9

Although the OC e-ratios at station SN-9 were not higher than for the other stations, the BSi e-ratios were about double those observed at the head of Saanich Inlet and in Jervis Inlet and, at all depths, the material intercepted by sediment traps at station SN-9 was more refractory than at the other stations; %OC and %BSi were lowest, while %Al was highest at this site (Figures 3.8 and 3.14). Refractory material was likely resuspended off the sill of Saanich Inlet and perhaps also travelled from the mouth of

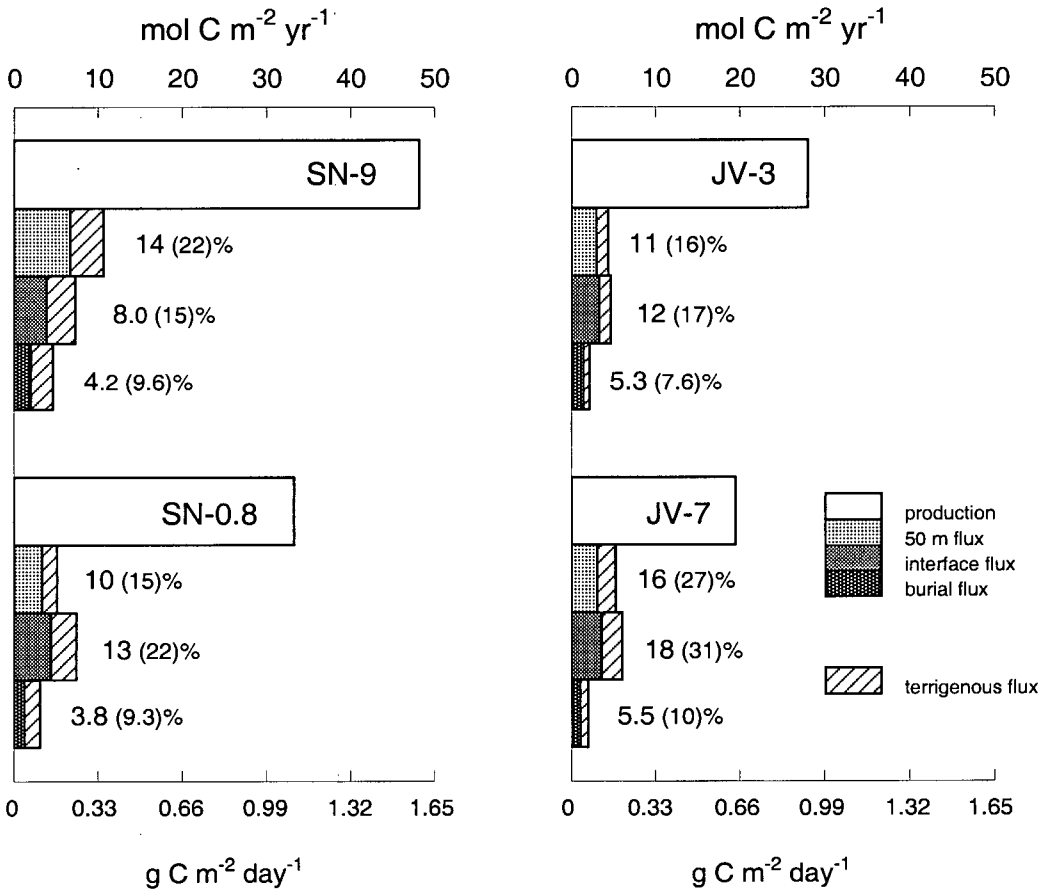

Figure 3.23: Summary of OC fluxes. Primary production is from Table 2.1, 50 m fluxes are from Tables 3.3 and 3.4 and sediment-water interface and burial fluxes are from Table 3.9. The sediment-trap and benthic fluxes are separated into marine (filled part of each bar) and terrigenous (hatched portion of bar) components, so that their sum is the total OC flux at each interval. Numbers associated with each bar are the percent of primary production accounted for by each flux. Numbers in parentheses are for total OC, while numbers before parentheses are for marine OC.

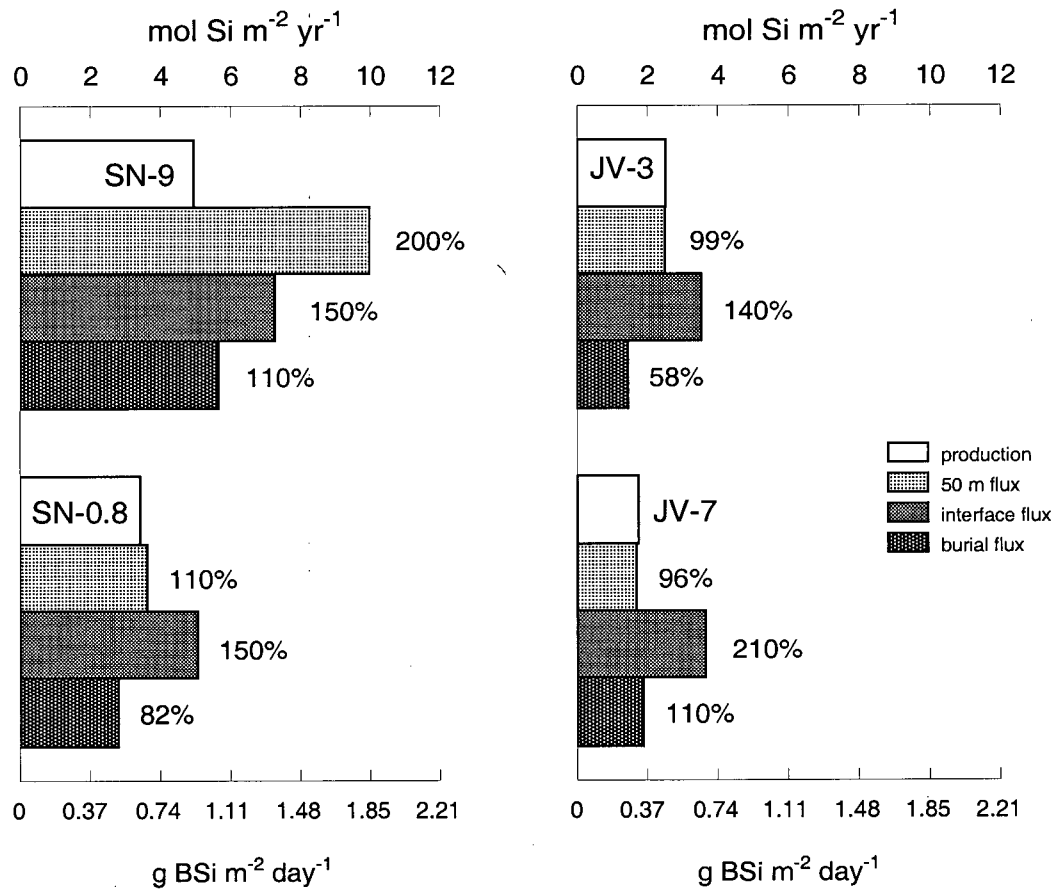

Figure 3.24: Summary of BSi fluxes. Si production is calculated as 0.13 x diatomaceous carbon assimilation (Table 3.6). 50 m fluxes are from Tables 3.3 and 3.4, and sediment-water interface and burial fluxes are from Table 3.9.

the Cowichan River to the vicinity of station SN-9. Nevertheless, the water-column fluxes of Al were higher than the MAR of Al in the sediments, resulting in a focusing factor less than one (Table 3.9). In fact, there is no evidence of enhanced sediment deposition at station SN-9 when comparing sedimentary fluxes of OC and BSi to local primary production (Figures 3.23 and 3.24). According to Gucluer and Gross (1964) and François (1987), station SN-9 is located at the northern edge of sediments characteristic of the central basin, and the large linear accumulation rates measured there (Table 3.8) argue against this as a location of winnowing. Therefore, it appears that a nepheloid layer or sediment plume extends from the sill of Saanich Inlet to station SN-9. This plume, furthermore, does not appear to deposit an amount of biogenic material to the sediments in excess of the focusing occurring at other stations. Remineralisation within the sediments at station SN-9, however, is less than at the other stations (Table 3.9). The enhanced preservation inside the sill of Saanich Inlet is probably caused by the very high accumulation rate, but may also be the result of particularly refractory sediments being deposited here. At all stations, the BSi interface flux is 1.4 to 2.1 times greater than estimated Si assimilation (Figures 3.23 and 3.24). While at stations JV-3, JV-7 and SN-0.8 these additional fluxes may represent relatively young, autochthonous debris focused toward the bottom, at station SN-9 the additional sediments coming from outside the fjord may be more diagenetically altered.

Oxygen and carbon budgets for the deep waters of Jervis Inlet

For the stagnant waters behind the sill of a fjord, the decay of dissolved oxygen over time allows estimation of the water-column and sediment oxygen demand in the deep basin. This exercise is complicated for Saanich Inlet because dissolved oxygen concentrations did not decay in a gradual manner (see Figures 1.4, 1.5 and 4.8), likely due to the oxidation of reduced chemical species during and shortly after deepwater renewals. However, in

Jervis Inlet, dissolved oxygen decayed in such a manner that this exercise is possible (Figures 1.6, 1.7 and 4.7).

A box model is used to compare the observed loss of oxygen behind the sill (240 m) of Jervis Inlet and the predicted oxygen demand based on organic carbon remineralisation within the deep waters and sediments. Oxygen contours (Figures 1.6 and 1.7) show that dissolved oxygen was often homogeneously distributed below about 300 m, while above this depth mid-water advection seasonally affected oxygen concentration. Thus, 300 m is taken as the top of the box within which advective sources of oxygen should be negligible and diffusion effects are ignored, noting that vertical gradients in dissolved oxygen concentration at 300 m at stations JV-3 and JV-7 were small. The mean depth of the center of Jervis Inlet is 495 m (Pickard, 1961). Accounting for the sloping sides below 300 m (see transects of Figure 1.3), the average depth of the box is 160 m. For sampling locations within the box (Figures 1.6 and 1.7), the rate of dissolved oxygen decay during periods between deepwater renewals was approximately 0.10 μM d^{-1} (see Figure 4.7 for an example), converting to an oxygen consumption rate of 5.8 mol m^{-2} yr^{-1} within the box. In Chapter 4, water-column remineralisation rates of organic carbon are estimated. From those results and using a mean flux of 130 mg OC m^{-2} d^{-1} (mean annual OC flux for sediment traps moored within the box; Table 3.4) at the top of the box, 0.64 mol OC m^{-2} yr^{-1} were lost within the water-column of the box. Finally, from Table 3.9, 2.6 to 4.0 mol OC m^{-2} yr^{-1} were lost within the sediments at stations JV-7 and JV-3, respectively, for an average sedimentary OC loss of 3.3 mol OC m^{-2} yr^{-1}. These water-column and sedimentary losses of organic matter can be converted to an oxygen demand using the stoichiometry outlined in section 3.3.1. For the OC:N ratios observed in Jervis Inlet, oxygen and organic carbon should be lost at a molar ratio of 126:106 during organic matter degradation (Timothy, 1994). Thus, the water-column and sediment oxygen demands are predicted to have been 0.76 and 3.9 mol O_2 m^{-2} yr^{-1},

respectively.

Considering the errors, these independent estimates of the oxygen demand for the bottom 160 m of Jervis Inlet (5.8 mol m^{-2} yr^{-1} based on the time-course of dissolved oxygen concentration and 4.7 mol m^{-2} yr^{-1} determined from remineralisation of organic matter) agree very well. The largest sources of error in the estimate based on dissolved oxygen concentrations is determining the upper boundary of the box, which could be off by about 50 m (±30%), and the rate of oxygen decay, which ranged between about 0.06 and 0.16 μM d^{-1} for different periods, depths, and stations of the time series. The average of 0.10 μM d^{-1} is probably accurate to within 20%. The predicted oxygen demand based on organic matter degradation is most sensitive to the sedimentary oxygen demand, as it accounted for 84% of predicted organic matter remineralisation within the box. It is difficult to put an error on the sediment oxygen demand, which is based on ^{210}Pb profiles and sediment-trap fluxes, but ±50% is probably a conservative estimate.

3.5 Conclusions

1. Water-column fluxes of organic carbon and biogenic silica follow local primary production in Saanich and Jervis Inlets. However, physical processes of resuspension and particle focusing in the vertically-narrowing channels, and possibly increased trapping efficiency with depth due to weak deepwater currents and accelerated sinking, cause increases in flux with depth. At station SN-9, the effect of mid and deepwater renewals on particle flux throughout the water column deceptively suggest late summer plankton blooms.

2. Although resuspension largely affects the Al fluxes at stations SN-9, JV-3 and JV-7, at station SN-0.8 the rain of aluminosilicates is controlled by terrigenous runoff, as Al fluxes closely follow local precipitation and flow of the Cowichan and Goldstream

Rivers. There is some evidence that the Cowichan River has a greater effect on Al fluxes than local runoff. The Fraser River as a significant source of aluminosilicates to Saanich Inlet is unlikely.

3. The relationship between stable carbon isotopes and BSi content reveals that 70-80% of the marine OC in these fjords is diatomaceous. This relationship was used to make estimates of the mean $\delta^{13}C$ signal of settling marine organic matter. In Saanich Inlet, an estimate of the mean $\delta^{13}C$ of marine organic matter is -17.3$^0/_{00}$ and, in Jervis Inlet, is -19.6$^0/_{00}$. The difference between fjords may be due to a greater predominance of fast-growing diatoms in Saanich Inlet. In the spring and summer, 20-40% of the sinking organic matter at 50 m is terrigenous while, in the fall and winter, 40-60% is terrigenous.

4. The sediment-trap export ratios of OC were very low in both fjords during this study, and may have been affected by solubilisation of organic material within the sediment traps and during laboratory processing. Export ratios of BSi were high, suggesting an efficient transfer of biogenic silica out of the euphotic zone. The observed BSi e-ratios may have furthermore been affected by resuspended or focused sediments reaching the shallow sediment traps. Exceptionally high fluxes of biogenic silica at station SN-9 mark a sediment plume or nepheloid layer associated with the sill.

5. Although a sediment plume extends from the sill into Saanich Inlet, when comparing to local primary production, biogenic material is not transmitted to the sediments in excess of the biogenic delivery to sediments at the head of Saanich Inlet or in Jervis Inlet. However, at station SN-9 organic matter and biogenic silica is better preserved in the sediments, probably because of the high accumulation rates and the refractory nature of the sedimenting material.

6. Comparing accumulation rates in the upper 30 cm of the sediments with local primary production, there is little evidence that either organic matter or biogenic silica is preferentially preserved in the periodically anoxic environment of Saanich Inlet; in both Saanich and Jervis Inlets, about 5% of the carbon and 60-110% of the Si assimilated in the euphotic zone is buried in the sediments beneath. In Chapter 4 it is estimated that water-column dissolution in Jervis Inlet causes about a 20% loss of biogenic silica as it sinks from 100 m to 200 m, and a 35% loss for sinking from 100 m to 600 m. Considering water-column dissolution yet the high proportion of assimilated Si buried in the sediments, there is a large amount of particle focusing occurring in these fjords and/or the Si:C uptake ratio of 0.13 used to estimate Si assimilation is too low. Away from station SN-9 where accumulation rates are highest and the sediment is of a more refractory nature, similar amounts of organic carbon (54-66%), nitrogen (60-78%) and biogenic silica (45-59%) are lost between the sediment-water interface and deeper in the sediment core at stations SN-0.8, JV-3 and JV-7.

Chapter 4

A model to interpret increases in flux with depth: remineralisation rate constants and the additional flux to deep sediment traps

4.1 Introduction

In studies of vertical particle flux in the ocean using moored sediment traps, increases in flux with depth are often observed, especially in coastal environments. For these situations, deducing particulate supply from surface waters as well as the alteration of material as it sinks is not straightforward without a means of separating primary fluxes from the additional material caught by deep traps.

Quantitative methods to interpret sediment-trap fluxes that increase with depth have considered either the decay of primary fluxes or the composition and amount of additional fluxes, but not both simultaneously. For instance, Noriki et al. (1985) determined regeneration rates for biogenic silica and organic matter in a shallow bay in Japan by normalising fluxes to aluminium (Al). Later, Noriki and Tsunogai (1986), for trap fluxes from the Pacific and Southern Oceans, and Walsh et al. (1988b), for the Equatorial North Pacific, also normalised fluxes of particulate organic carbon, calcium carbonate and biogenic silica to Al. The oceanic estimates of remineralisation give similar amounts of biogenous flux decay over comparable depth intervals. However, the normalisation procedure assumes compositional similarity between primary and additional fluxes, a constraint that is not everywhere appropriate. For example, artificially high decay rates are obtained if Al-rich material, such as refractory bottom sediment, is the cause of an

increase in flux with depth (Walsh et al., 1988a). Normalisation to Al also assumes that the Al flux is conservative, though dissolved Al is known to be scavenged by sinking particles (Orians and Bruland, 1986). In regions where Al fluxes are small, scavenging may cause over-estimates of decay. Bloesch (1982) applied a method to quantify the amount of resuspended material that reached near-bottom traps in the shallow and turbulent waters of Lake Erie. The method was able to detect that there were both locally resuspended sediments and material of a more organic-rich nature within the additional flux to hypolimnetic traps. Walsh and Gardner (1992) described a similar model and found that the composition of the additional flux to deeper traps moored in the Gulf of Mexico was more similar to the primary flux than to bottom sediments. However, these two techniques were not general because water-column decay was either not considered (Bloesch, 1982) or had to be estimated independently using the normalisation scheme (Walsh and Gardner, 1992).

Three common methods to unravel coastal sediment-trap fluxes that increase with depth were reviewed by Håkanson et al. (1989), and a combination of two of those methods (the base-line approach and the burial approach) was used by Pejrup et al. (1996) to separate primary from resuspended fluxes in a shallow, coastal environment. Techniques similar to the label approach of Håkanson et al. (1989) have been used to infer much about processes affecting particles as they sink. For instance, Blomqvist and Larsson (1994) used the Al concentration of primary and resuspended sediments to estimate the proportion of primary settling material to sediment traps moored at a single depth at two stations during a five year time series in the Baltic Sea. A greater abundance and different assemblages of intact phytoplankton cells in deep sediment traps relative to shallow traps was used to evaluate the degree of lateral transport from the shelf to the slope of the Middle Atlantic Bight (Falkowski et al., 1994). Also, the composition of sediment-trap material and underlying sediments has provided insight into the biochemical changes that

occur to particles as they sink through the water column and become incorporated into the sediments in Dabob Bay, WA (Hedges et al., 1988a; 1988b). However, none of the approaches outlined by Håkanson et al. (1989) describes remineralisation of the primary flux, a term that may be relatively large where water depths are greater than roughly 10 to 100 m (Pejrup et al., 1996).

The primary concern of this work is to estimate remineralisation rates of settling particulate material where observed fluxes increase with depth so that more accurate elemental budgets can be described for coastal regions. A general balance equation that treats as unknowns both water-column decay and the composition of additional material caught by a deeper trap was developed by Timothy (1994) and Timothy and Pond (1997). That model is applied to fluxes of organic carbon, nitrogen, biogenic silica and aluminium during the multi-year sediment-trap time-series from Saanich and Jervis Inlets presented in Chapter 3.

4.2 Description and solution of the model

Timothy (1994) and Timothy and Pond (1997) described a model to estimate rates of water-column decay where measured fluxes increase with depth for the general case where the rain to the deep sediment trap is a mixture of debris from different sources and with different compositional properties. The model (Figure 4.1) partitions the flux to a deep sediment trap into two components. The *anticipated flux* is the representative material expected to reach the deep sediment trap knowing the flux at the shallow sediment trap, and the *additional flux* is the material caught by a deep sediment trap in excess of the anticipated flux. The observed flux to a deep sediment trap, therefore, is the sum of anticipated and additional fluxes. In general, anticipated and additional fluxes might be equated with primary and resuspended fluxes, respectively, but the operational terms are

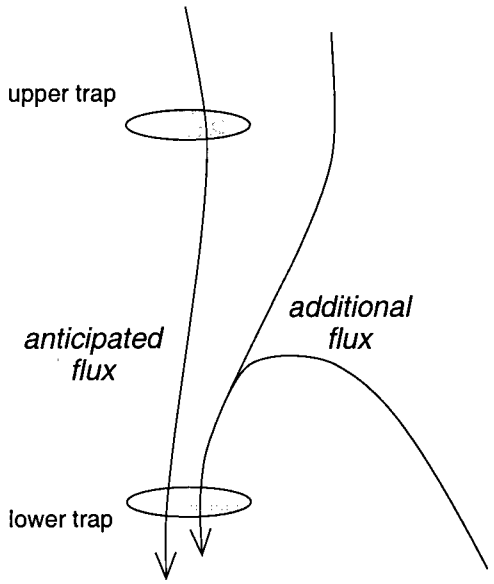

Figure 4.1: Schematic of the sediment-trap model. Anticipated fluxes are allowed to decay as they sink and there is no constraint on the source of additional fluxes.

used to emphasise that the model can be applied to a data set regardless of the sources of material reaching upper and lower sediment traps.

Fluxes are recorded by sediment traps at depths z_1 and z_2 (z is positive downward). j is a component of the mass flux, J. Anticipated and additional fluxes are identified by subscripts n and d, respectively, so that:

$$J_2 = J_n + J_d\,; \tag{4.1a}$$

$$j_2 = j_n + j_d\,. \tag{4.1b}$$

The model is designed largely to find rates of remineralisation of the sinking flux of j between depths z_1 and z_2 bounded by two sediment traps. Using the results of the modelling on the six depth intervals in Jervis Inlet, it will be shown in section 4.4.1 that rates of remineralisation of OC, N and BSi decreased with depth during the study in Jervis Inlet. However, because the depth distribution of loss cannot be determined from fluxes

measured at two depths, here it is assumed that the rate of remineralisation of constituent j between the depths of two sediment traps is constant, so that anticipated fluxes decrease exponentially with depth as they sink (e.g.; Walsh et al., 1988b). Equation 4.1*b* becomes:

$$j_2 = j_1 \, e^{-k_j \Delta z} + j_d \, . \tag{4.2}$$

k_j (m^{-1}) is the rate constant for component j. In order to estimate the rate constant, j_d must be quantified and in the model is written as the product of J_d and the fraction of j in J_d, $(j/J)_d$. Equation 4.2 is re-written as:

$$j_2 = j_1 \, e^{-k_j \Delta z} + \left(\frac{j}{J}\right)_d J_d \, . \tag{4.3a}$$

If an estimate of J_d can be made for each deployment period, then Equation 4.3*a* is linear with the measured (or estimated) variables j_2, j_1 and J_d. For data from n deployment periods, these variables can be plotted on three orthogonal axes. If a plane is fitted through the data points, the slope of the line representing intersection of the fitted plane with the $j_2 : j_1$ plane is a best-estimate of $e^{-k_j \Delta z}$, and the slope of the line where the fitted plane intersects the $j_2 : J_d$ plane is an estimate of $(j/J)_d$. The degree of fit of the plane to the data is a measure of the extent to which $e^{-k_j \Delta z}$ and $\{j/J\}_d$ behaved as constants over the period and depth interval considered.

As Equation 4.3*a* is written, the solution plane should pass through the origin and therefore should have a zero-intercept on the j_2-axis. However, there may be errors associated with the trapping experiment or with the assumptions of the model that might cause a non-zero intercept on the j_2-axis. A term (ϵ, the intercept on the j_2-axis) is included in Equation 4.3*a* to quantify these possible errors.

$$j_2 = j_1 \, e^{-k_j \Delta z} + \left(\frac{j}{J}\right)_d J_d + \epsilon \tag{4.3b}$$

This error term is discussed further in section 4.3.2.

In order to solve Equation 4.3*b*, the total additional flux, J_d, must be estimated for each deployment period. If fluxes settle conservatively, J_d can be estimated as the difference in flux between depths z_1 and z_2: $J_d = J_2 - J_1$. However, where water-column decay occurs, J_d will be greater than $J_2 - J_1$ by the amount of J_1 that is lost while it sinks to depth z_2. The sinking flux is composed of organic matter, biogenic silica, calcium carbonate and lithogenic debris. Lithogenous fluxes are expected to be conservative and $CaCO_3$ made up only about 2% of the observed fluxes in Saanich and Jervis Inlets. Only the degradation of POM and the dissolution of biogenic silica are therefore included in the expression for J_d in this study:

$$J_d = J_2 - J_1 + 2.7\,C_1\,(1 - e^{-k_C \Delta z}) + Si_1\,(1 - e^{-k_{Si} \Delta z})\,. \tag{4.4}$$

C_1 and Si_1 are fluxes of organic carbon and biogenic silica at the depth of the upper sediment trap, k_C and k_{Si} are decay constants for organic carbon and biogenic silica, and the factor 2.7 is used to convert POC to POM (section 3.3.1). In equation 4.4, the terms with C_1 and Si_1 account for the portion of J_1 lost to the water column between depths z_1 and z_2. Replacing J_d of Equation 4.3*b* with Equation 4.4,

$$j_2 = j_1\,e^{-k_j \Delta z} + \left(\frac{j}{J}\right)_d (J_2 - J_1 + 2.7C_1\,\{1 - e^{-k_C \Delta z}\} + Si_1\,\{1 - e^{-k_{Si} \Delta z}\}) + \epsilon\,. \tag{4.5}$$

For data collected over n deployment periods, Equation 4.3*b* is a set of n simultaneous equations.

$$\begin{bmatrix} j_{11} & J_{d1} & 1 \\ j_{12} & J_{d2} & 1 \\ \vdots & \vdots & \vdots \\ j_{1n} & J_{dn} & 1 \end{bmatrix} \begin{bmatrix} e^{-k_j \Delta z} \\ \left(\frac{j}{J}\right)_d \\ \epsilon \end{bmatrix} = \begin{bmatrix} j_{21} \\ j_{22} \\ \vdots \\ j_{2n} \end{bmatrix} \tag{4.6a}$$

Writing Equation 4.6*a* in abbreviated matrix notation:

$$X\ a\ =\ Y \tag{4.6b}$$

and matrix multiplication of both sides of Equation 4.6*b* by $\left(X^T X\right)^{-1} X^T$ gives:

$$a = \left(X^T X\right)^{-1} X^T Y \; . \tag{4.7}$$

periods represented. In applying Equation 4.7, $(J_2 - J_1)$ is used as a first approximation of J_d. First estimates of k_C and k_{Si} are made by solving Equation 4.7 for j = OC and j = BSi, respectively. These rate constants are used in Equation 4.4 to make improved estimates of J_d which, again applying Equation 4.7, give new estimates of k_C and k_{Si}. This iterative procedure is continued until the rate constants used to calculate J_d converge with k_C and k_{Si} given back when solving Equation 4.7 for OC and BSi fluxes. With final estimates of k_C and k_{Si} for the depth interval and deployment periods being addressed, best estimates of J_d (Equation 4.4) can be made, and k_j and $(j/J)_d$ of constituent fluxes (e.g.; N, Al) can be solved without iteration.

For the case where the rate constants do not converge, or where computational resources do not allow the iteration described here, an alternate solution to the model is described in Appendix B.

4.3 Results

4.3.1 Sensitivity analyses and examples of the planar fits

The model of Equation 4.5 and solved using Equation 4.7 has been applied to the sediment-trap fluxes from Saanich and Jervis Inlets reported in Chapter 3. A sensitivity analysis of the data from each depth interval (three at each station) was performed in order to find and remove records that heavily biased model solution (Appendices C and D). The model solutions presented in Tables C.1 and D.1 are the results after outliers have been removed. The rate constants estimated for Saanich Inlet (Table D.1, Figure 4.4) are spatially inconsistent, and the differences between constituents are not

clearly meaningful. Possible causes of these results are discussed in Appendix D; one is that the depth intervals separating the sediment traps may have been too small to resolve the decay of the settling flux. Rate constants from Saanich Inlet are plotted in Figure 4.4. Otherwise, this chapter will consider only the results for Jervis Inlet.

In Jervis Inlet, 11 of the surface records biased the model results for the surface-mid and/or the surface-deep intervals. Of these 11 records, eight were from station JV-7 and most were from periods of anomalously high fluxes of OC to the 50 m sediment traps (Figure C.7). The majority of these periods occurred in the spring and summer of 1985 and 1986, and were generally characterised by high OC:BSi ratios (compare Figures 3.11 and 3.10). Primary production was not measured throughout 1985, but in 1986 was higher than average in Jervis Inlet. It is possible that these high OC fluxes were associated with blooms of thecate dinoflagellates or nanoflagellates as described for Sechelt Inlet (Haigh et al., 1992; Taylor et al., 1994), adjoining Jervis Inlet near station JV-3 (Figure 1.1). Nutrient data from station JV-7 (Figure 2.6) further suggest that towards the head of Jervis Inlet autotrophic flagellates were more prevalent than at station JV-3 or in Saanich Inlet. The high OC fluxes with low OC:BSi ratios also may have represented a response by the zooplankton to blooms of diatoms or flagellates. While grazing heterotrophs may have died and sank to the depth of the 50 m sediment traps, it is also possible they were attracted to the debris in the 50 m traps and contaminated the samples (e.g.; Michaels et al., 1990). This latter explanation for the high OC fluxes is supported by the observation of polychaetes occasionally caught within the grids of the sediment traps (Chapter 3). Furthermore, for these fluxes to have resulted from naturally sinking phytoplankton or heterotrophs, remineralisation between the 50 m and the mid-depth traps would have been exceptionally high. Without a protective shell, sinking flagellates may remineralise quickly, but if so they would not be expected to sink in abundance to 50 m, a depth well below the euphotic zone in Jervis Inlet (Figure 2.7).

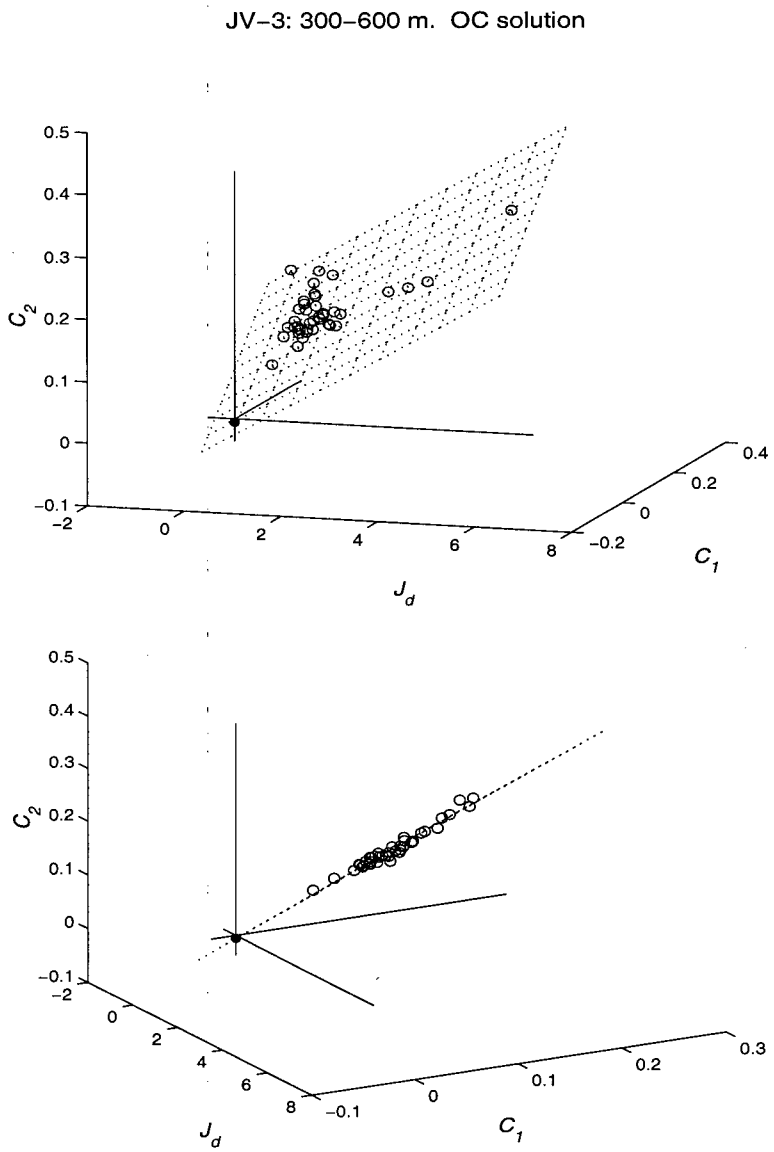

Figure 4.2: Plot of OC solution: station JV-3, 300-600 m. The upper plot depicts the plane relative to the OC_2, OC_1 and J_d axes. Below, the plot has been rotated to an angle where the plane intersects the data to show the goodness of fit of the model solution. Open circles are plotted data, filled circle is the OC_2-intercept.

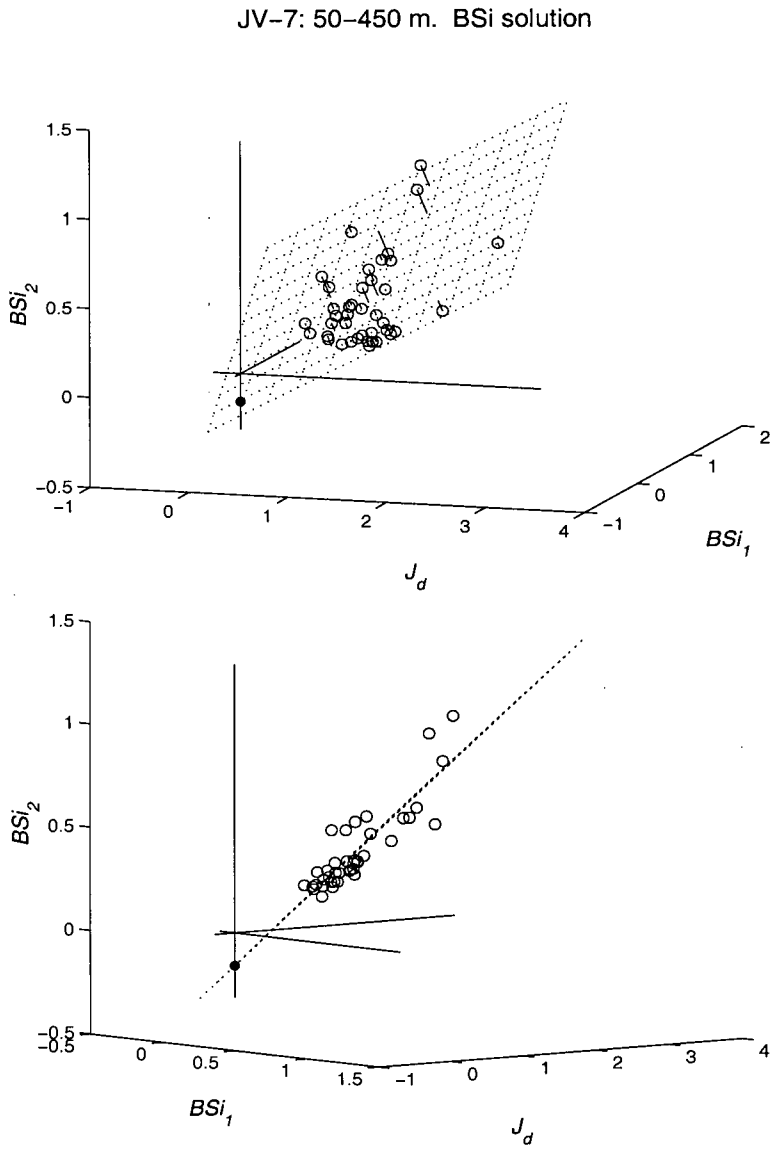

Figure 4.3: Plot of BSi solution: station JV-7, 50-450 m. The upper plot shows the plane relative to the BSi_2, BSi_1 and J_d axes and, below, is rotated to show the goodness of fit. Open circles are plotted data, filled circle is the BSi_2-intercept.

Swimmer contamination was therefore a likely cause of the anomalously high OC fluxes to the 50 m sediment traps in Jervis Inlet.

Figures 4.2 and 4.3 show examples of the solution plane fit to the sediment-trap data from Jervis Inlet. These examples were chosen because they represent the range of goodness-of-fit of the model to this data set (Table C.1). The fit to OC fluxes of 300-600 m at station JV-3 (Figures 4.2) was very good, while the fit to BSi flux for 50-450 m at station JV-7 was not as good, and a significant intercept on the BSi_2-axis occurred (Figure 4.3).

4.3.2 The error term

The error term included in the model and depicted as the intercept on the j_2 axis (e.g.; Figure 4.3) was small for the deep sediment-trap depth intervals in Jervis Inlet, but, for many cases from the more shallow intervals, the error was non-zero (Table C.1). The model assumes that the material representing the anticipated flux reaches the deep sediment trap, but this assumption may be at least partially invalid for a number of reasons including changes in trapping efficiency with depth and horizontal advection across a horizontal gradient in the settling flux. Thus, the anticipated flux might be over- or under-represented in the deep sediment trap, giving physical significance to ϵ.

The modelled fluxes to a deep sediment trap, including the error term (Equation 4.3*b*), can be equated with the true fluxes in a way that allows for the possibility that the deep sediment trap imperfectly captured the anticipated flux.

$$j_n + j_d + \epsilon = y\, j_n + j_d\,. \tag{4.8}$$

y is the fraction of j_n that reaches the deep sediment trap. Rearranging Equation 4.8:

$$\epsilon = (y - 1)\, j_n\,. \tag{4.9}$$

- $\epsilon > 0$: over-collection of j_n at z_2.
- $\epsilon < 0$: under-collection of j_n at z_2.

For the depth intervals associated with the surface sediment traps, positive errors (the intercepts reported in Table C.1) were common for OC, N and Al, and could be caused by increased trapping efficiency with depth. Improved trapping efficiency in deep water can be caused by reduced current speeds at depth, and by accelerated sinking of the settling debris (e.g.; Smetacek et al., 1978; Timothy and Pond, 1997; Yu et al., 2001). However, if improved trapping efficiency were causing these intercepts for the OC, N and Al solutions, it is expected the BSi solutions would also have positive intercepts, but they do not. The negative BSi intercepts could be caused by horizontal advection carrying the anticipated flux away from the deep sediment trap and replacing it with material from a region of small export flux (Deuser et al., 1988; Siegel et al., 1990; Yu et al., 2001). Timothy and Pond (1997) presented a scale analysis for Sechelt Inlet to determine whether increases in flux with depth could have been caused by the advection of sediment from a high export region. They concluded that horizontal gradients in the export flux, relative to local current speeds, were not sufficient to cause increases in flux with depth unless sinking rates were quite low (< 20 m d^{-1}).

Currently, the cause of the difference in sign of the BSi errors and those of OC, N and Al is unresolved. It remains to be seen whether sample artifacts, such as differential preservation and swimmer contamination, are affecting these results.

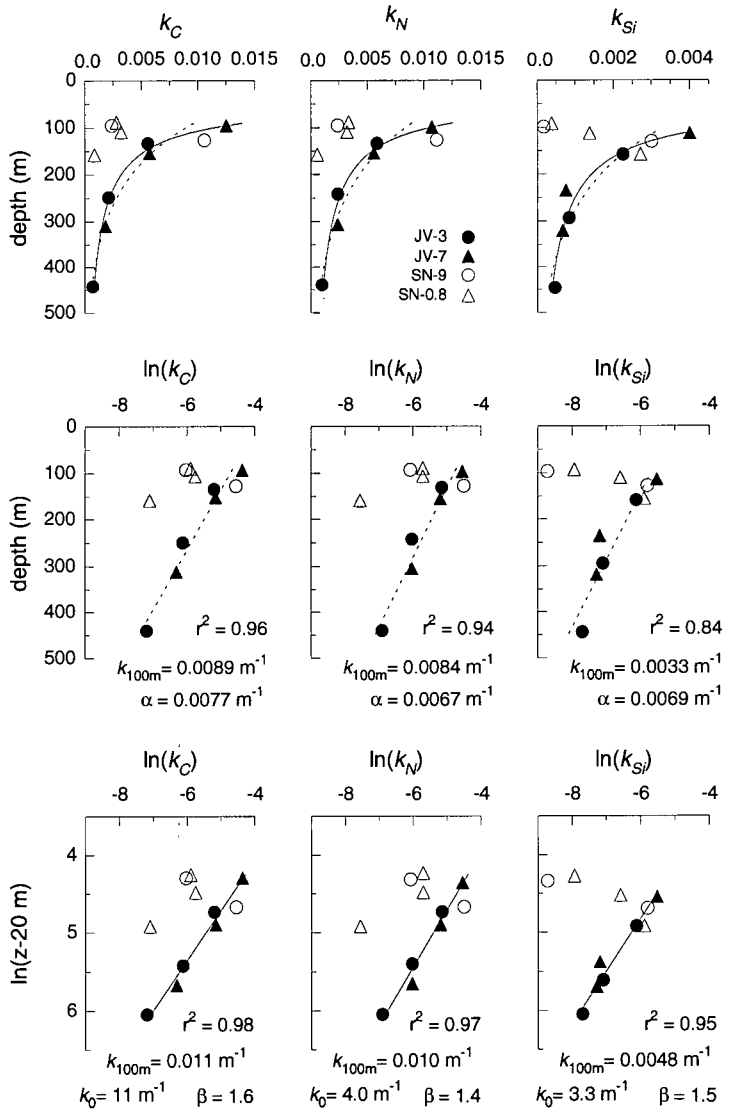

Figure 4.4: The relationship between rate constants (k_C, k_N and k_{Si}) and depth. Top row: rate constants plotted against depth. Middle row: semi-ln plots describing an exponential dependence (Equation E.2) of rate constants on depth. Bottom row: ln-ln plots showing the power function relationship (Equation 4.11). For the power functionality, z_0 is set at 20 m, the approximate base of the euphotic zone in Jervis Inlet. Solid and dashed lines are for semi-ln and ln-ln treatments, respectively. k_{100m}, α and β are from the regression equations of the semi-ln and ln-ln plots. See Appendix E for the exponential (semi-ln) treatment, and why it was rejected. The model results from Saanich Inlet are viewed skeptically (Appendix D), but the rate constants are plotted here for comparison.

4.4 Discussion

4.4.1 Describing depth dependence of the rate constants

At Equation 4.2, it was noted that the depth dependence of the rate constants cannot be determined from data collected at two sediment traps, so it was assumed that the rate parameters were constant with depth. However, results from the six depth intervals in Jervis Inlet (Figure 4.4) show that the rate parameters decreased with depth non-linearly. Organic matter is made of a range of constituents that differ in their susceptibility to degradation; the most labile compounds are oxidised quickly, while refractory components require more time (or depth) to decay (Toth and Lerman, 1977; Westrich and Berner, 1984; Harvey et al., 1995). Diatom frustules also exhibit a large range in their dissolution rate. Temperature plays an important role in silica dissolution (Lewin, 1961; Lawson et al., 1978; Kamatini and Riley, 1979), as does ambient silicic acid concentration (Hurd and Birdwhistell, 1983; Van Cappellen and Qiu, 1997). However, below 50 m in Jervis Inlet, these factors did not vary significantly ($T = 9^{o} \pm 1^{o}$; $[Si(OH)_4] = 54 - 68\mu M$). Susceptibility to dissolution varies widely between diatom species depending on the specific surface area and morphology of their frustules (e.g.; Lewin, 1961; Kamatini and Riley, 1979; Kamatini, 1980). Furthermore, organic coatings play an important role in protecting biogenic silica from dissolution (e.g.; Lewin, 1961; Bidle and Azam, 1999) and diatom fragmentation by grazing can also greatly accelerate BSi dissolution (Sancetta, 1989a, 1989b; Ragueneau et al., 2000). Indeed, Sancetta (1989c) found that the small and weakly silicified cells in Jervis Inlet were preferentially lost in the water column, while the dense taxa and diatom cysts better survived transit to the deep sediment traps.

The scenario where organic matter is composed of various fractions that decay with different reactivities has been described with the multi-G model (Jørgensen, 1978; Westrich and Berner, 1984), which predicts that changes in the rate constant with time (depth) are

most rapid near t_0 (z_0). Middleburg (1989) found that the power function describes rate constants of organic carbon ranging eight orders of magnitude in age, including laboratory data that had previously been characterised by the quantum-G model (a variant of the multi-G model that considers a finite number of reactive components; Westrich and Berner, 1984). Because the diatom assemblage in Jervis Inlet encompasses diverse taxa with variable susceptibility to dissolution, the power function may also be appropriate to describe changes with depth of biogenic silica rate constants.

In constructing the power function model, changes in k_j with depth are a function of depth:

$$\frac{dk}{dz} = -\beta k_0 z^{(-\beta-1)} . \tag{4.10}$$

β is a dimensionless constant that describes the dependence of k_j on z. Equation 4.10 is written as such so that integration gives the power function:

$$k = k_0 z^{-\beta} . \tag{4.11}$$

The natural logarithm of Equation 4.11 is:

$$\ln(k) = -\beta \ln(z) + \ln(k_0) . \tag{4.12}$$

β and k_0 can thus be determined as the slope and the intercept, respectively, of the regression line of $\ln(k)$ plotted against $\ln(z)$. β is sensitive to z_0, the depth where material begins sinking and equivalent to t_0 of Middleburg (1989). For the curve fitting of Figure 4.4, z_0 was set at 20 m, the approximate depth of 1% surface irradiance during the study (Figure 2.7).

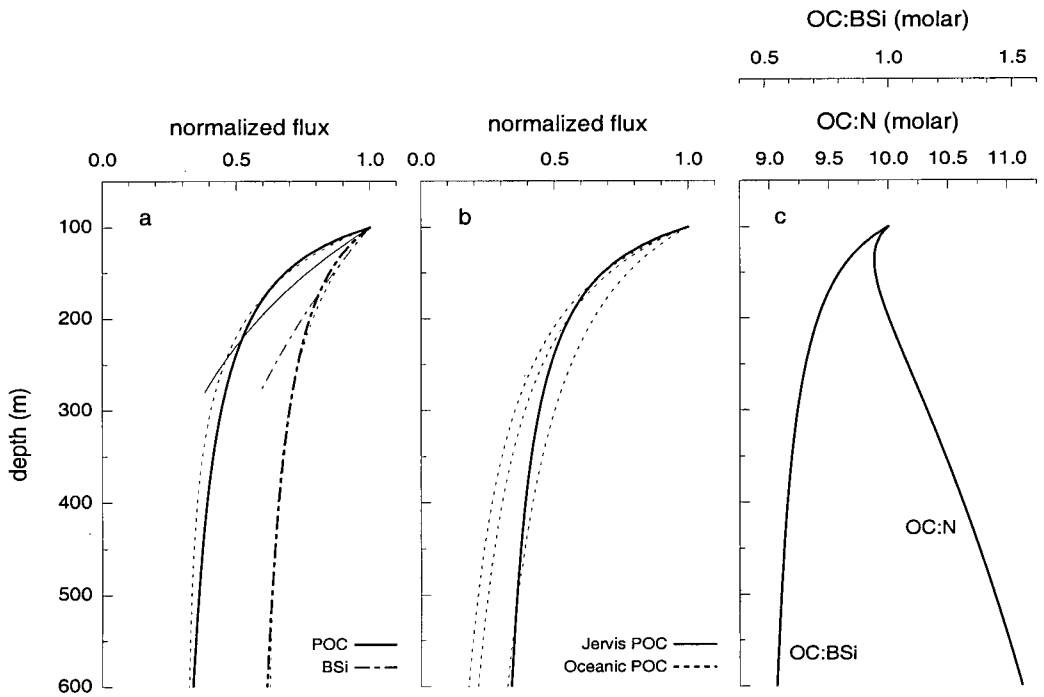

Figure 4.5: Flux versus depth in Jervis Inlet. a. Decrease with depth of the anticipated fluxes of POC and BSi for Jervis Inlet. The curves extending to ~300 m were generated from results from nearby Sechelt Inlet (Timothy and Pond, 1997). The longer curves are from the results of Figure 4.4; heavy lines are from the power-function description of rate constants (Equation 4.14) and light lines are from the exponential description of the rate constants (Equation E.5; the two curves for BSi flux are nearly identical and difficult to differentiate). b. Comparison of the Jervis POC curve with curves published by Martin et al. (1987; central dashed curve), Betzer et al. (1984; right-hand dashed curve) and Suess (1980; left-hand dashed curve). Other oceanic curves (Bishop, 1989) are within the envelope of those presented here. c. Flux ratios with depth in Jervis Inlet.

4.4.2 The anticipated flux

Having fitted the power function of Equation 4.11 to the rate constants of Table C.1, a description of changes in $flux$ with depth can be made.

$$\frac{dj}{dz} = -kj \tag{4.13}$$

Substituting Equation 4.11 into Equation 4.13 and integrating:

$$j = j_1 \exp\left(\frac{-k_0 z^{[-\beta+1]}}{-\beta+1}\right) \qquad (\beta \neq 1)\,. \tag{4.14}$$

Equation 4.14 is a description of the flux that would be observed if additional material did not reach deep sediment traps. From k_0 and β of Figure 4.4, the anticipated fluxes of OC and BSi in Jervis Inlet are given in Figure 4.5. OC:N and OC:BSi ratios of the particulate fraction are also given in Figure 4.5. The OC:BSi ratio of the settling flux decreases with depth, as remineralisation of OC exceeds that of BSi. In general, there is an increase in the particulate OC:N ratio with depth, as N remineralisation occurs slightly more rapidly than carbon, except for the surface-mid and surface-deep depth intervals at station JV-7 (Table C.1). Here, k_C is larger than k_N, though the difference was not significant. Therefore, the surface wiggle in the OC:N-ratio profile is not certain. Nevertheless, Timothy and Pond (1997) found $k_C > k_N$ for a portion of their study, and Harvey et al. (1995) observed that phytoplankton carbohydrates were lost more rapidly than proteins or lipids under oxic conditions during laboratory experiments of organic decay.

The power function is commonly used to describe water-column fluxes of settling material (review by Bishop, 1989) but to my knowledge a treatment such as presented here (using the power function to describe changes in k with depth, and Equation 4.14 for changes in flux with depth) has not been made previously. Although the shape is somewhat different between the curve for organic carbon flux in Jervis Inlet and oceanic

results, the two sets of curves give very similar amounts of decay over a 500 m depth interval. The faster fall-off of decay in Jervis Inlet, compared to the oceanic curves, is due to the small rate constants in the deep waters of Jervis Inlet and not the fitting procedures performed here, as the deepwater rate constants were very well fit by the power function. These small rate constants for OC and N in the deep waters of Jervis Inlet, compared to the oceanic rate constants implied from descriptions of flux (e.g.; Martin et al., 1987), are unlikely a model artifact because the model best described deepwater sediment-trap flux.

In order to evaluate the biogenic silica rate constants from Jervis Inlet, they can be converted to time-dependent dissolution rates (V_{diss}; h^{-1}) by multiplying by the sinking rate. Using a nominal sinking rate of 100 m d^{-1} (Suess, 1980; Fowler and Knauer, 1986; Alldredge and Gostchalk, 1988), the k_{Si} values of Table C.1 were 0.02 h^{-1} at 110 m and decreased to 0.002 h^{-1} at 450 m. These estimates are similar to those measured in the coastal waters off Northwest Africa (0.004-0.023 h^{-1}; Nelson and Goering, 1977), which were the highest dissolution rates reported in a compilation by Ragueneau et al. (2000). The conversion from k_{Si} to V_{diss} is dependent on the sinking rate and an interesting possibility is that sinking was less than 100 m d^{-1} in the upper water column and accelerated into deeper waters. However, it is likely that much of the curvature in the depth profile of k_{Si} (Figure 4.4) was in fact caused by decreasing V_{diss} with depth, as Sancetta (1989c) found that weakly silicified diatoms did not survive the fall into deep waters as well as did the larger diatoms. As noted above, this shift to more heavily silicified taxa occurred in waters with relatively homogeneous temperature and ambient silicic acid concentration.

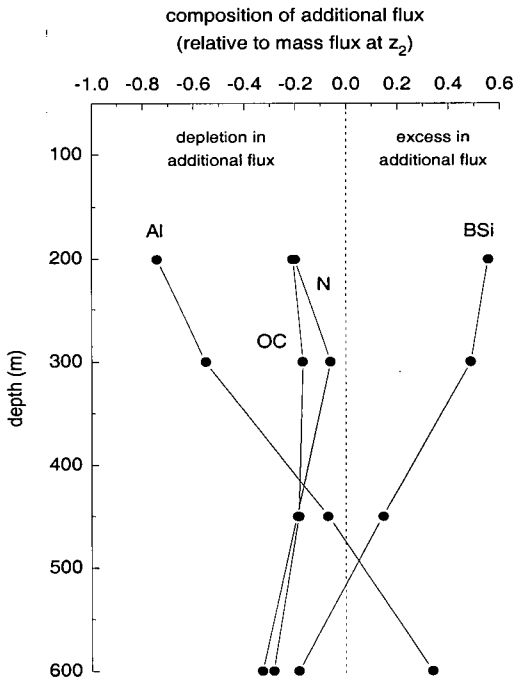

Figure 4.6: Composition of the additional flux in Jervis Inlet relative to the mass flux to the middle and deep sediment traps.

4.4.3 The additional flux in Jervis Inlet

The composition of the additional flux in Jervis Inlet, reported for each depth interval in Table C.1, is plotted relative to the mass flux intercepted by the deep sediment traps in Figure 4.6. Relative to the mass flux, the additional flux was depleted in organic carbon and nitrogen throughout the water column, and became increasingly enriched in aluminosilicates and depleted in biogenic silica with depth (Figure 4.6). The OM depletion is suggestive of diagenetically old sediment, likely resuspended from the boundaries of the fjord, including topographic peaks such as the sill and internal rises (see Figure 1.3). The vertical gradient of the contents of aluminosilicates and BSi may be explained by hydrodynamic sorting of this resuspended material (Smetacek, 1980a). As sediments are lifted away from the topographic boundaries, silts and clay will settle out more quickly than

the diatomaceous debris leaving increasingly BSi-rich sediments as the distance from the the bottom and sides increases.

Using Equation 4.4 and the rate constants of Table C.1, the total additional flux to middle and deep sediment traps has been calculated for each deployment period in Jervis Inlet (Figure 4.7). Bottom water O_2 concentration is plotted with the additional fluxes in Figure 4.7 and shows two large deepwater renewals occurring in the late summer and fall of 1985 and 1988, and a smaller renewal in the fall of 1986. In addition, the beginning of a renewal was observed at the end of the time-series in the fall of 1989, and the gradual O_2 increases in the winter of 1987/88 indicate a mid-depth renewal followed by downward diffusion of O_2 (eg; DeYoung and Pond, 1988). Historically, renewals occur every several years in Jervis Inlet (Lazier, 1963; Pickard, 1975), when dense, oxygen-rich waters penetrate Juan de Fuca and the Strait of Georgia during the summer-fall upwelling season (Chapters 1 and 2). Resuspension during deepwater renewals has been observed in two Norwegian fjords (Skei, 1980) and a Scottish fjord (Stanley et al., 1981).

Additional fluxes to the deep sediment traps were associated with each of the renewals observed in Jervis Inlet, especially at station JV-3 closer to the mouth, and show that the renewal events were sufficiently turbulent to resuspend sediment to depths 50 m off the bottom or carry material as a plume away from the sill and up-inlet. Additional fluxes to mid-depth traps, however, generally did not show peaks during deepwater renewals, although at 200 m at station JV-7 there were relatively large additional fluxes in the fall and winter of 1986/87 corresponding to an oxygen renewal. The additional flux was a substantial portion of the total to 200 m (station JV-7) and 300 m (station JV-3). Certainly with exceptions, the additional flux to the mid-depth traps was a relatively constant fraction of the total flux, suggesting a continual process such as particle focusing (e.g.; Wassmann, 1984; and discussed in Chapter 3) in the narrowing fjord, or regularly occurring resuspension caused by tidal currents. Using a version of the model described

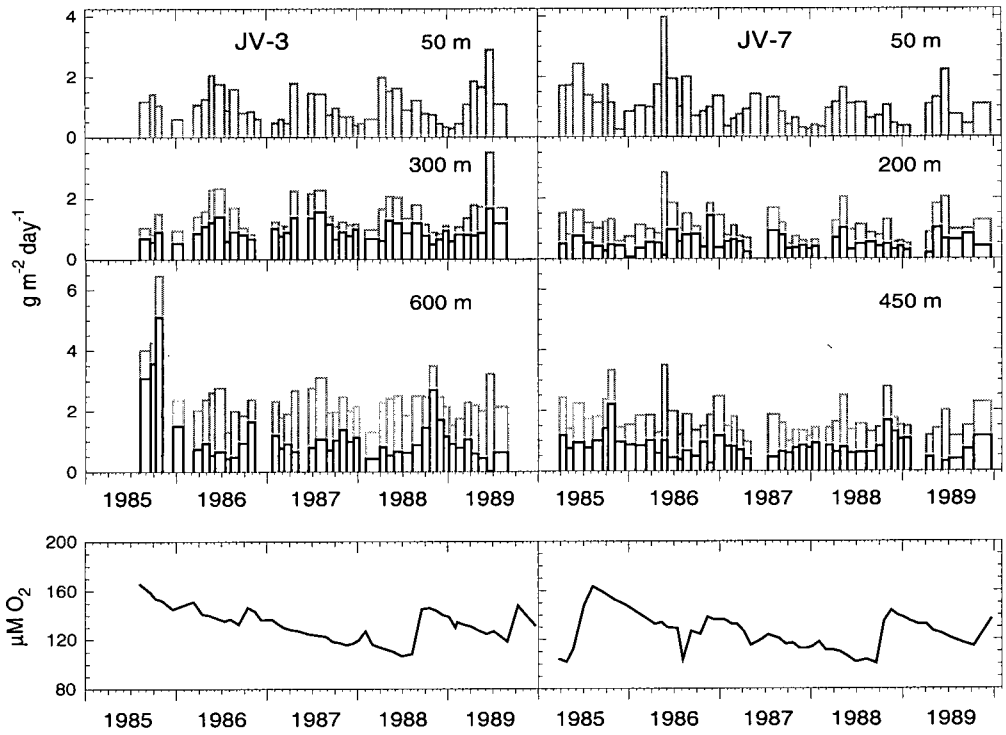

Figure 4.7: The additional flux in Jervis Inlet. Light bars are the total mass flux, dark bars are the additional flux. The additional flux to the deep sediment traps is with respect to the flux at the mid-depth traps. Below is oxygen concentration, showing the timing of deepwater renewals. The oxygen time series are from 650 m at station JV-3, and 500 m at station JV-7. The low O_2 value from JV-7 collected August 6, 1986, was accompanied by a slight *decrease* in density between 400 m and 500 m.

here, Timothy and Pond (1997) suggested that increases in flux with depth in Sechelt Inlet were partly caused by increasing trapping efficiency in deep waters.

4.4.4 The additional flux in Saanich Inlet

Although the solutions of the records from Saanich Inlet are suspect (Appendix D), additional fluxes can be calculated because the distance between the sediment traps was short and, therefore, the terms accounting for water-column decay in Equation 4.4 small. Considering a treatment similar to that of Figure 4.7 for Jervis Inlet, similar results are found in Saanich Inlet (Figure 4.8), where additional-flux peaks often coincide with oxygen-rich intrusions to the depths of the fjord. Although the Al fluxes at station SN-9 showed little seasonality, many of the peaks in the Al flux to 110 m coincided with renewal events. Specifically, the renewals of Feb-Mar, 1985; Aug-Dec, 1985; Aug, 1986 (this event was discussed by Ward and Kilpatrick, 1990); Jul-Aug, 1987 and Jul-Aug 1988 resulted in high additional fluxes to 150 m at station SN-9. Approximately one month later, muted versions of most of these events were recorded at station SN-0.8 near the head of Saanich Inlet (Figure 4.8). Effects of the renewal event of 1986 were observed in September by Ward and Kilpatrick (1990) at a station located in the central basin of Saanich Inlet.

The deepwater renewals were not clearly evident in the magnitude of the additional flux to the mid-depth sediment traps, even though the additional fluxes were significantly larger than to the deep sediment traps. As in Jervis Inlet, the additional flux to mid-depth followed the total flux and was likely the result of particle focusing (Wassmann, 1984; Timothy and Pond, 1997) and increasing trapping efficiency with depth (Smetacek, 1978; Timothy and Pond, 1997; Yu et al., 2001).

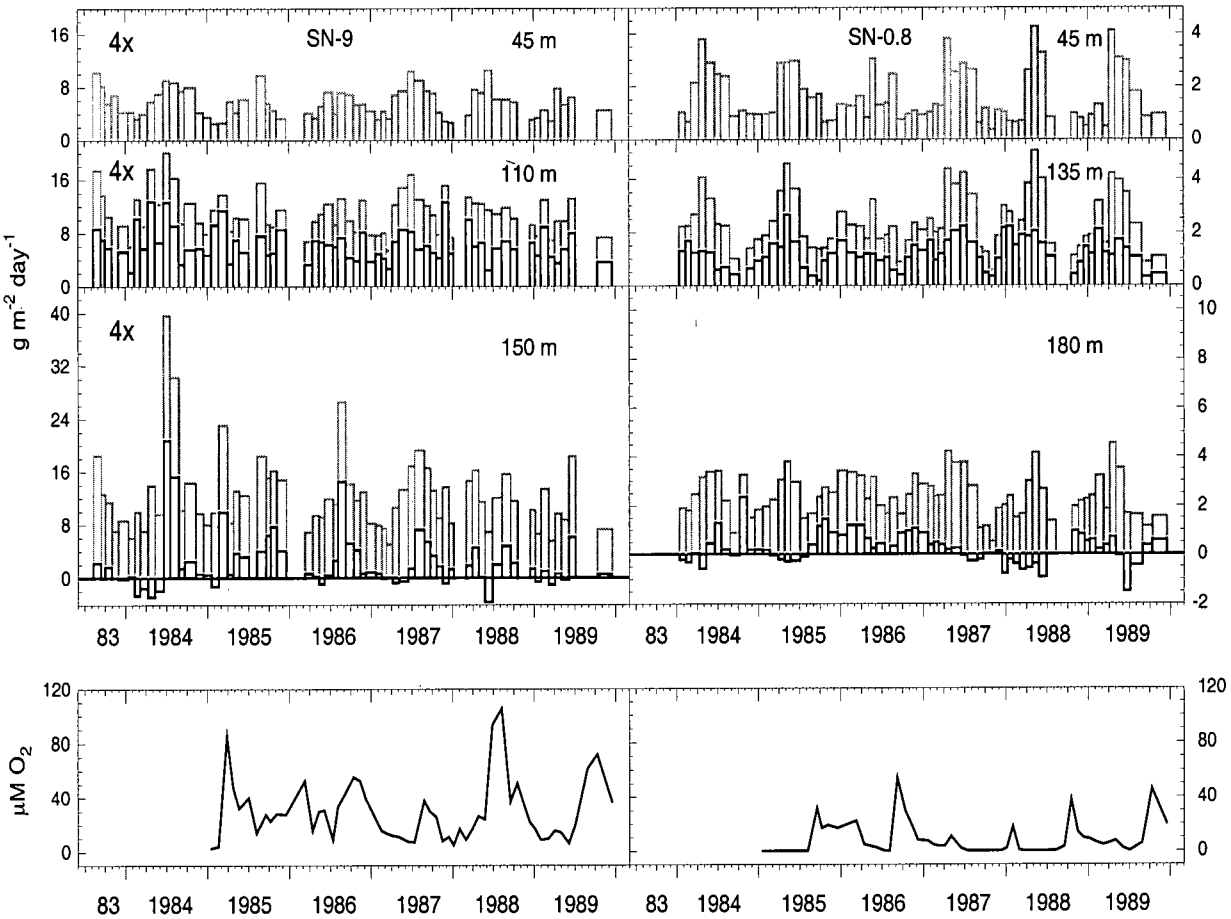

Figure 4.8: The additional flux in Saanich Inlet. Light bars are the total mass flux, dark bars are the additional flux. The additional flux to the deep sediment traps is with respect to the flux at the mid-depth traps. Oxygen concentrations below show intrusions spilling over the sill with weak penetration to station SN-0.8. The oxygen time series are from 140 m at station SN-9, and 190 m at station SN-0.8.

4.5 Conclusions

To my knowledge, there are very few depth-dependent rate constant estimates of organic matter or biogenic silica in the world's oceans. Those of Noriki and Tsunogai (1986) and Walsh et al. (1988b) for the deep ocean are the only explicit estimates of k_C or k_{Si}, and I know of none for the upper water column. However, upper ocean decay rates can be made from the first derivative of the oceanic curves of OC flux shown in Figure 4.5 (Martin et al., 1987). The agreement between the curves described from the k_C values in Jervis Inlet and the oceanic curves suggest, therefore, similarity in the processes causing water column loss of OM. BSi flux has not been described for oceanic and coastal settings to the extent of OC descriptions, but conversion from k_{Si} to V_{diss} using an estimated sinking rate suggests that BSi dissolution was rapid in Jervis Inlet. The model also described the additional flux to deep sediment traps, and it appears two processes largely contributed excess material to deep traps. Turbulent deepwater renewal events periodically contributed debris to deep sediment traps, and other processes such as particle focusing, tidally driven resuspension events and/or increasing trapping efficiency with depth were a continual source of additional fluxes to mid and deep sediment traps.

The model presented in this chapter is able to find decay rates of settling material by quantifying the operationally-defined 'anticipated' and 'additional' fluxes observed during a sediment trap experiment, and thus obviates many of the complications that occur when translating from the observed to the true, downward flux. The advantage of the model is also a weakness, as the rate constants it produces only apply to the material intercepted by sediment traps and measured in the laboratory. The results, therefore, should be considered accurate estimates of rate constants of the measured sinking flux. For example, the rate constants derived for the POM flux are not applicable to the slowly sinking organic matter that was not sampled by the sediment traps, or the fraction of the

rapidly sinking debris that may have been solubilised within the sediment traps (Knauer et al., 1990; Kumar et al., 1996) or during sample processing (i.e.; rinsing with distilled water and centrifugation). Finally, another advantage only recently recognised is the possibility that the error term might be an indication of changes in trapping efficiency with depth. In Jervis Inlet, the different sign of some of the constituent error terms make immediate interpretation difficult, but further application of the model to various data sets may find an explanation.

Chapter 5

Conclusions

This thesis has reported a multi-year time series of primary production and sediment-trap flux collected from Saanich and Jervis Inlets, two fjords of southern British Columbia with contrasting redox environments. The deep waters of Saanich Inlet are seasonally anoxic, even though its flushing rate is relatively high. This condition is rare among BC fjords, so part of the motivation of the study was to determine the cause of anoxia in Saanich Inlet.

Saanich Inlet was significantly more productive than Jervis Inlet, and these high rates of production were likely caused by the unique circulation and mixing of Saanich Inlet and the southern Strait of Georgia. In the summer and fall when nutrients typically limit phytoplankton growth, wind-driven upwelling brings nutrient-rich waters through Juan de Fuca and Haro Straits and toward the mouth of Saanich Inlet. Tidal and isopycnal mixing thus supplies Saanich Inlet with new nutrients, and surface density gradients furthermore pump nutrient-rich waters toward the head of Saanich Inlet as surface salinity at Satellite Channel increases during spring tides. The nutrient supply and high primary production result in large fluxes of diatomaceous debris to the deep waters, likely causing an increased deepwater oxygen demand. Other aspects of the physical oceanography of Saanich Inlet are also conducive to deep water anoxia. Downward mixing of oxygen may be less effective here than in other similar environments, and the weak or negative estuarine flow will tend to trap surface water properties within the fjord. Thus, a larger proportion of the high biomass of the euphotic zone may settle out within the fjord

instead of being transported seaward.

Settling fluxes in Saanich and Jervis Inlets were typical of coastal temperate seas in that the rain of diatomaceous material (biogenic silica and organic matter) was high in the spring and summer, while terrigenous clays and organic matter dominated the fall and winter fluxes. The mooring site near the mouth of Saanich Inlet received significant amounts of material washed into the fjord from the shallow sill of Satellite Channel. In both fjords, sediments from several real or apparent sources were superimposed on the seasonal cycle of diatom production. Deepwater renewals caused high fluxes to the deep sediment traps by resuspending debris from the sills and other topographic features of the fjords. The effect of deepwater renewal was most noticeable at the seaward stations, but weak sedimentary signals of the renewals were also recorded at the landward stations. Other processes caused "additional" fluxes to mid and deep sediment traps on a more continual basis. Particle focusing at depth due to the narrowing cross-sections of the fjords, resuspension caused by regular tidal currents or internal wave breaking, and increased trapping efficiency with depth (an apparent source of sediment to deep traps) likely all participated in the amplification of settling fluxes to the deeper sediment traps.

Several conclusions were obtained from the comparison of primary production, water-column fluxes and the accumulation of material in the bottom sediments. Despite the high water-column fluxes at the mouth of Saanich Inlet, the delivery of biogenic silica and organic carbon to the sediment-water interface at the station inside the sill was not in excess of the other stations if normalised to primary production at each station. Apparently, a sedimentary plume or nepheloid layer extended into Saanich Inlet from the sill and although it certainly deposited material to the sediments, it did not deliver more than did sediment focusing at the other stations. The mass accumulation rate was highest at the same station (proportionally with local primary production), and it is believed that this is why preservation of organic matter and biogenic silica were highest

in the sediments near the sill (Table 3.9). Otherwise, the preservation of organic carbon, nitrogen and biogenic silica were similar in Jervis Inlet (oxygenated surface sediments) and Saanich Inlet (anoxic sediments).

A model designed to estimate decay constants for constituents of the sinking flux and the composition of the material causing increases in flux with depth was applied to the sediment trap time series. Rate constants were inconsistent in Saanich Inlet, perhaps because the depth interval between sediment traps was too small to resolve water-column decay. However, rate constants from Jervis Inlet were self-consistent; organic carbon and nitrogen decayed similarly, and faster than the rate of biogenic silica dissolution, while aluminium rate constants were effectively zero. A power function described changes with depth of the organic carbon, nitrogen and biogenic silica rate constants, suggesting that OM and BSi in Jervis Inlet are composed of various components with different decay rates. The spectrum of organic matter in Jervis Inlet may range from fresh plankton to terrigenous organic matter and diagenetically altered, resuspended organics. For the biogenic silica of diatoms, a range of components dissolving at different rates can be explained by weakly silicified species and small fragmented remains of copepod grazing dissolving in shallow waters, while intact, heavily silicified cells transit the water column with less dissolution. The model also described the additional flux, which appeared to be resuspended and hydrodynamically sorted sediment; it was low in organic matter and became increasingly rich in BSi and depleted in Al away from the benthic boundaries.

A feature of the model that needs further exploration is the error term, ϵ, which may represent changes in trapping efficiency with depth or be influenced by lateral advection across horizontal gradients in the export flux. From the mid-to-deep depth interval in Jervis Inlet, the error terms were negligible, validating the basic assumptions of the model construction for the deep waters of Jervis Inlet. However, for the shallow-to-mid and shallow-to-deep depth intervals, the error terms suggested that, relative to measured

fluxes at 50 m, the anticipated fluxes of organic carbon, nitrogen and aluminium were over-collected in deep water (e.g.; trapping efficiency may have been greater for these constituents in deep water), while the anticipated flux of biogenic silica was under-collected (some process such as horizontal advection caused smaller-than-expected fluxes in deep waters). The meaning of these results (over-collection of OM and Al, under-collection of BSi) is unresolved, but application of the model on other data sets could reveal more of its features.

This time series began when sampling the marine environment with particle interceptors was in its early development. Some features of the experiment were well designed, and from what we have since learned others might be changed if the experiment were repeated. The cylindrical sediment traps were well chosen for these waters subject to high current speeds, although traps with a higher aspect (height to diameter) ratio might have resulted in less hydrodynamic uncertainty due to the possibility of downward mixing to the bottom of the trap. The sediment traps and deployment schedule (monthly) may have been well suited for accurate measurement of the lithic flux and to a lesser degree the rain of biogenic silica. However, it appears as though, at some stage of the sampling procedure, there was a general loss of organic matter; indeed, other studies have shown that a large fraction of particulate organic matter is solubilised within sediment traps while they are still deployed. This artifact is especially severe for sediment traps moored in shallow waters where the intercepted organic matter will tend to be more labile than in deeper waters. Shorter deployment periods, sediment traps with closing sample chambers and subsequent measurement of dissolved organic carbon on the chamber solution to quantify solubilised organic matter, and a more gentle laboratory treatment (without distilled-water rinse and centrifugation) would probably result in higher measured fluxes of organic matter and, to a lesser extent, biogenic silica.

The station locations and depth intervals chosen in Jervis Inlet were excellent, as was

the positioning of station SN-0.8 toward the head of Saanich Inlet. Interesting features of sedimentation off the sill in Saanich Inlet were gleaned from the record from station SN-9, but the time series may have been more significant biologically and geochemically if this mooring had been located in the central basin of Saanich Inlet. This said, the primary production time series at station SN-9 is very valuable as it appears to be from a location of maximal production due to high nutrient supply just inside the sill. The addition of chlorophyll measurements in a future study would certainly be valuable.

An intriguing possibility to obtaining higher depth-resolution of the rate constants determined from the sediment-trap model would be to place more sediment traps on a single mooring. It would be interesting to test the model on data collected from such an arrangement, but also the results from Saanich Inlet may indicate that decay between closely moored sediment traps cannot be resolved by the model. It would also be interesting to test the model on data from many short deployment periods (1/2 week) from a single season to determine the seasonality of rate constants. Such a high resolution data set would also be very telling of the timing of the various sedimentation events in these fjords.

Bibliography

Alldredge, A. L., and Gotschalk, C. (1988). In situ settling behavior of marine snow. Limnology and Oceanography, 33(3), 339-351.

Alldredge, A. L., Passow, U., and Logan, B. E. (1993). The abundance and significance of a class of large, transparent organic particles in the ocean. Deep-Sea Research I, 40(6), 1131-1140.

Anderson, J. J., and Devol, A. H. (1973). Deep water renewal in Saanich Inlet, an intermittently anoxic basin. Estuarine and Coastal Marine Science, 1, 1-10.

Anderson, R.F., Rowe, G.T., Kemp, P.F., Trumbore, S., Biscaye, P.E. (1994). Carbon budget for the mid-slope depocenter of the Middle Atlantic Bight. Deep-Sea Research II, 41(2/3), 669-703.

Baker, E. T., Milburn, H. B., and Tennant, D. A. (1988). Field assessment of sediment trap efficiency under varying flow conditions. Journal of Marine Research, 46(3), 573-592.

Baumgartner, T., Crusius, J., Thomson, R., Holmgren, D., Francis, R., Soutar, A., Ferreira, V., and Field, J. (in review). A sedimentary record of small pelagic fish abundances from the west coast of Vancouver Island. Canadian Journal of Fisheries and Aquatic Sciences.

Berner, R. A. (1982). Burial of organic carbon and pyrite sulfur in the modern ocean: its geochemical and environmental significance. American Journal of Science, 282, 451-473.

Berner, R. A. (1989). Biogeochemical cycles of carbon and sulfur and their effect on atmospheric oxygen over Phanerozoic time. Palaeogeography, Palaeoclimatology, Palaeoecology, 73, 97-122.

Betzer, P. R., Showers, W. J., Laws, E. A., Winn, C. D., DiTullio, G. R., and Kroopnick, P. M. (1984). Primary productivity and particle fluxes on a transect of the equator at 153°W in the Pacific Ocean. Deep-Sea Research, 31(1), 1-11.

Bidigare, R. R., Fluegge, A., Freeman, K. H., Hanson, K. L., Hayes, J. M., Hollander, D., Jasper, J. P., King, L. L., Laws, E. A., Milder, J., Millero, F. J., Pancost, R., Popp, B. N., Steinberg, P. A., and Wakeham, S. G. (1997). Consistent fractionation of ^{13}C in nature and in the laboratory: Growth-rate effects in some haptophyte algae. Global Biogeochemical Cycles, 11(2), 279-292.

Bidle, K. D., and Azam, F. (1999). Accelerated dissolution of diatom silica by marine bacterial assemblages. Nature, 397, 508-512.

Bishop, J. K. B. (1989). Regional extremes in particulate matter composition and flux: effects on the chemistry of the ocean interior. Productivity of the Oceans: Present and Past, W. H. Berger, V. S. Smetacek, and G. Wefer, eds., John Wiley and Sons Limited, 117-137.

Bloesch, J. (1982). Inshore-offshore sedimentation differences resulting from resuspension in the eastern basin of Lake Erie. Canadian Journal of Fisheries and Aquatic Sciences, 39, 748-759.

Blomqvist, S., and Køfoed, C. (1981). Sediment trapping - A subaquatic in situ experiment. Limnology and Oceanography, 26(3), 585-590.

Blomqvist, S., and Larsson, U. (1994). Detrital bedrock elements as tracers of settling resuspended particulate matter in a coastal area of the Baltic Sea. Limnology and Oceanography, 39(4), 880-896.

Bornhold, B. D., Ren, P., and Prior, D. B. (1994). High-frequency turbidity currents in British Columbia fjords. Geo-Marine Letters, 14, 238-243.

Bornhold, E. A. (2000). Interannual and interdecadal patterns in timing and abundance of phytoplankton and zooplankton in the central Strait of Georgia, BC: with special reference to *Neocalanus plumchrus*, M.Sc., UBC.

Boyd, P., and Newton, P. (1995). Evidence of the potential influence of planktonic community structure on the interannual variability of particulate organic carbon flux. Deep-Sea Research I, 42(5), 619-639.

Bruland, K. W. (1974). Pb-210 geochronology in the coastal margin environment, Ph.D., University of California.

Brzezinski, M. A. (1985). The Si:C:N ratio of marine diatoms: interspecific variability and the effect of some environmental variables. Journal of Phycology, 21, 347-357.

Buck, K. R., and Newton, J. (1995). Fecal pellet flux in Dabob Bay during a diatom bloom: Contribution of microzooplankton. Limnology and Oceanography, 40(2), 306-315.

Buesseler, K. O. (1991). Do upper-ocean sediment traps provide an accurate record of particle flux? Nature, 353, 420-423.

Buesseler, K. O., Michaels, A. F., Siegel, D.A., Knap, A.H. (1994). A three dimensional time-dependent approach to calibrating sediment trap fluxes. Global biogeochemical cycles, 8(2), 179-193.

Buesseler, K. O., Steinberg, D. K., Michaels, A. F., Johnson, R. J., Andrews, J. E., Valdes, J. R., and Price, J. F. (2000). A comparison of the quantity and composition of material caught in a neutrally buoyant versus surface-tethered sediment trap. Deep-Sea Research I, 47, 277-294.

Burdige, D. J., and Martens, C. S. (1988). Biogeochemical cycling in an organic-rich coastal marine basin: 10. The role of amino acids in sedimentary carbon and nitrogen cycling. Geochimica et Cosmochimica Acta, 52, 1571-1584.

Burkhardt, S., Riebesell, U., and Zondervan, I. (1999). Effects of growth rate, CO_2 concentration, and cell size on the stable carbon isotope fractionation in marine phytoplankton. Geochimica et Cosmochimica Acta, 63(22), 3729-3741.

Burrell, D. C. (1983). Patterns of carbon supply and distribution and oxygen renewal in two Alaskan fjords. Sedimentary Geology, 36, 93-115.

Burrell, D. C. (1988). Carbon flow in fjords. Oceanography and Marine Biology Annual Review, 26, 143-226.

Butman, C. A. (1986). Sediment trap biases in turbulent flows: Results from a laboratory flume study. Journal of Marine Research, 44(3), 645-693.

Butman, C. A., Grant, W. D., and Stolzenbach, K. D. (1986). Predictions of sediment trap biases in turbulent flows: A theoretical analysis based on observations from the literature. Journal of Marine Research, 44(3), 601-644.

Calvert, S. E., and Pedersen, T. F. (1992). Organic carbon accumulation and preservation in marine sediments: how important is anoxia? Organic Matter: Productivity, Accumulation, and Preservation in Recent and Ancient Sediments, J. K. Whelan and J. W. Farrington, eds., Columbia University Press, 231-263.

Calvert, S. E., Pedersen, T. F., and Karlin, R. E. (2001). Geochemical and isotopic evidence for post-glacial palaeoceanographic changes in Saanich Inlet, British Columbia. Marine Geology, 174, 287-305.

Clifford, P. J., Harrison, P. J., St. John, M. A., Yin, K., and Albright, L. J. (1991). Plankton production and nutrient dynamics in the Fraser River Plume, 1989. Manuscript report no. 54, University of British Columbia.

Clifford, P. J., Harrison, P. J., Yin, K., St. John, M. A., and Goldblatt, R. H. (1992). Plankton production and nutrient dynamics in the Fraser River Plume, 1991. Volume 1. Manuscript report no. 59, University of British Columbia.

Cochlan, W. P., Harrison, P. J., Thompson, P. A., and Parsons, T. R. (1986). Preliminary observations of the summer production of three British Columbian coastal inlets. Sarsia,

71, 161-168.

Conley, D. J., and Malone, T. C. (1992). Annual cycle of dissolved silicate in Chesapeake Bay: implications for the production and fate of phytoplankton biomass. Marine Ecology Progress Series, 81, 121-128.

Corner, E. D. S., and Davies, A. G. (1971). Plankton as a factor in the nitrogen and phosphorus cycles in the sea. Advances in Marine Biology, 9, 101-204.

Cowie, G. L., and Hedges, J. I. (1992). The role of anoxia in organic matter preservation in coastal sediments: relative stabilities of the major biochemicals under oxic and anoxic depositional conditions. Advances in Organic Geochemistry, 19(1-3), 229-234.

Cowie, G. L., Hedges, J. I., and Calvert, S. E. (1992). Sources and relative reactivities of amino acids, neutral sugars, and lignin in an intermittently anoxic marine environment. Geochimica et Cosmochimica Acta, 56, 1963-1978.

Crusius, J., and Anderson, R. F. (1995). Sediment focusing in six small lakes inferred from radionuclide profiles. Paleolimnology, 13, 143-155.

Dagg, M. J., Frost, B. W., and Walser, W. E. J. (1989). Copepod diel migration, feeding, and the vertical flux of pheopigments. Limnology and Oceanography, 34(6), 1062-1071.

de Young, B., and Pond, S. (1988). The deepwater exchange cycle in Indian Arm, British Columbia. Estuarine, Coastal and Shelf Science, 26, 285-308.

Deines, P. (1980). The isotopic composition of reduced organic carbon. Handbook of Environmental Isotope Geochemistry, P. Fritz and J. C. Fontes, eds., Elsevier Scientific, Amsterdam, 329-406.

Del Amo, Y., Quéguiner, B., Treguer, P., Breton, H., and Lampert, L. (1997). Impacts of high-nitrate freshwater inputs on macrotidal ecosystems. II. Specific role of the silicic acid pump in the year-round dominance of diatoms in the Bay of Brest (France). Marine Ecology Progress Series, 161, 225-237.

DeNiro, M. J., and Epstein, S. (1978). Influence of diet on the distribution of carbon isotopes in animals. Geochimica et Cosmochimica Acta, 42, 495-506.

Deuser, W. G., Muller-Karger, F. E., and Hemleben, C. (1988). Temporal variations of particle fluxes in the deep subtropical and tropical North Antlantic: Eulerian versus Lagrangian effects. Journal of Geophysical Research, 93(C6), 6857-6862.

Deuser, W. G. (1996). Temporal variability of particle flux in the deep Sargasso Sea. Particle Flux in the Ocean, V. Ittekkot, P. Schafer, S. Honjo, and P. J. Depetris, eds., John Wiley and Sons, Chichester, 185-198.

Downs, J.N. (1989). Export production in oceanic systems: Information from phaeopigment, carbon and nitrogen analyses, Ph.D., University of Washington.

Dugdale, R. C., and Goering, J. J. (1967). Uptake of new and regenerated forms of nitrogen in primary productivity. Limnology and Oceanography, 12(2), 196-206.

Dymond, J. (1984). Sediment traps, particle fluxes, and benthic boundary layer processes. Global Ocean Flux Study, Woods Hole, MA, 260-284.

Emerson, S. (1980). Redox species in a reducing fjord: the oxidation rate of manganese II. Fjord Oceanography, H. J. Freeland, D. M. Farmer, and C. D. Levings, eds., Plenum Press, New York, 681-687.

Emerson, S., Quay, P. D., Stump, C., Wilbur, D., and Schudlich, R. (1995). Chemical tracers of productivity and respiration in the subtropical Pacific Ocean. Journal of Geophysical Research, 100(C8), 15,873-15,887.

Eppley, R. W., and Peterson, B. J. (1979). Particulate organic matter flux and planktonic new production in the deep ocean. Nature, 282, 677-680.

Falkowski, P. G., Biscaye, P. E., and Sancetta, C. (1994). The lateral flux of biogenic particles from the eastern North American continental margin to the North Atlantic Ocean. Deep-Sea Research II, 41(2/3), 583-601.

Fleming, R. H. (1940). Composition of plankton and units for reporting populations and production. Proceedings of the Sixth Pacific Science Congress of the Pacific Science Association, University of California and Stanford, 535-540.

Fowler, S. W., and Knauer, G. A. (1986). Role of large particles in the transport of elements and organic compounds through the oceanic water column. Progress in Oceanography, 16, 147-194.

François, R. (1987). Some aspects of the geochemistry of sulphur and iodine in marine humic substances and transition metal enrichment in anoxic sediments, Ph.D., UBC.

François, R. (1988). A study on the regulation of the concentrations of some trace metals (Rb, Sr, Zn, Pb, Cu, V, Cr, Ni, Mn,and Mo) in Saanich Inlet sediments, British Columbia, Canada. Marine Geology, 83, 285-308.

Fry, B., and Wainright, S. C. (1991). Diatom sources of ^{13}C-rich carbon in marine food webs. Marine Ecology Progress Series, 76, 149-157.

Gardner, W. D. (1980a). Field assessment of sediment traps. Journal of Marine Research, 38(1), 41-52.

Gardner, W. D. (1980b). Sediment trap dynamics and calibration: a laboratory evaluation.

Journal of Marine Research, 38(1), 17-39.

Gardner, W. D. (1985). The effects of tilt on sediment trap efficiency. Deep-Sea Research, 32(3), 349-361.

Gardner, W. D., and Zhang, Y. (1997). The effect of brine on the collection efficiency of cylindrical sediment traps. Journal of Marine Research, 55, 1029-1048.

Gibbs, R. J., and Konwar, L. (1986). Coagulation and settling of Amazon river suspended sediment. Continental Shelf Research, 6(1/2), 127-149.

Gilmartin, M. (1964). The primary production of a British Columbia fjord. Journal of the Fisheries Research Board of Canada, 21(3), 505-538.

Goñi, M. A., Ruttenberg, K. C., and Eglinton, T. I. (1997). Sources and contributions of terrigenous organic carbon to surface sediments in the Gulf of Mexico. Nature, 389, 275-278.

Goñi, M. A., Ruttenberg, K. C., and Eglinton, T. I. (1998). A reassessment of the sources and importance of the land-derived organic matter in surface sediments from the Gulf of Mexico. Geochimica et Cosmochimica Acta, 62(18), 3055-3075.

Griffin, D. A., and LeBlond, P. H. (1990). Estuary/ocean exchange controlled by spring-neap tidal mixing. Estuarine, Coastal and Shelf Science, 30, 275-297.

Gucluer, S. M., and Gross, M. G. (1964). Recent marine sediments in Saanich Inlet, a stagnant marine basin. Limnology and Oceanography, 9(2), 359-376.

Guillard, R. R. L., and Kilham, P. (1977). The ecology of marine planktonic diatoms. The Biology of Diatoms, D. Werner, eds., Blackwell Scientific, Oxford, 372-469.

Gust, G., Byrne, R. H., Bernstein, R. E., Betzer, P. R., and Bowles, W. (1992). Particle fluxes and moving fluids: experience from synchronous trap collections in the Sargasso Sea. Deep-Sea Research, 39(7/8), 1071-1083.

Gust, G., Michaels, A. F., Johnson, R., Deuser, W. G., and Bowles, W. (1994). Mooring line motions and sediment trap hydromechanics: in situ intercomparison of three common deployment designs. Deep-Sea Research I, 41(5/6), 831-857.

Haigh, R., Taylor, F. J. R., and Sutherland, T. F. (1992). Phytoplankton ecology of Sechelt Inlet, a fjord system on the British Columbia coast. I. General features of the nano- and microplankton. Marine Ecology Progress Series, 89, 117-134.

Håkanson, L., Floderus, S., and Wallin, M. (1989). Sediment trap assemblages - a methodological description. Hydrobiologia, 176/177, 481-490.

Hansen, J. L. S., Timm, U., and Kiørboe, T. (1995). Adaptive significance of phytoplankton stickiness with emphasis on the diatom *Skeletonema costatum.* Marine Biology, 123, 667-676.

Hargrave, B. T., and Burns, N. M. (1979). Assessment of sediment trap collection efficiency. Limnology and Oceanography, 24(6), 1124-1136.

Hargrave, B. T., Bodungen, B., Stoffyn-Egli, P., and Mudis, P. J. (1994). Seasonal variability in particle sedimentation under permanent ice cover in the Arctic Ocean. Continental Shelf Research, 14, 279-293.

Harrison, P. J., Fulton, J. D., Taylor, F. J. R., and Parsons, T. R. (1983). Review of the biological oceanography of the Strait of Georgia: pelagic environment. Canadian Journal of Fisheries and Aquatic Sciences, 40, 1064-1094.

Harrison, P. J., Clifford, P. J., Cochlan, W. P., Yin, K., St. John, M. A., Thompson, P. A., Sibbald, M. J., and Albright, L. J. (1991). Nutrient and plankton dynamics in the Fraser River plume, Strait of Georgia, British Columbia. Marine Ecology Progress Series, 70, 291-304.

Harrison, W. G., Platt, T., and Lewis, M. R. (1987). f-Ratio and its relationship th ambient nitrate concentration in coastal waters. Journal of Plankton Research, 9(1), 235-248.

Harvey, H. R., Tuttle, J. H., and Bell, J. T. (1995). Kinetics of phytoplankton decay during simulated sedimentation: Changes in biochemical composition and microbial activity under oxic and anoxic conditions. Geochimica et Cosmochimica Acta, 59(16), 3367-3377.

Hawley, N. (1988). Flow in cylindrical sediment traps. Journal of Great Lakes Research, 14(1), 76-88.

Hecky, R. E., Mopper, K., Kilham, P., and Degens, E. T. (1973). The amino acid and sugar composition of diatom cell-walls. Marine Biology, 19, 323-331.

Hedges, J. I., Clark, W. A., Quay, P. D., Richey, J. E., Devol, A. H., and Santos, U. d. M. (1986). Compositions and fluxes of particulate organic material in the Amazon River. Limnology and Oceanography, 31(4), 717-738.

Hedges, J. I., Clark, W. A., and Cowie, G. L. (1988a). Organic matter sources to the water column and surficial sediments of a marine bay. Limnology and Oceanography, 33(5), 1116-1136.

Hedges, J. I., Clark, W. A., and Cowie, G. L. (1988b). Fluxes and reactivities of organic matter in a coastal marine bay. Limnology and Oceanography, 33(5), 1137-1152.

Hedges, J. I., and Bergamaschi, B. A. (1992). Seawater carbon measurement. Nature, 359,

202.

Hedges, J. I., and Keil, R. G. (1995). Sedimentary organic matter preservation: an assessment and speculative synthesis. Marine Chemistry, 49, 81-115.

Herlinveaux, R. H. (1962). Oceanography of Saanich Inlet in Vancouver Island, British Columbia. Journal of the Fisheries Research Board of Canada, 19(1), 1-37.

Hill, P. S., Milligan, T. G., and Geyer, W. R. (2000). Controls on effective settling velocity of suspended sediment in the Eel River flood plume. Continental Shelf Research, 20(C2), 2095-2111.

Hobson, L. A. (1981). Seasonal variations in maximum photosynthetic rates of phytoplankton in Saanich Inlet, Vancouver Island, British Columbia. Journal of Experimental Marine Biology and Ecology, 52, 1-13.

Hobson, L. A. (1983). Phytoplankton crops, bacterial metabolism and oxygen in Saanich Inlet, a fjord in Vancouver Island, British Columbia. Sedimentary Geology, 36, 117-130.

Hobson, L. A. (1985). Seasonal variations and spatial gradients of nitrogenous nutrients in waters of southeastern Vancouver Island, British Columbia, Canada. Netherlands Journal of Sea Research, 19(3/4), 251-256.

Hobson, L. A., and McQuoid, M. R. (1997). Temporal variations among plankton diatom assemblages in a turbulent environment of the southern Strait of Georgia, British Columbia, Canada. Marine Ecology Progress Series, 150, 263-274.

Hobson, L. A., and McQuoid, M. R. (2001). Pelagic diatom assemblages are good indicators of mixed water intrusions into Saanich Inlet, a stratified fjord in Vancouver Island. Marine Geology, 174, 125-138.

Honjo, S., Spencer, D. W., and Gardner, W. D. (1992). A sediment trap intercomparison experiment in the Panama Basin, 1979. Deep-Sea Research, 39(2), 333-358.

Hopkins, C. C. E. (1981). Ecological investigations on the zooplankton community of Balsfjorden, Northern Norway: changes in zooplankton abundance and biomass in relation to phytoplankton and hydrography, March 1976-February 1977. Kieler Meeresforschungen Sonderheft, 5(124-139).

Huntley, M. E., and Hobson, L. A. (1978). Medusa predation and plankton dynamics in a temperate fjord, British Columbia. Journal of the Fisheries Research Board of Canada, 35, 257-261.

Hurd, D. C., and Birdwhistell, S. (1983). On producing a more general model for biogenic silica dissolution. American Journal of Science, 283, 1-28.

Iseki, K., Whitney, F., and Wong, C.S. (1980). Biochemical changes of sedimented matter in sediment trap in shallow coastal waters. Bulletin of Plankton Society of Japan, 27(1), 27-36.

Ittekkot, V. (1993). The abiotically driven biological pump in the ocean and short-term fluctuations in atmospheric CO_2 contents. Global Planetary Change, 8, 17-25.

Jacobson, D. M., and Anderson, D. M. (1986). Thecate heterotrophic dinoflagellates: feeding behavior and mechanisms. Journal of Phycology, 22, 249-258.

Jørgensen, B. B. (1978). A comparison of methods for the quantification of bacterial sulfate reduction in coastal marine sediments II. calculation from mathematical models. Geomicrobiology Journal, 1(1), 29-47.

Jumars, P. A., Penry, D. L., Baross, J. A., Perry, M. J., and Frost, B. W. (1989). Closing the microbial loop: dissolved carbon pathway to heterotrophic bacteria from incomplete ingestion, digestion and absorption in animals. Deep-Sea Research, 36, 483-495.

Kamatani, A., and Riley, J. P. (1979). Rate of dissolution of diatom silica walls in seawater. Marine Biology, 55, 29-35.

Kamatani, A., Riley, J. P., and Skirrow, G. (1980). The dissolution of opaline silica of diatom tests in seawater. Journal of the Oceanographical Society of Japan, 36, 201-208.

Karl, D. M., Knauer, G. A., and Martin, J. H. (1988). Downward flux of particulate organic matter in the ocean: a particle decomposition paradox. Nature, 332(6163), 438-441.

Karl, D. M., and Knauer, G. A. (1989). Swimmers: a recapitulation of the problem and a potential solution. Oceanography, 32-35.

Kineke, G. C., Sternberg, R. W., and Johnson, R. (1989). A new instrument for measuring settling velocities in situ. Marine Geology, 90, 149-158.

Kiørboe, T., Lundsgaard, C., Olesen, M., and Hansen, J. L. S. (1994). Aggregation and sedimentation processes during a spring phytoplankton bloom: A field experiment to test coagualation theory. Journal of Marine Research, 52, 297-323.

Kiørboe, T., Hansen, J. L. S., Alldredge, A. L., Jackson, G. A., Passow, U., Dam, H. G., Drapeau, D. T., Waite, A., and Garcia, C. M. (1996). Sedimentation of phytoplankton during a diatom bloom: Rates and mechanisms. Journal of Marine Research, 54, 1123-1148.

Knauer, G. A., Karl, D. M., Martin, J. H., and Hunter, C. N. (1984). In situ effects of selected preservatives on total carbon, nitrogen and metals collected in sediment traps. Journal of Marine Research, 42(2), 445-462.

Knauer, G., and Asper, V. (1989). Sediment trap technology and sampling: report of the U.S. GOFS working group on sediment trap technology and sampling, November 1988. U.S. GOFS Planning Report Number 10.

Knauer, G. A., Redalje, D. G., Harrison, W. G., and Karl, D. M. (1990). New production at the VERTEX time-series site. Deep-Sea Research, 37(7), 1121-1134.

Koeller, P. A., Barwell-Clarke, J. E., Whitney, F., and Takahashi, M. (1979). Winter condition of marine plankton populations in Saanich Inlet, B.C., Canada. III. Mesozooplankton. Journal of Experimental Marine Biology and Ecology, 37, 161-174.

Kukert, H., and Riebesell, U. (1998). Phytoplankton carbon isotope fractionation during a diatom spring bloom in a Norwegian fjord. Marine Ecology Progress Series, 173, 127-137.

Kumar, N., Anderson, R. F., and Biscaye, P. E. (1996). Remineralization of particulate authigenic trace metals in the Middle Atlantic Bight: Implications for proxies of export production. Geochimica et Cosmochimica Acta, 60(18), 3383-3397.

Lampitt, R. S., Newton, P. P., Jickells, T. D., Thomson, J., and King, P. (2000). Near-bottom particle flux in the abyssal northeast Atlantic. Deep-Sea Research II, 47, 2051-2071.

Langdon, C. (1993). The significance of respiration in production measurements based on oxygen. Measurement of Primary Production from the Molecular to the Global Scale, La Rochelle, 69-78.

Lau, Y. L. (1979). Laboratory study of cylindrical sedimentation traps. Journal of the Fisheries Research Board of Canada, 36, 1288-1291.

Laws, E. A., and Archie, J. W. (1981). Appropriate use of regression analysis in marine biology. Marine Biology, 65, 13-16.

Laws, E. A., DiTullio, G. R., Betzer, P. R., Karl, D. M., and Carder, K. L. (1989). Autotrophic production and elemental fluxes at 26°N, 155°W in the North Pacific subtropical gyre. Deep-Sea Research, 36(1), 103-120.

Laws, E. A., Popp, B. N., Bidigare, R. R., Kennicutt, M. C., and Macko, S. A. (1995). Dependence of phytoplankton carbon isotopic composition on growth rate and $[CO_2]$aq: Theoretical considerations and experimental results. Geochimica et Cosmochimica Acta, 59(6), 1131-1138.

Lawson, D. S., Hurd, D. C., and Pankratz, H. S. (1978). Silica dissolution rates of decomposing phytoplankton assemblages at various temperatures. American Journal of Science, 278, 1373-1393.

Lazier, J. R. N. (1963). Some aspects of the oceanographic structure of the Jervis Inlet system, M.Sc., U.B.C.

LeBlond, P. H., Griffin, D. A., and Thomson, R. E. (1994). Surface salinity variations in the Juan de Fuca Strait: test of a predictive model. Continental Shelf Research, 14(1), 37-56.

Lee, C., Wakeham, S. G., and Hedges, J. I. (1988). The measurement of oceanic particle flux - are "swimmers" a problem? Oceanography, 34-36.

Lee, C., Hedges, J. I., Wakeman, S. G., and Zhu, N. (1992). Effectiveness of various treatments in retarding microbial activity in sediment trap material and their effects on the collection of swimmers. Limnology and Oceanography, 37(1), 117-130.

Lewin, J. C. (1961). The dissolution of silica from diatom walls. Geochimica et Cosmochimica Acta, 21, 182-198.

Lewis, A. G. (1978). Concentrations of nutrients and chlorophyll on a cross-channel transect in Juan de Fuca Strait, British Columbia. Journal of the Fisheries Research Board of Canada, 35, 305-314.

Lewis, A. G., and Thomas, A. C. (1986). Tidal transport of planktonic copepods across the sill of a British Columbia fjord. Journal of Plankton Research, 8(6), 1079-1089.

Lilley, M. D., Baross, J. A., and Gordon, L. I. (1982). Dissolved methane and hydrogen in Saanich Inlet, British Columbia. Deep-Sea Research, 29(12A), 1471-1484.

Liu, K. K., Iseki, K., and Chao, S. Y. (2000). Continental margin carbon fluxes. The changing ocean carbon cycle, R. B. Hanson, H. W. Ducklow, and J. G. Field, eds., Cambridge University Press, Cambridge, 187-239.

Mackas, D. L., Denman, K. L., and Bennett, A. F. (1987). Least squares multiple tracer analysis of water mass composition. Journal of Geophysical Research, 92(C3), 2907-2918.

Mackas, D. L., and Harrison, P. J. (1997). Nitrogenous nutrient sources and sinks in the Juan de Fuca Strait/Strait of Georgia/Puget Sound estuarine system: assessing the potential for eutrophication. Estuarine, Coastal and Shelf Science, 44, 1-21.

Margalef, R. (1958). Temporal succession and spatial heterogeneity in phytoplankton. Perspectives in Marine Biology, A. A. Buzzati-Traverso, eds., University of California Press, Berkeley and Los Angeles, 323-349.

Mark, D. M., and Church, M. (1977). On the misuse of regression in earth science. Mathematical Geology, 9(1), 63-75.

Martin, J. H., Knauer, G. A., Karl, D. M., and Broenkow, W. W. (1987). VERTEX:

carbon cycling in the northeast Pacific. Deep-Sea Research, 34(2), 267-285.

Masson, D., and Cummins, P. F. (1999). Numerical simulations of a buoyancy-driven coastal countercurrent off Vancouver Island. Journal of Physical Oceanography, 29, 418-435.

McCave, I. N. (1975). Vertical flux of particles in the ocean. Deep-Sea Research, 22, 491-502.

McKee, B., and Skei, J. (1999). Framvaren Fjord as a natural laboratory for examining biogeochemical processes in anoxic environments. Marine Chemistry, 67, 147-148.

McQuoid, M. R., and Hobson, L. A. (1995). Importance of resting stages in diatom seasonal succession. Journal of Phycology, 31, 44-50.

Meybeck, M. (1982). Carbon, nitrogen and phosphorus transport by world rivers. American Journal of Science, 282, 401-450.

Michaels, A. F., Silver, M. W., Gowing, M. M., and Knauer, G. A. (1990). Cryptic zooplankton "swimmers" in upper ocean sediment traps. Deep-Sea Research, 37(8), 1285-1296.

Michaels, A. F., Bates, N. R., Buesseler, K. O., Carlson, C. A., and Knap, A. H. (1994). Carbon-cycle imbalances in the Sargasso Sea. Nature, 372, 537-540.

Middleburg, J. J. (1989). A simple rate model for organic matter decomposition in marine sediments. Geochimica et Cosmochimica Acta, 53, 1577-1581.

Middleburg, J. J., Soetaert, K., and Herman, P. M. (1997). Emperical relationships for use in global diagenetic models. Deep-Sea Research I, 44(2), 327-344.

Milligan, T. G. (1995). An examination of the settling behaviour of a flocculated suspension. Netherlands Journal of Sea Research, 33(2), 163-171.

Mortlock, R. A., and Froelich, P. N. (1989). A simple method for the rapid determination of biogenic opal in pelagic marine sediments. Deep-Sea Research, 36(9), 1415-1426.

Nelson, D. M., and Goering, J. J. (1977). Near-surface silica dissolution in the upwelling region off northwest Africa. Deep-Sea Research, 24, 65-73.

Nelson, D. M., Tréguer, P., Brzezinski, M. A., Leynaert, A., and Quéguiner, B. (1995). Production and dissolution of biogenic silica in the ocean: Revised global estimates, comparisons with regional data and relationship to biogenic sedimentation. Global Biogeochemical Cycles, 9(3), 359-372.

Nodder, S. D., and Alexander, B. L. (1999). The effects of multiple trap spacing, baffles

and brine volume on sediment trap collection efficiency. Journal of Marine Research, 57, 537-559.

Noji, T. T., Estep, K. W., MacIntyre, F., and Norrbin, F. (1991). Image analysis of faecal material grazed upon by three species of copepods: evidence for coprohexy, coprophagy and coprochaly. Journal of the Marine Biological Association of the United Kingdom, 71, 465-480.

Noji, T. T., Børsheim, K. Y., Rey, F., and Nortvedt, R. (1999). Dissolved organic carbon associated with sinking particles can be crucial for estimates of vertical carbon flux. Sarsia, 84, 129-135.

Noriki, S., Ishimori, N., and Tsunogai, S. (1985). Regeneration of chemical elements from settling particles collected by sediment trap in Funka Bay, Japan. Journal of the Oceanographical Society of Japan, 41, 113-120.

Noriki, S., and Tsunogai, S. (1986). Particulate fluxes and major components of settling particles from sediment trap experiments in the Pacific Ocean. Deep-Sea Research, 33(7), 903-912.

Northcote, T. G., Wilson, M. S., and Hurn, D. R. (1964). Some characteristics of Nitinat Lake, an inlet on Vancouver Island, British Columbia. Journal of the Fisheries Research Board of Canada, 21(5), 1069-1081.

Nuszdorfer, F. C., Klinka, K., and Demarchi, D. A. (1991). Coastal douglas-fir zone. Ecosystems of British Columbia, D. Meidinger and J. Pojar, eds., Research Branch, Ministry of Forests, Victoria, BC, 81-94.

Orians, K. J., and Bruland, K. W. (1986). The biogeochemistry of aluminum in the Pacific Ocean. Earth and Planetary Science Letters, 78, 397-410.

Overnell, J., Edwards, A., Grantham, B. E., Harvey, S. M., Jones, K. J., Leftley, J. W., and Smallman, D. J. (1995). Sediment-water column coupling and the fate of the spring phytoplankton bloom in Loch Linnhe, a Scottish fjordic sea-loch. Sediment processes and sediment-water fluxes. Estuarine, Coastal and Shelf Science, 41, 1-19.

Pace, M. J., Knauer, G. A., Karl, D. M., and Martin, J. H. (1987). Primary production, new production and vertical flux in the eastern Pacific Ocean. Nature, 325, 803-804.

Pancost, R. D., Freeman, K. H., Wakeham, S. G., and Robertson, C. Y. (1997). Controls on carbon isotope fractionation by diatoms in the Peru upwelling region. Geochimica et Cosmochimica Acta, 61(23), 4983-4991.

Parsons, T. R., Stephens, K., and Strickland, J. D. H. (1961). On the chemical composition of eleven species of marine phytoplankters. Journal of the Fisheries Research Board of

Canada, 18(6), 1001-1025.

Parsons, T. R. (1979). The Strait of Georgia program. Marine production mechanisms, M. J. Dunbar, eds., Cambridge University Press, Cambridge, 133-149.

Parsons, T. R., Stronach, J., Borstad, G. A., Louttit, G., and Perry, R. I. (1981). Biological fronts in the Strait of Georgia, British Columbia, and their relation to recent measurements of primary productivity. Marine Ecology Progress Series, 6, 237-242.

Parsons, T. R., Perry, R. I., Nutbrown, E. D., Hsieh, W., and Lalli, C. M. (1983). Frontal Zone analysis at the mouth of Saanich Inlet, British Columbia, Canada. Marine Biology, 73, 1-5.

Parsons, T. R., Maita, Y., and Lalli, C. M. (1984a). A Manual of Chemical and Biological Methods for Seawater Analysis, Pergamon press, Oxford.

Parsons, T. R., Dovey, H. M., Cochlan, W. P., Perry, R. I., and Crean, P. B. (1984b). Frontal zone analysis at the mouth of a fjord - Jervis Inlet, British Columbia. Sarsia, 69, 133-137.

Pawlowicz, R., and Farmer, D. M. (1998). Diagnosing vertical mixing in a two-layer exchange flow. Journal of Geophysical Research, 103(C13), 30,695-30,711.

Pedersen, T. F., Malcolm, S. J., and Sholkovitz, E. R. (1985). A lightweight gravity corer for undisturbed sampling of soft sediments. Canadian Journal of Earth Science, 22, 133-135.

Pejrup, M., Valeur, J., and Jensen, A. (1996). Vertical fluxes of particulate matter in Aarhus Bight, Denmark. Continental Shelf Research, 16(8), 1047-1064.

Peña, M. A., Denman, K. L., Calvert, S. E., Thomson, R. E., and Forbes, J. R. (1999). The seasonal cycle in sinking particle fluxes off Vancouver Island, British Columbia. Deep-Sea Research II, 46, 2969-2992.

Perry, M. J., Bolger, J. P., and English, D. C. (1989). Primary production in Washington coastal waters. Coastal Oceanography of Washington and Oregon, M. R. Landry and B. M. Hickey, eds., Elsevier Science Publishers, Amsterdam, 117-138.

Pickard, G. L. (1961). Oceanographic features of inlets in the British Columbia mainland coast. Journal of the Fisheries Research Board of Canada, 18(6), 907-999.

Pickard, G. L. (1963). Oceanographic characteristics if inlets of Vancouver Island, British Columbia. Journal of the Fisheries Research Board of Canada, 20(5), 1109-1144.

Pickard, G. L. (1975). Annual and longer term variations of deepwater properties in the coastal waters of southern British Columbia. Journal of the Fisheries Research Board of

Canada, 32, 1561-1587.

Pike, J., and Kemp, A. E. S. (1999). Diatom mats in Gulf of California sediments: Implications for the paleoenvironmental interpretation of laminated sediments and silica burial. Geology, 27(4), 311-314.

Pitcher, G. C. (1986). Sedimentary flux and the formation of resting spores of selected Chaetoceros species at two sites in the southern Benguela system. South African Journal of Marine Science, 4, 231-244.

Platt, T., and Harrison, W. G. (1985). Biogenic fluxes of carbon and oxygen in the ocean. Nature, 318(6041), 55-58.

Platt, T., Sathyendranath, S., and Ravindran, P. (1990). Primary production by phytoplankton: analytic solutions for daily rates per unit area of water surface. Proceedings of the Royal Society of London B, 241, 101-111.

Pojar, J., Klinka, K., and Demarchi, D. A. (1991). Coastal western hemlock zone. Ecosystems of British Columbia, D. Meidinger and J. Pojar, eds., Research Branch, Ministry of Forests, Victoria, BC, 95-112.

Popp, B. N., Laws, E. A., Bidigare, R. R., Dore, J. E., Hanson, K. L., and Wakeham, S. G. (1998). Effect of phytoplankton cell geometry on carbon isotopic fractionation. Geochimica et Cosmochimica Acta, 62(1), 69-77.

Prahl, F. G., Ertel, J. R., Goñi, M. A., Sparrow, M. A., and Eversmeyer, B. (1994). Terrestrial organic carbon contributions to sediments on the Washington margin. Geochimica et Cosmochimica Acta, 58(14), 3035-3048.

Quéguiner, B., Tréguer, P., Peeken, I., and Scharek, R. (1997). Biogeochemical dynamics and the silicon cycle in the Atlantic sector of the Southern Ocean during austral spring 1992. Deep-Sea Research II, 44(1-2), 69-89.

Ragueneau, O., Tréguer, P., Leynaert, A., Anderson, R. F., Brzezinski, M. A., DeMaster, D. J., Dugdale, R. C., Dymond, J., Fischer, G., François, R., Heinze, C., Maier-Reimer, E., Martin-Jézéquel, V., Nelson, D. M., and Quéguiner, B. (2000). A review of the Si cycle in the modern ocean: recent progress and missing gaps in the application of biogenic opal as a paleoproductivity proxy. Global Planetary Change, 26, 317-365.

Rau, G. H., Chavez, F. P., and Friederich, G. E. (2001). Plankton $^{13}C/^{12}C$ variations in Monterey Bay, California: evidence of non-diffusive inorganic carbon uptake by phytoplankton in an upwelling environment. Deep-Sea Research I, 48, 79-94.

Redfield, A. C., Ketchum, B. H., and Richards, F. A. (1963). The influence of organisms on the composition of sea-water. The Sea, M. N. Hill, eds., John Wiley & Sons, New

York, 26-77.

Reinfelder, J. R., Kraepiel, A. M. L., and Morel, F. M. M. (2000). Unicellular C_4 photosynthesis in a marine diatom. Nature, 407, 996-999.

Richards, F. A. (1965). Anoxic basins and fjords. Chemical Oceanography, J. P. Riley and G. Skirrow, eds., Academic Press, London, 611-645.

Ricker, W. E. (1973). Linear regressions in fishery research. Journal of the Fisheries Research Board of Canada, 30, 409-434.

Ricker, W. E. (1975). Computation and Interpretation of Biological Statistics of Fish Populations, Department of the environment fisheries and marine service.

Ricker, W. E. (1984). Computation and uses of central trend lines. Canadian Journal of Zoology, 62, 1897-1905.

Ross, A. H., Gurney, S. C., Heath, M. R., Hay, S. J., and Henderson, E. W. (1993). A strategic simulation model of a fjord ecosystem. Limnology and Oceanography, 38(1), 128-153.

Ruttenberg, K. C., and Goñi, M. A. (1997). Phosphorus distribution, C:N:P ratios, and $\delta^{13}C$ in arctic, temperate, and tropical coastal sediments: tools for characterizing bulk sedimentary organic matter. Marine Geology, 139, 123-145.

Sackett, W. M., and Thompson, R. R. (1963). Isotopic organic carbon composition of recent continental derived clastic sediments of eastern gulf coast, Gulf of Mexico. Bulletin of the American Association of Petroleum Geologists, 47(3), 525-531.

Sage, D. (1994). Rhenium and molybdenum in Saanich and Jervis Inlet sediments: analysis and distribution, B.Sc., UBC.

Sakshaug, E., and Myklestad, S. (1973). Studies on the phytoplankton ecology of the Trondheimsfjord. III. Dynamics of phytoplankton blooms in relation to environmental factors, bioassay experiments and parameters for the physiological state of the populations. Journal of Experimental Marine Biology and Ecology, 11, 157-188.

Sakshaug, E. (1977). Limiting nutrients and maximum growth rates for diatoms in Narragansett Bay. Journal of Experimental Marine Biology and Ecology, 28, 109-123.

Sakshaug, E., Andersen, K., Myklestad, S., and Olsen, Y. (1983). Nutrient status of phytoplankton communities in Norwegian waters (marine, brackish, and fresh) as revealed by their chemical composition. Journal of Plankton Research, 5(2), 175-196.

Sakshaug, E., and Olsen, Y. (1986). Nutrient status of phytoplankton blooms in Norwegian waters and algal strategies for nutrient competition. Canadian Journal of Fisheries and

Aquatic Sciences, 43, 389-396.

Sakshaug, E., Andersen, K., and Kiefer, D. A. (1989). A steady state description of growth and light absorption in the marine planktonic diatom Skeletonema costatum. Limnology and Oceanography, 34(1), 198-205.

Sakshaug, E. (1993). The relationship between phytoplankton growth rate and production with emphasis on respiration and excretion. Measurement of Primary Production from the Molecular to the Global Scale, La Rochelle, 63-68.

Sancetta, C., and Calvert, S. E. (1988). The annual cycle of sedimentation in Saanich Inlet, British Columbia: implications for the interpretation of diatom fossil assemblages. Deep-Sea Research, 35(1), 71-90.

Sancetta, C. (1989a). Spatial and temporal trends of diatom flux in British Columbian fjords. Journal of Plankton Research, 11(3), 503-520.

Sancetta, C. (1989b). Sediment transport by fecal pellets in British Columbian fjords. Marine Geology, 89, 331-346.

Sancetta, C. (1989c). Processes controlling the accumulation of diatoms in sediments: a model derived from British Columbia fjords. Paleoceanography, 4(3), 235-251.

Scharek, R., Tupas, L. M., and Karl, D. M. (1999). Diatom fluxes to the deep sea in the oligotrophic North Pacific gyre at Station ALOHA. Marine Ecology Progress Series, 182, 55-67.

Sholkovitz, E. R. (1976). Flocculation of dissolved organic and inorganic matter during the mixing of river water and seawater. Geochimica et Cosmochimica Acta, 40, 831-845.

Siegel, D. A., Granata, T. C., Michaels, A. F., and Dickey, T. D. (1990). Mesoscale eddy diffusion, particle sinking, and the interpretation of sediment trap data. Journal of Geophysical Research, 95(C4), 5305-5311.

Siegel, D. A., and Deuser, W. G. (1997). Trajectories of sinking particles in the Sargasso Sea: modeling of statistical funnels above deep-ocean sediment traps. Deep-Sea Research I, 44(9-10), 1519-1541.

Siegenthaler, U., and Sarmiento, J. L. (1993). Atmospheric carbon dioxide and the ocean. Nature, 365, 119-125.

Skei, J. M., and Paus, P. E. (1979). Surface metal enrichment and partitioning of metals in a dated sediment core from a Norwegian fjord. Geochimica et Cosmochimica Acta, 43, 239-246.

Skei, J. (1980). The chemistry of suspended particulate matter from two oxygen deficient

Norwegian fjords - with special reference to manganese. Fjord Oceanography, H. J. Freeland, D. M. Farmer, and C. D. Levings, eds., Plenum Press, New York, 693-697.

Skei, J. M. (1981). Dispersal and retention of pollutants in Norwegian fjords. Rapport Proces-Verbal Conseil International Exploration de la Mer, 181, 78-86.

Skei, J. (1983). Why sedimentologists are interested in fjords. Sedimentary Geology, 36, 75-80.

Smetacek, V., von Brockel, K., Zeitzschel, B., and Zenk, W. (1978). Sedimentation of particulate matter during a phytoplankton spring bloom in relation to the hydrographical regime. Marine Biology, 47, 211-226.

Smetacek, V. (1980a). Annual cycle of sedimentation in relation to plankton ecology in western Kiel Bight. Ophelia, 1 (suppl.), 65-76.

Smetacek, V. (1980b). Zooplankton standing stock, copepod fecal pellets and particulate detritus in Kiel Bight. Estuarine and Coastal Marine Science, 11, 477-490.

Smetacek, V. S. (1985). Role of sinking in diatom life-history cycles: ecological, evolutionary and geological significance. Marine Biology, 84, 239-251.

Smethie, W. M. J. (1981). Vertical mixing rates in fjords determined using radon and salinity as tracers. Estuarine, Coastal and Shelf Science, 12, 131-153.

Smethie, W. M. J. (1987). Nutrient regeneration and denitrification in low oxygen fjords. Deep-Sea Research, 34(5/6), 983-1006.

Smith, S. V., and Hollibaugh, J. T. (1993). Coastal metabolism and the oceanic organic carbon balance. Reviews of Geophysics, 31(1), 75-89.

Smith, P. J., and Hobson, L. A. (1994). Temporal variations in the taxonomic composition of flagellated nanoplankton in a temperate fjord. Journal of Phycology, 30, 369-375.

Söderström, J. (1996). The significance of observed nutrient concentrations in the discussion about nitrogen and phosphorus as limiting nutrients for the primary carbon flux in coastal water ecosystems. Sarsia, 81, 81-96.

Sokal, R. R., and Rohlf, F. J. (1995). Biometry: the principles and practice of statistics in biological research, W.H. Freeman and Company, New York.

Stanley, S. O., Leftley, J. W., Lightfoot, A., Robertson, N., Stanley, I. M., and Vance, I. (1978). The Loch Eil project: sediment chemistry, sedimentation and the chemistry of the overlying water in Loch Eil. Journal of Experimental Marine Biology and Ecology, 55, 299-313.

Sternberg, R. W., Berhane, I., and Ogston, A. S. (1999). Measurement of size and settling velocity of suspended aggregates on the northern California continental shelf. Marine Geology, 154, 43-54.

Stockner, J. G., and Cliff, D. D. (1975). Marine phytoplankton production, distribution and species composition in Pendrell and Hotham Sounds, British Columbia. 516, Fisheries Research Board of Canada.

Stockner, J. G., Cliff, D. D., and Buchanan, D. B. (1977). Phytoplankton production and distribution in Howe Sound, British Columbia: a coastal marine embayment - fjord under stress. Journal of the Fisheries Research Board of Canada, 34, 907-917.

Stockner, J. G., Cliff, D. D., and Shortreed, K. R. S. (1979). Phytoplankton ecology of the Strait of Georgia, British Columbia. Journal of the Fisheries Research Board of Canada, 36, 657-666.

Stucchi, D., and Whitney, F. (1997). Circulation and nitrogen transport in Saanich Inlet, B.C. Canadian Meteorological and Oceanographic Society Bulletin, 25(2), 39-44.

Suess, E. (1980). Particulate organic carbon flux in the oceans - surface productivity and oxygen utilization. Nature, 288, 260-263.

Suess, E., and Müller, P. J. (1980). Productivity, sedimentation rate and sedimentary organic matter in the oceans II. - elemental fractionation. Biogeochimie de la Matiere Organique A L'Interface Eau-Sediment Marin, 18-26.

Syvitski, J. P. M., Asprey, K. W., Clattenburg, D. A., and Hodge, G. D. (1985). The prodelta environment of a fjord: suspended particle dynamics. Sedimentology, 32, 83-107.

Syvitski, J. P. M., Burrell, D. C., and Skei, J. M. (1987). Fjords: processes and products, Springer-Verlag New York, Inc., New York.

Syvitski, J. P. M., Smith, J. N., Calabrese, E. A., and Boudreau, B. P. (1988). Basin sedimentation and the growth of prograding deltas. Journal of Geophysical Research, 93(C6), 6895-6908.

Takahashi, M., Fujii, K., and Parsons, T. R. (1973). Simulation study of phytoplankton photosynthesis and growth in the Fraser River estuary. Marine Biology, 19, 102-116.

Takahashi, M., Thomas, W. H., Seibert, D. L., Beers, J., Koeller, P., and Parsons, T. R. (1975). The replication of biological events in enclosed water columns. Archiv fur Hydrobiologie, 76(1), 5-23.

Takahashi, M., Seibert, D. L., and Thomas, W. H. (1977). Occasional blooms of phytoplankton during summer in Saanich Inlet, B.C., Canada. Deep-Sea Research, 24, 775-780.

Takahashi, M., Barwell-Clarke, J., Whitney, F., and Koeller, P. (1978). Winter condition of marine plankton populations in Saanich Inlet, B.C., Canada. I. phytoplankton and its surrounding environment. Journal of Experimental Marine Biology and Ecology, 31, 283-301.

Takahashi, M., and Hoskins, K. D. (1978). Winter condition of marine plankton populations in Saanich Inlet, B.C., Canada. II. Micro-zooplankton. Journal of Experimental Marine Biology and Ecology, 32, 27-37.

Takahashi, T., Broecker, W. S., and Langer, S. (1985). Redfield ratio based on chemical data from isopycnal surfaces. Journal of Geophysical Research, 90(C4), 6907-6924.

Taylor, S. R., and McClennan, S. M. (1985). The Continental Crust: its Composition and Evolution, Blackwell Scientific.

Taylor, F. J. R., Haigh, R., and Sutherland, T. F. (1994). Phytoplankton ecology of Sechelt Inlet, a fjord system on the British Columbia coast. II. Potentially harmful species. Marine Ecology Progress Series, 103, 151-164.

Teeri, J. A., and Stowe, L. G. (1976). Climate patterns and the distribution of C_4 grasses in North America. Oecologia, 23, 1-12.

Thunell, R. C., Varela, R., Llano, M., Collister, J., Muller-Karger, F., and Bohrer, R. (2000). Organic carbon fluxes, degradation, and accumulation in an anoxic basin: Sediment trap results from the Cariaco Basin. Limnology and Oceanography, 45(2), 300-308.

Timothy, D. A. (1994). Production and consumption of organic carbon and oxygen in Sechelt Inlet, British Columbia, M.Sc., University of British Columbia.

Timothy, D. A., and Pond, S. (1997). Describing additional fluxes to deep sediment traps and water-column decay in a coastal environment. Journal of Marine Research, 55, 383-406.

Timothy, D. A., and Soon, M. Y. S. (2001). Primary production and deep-water oxygen content of two British Columbian fjords. Marine Chemistry, 73(1), 37-51.

Tiselius, P., and Kuylenstierna, M. (1996). Growth and decline of a diatom spring bloom: phytoplankton species composition, formation of marine snow and the role of heterotrophic dinoflagellates. Journal of Plankton Research, 18(2), 133-155.

Tortell, P. D., Rau, G. H., and Morel, F. M. M. (2000). Inorganic carbon acquisition in

coastal Pacific phytoplankton communities. Limnology and Oceanography, 45(7), 1485-1500.

Toth, D. J., and Lerman, A. (1977). Organic matter reactivity and sedimentation rates in the ocean. American Journal of Science, 277, 465-485.

Tunnicliffe, V. (2000). A fine-scale record of 130 years of organic carbon deposition in an anoxic fjord, Saanich Inlet, British Columbia. Limnology and Oceanography, 45(6), 1380-1387.

Van Cappellen, P., and Qiu, L. (1997). Biogenic silica dissolution in sediments of the Southern Ocean. II. Kinetics. Deep-Sea Research II, 44(5), 1129-1149.

Verardo, D. J., Froelich, P. N., and McIntyre, A. (1990). Determination of organic carbon and nitrogen in marine sediments using the Carlo Erba NA-1500 Analyzer. Deep-Sea Research, 37(1), 157-165.

Wada, E., Terazaki, M., Kabaya, Y., and Nemoto, T. (1987). ^{15}N and ^{13}C abundances in the Antarctic Ocean with emphasis on the biogeochemical structure of the food web. Deep-Sea Research, 34(5/6), 829-841.

Waite, A., Bienfang, P. K., and Harrison, P. J. (1992). Spring bloom sedimentation in a subarctic ecosystem II. Succession and sedimentation. Marine Biology, 114, 131-138.

Walsh, J. J. (1988). On the nature of continental shelves, Academic Press, Inc., San Diego.

Walsh, I., Fischer, K., Murray, D., and Dymond, J. (1988a). Evidence for resuspension of rebound particles from near-bottom sediment traps. Deep-Sea Research, 35(1), 59-70.

Walsh, I., Dymond, J., and Collier, R. (1988b). Rates of recycling of biogenic components of settling particles in the ocean derived from sediment trap experiments. Deep-Sea Research, 35(1), 43-58.

Walsh, I. D. (1992). Large aggregate flux and fate at the seafloor: Diagenesis during the rebound process. Deep-Sea Food Chains and the Global Carbon Cycle, G. T. Rowe and V. Pariente, eds., Kluwer Academic Publishers, Netherlands, 365-373.

Walsh, I. D., and Gardner, W. D. (1992). A comparison of aggregate profiles with sediment trap fluxes. Deep-Sea Research, 39(11/12), 1817-1834.

Ward, B. B., Kilpatrick, K. A., Wopat, A. E., Minnich, E. C., and Lidstrom, M. E. (1989). Methane oxidation in Saanich Inlet during summer stratification. Deep-Sea Research, 9(1), 65-75.

Ward, B. B., and Kilpatrick, K. A. (1990). Relationship between substrate concentration and oxidation of ammonium and methane in a stratified water column. Continental Shelf

Research, 10(12), 1193-1208.

Wassmann, P. (1984). Sedimentation and benthic mineralization of organic detritus in a Norwegian fjord. Marine Biology, 83, 83-94.

Wassmann, P. (1990). Relationship between primary and export production in the boreal coastal zone of the North Atlantic. Limnology and Oceanography, 35(2), 464-471.

Wassmann, P. (1991). Dynamics of primary production and sedimentation in shallow fjords and polls of western Norway. Oceanography and Marine Biology Annual Review, 29, 87-154.

Wassmann, P., Svendsen, H., Keck, A., and Reigstad, M. (1996). Selected aspects of the physical oceanography and particle fluxes in fjords of northern Norway. Journal of Marine Systems, 8, 53-71.

Westrich, J. T., and Berner, R. A. (1984). The role of sedimentary organic matter in bacterial sulfate reduction: The G-model tested. Limnology and Oceanography, 29(2), 236-249.

Wong, C. S., Whitney, F. A., Crawford, D. W., Iseki, K., Matear, R. J., Johnson, W. K., Page, J. S., and Timothy, D. (1999). Seasonal and interannual variability in particle fluxes of carbon, nitrogen and silicon from time series of sediment traps at Ocean Station P, 1982-1993: relationship to changes in subarctic primary productivity. Deep-Sea Research II, 46, 2735-2760.

Yu, E.-F., François, R., Bacon, M. P., Honjo, S., Fleer, A. P., Manganini, S. J., Rutgers van der Loeff, M. M., and Ittekot, V. (2001). Trapping efficiency of bottom-tethered sediment traps estimated from the intercepted fluxes of ^{230}Th and ^{231}Pa. Deep-Sea Research I, 48, 865-889.

Appendix A

Separating marine from terrigenous organic matter

If all marine OC in Saanich and Jervis Inlets were diatomaceous, then the y-intercepts of the regressions of Figure 3.19 would be good approximations of $\delta^{13}C$ of the settling terrigenous OC. The terrigenous endmembers have been measured directly, giving -25.1$^0/_{00}$ in Saanich Inlet and -26.5$^0/_{00}$ in Jervis Inlet (Cowie, unpublished data). Assuming the shifts of the y-intercepts of Figure 3.19 away from these endmember values are caused by the presence of non-diatomaceous, marine OC that is isotopically heavier than terrigenous OM, the following exercise gives estimates of marine $\delta^{13}C$ endmembers and the composition of 'typical' marine samples.

1. Estimate the BSi content of a prototypical marine sample by assuming it is entirely diatomaceous. The slopes of Figure 3.16 give the mean diatomaceous OC to BSi (OC_d:BSi) ratios of the settling particulates. All data for each fjord (both stations, all seasons) were combined to obtain the following ratios. Conversion from OC_d:BSi to OM_d:BSi uses an OM:OC ratio of 2.7 (section 3.3.1).

    - Saanich Inlet: OC_d:BSi = 0.84 (moles) = 0.15 (weight) $\rightarrow$ OM_d:BSi = 0.40. This ratio gives 71% as the proportion of BSi in a 'typical' marine sample.
    - Jervis Inlet: OC_d:BSi = 0.79 (moles) = 0.14 (weight) $\rightarrow$ OM_d:BSi = 0.38, giving a 'typical' marine sample with 73% BSi.

2. Using %BSi of these diatomaceous samples, a first estimate of $\delta^{13}C$ of the marine

endmember can be made (Figure 3.19).

$$\delta^{13}C_{mar} = \%BSi \text{ (slope)} + \text{intercept} \tag{A.1}$$

The slope and intercept are those of the regression lines of Figure 3.19.

- Saanich Inlet: $\delta^{13}C = 0.093$ %BSi - 23.5; r = 0.78.
- Jervis Inlet: $\delta^{13}C = 0.074$ %BSi - 24.4; r = 0.40.

3. From Equation A.1, a first partitioning of the marine organic matter into diatomaceous and non-diatomaceous components can be made.

$$\frac{OM_{nd}}{OM_d} \equiv \frac{OC_{nd}}{OC_d} = \frac{\delta^{13}C_{int} - \delta^{13}C_{ter}}{\delta^{13}C_{mar} - \delta^{13}C_{int}} \tag{A.2}$$

$\delta^{13}C_{int}$ is the intercept on the $\delta^{13}C$ axes of Figure 3.19 (the intercept of Equation A.1). OM_{nd} and OC_{nd} are the non-diatomaceous, marine organic components of a typical marine sample including as photosynthetic flagellates, heterotrophs and transparent exopolymer particles (TEP). They do not include terrigenous organics. Equivalence between OM_{nd} and OC_{nd} assumes the proportions of carbon in diatomaceous and non-diatomaceous, marine organic matter are similar.

4. Equation A.3 estimates %BSi of a marine sample containing BSi, OM_d and OM_{nd}. This estimate will be less than the BSi content of the prototypic marine sample of step 1, because of the presence of OM_{nd}.

$$\%BSi = 100 \left(1 + \frac{OM_d}{BSi}\left[1 + \frac{OM_{nd}}{OM_d}\right]\right)^{-1} \tag{A.3}$$

OM_d:BSi is from step 1 and OM_{nd}:OM_d is from Equation A.2. (Equation A.3 can be simplified, but a new term would be introduced.) The proportion of BSi from Equation A.3 is used to make an improved estimate of $\delta^{13}C_{mar}$ (Equation A.1), which is then used to re-estimate OM_{nd}:OM_d of Equation A.2. This new estimate

	Saanich Inlet	Jervis Inlet
	marine endmember	
δ^{13}**C**	-17.3 ± 0.41	-19.6 ± 0.69
	typical marine sample	
%BSi	66.2 ± 1.8	64.8 ± 4.5
%OM$_d$	26.7 ± 0.25	24.5 ± 0.50
%OM$_{nd}$	7.04 ± 1.6	10.7 ± 4.0
	diatomaceous proportion of marine OM	
100 x $\frac{OM_d}{OM_{mar}}$	79.2 ± 3.5	69.7 ± 7.3

Table A.1: Estimates of δ^{13}C of the marine OC endmembers and the composition of typical marine samples from Saanich and Jervis Inlets. Error estimates are described in the text.

of OM_{nd}:OM_d is then used in Equation A.3 to make a better estimate of the BSi content of a typical marine sample. Iteration is performed until the value used for %BSi in Equation A.1 converges with the %BSi value calculated from Equation A.3.

5. The largest errors of this exercise are from uncertainty in the OC_d:BSi ratios (Figure 3.16, step 1) and in the uncertainty of the regression lines of Figure 3.19 (Equation A.1). Table A.1 gives results with the 95% confidence interval of both sources of error. The degree to which it is incorrect to assume $CaCO_3$ makes up a negligible portion of the "typical" marine sample (section 3.3.1) will make the final estimates of the marine OC δ^{13}C endmember lighter.

Appendix B

Using a conservative tracer with the trap model

B.1 An alternate model for when rate constants do not converge

For certain sub-sets of the time series, the iterative procedure did not result in convergence of the rate constants of Equations 4.4 and 4.7. Although only results where convergence occurred are presented in this thesis, in exploring the data sets it was useful to otherwise estimate k_C and k_{Si} where converge did not occur.

The additional flux of Equation 4.4 is written as the mass flux at depth z_2 not attributable to the anticipated flux. Because the anticipated flux decays as it sinks, the iteration described in section 4.2.2 is required to solve the model. However, if a conservative element were considered, accommodation of loss during sinking would not be required to quantify the additional flux, and the iteration of section 4.2.2 would be avoided. Aluminosilicates are not biologically or chemically reactive on the time scales considered here, and the flux of adsorbed Al (section 4.1) affects the total flux of Al only where the rain rate of aluminosilicates is very small. Using Al as a conservative tracer,

$$Al_d = Al_2 - Al_1 \,. \tag{B.1}$$

Replacing J_d with Al_d, Equation 4.5 can be written as:

$$j_2 = j_1 \, e^{-k_j \Delta z} + \left(\frac{j}{Al}\right)_d (Al_2 - Al_1) + \epsilon \,. \tag{B.2}$$

The set of linear equations used to solve for $e^{-k_j \Delta z}$ and $(j/J)_d$ then becomes:

$$\begin{bmatrix} j_{11} & Al_{d1} & 1 \\ j_{12} & Al_{d2} & 1 \\ \vdots & \vdots & \vdots \\ j_{1n} & Al_{dn} & 1 \end{bmatrix} \begin{bmatrix} e^{-k_j \Delta z} \\ \left(\frac{j}{Al}\right)_d \\ \epsilon \end{bmatrix} = \begin{bmatrix} j_{21} \\ j_{22} \\ \vdots \\ j_{2n} \end{bmatrix}. \tag{B.3}$$

Equation B.2 can be applied to all constituent fluxes. Another approach, however, is to use Equation B.2 to solve for k_C and k_{Si}, put these values into Equation 4.4, and non-iteratively solve for constituent fluxes, including OC and BSi, using Equation 4.5 as described in section 4.2.2.

Model Equation B.2 was developed, and Al and Ti measured on the sediment-trap samples, to test the possibility that this model would produce meaningful solutions of $e^{-k_j \Delta z}$ for data sub-sets where early use of Equation 4.5 was not successful. However, it was found that the use of Equation B.2 (using either Al or Ti as the conservative tracer) did not improve model solution. Nevertheless, one advantage of Equation B.2 is that no iterations are required to solve the model. This may be especially useful depending on the computational method used to solve for a of Equation 4.7. I have written a routine that performs the iterations, and it was not time-consuming to run the model of Equation 4.5. Furthermore, a disadvantage of Equation B.2 is that the information returned about the composition of the additional flux, $(j/Al)_d$, is physically less meaningful than $(j/J)_d$ as determined by Equations 4.5. Thus, use of Equation B.2 has been reserved for the case where the rate constants of Equations 4.4 and 4.6 do not converge.

B.2 The normalisation scheme

If the composition of the additional flux is identical to the composition of the bulk flux to the deep sediment trap, Equation B.2 can be written as:

$$j_2 = j_1\, e^{-k_j \Delta z} + \frac{j_2}{Al_2}(Al_2 - Al_1)\,. \tag{B.4}$$

Equation B.4 simplifies to:

$$\frac{j_2}{Al_2} = \frac{j_1}{Al_1}\, e^{-k_j \Delta z}\,. \tag{B.5}$$

Walsh et al. (1988b) used Equation B.5 to estimate decay rates of organic carbon, biogenic silica and $CaCO_3$ for the deep Equatorial North Pacific, and Noriki and Tsunogai (1986) used a form of this model on the same fluxes from data collected in the Pacific and Southern Oceans. Walsh et al. (1988b) noted that an assumption of Equation B.5 is compositional similarity between additional fluxes and the bulk material reaching the deep sediment traps. However, they also demonstrated (Walsh et al., 1988a) that the increase in flux with depth as the bottom boundary layer of the ocean is approached was caused by material that was indeed more similar to the material sinking from above than to bottom sediments. They postulated that a 'rebound' flux of relatively young sediments caused observed increases in flux with depth, and others have found additional fluxes less like bottom sediment than expected if resuspended material were causing increases in flux with depth (Smetacek, 1978; Walsh and Gardner, 1992; Timothy and Pond, 1997). An alternative to the rebound hypothesis is that upper sediment traps catch material less efficiently than deep traps, causing an apparent, but not a real, increase in flux with depth (Smetacek, 1978; Timothy and Pond, 1997; Yu et al., 2001).

Appendix C

Sensitivity analysis and results for Jervis Inlet

Data from some deployment periods heavily weighted the model results for Jervis Inlet. In general, the decay terms ($e^{-k_j \Delta z}$) were more sensitive to data removal than were the terms describing the composition of the additional flux ($\{j/J\}_d$) and, furthermore, k_C (and k_N) were more sensitive than k_{Si}. Also, while $(j/J)_d$ has locally useful information about sedimentation in Jervis Inlet, the decay constants are more important for elemental budgets and can be applied to other temperate coastal settings. Therefore, solutions for $e^{-k_c \Delta z}$ (the OC decay terms) were used to find records from deployment periods that largely affected model results.

The method used was to remove data from one deployment period at a time, successively from the first to the last deployment, and to re-solve the model of Equation 4.6*a*. If the removal of a certain deployment period resulted in a significantly different solution, that deployment was removed from the data set and the exercise was repeated. The criterion used to determine whether to reject a deployment period's data was whether removal of those data caused a change in $e^{-k_c \Delta z}$ of more than 30% (dashed lines in the following figures). Figures C.1 through C.6 show the sensitivity analysis, and Figure C.7 shows the deployment periods that were permanently removed from the modelling exercise in Jervis Inlet.

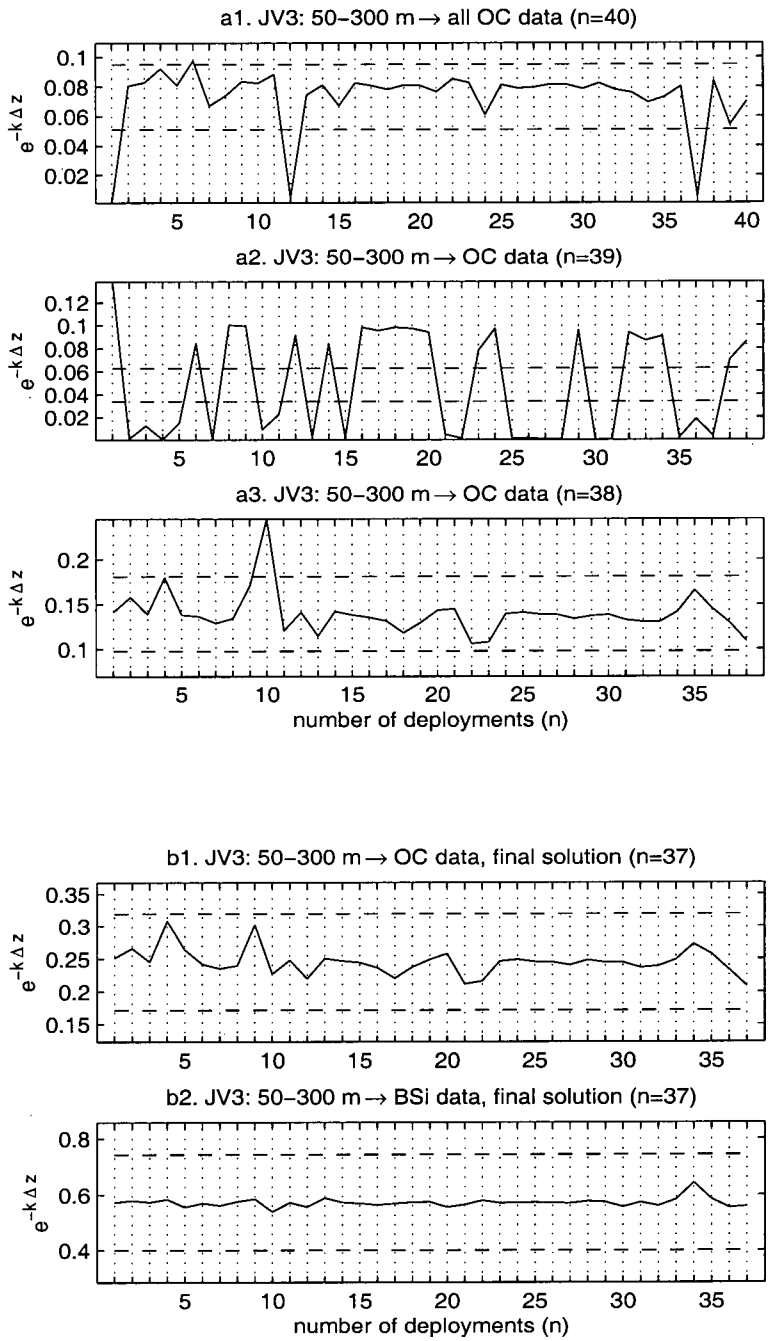

Figure C.1: Sensitivity analysis for station JV-3, 50-300 m. a1: $e^{-k_c \Delta z}$ when successive deployment periods are removed from the entire data set. a2: One period has been permanently removed and the sensitivity analysis repeated (and again for a3). b1 and b2: Sensitivity analysis for OC and BSi on the final subset used for this depth interval.

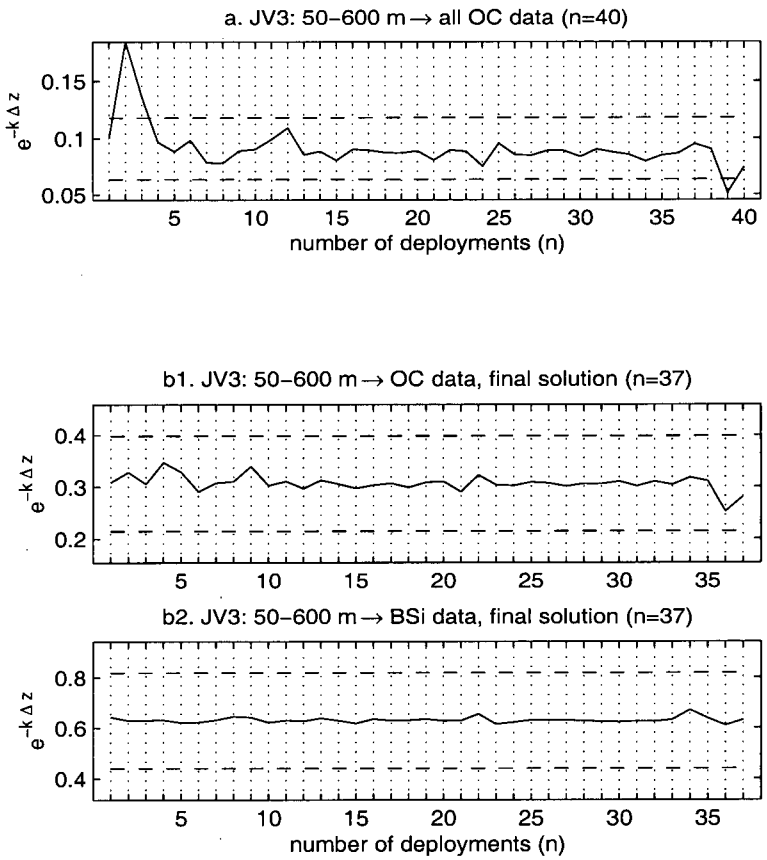

Figure C.2: Sensitivity analysis for station JV-3, 50-600 m. a: $e^{-k_c \Delta z}$ when successive deployment periods are removed from the entire data set. b1 and b2: Sensitivity analysis for OC and BSi after removing the three deployment periods that were taken out of the 50-300 m depth interval (Figure C.1).

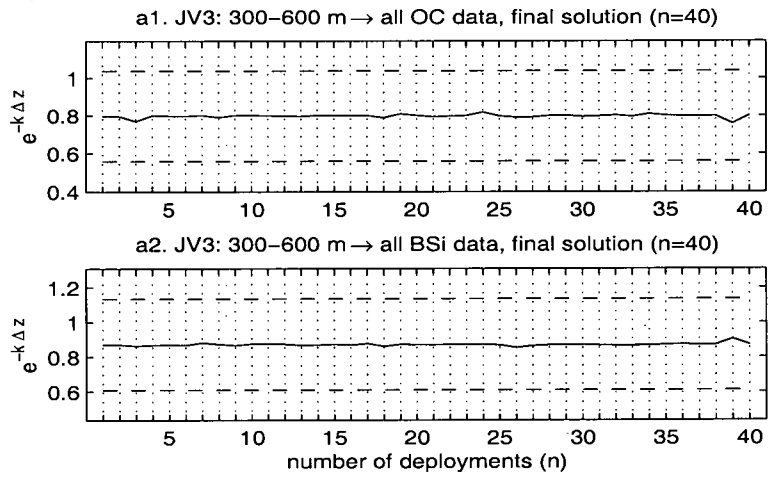

Figure C.3: Sensitivity analysis for station JV-3, 300-600 m. The entire data set is used for this depth interval.

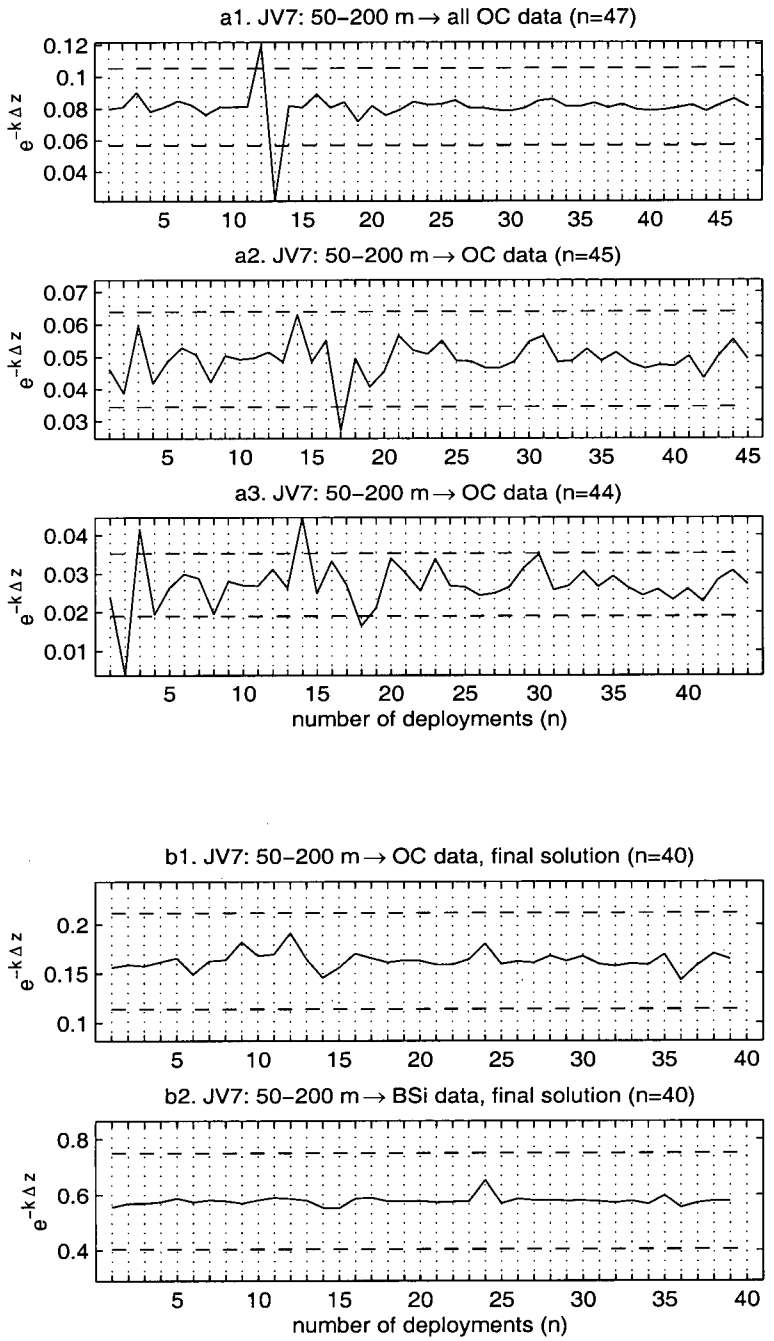

Figure C.4: Sensitivity analysis for station JV-7, 50-200 m. a1: $e^{-k_c \Delta z}$ when successive deployment periods are removed from the entire data set. a2: Two periods have been permanently removed and the sensitivity analysis repeated (and, again, one period removed for a3). b1 and b2: Sensitivity analysis for OC and BSi on the final data subset.

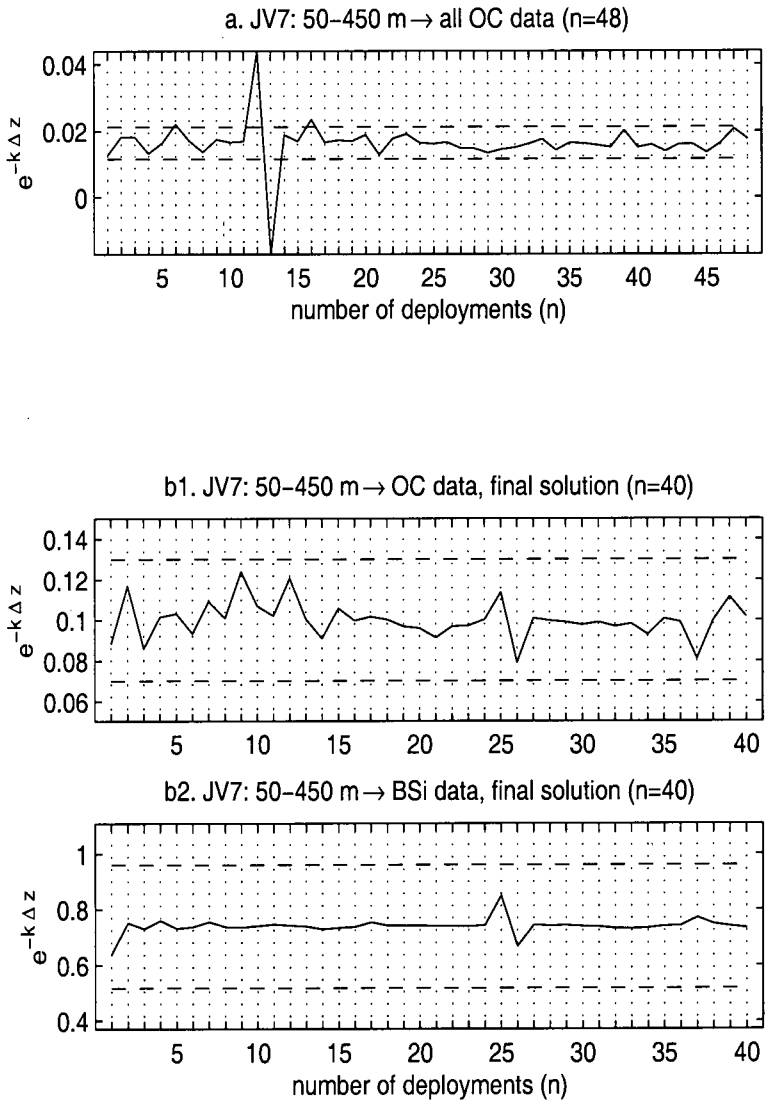

Figure C.5: Sensitivity analysis for station JV-7, 50-450 m. a: $e^{-k_c \Delta z}$ when successive deployment periods are removed from the entire data set. b1 and b2: Sensitivity analysis for OC and BSi after the seven deployment periods that were taken out of the 50-200 m depth interval (Figure C.4), plus one more, have been removed from this depth interval.

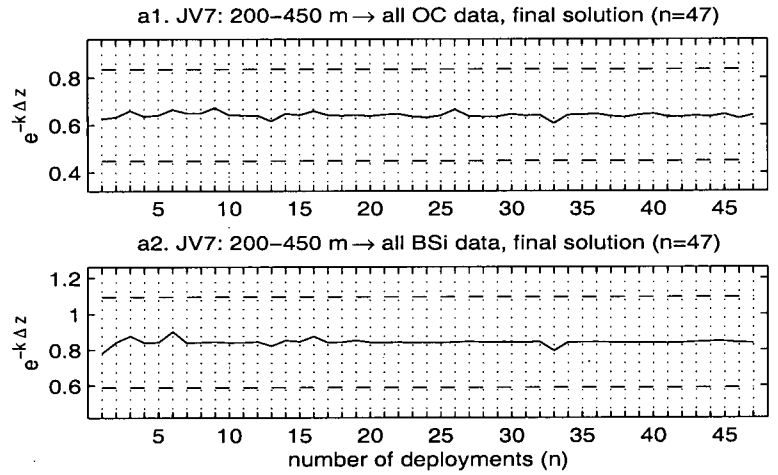

Figure C.6: Sensitivity analysis for station JV-7, 200-450 m. The entire data set is used for this depth interval.

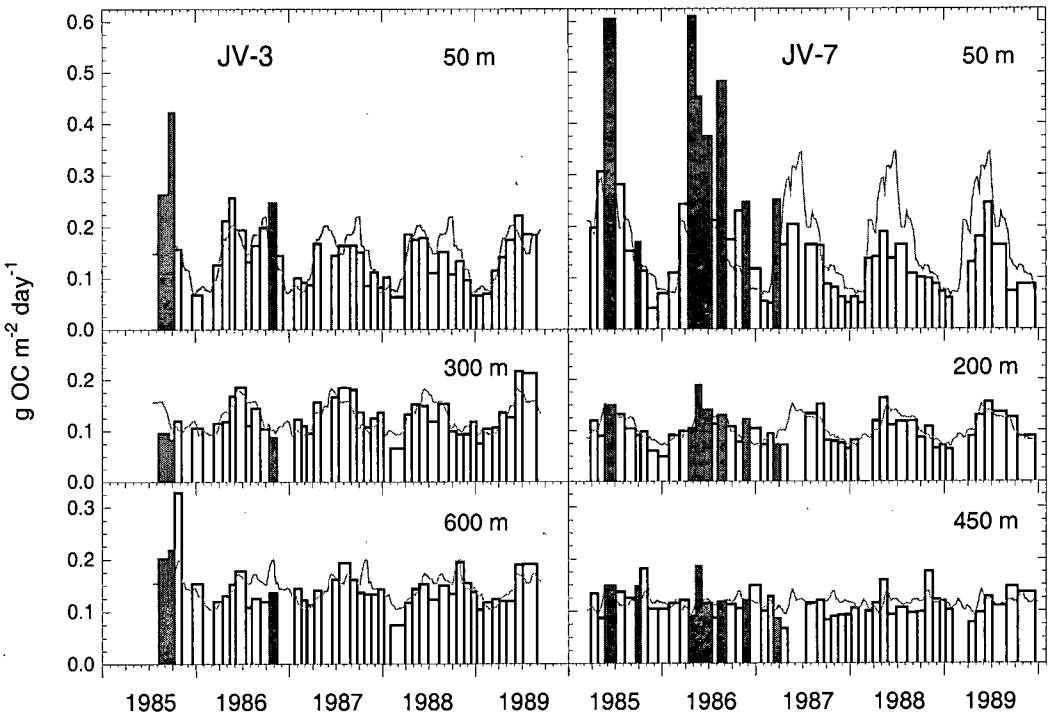

Figure C.7: Data removed from shallow-mid and shallow-deep analyses (dark bars). Most of these deployment periods are characterised by high OC fluxes to the shallow sediment traps and large decreases with depth of the OC rain rate. In Sept/Oct, 1985, while the 50-200 m data from station JV-7 did not stand out in the sensitivity analysis, the data from the 50-450 m depth interval did. The entire time series was used for the mid-deep depth interval at each stations.

	50-200 m JV-7 n = 40	**50-300 m** JV-3 n = 37	**50-450 m** JV-7 n = 40	**50-600 m** JV-3 n = 37	**200-450 m** JV-7 n = 47	**300-600 m** JV-3 n = 40
			organic carbon solution			
r^2	0.76	0.76	0.72	0.85	0.85	0.97
$z_{1/2}$	94	134	154	248	311	442
k_C	0.012 (12)	0.0056 (22)	0.0058 (15)	0.0022 (15)	0.0018 (19)	0.00075 (21)
$\%OC_d$	7.9 (12)	7.8 (16)	5.7 (10)	4.4 (7.7)	5.5 (7.7)	4.5 (3.2)
OC int	37 (17)	27 (40)	35 (26)	30 (34)	6.5†(>100)	-5.8†(>100)
			biogenic silica solution			
r^2	0.92	0.95	0.79	0.90	0.86	0.97
$z_{1/2}$	114	158	235	293	320	445
k_{Si}	0.0040 (12)	0.0022 (11)	0.00076 (30)	0.00084 (14)	0.00069 (35)	0.00046 (22)
$\%BSi_d$	40 (12)	45 (11)	30 (14)	22 (9.0)	22 (15)	20 (4.4)
BSi int	-81 (32)	-190 (21)	-160 (38)	-70†(66)	-38†(95)	-16†(>100)
			nitrogen solution			
r^2	0.79	0.79	0.65	0.80	0.72	0.94
$z_{1/2}$	98	133	156	242	307	439
k_N	0.011 (8.4)	0.0058 (19)	0.0056 (13)	0.0024 (15)	0.0024 (21)	0.00099 (20)
$\%N_d$	0.91 (12)	1.0 (14)	0.61 (12)	0.46 (9.1)	0.66 (11)	0.49 (4.3)
N int	3.3 (22)	2.2†(54)	4.3 (26)	0.0†(>100)	1.6†(73)	0.20†(>100)
			aluminium solution			
r^2	0.89	0.56	0.88	0.95	0.94	0.98
$z_{1/2}$	124	171	253	333	326	451
k_{Al}	0.0004 (96)	0.0006 (>100)	-0.0002 (>100)	-0.0002 (>100)	-0.0001 (>100)	-0.00008 (>100)
$\%Al_d$	0.96 (44)	1.7 (31)	3.5 (14)	5.8 (5.1)	4.4 (7.9)	6.1 (2.4)
Al int	8.1 (35)	22 (24)	4.9†(>100)	-10 (52)	0.30†(>100)	-9.4†(57)

Table C.1: Results of the model applied to each depth interval in Jervis Inlet after the sensitivity analysis was used to remove some deployment periods. Standard errors (percent of the value represented) are in parentheses and results that are not significantly different from zero ($P > 0.05$) are tagged (†; for a rate constant of zero, $e^{-k_j \Delta z}$ of the model is one and, therefore, significant). $z_{1/2}$ is the depth between z_1 and z_2 at which half of the decay of the anticipated flux has occurred (where $j_n = 0.5\{1 + e^{-k_j[z_2 - z_1]}\}$) and is used as the reference depth for which decay constants are characteristic. Rate constants (k_j) have units m^{-1}, intercepts are mg m^{-2} d^{-1}.

Appendix D

Sensitivity analysis and results for Saanich Inlet

This Appendix shows the results of the sensitivity analyses for the data from Saanich Inlet. For a description of the procedure, see Appendix C. On the whole, the data of only one deployment period and one depth interval (station SN-0.8, 135-180 m; Figure D.6) were removed from final analyses.

From the sensitivity analyses and the regression coefficients (compare r^2 of Tables C.1 and D.1), it appears that the model described the data from Saanich Inlet relatively well, yet the rate constants are spatially inconsistent and differences between constituents are not easily explained. For instance, for the 45-110 m depth interval at station SN-9, rate constants are negative and, comparing the 45-150 and the 110-150 m depth intervals, the rate constants increase with depth (Table D.1). At station SN-0.8, although k_C and k_N are spatially reasonable (decreasing with depth) and of similar magnitude, k_{Si} increases with depth and, for the 135-180 m depth interval, the magnitude of the rate constants ($k_{Al} > k_{Si} > k_C > k_N$) is the reverse of that expected. Other evidence that the model results from Saanich Inlet are suspect is the composition of the additional flux. Although not shown explicitly (e.g.; as is for Jervis Inlet at Figure 4.6), for each depth interval in Saanich Inlet, OC, N, BSi and Al are all depleted in the additional flux when compared to the total mass flux reaching the deep sediment traps. In the real case, constituents that are depleted must be balanced by others in excess. Thus, the model appears to be partitioning too much material into the anticipated flux to depth z_2 in Saanich Inlet. If this is the case, the rate constants are too small (resulting in a large anticipated flux),

and the size of the additional flux (parameterised by $\{j/J\}_d$) is too small.

A number of factors might have contributed to these peculiar results from Saanich Inlet. The depth intervals between sediment traps was much less than in Jervis Inlet and possibly too small to resolve decay of the settling flux. At station SN-9, extremely high additional fluxes occurred for the two depth intervals anchored above by the 45 m sediment trap. Determining the size of the anticipated flux for these intervals may be inaccurate because it is the difference between two large numbers (Equations 4.1*a* and 4.1*b*). Horizontal gradients in the export flux, combined with horizontal currents, might have occurred such that the construction of the model (Figure 4.1) was not valid, especially at station SN-9 where large horizontal gradients in surface biomass (e.g.; Hobson and McQuoid, in press) and significant horizontal transport of resuspended material occurred. However, Equations 4.8 and 4.9 suggest that horizontal advection, enhancing or diminishing the downward flux from one depth to the next, would result in a positive (advection from high export region) or a negative (advection from regions of low export) error term without necessarily compromising estimates of rate constants.

It is unlikely that seasonal anoxia affected the sinking flux; only the 180 m sediment trap at station SN-0.8 would have been exposed to anoxic waters for extended periods of time. Indeed, Thunell et al. (2000) found that decreases with depth of POC fluxes in the anoxic waters of the Cariaco Trench were not different than those predicted from oxygenated settings, and certain results (high rate constants for Al, depletion of all constituents in the additional fluxes) cannot be explained by low redox conditions.

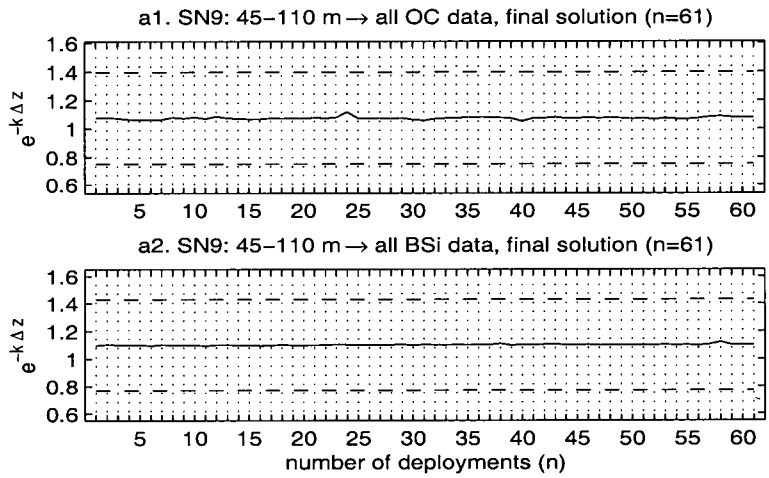

Figure D.1: Sensitivity analysis for station SN-9, 45-110 m. No data were removed from final analysis.

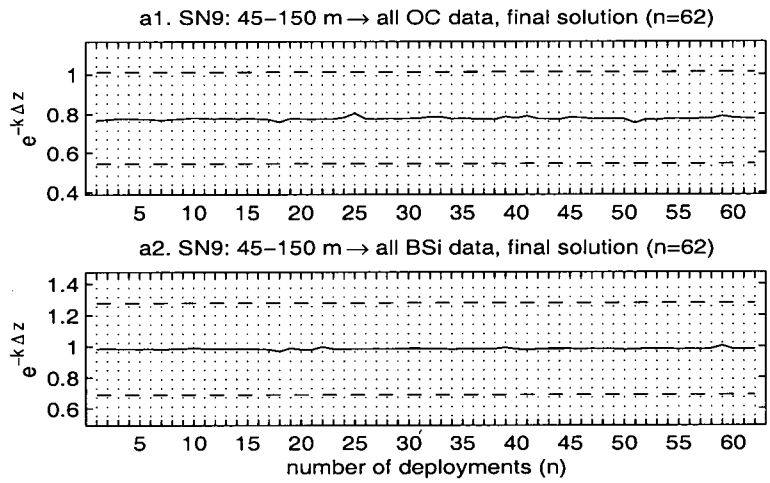

Figure D.2: Sensitivity analysis for station SN-9, 45-150 m. No data were removed from final analysis.

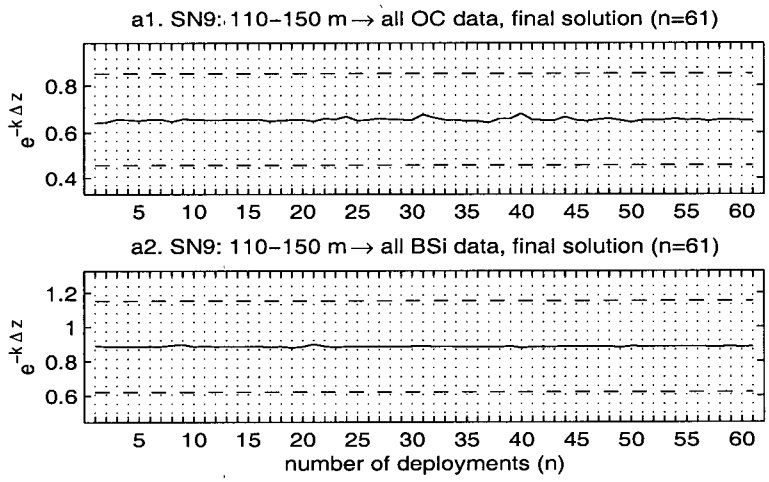

Figure D.3: Sensitivity analysis for station SN-9, 110-150 m. No data were removed from final analysis.

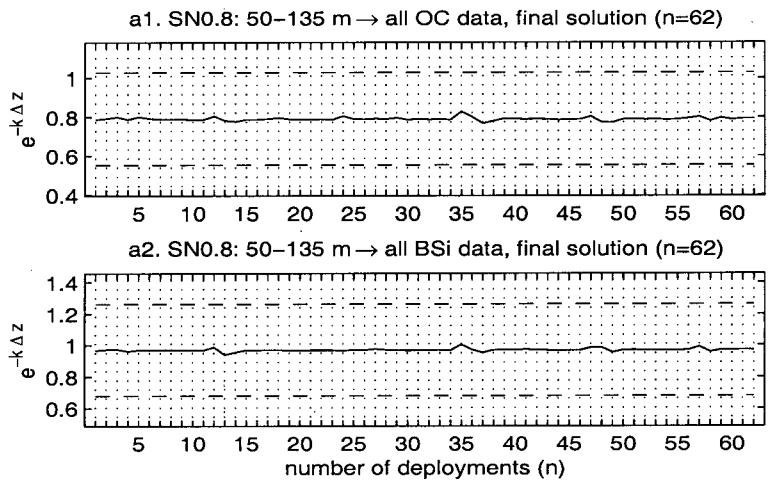

Figure D.4: Sensitivity analysis for station SN-0.8, 50-135 m. No data were removed from final analysis.

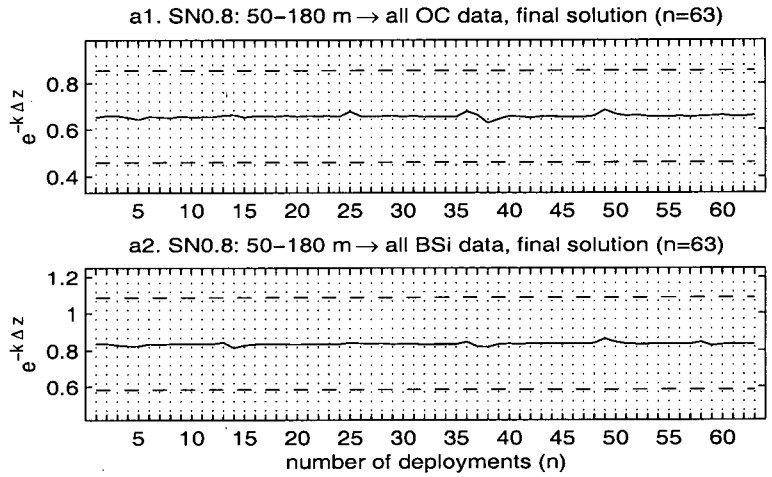

Figure D.5: Sensitivity analysis for station SN-0.8, 50-180 m. were removed from final analysis.

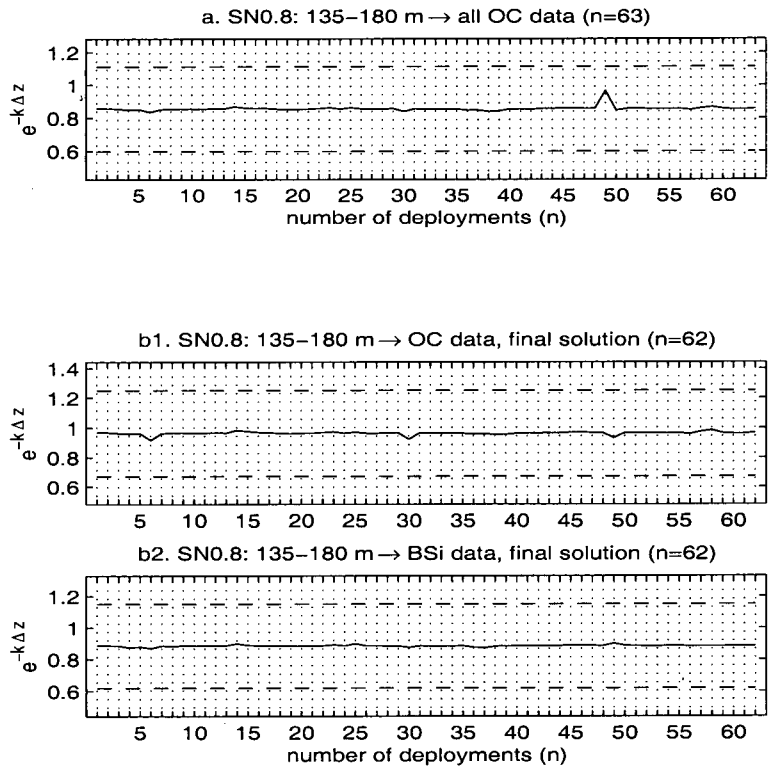

Figure D.6: Sensitivity analysis for station SN-0.8, 135-180 m. Although it passed the 30% criteria used in Jervis Inlet (Appendix C), One deployment period's data (a) stood out and was removed from the final analysis (b1 and b2).

	45-110 m SN-9 n = 61	**50-135 m** SN-0.8 n = 62	**45-150 m** SN-9 n = 62	**50-180 m** SN-0.8 n = 63	**110-150 m** SN-9 n = 61	**135-180 m** SN-0.8 n = 62
			organic carbon solution			
r^2	0.86	0.89	0.96	0.71	0.94	0.91
$z_{1/2}$	78	90	94	108	128	157
k_C	-0.0011 (78)	0.0028 (19)	0.0024 (19)	0.0032 (20)	0.011 (15)	0.00082 (>100)
$\%OC_d$	2.9 (12)	5.1 (12)	2.7 (4.0)	4.8 (16)	2.7 (6.5)	6.0 (7.5)
OC int	12†(>100)	1.2†(>100)	29†(54)	17†(95)	79 (28)	-0.30†(>100)
			biogenic silica solution			
r^2	0.97	0.96	0.98	0.89	0.99	0.90
$z_{1/2}$	78	92	97	112	129	157
k_{Si}	-0.0015 (25)	0.00036 (83)	0.00017 (>100)	0.0014 (25)	0.0030 (18)	0.0027 (37)
$\%BSi_d$	16 (7.5)	26 (11)	15 (4.0)	15 (24)	14 (4.0)	20 (20)
BSi int	-180†(52)	-120 (31)	-84†(80)	-33†(>100)	64†(82)	1.8†(>100)
			nitrogen solution			
r^2	0.88	0.89	0.94	0.71	0.93	0.91
$z_{1/2}$	78	90	94	108	128	157
k_N	-0.0014 (54)	0.0033 (16)	0.0023 (21)	0.0033 (19)	0.011 (16)	0.00052 (>100)
$\%N_d$	0.32 (14)	0.58 (14)	0.31 (5.2)	0.57 (18)	0.32 (7.9)	0.79 (8.3)
N int	-0.40†(>100)	1.2†(>100)	1.4†(>100)	2.6†(78)	8.8 (32)	-0.30†(>100)
			aluminium solution			
r^2	0.94	0.85	0.96	0.70	0.99	0.77
$z_{1/2}$	77	97	94	120	130	156
k_{Al}	0.00080 (>100)	-0.0052 (19)	0.0023 (62)	-0.0023 (43)	0.00075 (>100)	0.0047 (35)
$\%Al_d$	6.68 (3.5)	3.2 (14)	6.8 (2.6)	2.5 (20)	7.0 (2.1)	2.3 (20)
Al int	16†(>100)	-3.3†(>100)	47†(64)	4.0†(>100)	-19†(>100)	10†(53)

Table D.1: Results of the model applied to each depth interval in Saanich Inlet. From the sensitivity analyses, one deployment period (135-180 m depth interval at station SN-0.8) was removed. Standard errors (percent of the value represented) are in parentheses and results that are not significantly different from zero ($P > 0.05$) are tagged (†; for a rate constant of zero, $e^{-k_j \Delta z}$ of the model is one and, therefore, significant, so rate constants not different than zero are not tagged). $z_{1/2}$ is the depth between z_1 and z_2 at which half of the decay of the anticipated flux has occurred (where $j_n = 0.5\{1 + e^{-k_j[z_2 - z_1]}\}$). Rate constants ($k_j$) have units m^{-1} and intercepts are in mg m^{-2} d^{-1}.

Appendix E

Exponential fit to rate constants

Originally I had intended to fit an exponential function to the depth profiles of k. The reasoning was simply that the curvature of these profiles might be well explained by an exponential function. However, the power function discussed in Chapter 4 describes the profiles better, especially the plot of k_{Si} versus depth. The power function, furthermore, has more physical meaning than the exponential function, as it describes the realistic case where the decaying material (OM or BSi) is made up of a suite of components, each decaying at a different rate (Middleburg, 1989). Although the power function is the better model with which to describe variations in k with depth, the formulation of the exponential fit is given here. Figure 4.4 shows the exponential fits to the rate constants, and Figure 4.5 uses Equation E.5 to compare the description of flux with depth arrived at using the power function and the exponential model of k versus depth.

If the decay parameter k is modelled to decrease with depth at a constant rate, α (m^{-1}):

$$\frac{dk}{dz} = -\alpha k \; . \tag{E.1}$$

Integrating Equation E.1 gives the exponential relationship:

$$k = k_0 \, e^{-\alpha z} \; , \tag{E.2}$$

where k_0 is the value of k at a reference depth, which can be chosen arbitrarily because the shape of this first-order exponential function does not change with depth. Taking the logarithm of Equation E.2 provides a means to find k_0 and α of the rate constants

presented in Figure 4.4.

$$\ln(k) = -\alpha z + \ln(k_0) \tag{E.3}$$

Thus, for a plot of $\ln(k_j)$ versus z, the slope of the regression line is $-\alpha$ and the intercept at $z = 0$ is $\ln(k_0)$ (Figure 4.4).

Change in the $flux$ of j with depth is written as:

$$\frac{dj}{dz} = -kj \; . \tag{E.4}$$

Substituting k of Equation E.2 into Equation E.4 and integrating gives an expression for the change with depth of j for the case where k decreases exponentially with depth:

$$j = j_1 \; \exp\left(\frac{k_0}{\alpha}\left[e^{-\alpha z_2} - e^{-\alpha z_1}\right]\right) . \tag{E.5}$$

Appendix F

Tabulation of primary production data

This appendix presents the primary production data collected during the study (see section 2.2 for methods). Tables F.1 through F.4 give ^{14}C-uptake rates (mg C m^{-3} d^{-1}) at the depths of sampling (z: meters); section 2.2 explains how hourly rates were converted to the daily rates presented here. The header at the top of each block of data in Tables F.1 through F.4 is the date of sampling (yymmdd); depth and ^{14}C-uptake rates are given in the left and right columns of each block. The first 5 depths in each block are those that corresponded to 56, 32, 18 and 7% surface irradiance. The last depth in each group is an extrapolated estimate of the depth of 1% surface irradiance, and the corresponding rate of ^{14}C uptake is also an extrapolation (see section 2.2 for details). The ^{14}C-uptake value under the line at the end of each block is the vertically integrated estimate of primary production (mg C m^{-2} d^{-1}), obtained by trapezoidal integration from the surface to the depth of 7% surface irradiance (where the ^{14}C-uptake rate at the depth of 56% surface irradiance was extrapolated to the surface) and by assuming that primary production decreased exponentially with depth in proportion to light between 7% and 1% surface irradiance. See section 2.2 for the manner in which extinction coefficients for light were estimated.

z	^{14}C	z	^{14}C	z	^{14}C	z	^{14}C	z	^{14}C	z	^{14}C	z	^{14}C	z	^{14}C
850807		**851104**		**851216**		**860127**		**860310**		**860414**		**860512**		**860605**	
1	284	1	31.2	2	18.7	1	7.18	1	45.5	2	23.7	1	2791	1.5	870
3	162	3.5	6.77	4.5	6.59	2	10.2	2	91.9	4.5	9.67	1.5	2677	2.5	831
4.5	197	5.5	10.2	7.5	10.4	4	10.8	4.5	73.0	7	1.06	2.5	2026	4	717
7.5	20.6	9	6.10	12	8.24	6	16.1	6.5	46.3	9.5	0	3	1651	5.5	392
14	30.9	16	6.10	20	6.59	12	13.8	9	35.3	12	0	4	791	6.5	229
23.6	4.41	27.3	0.87	33.8	0.94	20.2	1.96	15.9	5.05	20.9	0	6.6	113	11.3	32.8
	1627		197		237		204		648		104		9610		4942
860714		**860805**		**860908**		**861014**		**861112**		**861208**		**870120**		**870216**	
2.5	858	1.5	2094	1	883	1	230	1.5	12.4	1	13.1	1.5	18.0	1.5	19.0
4	384	2.5	1705	3	182	2	206	3	9.32	2	4.72	3	7.94	3	8.84
5.5	291	3.5	1778	4	26.8	3.5	205	5	9.32	3.5	9.10	5	2.81	4.5	1.90
7.5	129	5	1860	5	34.4	4.5	152	7	7.46	4.5	5.69	7	1.22	6	0
9	74.3	6	694	6.5	4.69	6	57.9	10	6.84	5.5	3.01	8	0.0	7.5	0
15.1	10.6	10.2	99.1	11.2	0.67	10.3	8.27	16.9	0.98	9.7	0.43	14.4	0.0	12.9	0
	4362		12094		2121		1202		113		49.6		61.8		58.9
870309		**870504**		**870615**		**870713**		**870826**		**870921**		**871019**		**871116**	
1	17.1	1.5	17.8	1.5	173	2	254	1.5	73.5	1.5	949	1	26.5	1	98.0
2	8.90	3.5	17.8	3	193	3	144	4	101	3	843	2.5	22.1	2	103
3.5	7.12	6	11.9	4.5	98.6	4.5	124	6	95.0	4	497	5	9.58	3	63.7
5	0	8.5	8.89	6.5	141	6	58.7	7.5	53.8	4.5	1555	6.5	11.8	4	51.9
7	0	11	5.93	7	113	7	28.8	10.5	15.2	5.5	379	9	5.90	5.5	15.3
12.0	0	19.3	0.85	12.7	16.2	11.9	4.12	17.9	2.18	9.3	54.1	15.8	0.84	9.2	2.19
	47.4		165		1329		1153		790		5569		158		416
871214		**880105**		**880201**		**880229**		**880328**		**880425**		**880524**		**880627**	
1.5	6.06	1.5	22.4	1.5	8.19	1.5	5.86	1	36.9	1	602	1	1130	1	365
3	0	3.5	12.3	3	7.45	3	3.73	2.5	38.7	2	852	2	917	2	300
4.5	0.46	5	5.16	5	3.36	5.5	4.27	4	41.4	3.5	1417	3	822	3	179
6	0	7	0	7	1.16	7.5	9.06	6	15.2	4.5	674	4	384	4	136
8	0	10	0	9	0	10.5	6.66	7.5	3.77	5	228	5	533	5	79.8
13.5	0	16.8	0	15.6	0	18.0	0.95	13.3	0.54	9.1	32.6	8.6	76.1	8.6	11.4
	14.3		86.5		40.5		85.2		234		4698		4932		1329
880808		**880916**		**881017**		**881115**		**881212**		**890104**		**890130**		**890306**	
1	321	1	109	2	17.5	1.5	7.87	1.5	4.19	1.5	5.13	2	5.22	1	19.7
2.5	261	3.5	73.9	4	7.71	3	3.31	4	1.07	3	1.43	4	5.22	2.5	16.6
4	196	5	31.8	6	3.44	5	0.79	6.5	1.40	5	0	6	4.31	4	6.83
5.5	113	8	18.0	9	0	7	0	9	0	7	3.80	7.5	3.82	6	0.17
6.5	72.3	10	10.3	13	0	9	0	11	0	9	2.54	9	2.31	7	0
11.7	10.3	17.9	1.47	21.8	0	15.6	0	19.7	0	15.6	0.36	15.6	0.33	12.7	0
	1583		555		76.6		25.1		17.7		31.6		47.8		71.5
890403		**890501**		**890704**		**890828**		**891010**							
1.5	56.5	1.5	303	1.5	26.9	1	1436	2	26.6						
3	53.3	3	275	3	109	2.5	103	4	45.6						
5	39.2	4.5	140	5	29.0	4	72.7	6	57.2						
7	29.1	6.5	75.3	7	0	5.5	75.8	9	25.8						
8.5	13.1	9	9.37	9.5	0	8.5	43.7	12.5	5.03						
15.0	1.87	15.2	1.34	16.3	0	14.3	6.24	21.1	0.72						
	396		1546		310		3129		426						

Table F.1: Volumetric (mg C m^{-3} d^{-1}) and areal (mg C m^{-2} d^{-1}) rates of ^{14}C uptake versus depth (z: meters) at station SN-9. See text of this appendix for details.

Z	^{14}C	Z	^{14}C	Z	^{14}C	Z	^{14}C	Z	^{14}C	Z	^{14}C	Z	^{14}C	Z	^{14}C
850809		**851104**		**851216**		**860127**		**860310**		**860414**		**860512**		**860605**	
1	583	1.5	3.97	1.5	40.7	1	47.3	1	195	1	21.0	1	795	1	316
2	504	3	9.92	3.5	32.2	2.5	43.9	2	108	3.5	6.67	2.5	593	2	189
3	290	4	3.97	6	20.3	4	54.1	4	71.1	6	0	4.5	265	3.5	143
6	24.2	6	3.97	11	18.6	6	32.1	6	62.6	9	0	6	117	5	71.5
15	0	13	1.98	20	1.69	12	28.7	10	53.0	12	0	7	96.6	6	23.1
25.4	0	21.1	0.28	34.2	0.24	20.0	4.10	17.0	7.57	21.4	0	12.8	13.8	10.7	3.30
	2104		59.6		399		563		1058		63.8		3323		1073
860714		**860805**		**860908**		**861014**		**861112**		**861208**		**870120**		**870216**	
1.5	699	1.5	448	1	900	1.5	233	1	8.42	1	26.3	1	15.8	1.5	27.3
3	161	3	320	2	1965	2.5	203	2	0	2	11.1	2.5	1.16	3	20.1
4.5	152	5	224	3	591	4	131	3	0	3.5	11.6	4	0.44	5.5	9.65
5.5	38.4	6.5	331	3.5	182	5.5	91.6	5	0	5	4.56	6	2.25	7.5	10.5
7	0	8	92.0	4.5	182	6.5	8.28	6.5	0	6.5	0	8	1.09	9.5	7.16
11.9	0	14.0	13.1	7.6	26.1	11.3	1.18	11.3	0	11.3	0	14.0	0.16	16.7	1.02
	2052		2768		4244		1051		12.6		77.5		38.5		174
870309		**870406**		**870504**		**870615**		**870713**		**870826**		**870921**		**871019**	
0.5	25.3	1	26.8	1.5	39.6	1	136	2.5	529	1.5	192	1	988	1.5	101
1.5	13.7	2	36.1	4	18.2	3	53.7	4.5	1081	2.5	57.6	2	1014	3	94.4
3	10.6	3	141	7	20.3	4.5	45.5	6	1149	4.5	35.2	3	1013	5	77.2
4.5	2.64	4.5	78.6	10	7.48	5.5	57.9	8	145	6	6.40	4	398	7	21.3
5.5	0.32	7	35.1	13	3.21	6.5	57.9	9	106	8	0	5	371	9	8.21
10.2	0	11.6	5.02	23.1	0.46	11.7	8.27	15.6	15.1	13.7	0	8.6	53.1	15.6	1.17
	62.4		528		261		639		6328		544		4684		621
871116		**871214**		**880105**		**880201**		**880229**		**880328**		**880425**		**880524**	
1	137	2	0	1.5	55.7	1.5	43.0	1.5	7.48	1.5	46.0	1.5	447	1	407
2	59.6	6	0	3	29.3	3	32.6	3	9.05	3	32.0	3	811	3	365
3	49.4	10	0	4.5	12.6	4.5	21.0	5	6.91	5	19.2	4.5	582	4	347
5	33.0	13.5	0	7	2.04	6.5	12.1	7	7.48	7	0.27	5.5	365	6	309
7	5.83	17	0	9.5	0.40	8	4.07	9.5	0.33	9.5	0	7	98.6	7	255
12.0	0.83	30.4	0	16.2	0.06	13.9	0.58	16.3	0	16.3	0	11.9	14.1	12.6	36.4
	424		0		201		217		64.7		198		3696		3078
880627		**880808**		**880916**		**881017**		**881115**		**881212**		**890104**		**890130**	
1	202	1.5	213	1.5	38.3	1	43.0	1.5	0	1	0	1.5	1.49	1.5	0.41
2.5	157	3	187	3	27.4	2	28.2	3	0	4	0	3.5	1.10	3.5	0.82
4	85.6	4	81.2	5	15.1	3	29.5	4.5	0	5	0	4.5	1.17	6	0
5.5	141	6	71.3	7	17.1	5	13.5	6.5	0	7	0	7	0	9	0.26
7	44.6	7	7.24	9.5	0	8	2.70	8.5	0	11	0	11.5	0	14	0.29
12.3	6.37	12.2	1.03	16.3	0	13.4	0.39	14.5	0	18.5	0	19.0	0	23.8	0
	1064		961		203		181		0		0		7.42		5.95
890306		**890403**		**890501**		**890704**		**890828**		**891010**					
2	16.3	1.5	23.8	1.5	94.6	2	69.1	1	684	1	286				
4	17.7	3.5	30.1	3.5	93.9	4	67.0	1.5	948	2	185				
5.5	16.9	7	16.1	6	55.5	6.5	45.4	2	282	3	10.9				
7	7.70	9	5.19	8.5	79.6	8.5	34.6	3	0	4	0				
10.5	5.56	11	0	11	71.5	11	29.2	4.5	201	5	0				
17.1	0.79	20.0	0	19.3	10.2	18.9	4.18	7.3	28.7	8.6	0				
	151		197		1133		677		1953		625				

Table F.2: Volumetric (mg C m^{-3} d^{-1}) and areal (mg C m^{-2} d^{-1}) rates of ^{14}C uptake versus depth (z: meters) at station SN-0.8. See text of this appendix for details.

Z	^{14}C	Z	^{14}C	Z	^{14}C	Z	^{14}C	Z	^{14}C	Z	^{14}C	Z	^{14}C	Z	^{14}C
850808		**851105**		**851217**		**860128**		**860311**		**860415**		**860513**		**860604**	
1.5	80.1	2.5	7.94	2	24.3	1.5	29.8	1	59.1	1.5	336	1	567	0.75	670
4	127	6	5.95	4	18.3	3	26.5	3	44.6	3	264	2	438	2.5	526
5	101	9.5	13.9	8	0	5	6.63	5.5	29.0	5	179	3.5	353	3.5	653
7	59.1	13	6.61	13.5	0	8	13.3	7.5	21.8	7	99.2	4.5	186	4.5	241
13	30.0	20	6.61	25	2.03	18	19.9	10	12.4	9	59.5	5.5	108	5.5	140
21.1	4.29	33.6	0.94	42.6	0.29	30.0	2.84	17.8	1.78	15.6	8.50	9.7	15.4	9.8	20.0
	1035		202		155		425		390		2007		2274		3035
860715		**860806**		**860909**		**861015**		**861113**		**861209**		**870121**		**870217**	
1	731	1	464	1.5	362	1	70.7	1.5	26.8	1	9.80	1	9.01	1.5	19.3
2.5	469	2	547	3	359	2	62.9	3	13.0	3.5	4.60	2	9.01	3.5	16.3
4	616	3	249	5	131	4	62.9	5	8.93	6	3.24	3.5	6.43	5.5	13.4
5	227	4.5	259	7.5	56.9	5.5	12.4	7	2.68	8	2.56	6	5.02	8	8.17
6.5	48.1	5.5	111	9	45.0	7	14.8	9	0	11.5	2.19	8	3.67	10.5	5.79
11.3	6.88	9.6	15.9	16.0	6.43	12.5	2.11	15.6	0	20.1	0.31	14.1	0.52	18.2	0.83
	3175		2134		2021		375		106		59.9		62.3		158
870310		**870407**		**870505**		**870616**		**870714**		**870827**		**870922**		**871020**	
1	8.02	1	159	1	96.6	1	244	1	218	1.5	247	1	261	0.5	170
2.5	7.23	2	110	2	62.1	2	419	2	322	2.5	220	2	124	2	85.2
5	2.96	3	107	3	71.8	4	317	4	246	4	198	3.5	103	3	89.5
7	0	5	59.1	4.5	41.4	5	248	6	677	5	105	5	57.9	4	58.2
9	0	6.5	30.1	6	35.9	6.5	189	9	193	6.5	50.2	6	36.7	5	30.4
16.2	0	11.3	4.29	10.2	5.13	11.5	27.0	15.5	27.6	10.9	7.17	10.7	5.25	9.0	4.34
	35.2		697		454		2330		3841		1285		865		533
871117		**871215**		**880106**		**880202**		**880301**		**880329**		**880426**		**880525**	
1.5	22.6	1	11.0	2	3.74	2	0	2	41.9	2	72.1	1.5	128	2	111
3	17.0	3	8.75	5	3.91	4.5	0	4	23.3	3	58.3	3.5	188	3	704
4.5	13.2	4.5	8.12	7	1.69	8.5	0	6	9.84	5	36.1	5.5	99.5	4	513
6.5	6.91	7	5.87	9.5	0	12.5	0	8	6.46	7	22.1	8	70.1	5	373
8	4.65	9	7.37	14	0	16	0	10	0	9	13.0	9	37.8	6	199
13.9	0.66	15.9	1.05	23.4	0	28.5	0	17.2	0	15.3	1.86	16.4	5.41	9.9	28.5
	127		96.2		26.7		0		205		434		1178		2327
880628		**880809**		**880917**		**881018**		**881116**		**881213**		**890105**		**890131**	
1	96.2	1.5	198	1.5	104	1.5	0	2	24.5	2	8.75	1.5	13.7	1.5	8.83
3	115	3	190	3.5	57.7	2.5	0	3.5	15.7	4.5	5.56	4	11.4	3.5	8.90
4	139	5	180	5.5	51.9	4	0	5	12.7	7	4.22	6.5	11.3	5.5	5.26
5.5	132	6.5	119	7.5	37.9	6	0	7	9.49	9	3.91	9	8.30	7	1.07
7	40.1	8	56.7	9	24.7	7.5	0	8	7.04	12	2.16	12	8.68	9.5	0
12.2	5.73	14.0	8.10	16.0	3.53	12.9	0	13.9	1.01	20.5	0.31	20.9	1.24	16.2	0
	856		1463		638		0		149		73.0		164		51.2
890307		**890404**		**890502**		**890606**		**890705**		**890829**		**891011**			
2	16.5	1	69.4	1.5	336	2	608	1	94.5	1.5	53.8	1	58.6		
4	16.1	2.5	69.9	3	511	3.5	531	2	69.3	3	65.3	2	32.6		
6.5	11.2	4.5	32.3	4	453	4.5	267	4	33.8	4	53.0	4	9.41		
9.5	12.2	6.5	10.6	5	128	6	78.6	5	12.6	5.5	41.2	5.5	2.54		
12.5	4.92	8.5	4.01	6	70.7	7.5	13.8	7.5	5.01	7	0	8	0		
21.6	0.70	15.1	0.57	10.2	10.1	12.4	1.97	12.8	0.72	11.8	0	13.8	0		
	180		345		2144		2829		337		331		158		

Table F.3: Volumetric (mg C m^{-3} d^{-1}) and areal (mg C m^{-2} d^{-1}) rates of ^{14}C uptake versus depth (z: meters) at station JV-3. Samples for the first four periods (850808 to 860128) were collected at station JV-11.5. See text of this appendix for details.

Z	^{14}C	Z	^{14}C	Z	^{14}C	Z	^{14}C	Z	^{14}C	Z	^{14}C	Z	^{14}C	Z	^{14}C
850808		**851105**		**851217**		**860128**		**860311**		**860415**		**860513**		**860604**	
1.5	79.8	1.5	20.8	2.5	9.50	2.5	0	1	67.1	1	373	1	485	1	96.0
3.5	56.3	3	9.02	5.5	0	5	11.7	3	50.5	2.5	235	2	503	2	81.5
6	83.9	5.5	6.94	9.5	6.71	9	14.2	5	31.7	5	118	3.5	434	3	374
8.5	61.4	9	7.63	15	0	14	6.79	8	34.7	7	64.5	4.5	188	4.5	788
13	22.5	18	5.55	25	0	20	4.32	10	24.1	9	37.2	6	58.4	5.5	282
22.1	3.22	30.3	0.79	42.3	0	34.5	0.62	18.1	3.45	16.2	5.32	10.3	8.34	9.6	40.3
	893		189		69.9		180		508		1669		2290		2324
860715		**860806**		**860909**		**861015**		**861113**		**861209**		**870121**		**870217**	
1	216	1	344	1.5	204	1.5	40.7	1.5	61.8	0.5	15.5	1.5	11.5	1.5	13.9
3	182	2	232	3	93.5	2.5	46.5	3	27.3	2	9.78	3	7.14	3	10.2
4.5	218	3	371	5	60.0	4.5	26.8	5	18.0	4.5	5.29	5	3.61	5	3.70
6	102	4.5	313	6.5	54.4	6.5	9.08	7	6.54	6.5	5.76	7.5	1.31	8	0
7.5	0	5.5	141	8	29.3	8	1.63	9	1.36	8	4.89	11	0.92	10	0
13.3	0	9.6	20.2	14.0	4.19	14.0	0.23	15.6	0.19	15.0	0.70	18.7	0.13	17.7	0
	1232		1926		907		226		241		78.8		55.2		58.3
870310		**870407**		**870505**		**870616**		**870714**		**870827**		**870922**		**871020**	
0.5	27.3	1	227	1	137	1	205	2	96.3	2	102	1.5	152	1	163
2	11.1	2	151	2	190	2	198	3	227	3.5	111	3	69.1	2	82.3
4	9.55	3	110	4	60.1	3	142	4.5	150	5	127	4.5	38.5	3.5	20.6
6	5.12	4.5	46.6	6	45.8	4	81.6	6.5	45.9	7	84.0	6.5	14.9	5	10.7
8.5	3.41	6	10.6	7	43.9	6	54.4	8.5	17.9	8.5	37.9	8.5	7.87	6	5.10
15.2	0.49	10.2	1.51	12.9	6.27	9.9	7.78	14.2	2.56	14.5	5.41	14.5	1.12	10.7	0.73
	98.2		727		810		923		944		944		572		405
871117		**871215**		**880106**		**880202**		**880301**		**880329**		**880426**		**880525**	
1.5	17.6	1.5	10.6	2	5.10	2	0	1	31.3	1.5	95.3	1	171	1	63.9
3	16.8	3.5	7.68	4.5	6.93	4	0	2.5	17.2	3	85.6	2	161	2.5	52.7
5	3.92	6	3.14	7	3.19	7.5	0	4	7.88	5	69.2	3	149	4	58.3
7.5	2.72	8.5	0.0	10	3.19	11	0	6	4.13	7	21.8	4	174	5	71.8
9.5	1.36	11	0.0	14	3.82	15	0	8	0	9	6.32	5	98.4	6.5	46.0
16.6	0.19	19.3	0.0	23.8	0.55	26.1	0	14.0	0	15.6	0.90	8.6	14.1	11.3	6.57
	89.6		51.6		78.3		0		103		571		947		485
880628		**880809**		**880917**		**881018**		**881116**		**881213**		**890105**		**890131**	
1.5	69.6	2	137	1	138	1	26.3	2	10.9	1.5	3.87	2	3.73	1.5	5.81
3	51.3	4	102	2	161	2	20.8	3.5	7.25	3	2.52	4	2.02	3.5	0
4.5	30.5	6	130	4	127	4	7.62	5.5	6.64	4.5	4.19	6.5	0.73	5.5	3.95
6	25.6	7.5	213	5.5	109	6	5.26	8	1.21	6	4.73	10	2.02	7.5	5.16
7	9.89	9	81.5	7	42.4	8.5	1.52	10	0	8	1.93	13	1.35	10	3.73
12.3	1.41	15.6	11.6	12.5	6.06	14.8	0.22	17.2	0	13.5	0.28	22.6	0.19	17.2	0.53
	339		1459		965		104		60.2		33.8		32.2		50.6
890307		**890404**		**890502**		**890606**		**890705**		**890829**		**891011**			
1.5	29.5	1.5	108	1.5	273	2	89.5	1.5	76.5	1	146	0.5	114		
4	29.3	3	71.2	2.5	272	3.5	91.4	3	45.4	2	175	1.5	32.9		
6.5	25.4	5	21.3	3.5	229	5	245	5.5	75.2	3.5	269	2.5	6.68		
9	14.9	7	14.7	4.5	167	7	212	7	44.3	5	269	4	2.71		
10.5	3.46	9	9.15	6	82.9	9	93.4	8	17.5	6	43.0	5.5	0		
19.1	0.49	15.6	1.31	9.8	11.8	15.1	13.3	14.6	2.49	10.7	6.14	9.7	0		
	263		476		1466		1588		526		1286		160		

Table F.4: Volumetric (mg C m^{-3} d^{-1}) and areal (mg C m^{-2} d^{-1}) rates of ^{14}C uptake versus depth (z: meters) at station JV-7. See text of this appendix for details.

Appendix G

Sediment-trap data of Saanich Inlet

This appendix presents the sediment-trap data collected from Saanich Inlet during the study (see section 3.2 for methods). Sediment traps were moored in pairs with a brine solution at the base of each. In addition, NaN_3 was used in one sediment trap of each pair while no preservative was used in the other (section 3.2). The total mass, OC and N fluxes presented in these tables are the averages of the fluxes to the two traps in each pair. BSi, Al and Ti were measured on samples collected by the NaN_3-treated sediment traps and stable isotope ratios were determined for samples collected by sediment traps without NaN_3. The $CaCO_3$ fluxes presented in these tables are those collected by the sediment traps treated with sodium azide, as NaN_3 buffers $CaCO_3$ dissolution. "start" and "end" are the beginning and end of each deployment period.

start	end	mass	OC	N	BSi	$CaCO_3$	Al	Ti	$\delta^{13}C$	$\delta^{15}N$
ddmmyy					mg m^{-2} day^{-1}					
830809	830912	10197	531	64.2	3751	203	428	28.1	-19.9	-
830912	830930	8135	498	59.3	3715	176	265	16.5	-19.1	-
830930	831031	5511	309	34.2	1873	79.3	243	16.5	-20.2	-
831031	831128	6812	313	32.7	1312	26.4	-	-	-	-
831128	840112	4300	163	17.0	528	44.1	267	17.8	-22.4	-
840112	840209	4311	206	24.5	569	61.7	273	17.3	-	-
840209	840305	3226	165	21.9	527	0	204	13.1	-	-
840305	840409	3999	233	35.2	1499	0	174	11.4	-19.9	-
840409	840510	5802	337	47.9	1920	0	275	18.1	-19.5	-
840510	840618	6982	413	60.1	2943	70.5	246	16.5	-19.6	-
840618	840716	9039	554	80.1	3349	132	335	21.1	-19.2	-
840716	840824	8690	570	82.2	3510	52.9	321	19.8	-19.1	-
840824	840919	7415	543	73.9	2095	52.9	365	22.6	-20.3	-
840919	841108	7954	402	46.5	1803	177	391	24.1	-20.9	-
841108	841213	4230	174	19.7	580	59.8	264	17.2	-22.8	-
841213	850117	3495	163	18.2	504	80.0	220	13.8	-22.6	8.9
850117	850218	2550	142	16.8	391	63.1	156	10.2	-22.3	9.4
850218	850328	2656	134	14.7	525	53.2	153	9.42	-23.0	7.3
850328	850425	5891	331	45.7	2392	93.4	264	17.0	-21.1	7.3
850425	850521	4206	329	45.6	2201	69.3	102	6.56	-19.3	7.3
850521	850703	6148	419	56.3	2532	168	220	14.2	-19.4	6.9
850807	850917	9775	574	71.2	4709	165	378	24.4	-19.3	6.1
850917	851008	5571	388	49.9	2105	26.8	229	14.3	-19.9	7.1
851008	851104	4500	229	27.9	991	63.9	280	17.7	-21.1	6.9
851104	851216	3302	175	20.1	560	50.3	191	11.9	-21.9	7.5
860310	860414	4172	258	32.6	1578	56.0	195	12.3	-20.6	7.3
860414	860512	3360	211	28.9	892	48.7	182	11.5	-21.2	7.5
860512	860605	5127	363	50.4	2174	79.4	187	12.2	-20.5	7.3
860605	860714	7234	485	64.2	2075	97.2	345	21.4	-20.5	7.6
860714	860805	4067	356	48.7	1215	64.5	172	11.1	-19.8	8.4
860805	860908	7180	466	57.6	3086	70.5	242	15.5	-19.3	7.3
860908	861014	6893	542	65.0	2536	85.4	266	16.3	-20.1	7.7
861014	861112	5405	490	57.9	1527	55.8	246	15.7	-20.5	8.6
861112	861208	5437	316	37.2	793	59.9	361	23.0	-21.4	8.7
861208	870120	4451	221	25.6	594	50.1	310	20.0	-21.9	8.9

Table G.1: Sediment-trap fluxes measured at station SN-9: 45 m.

start	end	mass	OC	N	BSi	$CaCO_3$	Al	Ti	$\delta^{13}C$	$\delta^{15}N$
ddmmyy		mg m^{-2} day^{-1}								
870120	870216	3128	176	20.2	432	34.0	206	12.4	-22.0	9.4
870216	870309	4368	236	28.8	735	53.6	286	17.2	-22.9	9.4
870309	870406	3266	206	26.6	872	36.1	179	11.2	-22.4	8.5
870406	870504	6808	431	59.9	3457	34.7	193	12.3	-19.6	7.1
870504	870615	7427	420	56.4	2830	89.5	303	18.8	-19.5	5.9
870615	870713	10333	697	91.4	3748	193	362	22.4	-19.3	8.0
870713	870826	9008	577	73.8	3531	159	328	19.2	-19.7	6.3
870826	870921	7417	558	83.5	2933	116	241	15.5	-19.4	7.4
870921	871019	7053	536	61.0	3037	59.2	189	12.0	-19.7	7.0
871019	871116	4207	258	31.3	1442	49.8	175	11.2	-21.5	7.1
871116	871214	2885	147	16.9	849	45.0	152	10.3	-22.7	-
871214	880105	2647	158	18.7	352	28.1	166	10.4	-21.6	-
880229	880328	3788	215	26.1	802	59.1	209	12.4	-22.2	8.6
880328	880425	7614	420	52.9	2816	51.1	282	18.0	-20.6	6.4
880425	880524	7146	497	59.2	3009	22.5	140	9.62	-19.3	6.5
880524	880627	10534	525	61.1	3452	65.0	418	26.8	-19.7	6.3
880627	880808	6166	446	58.0	1797	99.6	255	15.4	-20.0	7.0
880808	880916	6130	452	59.1	2284	110	196	12.6	-20.1	6.7
880916	881017	5754	449	54.9	2411	95.6	183	11.4	-20.1	7.7
881212	890104	3065	172	20.8	443	47.1	171	11.7	-21.4	8.8
890104	890130	3368	207	24.4	476	51.5	206	13.0	-21.8	8.8
890130	890306	4530	230	25.3	758	95.2	283	18.0	-22.3	7.2
890306	890403	2852	161	19.2	517	39.7	160	9.91	-19.8	-
890403	890501	7778	488	65.6	3650	43.0	193	12.3	-19.3	6.0
890501	890605	5336	448	55.5	2292	28.7	92.9	6.45	-18.7	6.4
890605	890704	6430	508	66.2	2681	37.6	135	9.00	-18.7	6.9
891010	891215	4504	300	33.8	1431	41.9	180	12.3	-19.8	6.4

Table G.2: Sediment-trap fluxes measured at station SN-9: 45 m (continued).

start ddmmyy	end	mass	OC	N	BSi	$CaCO_3$	Al	Ti	$\delta^{13}C$	$\delta^{15}N$
					mg m^{-2} day^{-1}					
830809	830912	17369	765	86.8	5184	247	835	50.9	-	-
830912	830930	13688	669	73.9	4625	344	642	40.2	-	-
830930	831031	10451	446	49.1	2852	61.7	606	39.6	-	-
831031	831128	-	-	-	-	-	-	-	-	-
831128	840112	9182	280	28.9	1134	0	590	36.7	-	-
840112	840209	5998	211	22.2	743	-	389	24.4	-	-
840209	840305	13064	386	39.8	1690	0	902	58.4	-	-
840305	840409	9060	316	42.1	2447	0	528	34.6	-	-
840409	840510	17655	608	79.4	4142	88.2	1108	73.5	-	-
840510	840618	12376	615	86.1	4058	106	608	41.3	-	-
840618	840716	20146	891	126	5290	167	1082	69.7	-	-
840716	840824	16259	844	111	5124	52.9	733	49.2	-	-
840824	840919	9504	560	76.6	2380	52.9	507	34.3	-	-
840919	841108	12516	547	58.5	2328	162	669	42.8	-	-
841108	841213	9567	331	39.7	1223	121	593	38.9	-	-
841213	850117	7873	282	30.3	1036	104	495	33.4	-	7.6
850117	850218	11517	392	43.2	1422	129	855	51.3	-	7.7
850218	850328	13742	480	52.2	1862	157	1043	67.8	-	7.7
850328	850425	8323	408	52.0	2492	88.2	462	27.4	-	8.6
850425	850521	10255	551	73.9	3796	82.4	487	30.6	-	8.8
850521	850703	10173	611	79.8	3636	84.7	484	32.2	-	8.3
850807	850917	15572	765	94.1	5930	167	765	45.6	-	6.0
850917	851008	9320	527	65.2	2898	35.7	474	30.5	-	7.1
851008	851104	8960	424	48.4	1733	74.2	570	36.7	-	6.3
851104	851216	11499	794	79.3	1686	121	644	43.0	-	8.2
860310	860414	6739	352	42.1	1880	53.9	367	23.3	-	8.1
860414	860512	9744	395	48.7	1851	75.1	575	38.5	-	8.0
860512	860605	10847	594	79.1	3183	96.7	555	34.8	-	8.9
860605	860714	12360	707	95.4	2972	91.8	641	41.3	-	9.1
860714	860805	9260	571	75.9	2374	70.7	511	31.5	-	8.3
860805	860908	13175	768	93.5	4290	106	578	37.6	-	7.8
860908	861014	9845	789	92.6	2679	79.6	457	29.0	-	8.6
861014	861112	8196	668	79.2	1921	64.0	456	29.0	-	9.4
861112	861208	12913	551	62.0	1786	112	852	54.9	-	8.4
861208	870120	7720	343	39.0	1084	71.1	476	31.9	-	8.8

Table G.3: Sediment-trap fluxes measured at station SN-9: 110 m.

start	end	mass	OC	N	BSi	$CaCO_3$	Al	Ti	$\delta^{13}C$	$\delta^{15}N$
ddmmyy		mg m^{-2} day^{-1}								
870120	870216	7686	378	43.8	1028	65.2	513	31.1	-	9.7
870216	870309	8057	423	49.9	1317	77.3	523	33.5	-	10.4
870309	870406	5425	327	42.6	1174	48.6	332	20.2	-	10.0
870406	870504	12222	595	79.4	4058	66.9	545	35.0	-	-
870504	870615	14779	677	87.2	4316	96.9	744	48.7	-	7.1
870615	870713	16751	1000	136	4799	118	685	46.9	-	8.8
870713	870826	13005	734	90.9	4291	104	629	38.8	-	7.0
870826	870921	12099	745	92.4	3495	89.4	571	34.6	-	7.6
870921	871019	10699	640	72.7	3415	50.4	456	27.5	-	6.7
871019	871116	7797	369	43.7	1967	53.0	414	26.5	-	6.9
871116	871214	15130	516	54.5	2567	109	931	61.3	-	6.3
871214	880105	7300	342	37.2	1049	41.1	464	30.4	-	-
880229	880328	13348	501	58.1	2073	65.2	852	55.4	-	-
880328	880425	12419	502	59.1	3641	54.3	644	40.3	-	7.1
880425	880524	12359	689	76.4	3961	49.4	441	29.9	-	8.2
880524	880627	11439	633	74.2	3801	77.7	452	29.0	-	7.8
880627	880808	10847	618	76.5	2858	74.3	600	37.7	-	6.6
880808	880916	11783	764	92.4	3464	91.4	504	32.4	-	7.6
880916	881017	10169	618	75.7	2880	65.4	445	29.1	-	6.9
881212	890104	9248	335	36.6	1177	64.2	561	37.8	-	7.6
890104	890130	7573	306	33.0	1075	55.9	491	32.1	-	7.3
890130	890306	12955	492	54.9	1770	113	804	56.0	-	7.6
890306	890403	6927	341	41.6	1173	63.4	357	24.3	-	8.8
890403	890501	9776	468	59.1	3266	36.6	377	23.3	-	7.6
890501	890605	9754	532	65.3	3197	57.7	402	25.9	-	-
890605	890704	13117	711	87.8	3856	53.7	453	30.9	-	8.0
891010	891215	7330	449	47.3	1914	49.0	335	22.7	-	7.2

Table G.4: Sediment-trap fluxes measured at station SN-9: 110 m (continued).

start	end	mass	OC	N	BSi	$CaCO_3$	Al	Ti	$\delta^{13}C$	$\delta^{15}N$
ddmmyy		mg m^{-2} day^{-1}								
830809	830912	18459	724	83.0	4854	414	960	62.5	-20.5	-
830912	830930	12662	592	64.5	4151	212	593	37.9	-19.7	-
830930	831031	11456	446	51.5	2791	70.5	626	41.8	-20.5	-
831031	831128	7087	289	34.7	1308	0	461	30.1	-20.9	-
831128	840112	8658	260	25.6	1075	52.9	554	37.2	-22.4	-
840112	840209	6008	209	21.1	788	0	393	24.9	-22.0	-
840209	840305	9965	291	30.4	1292	0	652	42.6	-22.1	-
840305	840409	7066	264	34.6	1842	0	417	26.4	-21.0	-
840409	840510	13905	468	58.4	3114	79.3	821	54.5	-20.7	-
840510	840618	9626	429	57.2	2973	150	473	31.8	-20.0	-
840618	840716	39631	1273	161	7821	194	2437	162	-19.7	-
840716	840824	30306	1069	139	6625	79.3	1894	119	-20.5	-
840824	840919	10208	521	69.9	2244	0	565	38.3	-20.9	-
840919	841108	14308	530	58.5	2466	212	794	50.8	-21.4	-
841108	841213	9750	317	39.0	1241	117	587	37.1	-21.8	-
841213	850117	8041	277	30.2	1045	119	507	33.0	-22.7	7.2
850117	850218	9886	320	34.1	1277	119	714	44.8	-22.7	6.4
850218	850328	23082	631	64.6	3007	264	1737	112	-22.8	5.9
850328	850425	8289	333	41.0	2197	89.9	512	30.9	-22.1	7.4
850425	850521	13145	536	69.7	4595	100	645	45.7	-20.6	7.1
850521	850703	12460	563	72.9	3842	113	638	43.1	-20.2	-
850807	850917	18396	752	92.8	5619	204	1040	65.0	-20.3	6.7
850917	851008	15026	665	78.9	3669	148	874	54.1	-20.8	-
851008	851104	16156	580	64.6	2490	157	1132	70.1	-21.6	6.4
851104	851216	14742	633	71.7	2110	142	859	56.7	-21.4	7.4
860310	860414	6924	299	34.6	1912	49.7	387	24.1	-21.3	6.6
860414	860512	9462	337	38.3	1802	57.8	638	41.2	-21.8	5.9
860512	860605	9191	385	49.2	2732	75.5	526	32.4	-21.1	6.4
860605	860714	11909	545	70.4	2719	85.4	645	40.6	-21.2	9.1
860714	860805	11138	498	61.7	2503	79.7	670	41.8	-20.9	7.9
860805	860908	26615	896	101	5564	169	1591	101	-21.0	6.3
860908	861014	14135	594	69.3	3482	135	803	50.0	-20.9	6.4
861014	861112	11665	508	60.1	2382	88.1	692	43.8	-21.2	7.1
861112	861208	12947	474	53.7	1748	114	868	58.4	-22.7	6.5
861208	870120	8205	322	36.9	1099	64.9	567	34.5	-22.3	8.0

Table G.5: Sediment-trap fluxes measured at station SN-9: 150 m.

start	end	mass	OC	N	BSi	$CaCO_3$	Al	Ti	$\delta^{13}C$	$\delta^{15}N$
ddmmyy		mg m^{-2} day^{-1}								
870120	870216	7943	292	31.0	1016	52.6	542	33.1	-22.6	7.2
870216	870309	7457	277	27.6	1102	43.1	437	28.1	-23.0	5.6
870309	870406	5080	204	22.1	1055	28.8	311	19.4	-22.8	6.5
870406	870504	10614	400	48.8	3704	36.5	496	30.6	-20.7	5.8
870504	870615	13316	489	58.0	3760	61.5	772	50.5	-20.5	5.7
870615	870713	16842	711	85.1	4825	81.4	886	56.0	-20.3	7.1
870713	870826	19208	765	96.0	5025	144	1099	67.5	-20.5	7.1
870826	870921	16580	732	90.3	4153	138	769	51.1	-20.7	7.2
870921	871019	13173	650	75.8	3800	80.7	596	36.5	-20.3	6.4
871019	871116	9030	462	54.2	2134	62.5	481	31.4	-21.4	7.4
871116	871214	13688	463	51.5	2308	93.1	844	56.1	-22.4	6.0
871214	880105	8239	302	33.0	1146	37.4	527	32.5	-22.1	-
880229	880328	14590	491	52.6	2341	92.7	922	55.7	-21.6	6.1
880328	880425	16218	604	67.3	4020	90.6	895	54.9	-21.2	-
880425	880524	11491	543	64.9	3846	59.2	495	33.1	-19.6	6.8
880524	880627	6931	464	56.1	2837	45.1	173	11.0	-19.0	7.3
880627	880808	12062	579	69.9	2768	92.9	664	43.1	-20.5	7.7
880808	880916	15643	718	80.6	3865	124	808	53.5	-20.6	7.0
880916	881017	11594	558	66.7	2994	110	553	36.0	-20.4	6.7
881212	890104	10241	361	38.4	1304	84.6	634	42.9	-21.5	6.9
890104	890130	6655	257	28.3	926	44.6	425	27.7	-21.5	6.9
890130	890306	13411	456	49.0	1798	119	813	54.8	-22.1	6.7
890306	890403	5554	230	25.5	920	34.8	318	21.9	-21.8	6.9
890403	890501	9699	416	49.5	3278	40.5	399	27.4	-20.7	6.4
890501	890605	8734	424	49.8	2801	43.9	330	22.2	-19.9	6.5
890605	890704	18274	729	84.0	4729	63.3	838	56.8	-19.9	7.4
891010	891215	7298	350	40.8	1851	49.7	339	22.6	-20.4	6.4

Table G.6: Sediment-trap fluxes measured at station SN-9: 150 m (continued).

start ddmmyy	end ddmmyy	mass	OC	N	BSi	$CaCO_3$	Al	Ti	$\delta^{13}C$	$\delta^{15}N$
					mg m^{-2} day^{-1}					
840112	840209	1042	60.8	7.09	-	17.6	-	-	-	-
840209	840305	682	50.2	6.35	111	44.1	39.5	2.34	-22.5	-
840305	840409	2142	226	37.1	1229	159	36.1	2.19	-19.6	-
840409	840510	3787	305	42.7	1920	0	50.3	3.02	-18.4	-
840510	840618	2898	266	37.4	1615	0	25.2	1.59	-18.4	-
840618	840716	2459	300	47.1	794	26.4	27.2	1.67	-19.2	-
840716	840824	2385	317	47.0	996	44.1	27.2	1.50	-18.8	-
840824	841006	894	122	16.8	294	35.3	11.9	0.795	-19.5	-
841006	841108	1102	110	12.8	294	53.7	47.5	3.02	-21.7	-
841108	841213	981	101	14.5	135	38.4	44.5	2.96	-22.4	-
841213	850117	969	75.4	8.24	127	36.2	62.5	3.75	-22.9	9.3
850117	850218	973	65.6	8.38	170	43.6	56.0	3.18	-22.1	9.5
850218	850328	1027	76.1	10.4	227	44.9	54.8	3.22	-22.3	8.7
850328	850425	2896	213	29.5	1669	43.4	51.5	3.23	-20.8	6.6
850425	850521	2917	298	41.9	1885	40.8	23.2	1.52	-19.4	7.8
850521	850703	2960	326	44.0	1591	81.7	36.7	2.06	-18.9	8.9
850703	850807	1898	283	38.3	883	25.7	23.0	1.34	-19.5	8.7
850807	850917	1584	176	21.6	809	57.3	15.0	1.11	-19.0	9.2
850917	851008	1716	183	22.7	791	5.20	14.5	0.989	-19.0	8.1
851008	851104	673	79.2	10.3	177	23.9	23.5	1.52	-20.2	9.4
851104	851216	720	79.3	10.9	140	3.18	32.0	2.07	-21.2	10.6
851216	860127	1333	112	12.5	216	35.1	76.9	4.41	-21.8	8.5
860127	860310	1275	106	13.2	131	19.8	85.0	5.12	-22.2	8.8
860310	860414	1629	145	19.4	821	25.2	35.6	2.14	-20.2	9.0
860414	860512	849	116	16.0	289	25.1	23.9	1.48	-20.9	8.4
860512	860605	3035	323	40.1	1650	84.2	39.7	2.42	-20.3	8.8
860605	860714	1305	201	26.8	500	25.2	-	-	-20.1	8.7
860714	860805	1386	217	27.6	680	13.9	12.7	0.861	-19.3	9.0
860805	860908	2468	268	34.4	1378	53.3	19.0	1.49	-18.8	8.2
860908	861014	746	103	12.6	322	28.1	11.2	0.756	-19.3	8.5
861014	861112	969	131	16.8	404	21.5	10.1	0.735	-19.4	8.7
861112	861208	1088	113	12.9	177	24.9	47.0	3.20	-21.2	8.9
861208	870120	947	69.7	8.24	151	15.7	56.2	3.26	-22.4	9.8

Table G.7: Sediment-trap fluxes measured at station SN-0.8: 50 m.

start ddmmyy	end ddmmyy	mass	OC	N	BSi	$CaCO_3$	Al	Ti	$\delta^{13}C$	$\delta^{15}N$
		mg m^{-2} day^{-1}								
870120	870216	1042	97.6	11.6	160	18.9	62.9	3.65	-21.4	10.7
870216	870309	1325	117	14.6	233	33.8	70.1	4.26	-22.4	9.3
870309	870406	1274	124	16.0	431	7.99	49.9	2.91	-22.7	8.6
870406	870504	3807	310	42.1	2312	18.4	43.4	2.49	-19.5	7.9
870504	870615	2537	249	32.7	1442	27.7	31.0	1.60	-19.2	8.0
870615	870713	2866	291	36.9	1319	42.8	29.0	2.33	-19.1	-
870713	870826	2630	292	37.6	1253	58.7	27.8	1.97	-19.4	8.0
870826	870921	622	108	14.3	176	20.9	9.74	0.720	-20.9	8.6
870921	871019	1175	142	17.8	510	6.95	6.36	0.514	-19.1	7.8
871019	871116	353	58.1	6.33	70.4	22.0	10.3	0.736	-	-
871116	871214	1110	88.6	10.2	355	29.4	35.6	2.42	-23.0	7.9
871214	880105	1036	105	12.2	125	23.3	59.5	3.70	-22.2	6.3
880105	880201	688	65.9	7.21	113	29.0	33.0	1.91	-22.4	6.5
880201	880229	645	67.5	7.76	131	17.6	29.9	1.86	-23.1	7.3
880229	880328	694	69.6	8.71	182	39.9	29.8	1.84	-20.3	7.1
880328	880425	2610	191	22.6	1174	11.9	45.2	2.63	-19.8	5.8
880425	880524	4266	368	46.1	2404	29.1	26.4	1.59	-19.0	7.1
880524	880627	3262	232	28.2	1702	25.1	45.0	2.86	-20.8	8.2
880627	880808	836	173	23.1	206	36.6	12.1	0.786	-21.9	6.4
881017	881115	988	117	11.1	350	30.0	17.2	1.23	-21.8	6.4
881115	881212	805	93.3	10.4	158	25.6	31.9	2.17	-20.4	8.4
881212	890104	513	56.3	6.23	75.3	19.2	25.1	1.62	-22.3	8.9
890104	890130	925	96.3	10.6	128	27.0	49.2	2.93	-21.7	9.0
890130	890306	1305	117	14.4	187	87.1	60.6	3.87	-21.9	9.0
890306	890403	481	56.0	7.82	104	12.2	23.2	1.35	-22.9	9.3
890403	890501	4120	296	40.0	2104	24.7	58.4	3.33	-20.9	6.7
890501	890605	3077	300	36.7	1246	22.2	14.6	1.10	-19.1	7.5
890605	890704	2963	327	40.9	1160	33.2	25.4	1.61	-19.1	7.4
890704	890828	1790	243	29.3	507	33.0	12.1	0.906	-19.7	7.9
890828	891010	863	142	16.8	146	7.24	5.95	0.488	-20.4	7.1
891010	891215	961	105	11.4	414	17.1	19.2	1.31	-19.9	7.1

Table G.8: Sediment-trap fluxes measured at station SN-0.8: 50 m (continued).

start	end	mass	OC	N	BSi	$CaCO_3$	Al	Ti	$\delta^{13}C$	$\delta^{15}N$
ddmmyy		mg m^{-2} day^{-1}								
840112	840209	2237	108	11.3	289	26.4	150	8.89	-22.1	-
840209	840305	2253	117	14.8	370	0	139	8.07	-22.0	-
840305	840409	2682	198	29.9	1120	79.3	94.3	5.60	-20.1	-
840409	840510	4073	236	31.3	1818	0	110	6.61	-18.7	-
840510	840618	3274	239	33.5	1728	52.9	64.8	3.88	-18.9	-
840618	840716	2322	188	29.2	447	17.6	47.2	2.84	-19.6	-
840716	840824	2258	242	32.9	963	52.9	39.9	2.30	-19.4	-
840824	841006	1015	98.4	14.2	280	-	12.0	0.787	-19.6	-
841006	841108	-	-	-	-	-	-	-	-	-
841108	841213	1410	103	13.9	200	46.4	74.6	4.96	-22.4	-
841213	850117	1740	97.1	10.9	238	51.5	111	6.46	-22.8	8.4
850117	850218	1884	94.3	11.0	309	60.8	116	6.85	-22.3	8.4
850218	850328	2425	124	14.4	415	56.3	150	9.03	-22.4	8.1
850328	850425	3558	212	26.9	1539	66.4	131	7.83	-21.3	7.9
850425	850521	4578	323	41.7	2557	73.2	70.4	3.98	-19.9	8.2
850521	850703	3642	323	43.5	1896	67.2	64.2	3.52	-19.5	8.9
850703	850807	1845	240	31.9	744	29.3	33.3	2.11	-19.6	8.9
850807	850917	1432	124	17.1	604	25.7	20.2	1.32	-18.8	8.9
850917	851008	1381	155	19.4	616	7.00	17.8	1.24	-19.1	7.8
851008	851104	1422	134	18.2	279	54.8	49.8	3.28	-21.2	9.2
851104	851216	1762	123	14.9	242	74.5	71.4	4.75	-22.3	8.4
851216	860127	2775	139	15.3	406	99.0	161	9.21	-22.1	7.8
860127	860310	2293	138	15.7	284	56.9	144	8.48	-23.2	8.5
860310	860414	2234	157	20.2	927	41.2	76.5	4.38	-20.9	8.4
860414	860512	1765	120	15.7	443	31.1	74.2	5.23	-21.5	-
860512	860605	3241	227	30.0	1705	82.2	83.0	4.94	-20.4	7.1
860605	860714	1756	176	23.0	654	45.0	40.4	2.22	-20.2	8.3
860714	860805	1899	205	27.4	827	50.8	36.7	2.37	-19.7	8.2
860805	860908	2228	210	27.1	951	48.0	36.0	2.34	-19.4	9.5
860908	861014	884	94.8	12.3	299	24.0	19.4	1.30	-20.8	10.2
861014	861112	1694	215	26.6	441	51.3	29.9	2.03	-20.4	9.7
861112	861208	2359	139	16.5	329	71.7	103	6.94	-21.8	9.2
861208	870120	2100	125	16.0	301	52.4	119	7.01	-21.8	10.5

Table G.9: Sediment-trap fluxes measured at station SN-0.8: 135 m.

start ddmmyy	end ddmmyy	mass	OC	N	BSi	$CaCO_3$	Al	Ti	$\delta^{13}C$	$\delta^{15}N$
		mg m^{-2} day^{-1}								
870120	870216	2520	145	17.6	372	52.4	145	8.71	-22.1	9.7
870216	870309	2013	132	15.5	351	48.4	107	6.61	-22.6	8.5
870309	870406	2146	130	15.7	457	11.7	112	6.38	-22.7	8.2
870406	870504	4379	227	30.2	2076	45.7	111	6.38	-20.2	7.3
870504	870615	3810	230	30.8	1632	47.0	86.8	4.98	-19.5	7.9
870615	870713	4254	353	44.1	1899	74.3	89.1	4.68	-18.8	8.5
870713	870826	3424	312	41.7	1296	84.5	64.8	4.04	-21.0	9.3
870826	870921	1437	151	21.5	355	48.5	32.2	2.12	-20.9	9.3
870921	871019	1263	128	17.6	435	10.5	15.4	1.11	-19.5	-
871019	871116	563	54.0	6.82	127	21.6	17.6	1.13	-20.9	9.4
871116	871214	1869	114	13.5	468	51.7	77.7	5.15	-22.6	8.6
871214	880105	2994	185	23.5	530	80.0	150	9.25	-22.3	9.9
880105	880201	2762	145	17.0	414	75.7	146	8.36	-22.5	9.0
880201	880229	2006	120	14.8	316	58.0	80.7	4.58	-22.4	9.7
880229	880328	2437	147	18.0	460	62.7	111	6.91	-22.5	9.1
880328	880425	3824	234	29.2	1170	53.1	135	8.05	-21.2	8.6
880425	880524	5062	405	46.1	2398	60.8	74.0	4.43	-19.8	8.5
880524	880627	4023	313	37.4	1973	30.0	46.4	2.96	-19.1	8.0
880627	880808	1566	202	27.3	314	33.6	37.0	2.46	-20.5	8.5
881017	881115	1122	112	10.4	323	26.7	28.6	2.01	-21.6	7.5
881115	881212	1464	102	11.6	252	31.9	61.2	4.14	-21.4	8.2
881212	890104	1842	115	12.4	286	47.7	101	6.03	-21.8	8.6
890104	890130	1913	111	12.9	283	42.4	103	6.19	-22.4	8.8
890130	890306	3165	178	21.2	470	114	163	10.1	-21.9	9.3
890306	890403	1603	121	15.9	294	37.5	-	-	-	8.6
890403	890501	4214	267	35.4	1839	40.1	117	6.61	-21.2	8.0
890501	890605	3959	307	40.2	1685	44.1	61.0	3.88	-19.3	8.3
890605	890704	3496	282	37.8	1150	22.6	47.5	2.85	-18.9	8.5
890704	890828	2310	247	30.2	621	35.2	34.2	2.21	-20.2	8.4
890828	891010	884	129	16.1	131	40.6	13.7	0.976	-21.0	9.4
891010	891215	1094	105	12.2	387	26.1	32.4	2.15	-20.3	7.7

Table G.10: Sediment-trap fluxes measured at station SN-0.8: 135 m (continued).

start	end	mass	OC	N	BSi	$CaCO_3$	Al	Ti	$\delta^{13}C$	$\delta^{15}N$
ddmmyy		mg m^{-2} day^{-1}								
840112	840209	1909	93.1	9.36	259	0	134	8.00	-22.3	-
840209	840305	1814	95.2	11.5	289	52.9	118	6.87	-22.1	-
840305	840409	2481	189	28.1	1012	0	87.6	5.22	-19.9	-
840409	840510	3152	191	26.2	1686	0	91.9	5.73	-19.1	-
840510	840618	3390	242	33.8	1675	44.1	68.6	4.06	-18.8	-
840618	840716	3433	303	46.4	1626	70.5	76.5	4.65	-19.3	-
840716	840824	2206	242	33.8	919	44.1	45.0	2.67	-19.5	-
840824	841006	894	95.2	13.3	173	8.82	14.2	0.946	-20.4	-
841006	841108	3253	309	40.9	209	32.3	134	8.74	-21.6	-
841108	841213	1515	112	14.7	214	49.9	79.5	5.30	-21.7	-
841213	850117	1845	99.3	11.3	253	37.0	115	7.07	-23.0	8.3
850117	850218	1973	100	11.9	322	64.2	125	7.26	-22.5	7.8
850218	850328	2248	115	14.3	398	61.9	137	8.29	-21.9	8.1
850328	850425	3050	176	22.9	1245	48.0	118	7.26	-21.1	6.8
850425	850521	3805	254	33.2	2045	41.0	58.6	3.46	-19.6	7.6
850521	850703	2963	263	36.6	1534	52.5	55.4	3.02	-19.0	8.3
850703	850807	1493	192	22.5	594	8.81	27.4	1.81	-19.5	9.4
850807	850917	1690	155	20.9	717	33.0	30.2	2.09	-19.8	8.5
850917	851008	2367	224	31.0	775	68.1	30.7	2.02	-19.7	-
851008	851104	2741	235	27.7	286	132	58.8	3.85	-20.3	9.6
851104	851216	2548	152	19.2	236	104	88.9	6.04	-21.5	9.0
851216	860127	3430	166	18.7	367	142	157	9.32	-21.9	7.7
860127	860310	3364	161	18.7	261	137	155	9.56	-22.6	8.1
860310	860414	3226	186	22.9	888	121	90.8	5.51	-20.9	8.0
860414	860512	2294	147	19.0	466	88.1	95.2	5.87	-21.6	-
860512	860605	3170	216	29.5	1322	81.6	83.5	5.25	-21.1	7.6
860605	860714	2009	202	27.0	856	49.2	49.1	2.73	-20.4	7.8
860714	860805	1686	200	27.5	749	31.4	33.3	2.12	-19.6	8.2
860805	860908	2326	212	27.8	989	44.0	38.7	2.73	-19.7	8.9
860908	861014	1668	152	21.0	327	79.8	26.3	1.70	-21.3	10.2
861014	861112	2463	297	37.4	473	114	34.1	2.29	-20.1	10.5
861112	861208	3299	178	22.9	331	132	116	7.52	-21.3	9.8
861208	870120	2869	137	17.2	248	124	115	6.88	-21.6	9.6

Table G.11: Sediment-trap fluxes measured at station SN-0.8: 180 m.

start	end	mass	OC	N	BSi	$CaCO_3$	Al	Ti	$\delta^{13}C$	$\delta^{15}N$
ddmmyy		mg m^{-2} day^{-1}								
870120	870216	2783	138	17.1	294	100	129	7.78	-22.0	8.9
870216	870309	2389	137	16.7	318	83.4	110	6.97	-22.2	-
870309	870406	2414	131	15.9	423	41.1	128	7.08	-22.0	8.2
870406	870504	4219	232	30.6	1942	56.4	119	6.81	-20.0	7.5
870504	870615	3753	230	30.2	1689	65.1	92.0	5.59	-19.3	7.7
870615	870713	3774	330	40.9	1663	55.3	82.7	4.16	-17.8	8.3
870713	870826	2797	284	38.0	1123	66.2	65.1	4.16	-19.6	7.9
870826	870921	1078	116	16.9	258	8.58	30.7	2.25	-20.6	9.2
870921	871019	1153	115	15.9	383	4.94	14.0	1.02	-19.4	7.7
871019	871116	545	52.7	6.79	119	11.5	18.7	1.27	-20.9	9.3
871116	871214	1881	116	14.0	452	40.9	108	7.02	-22.8	-
871214	880105	2026	126	15.0	293	26.2	-	-	-	-
880105	880201	2403	132	15.4	397	62.2	130	7.58	-22.5	8.8
880201	880229	1514	92.9	11.5	272	28.9	-	-	-	8.5
880229	880328	1664	102	12.3	308	52.5	82.2	5.09	-	8.3
880328	880425	2994	169	21.4	843	35.6	111	6.48	-21.4	7.1
880425	880524	4157	255	30.5	1771	45.8	62.1	3.86	-19.4	6.6
880524	880627	2671	289	35.6	1049	20.3	19.8	1.34	-19.3	7.6
880627	880808	1383	186	26.8	317	-	37.5	2.68	-20.7	7.9
881017	881115	1965	187	18.7	377	63.0	41.5	3.00	-22.0	8.0
881115	881212	2191	147	17.6	296	60.4	72.2	4.81	-20.9	8.2
881212	890104	2273	138	15.7	297	61.4	103	6.24	-21.8	8.3
890104	890130	2411	133	15.8	321	61.8	119	7.16	-22.1	8.2
890130	890306	3219	176	19.7	454	115	160	9.67	-22.0	8.0
890306	890403	1866	110	14.0	255	55.8	77.4	5.05	-22.2	8.9
890403	890501	4549	271	35.9	1750	76.6	118	6.82	-21.3	7.2
890501	890605	3526	246	32.4	1479	45.5	61.2	3.57	-19.3	7.6
890605	890704	1686	141	18.6	650	15.5	26.7	1.67	-19.4	7.8
890704	890828	1631	223	26.6	463	26.0	28.7	1.89	-20.0	8.2
890828	891010	1154	127	16.2	148	56.6	16.5	1.31	-	8.5
891010	891215	1564	141	15.6	422	57.0	39.6	2.61	-20.1	8.8

Table G.12: Sediment-trap fluxes measured at station SN-0.8: 180 m (continued).

Appendix H

Sediment-trap data of Jervis Inlet

This appendix presents the sediment-trap data collected from Jervis Inlet during the study (see section 3.2 for methods). Sediment traps were moored in pairs with a brine solution at the base of each. In addition, NaN_3 was used in one sediment trap of each pair while no preservative was used in the other (section 3.2). The total mass, OC and N fluxes presented in these tables are the averages of the fluxes to the two traps in each pair. BSi, Al and Ti were measured on samples collected by the NaN_3-treated sediment traps and stable isotope ratios were determined for samples collected by sediment traps without NaN_3. The $CaCO_3$ fluxes presented in these tables are those collected by the sediment traps treated with sodium azide, as NaN_3 buffers $CaCO_3$ dissolution. "start" and "end" are the beginning and end of each deployment period.

start ddmmyy	end ddmmyy	mass	OC	N	BSi	$CaCO_3$	Al	Ti	$\delta^{13}C$	$\delta^{15}N$
		mg m^{-2} day^{-1}								
850808	850918	1179	263	33.3	525	38.0	6.53	0.350	-21.8	10.9
850918	851009	1416	422	58.3	502	37.5	8.53	0.461	-22.2	12.0
851009	851105	1049	157	17.2	216	45.4	42.7	2.34	-23.4	10.7
851217	860128	590	67.9	7.31	58.1	27.2	32.6	1.75	-22.9	9.9
860311	860415	1059	127	14.2	528	29.9	23.5	1.21	-22.8	8.7
860415	860513	1250	213	25.6	607	55.2	10.6	0.529	-22.6	9.3
860513	860604	2050	257	33.8	907	51.4	36.1	1.71	-22.3	8.6
860604	860715	1754	195	25.3	881	87.7	29.4	1.18	-20.3	7.3
860715	860806	872	132	16.4	377	16.8	10.4	0.410	-20.5	8.0
860806	860909	1592	164	18.9	987	19.5	9.17	0.501	-20.1	7.3
860909	861015	795	199	25.1	284	25.5	5.39	0.303	-21.5	9.2
861015	861113	841	247	31.2	285	19.4	7.22	0.372	-21.6	12.5
861113	861209	592	144	14.0	112	39.2	13.5	0.844	-23.1	9.7
870121	870217	459	100	11.1	50.2	22.7	19.7	1.03	-22.5	10.6
870217	870310	587	92.3	10.8	61.7	22.6	32.1	1.64	-22.5	10.8
870310	870407	453	87.0	10.8	129	13.2	11.6	0.723	-22.9	9.9
870407	870505	1783	167	21.7	1227	34.4	13.2	0.570	-21.9	7.8
870616	870714	1455	145	19.0	743	52.5	15.8	0.741	-20.4	8.3
870714	870827	1429	164	19.7	800	55.4	8.98	0.561	-20.1	7.3
870827	870922	732	164	19.7	242	29.3	5.10	0.286	-21.7	7.6
870922	871020	958	151	18.7	454	10.9	5.58	0.349	-22.0	8.0
871020	871117	661	85.1	9.71	329	21.7	6.89	0.353	-23.9	8.0
871117	871215	669	112	12.4	126	85.8	21.3	1.08	-22.4	10.5
871215	880106	382	82.3	8.21	53.3	31.0	11.0	0.625	-23.2	10.1
880106	880202	444	102	8.08	64.9	34.6	10.3	0.628	-21.0	9.0
880202	880329	590	63.4	7.19	348	18.5	6.12	0.300	-22.9	9.1
880329	880426	1982	186	22.2	1217	33.5	9.01	0.480	-21.4	8.0
880426	880525	1514	175	20.0	752	29.3	13.8	0.788	-20.8	-
880525	880628	1614	178	20.4	862	29.0	13.8	0.640	-21.2	7.6
880628	880809	898	111	13.7	372	32.0	8.38	0.361	-21.4	7.3
880809	880917	1214	152	18.3	627	40.4	7.13	0.332	-23.0	6.8
880917	881018	776	108	13.1	399	49.1	5.32	0.331	-23.4	7.1
881018	881116	736	133	14.1	98.2	53.2	24.2	1.37	-23.4	8.8
881116	881213	431	96.1	10.0	51.8	34.9	14.4	0.854	-22.8	9.9
881213	890105	325	66.6	6.98	43.7	36.7	9.89	0.708	-23.1	9.8
890105	890131	284	66.3	7.40	38.2	24.0	7.69	0.467	-23.3	-
890131	890307	431	69.9	7.47	73.3	31.6	16.6	0.864	-22.1	9.3
890307	890404	1074	115	14.0	616	28.5	7.68	0.389	-22.7	8.0
890404	890502	1849	141	17.8	1267	56.8	14.0	0.715	-22.5	6.9
890502	890606	1659	174	22.2	925	34.6	10.6	0.471	-22.3	6.9
890606	890705	2885	223	28.1	1296	91.0	28.5	1.68	-19.9	7.2
890705	890829	1086	185	19.6	340	40.5	8.67	0.377	-20.2	7.5

Table H.1: Sediment-trap fluxes measured at station JV-3: 50 m.

start ddmmyy	end ddmmyy	mass	OC	N	BSi	$CaCO_3$	Al	Ti	$\delta^{13}C$	$\delta^{15}N$
		mg m^{-2} day^{-1}								
850808	850918	1032	95.4	11.8	479	21.1	31.7	1.33	-	8.6
850918	851009	789	82.1	10.3	307	3.59	27.6	1.23	-	9.2
851009	851105	1482	120	11.7	320	21.8	77.8	3.84	-	7.8
851217	860128	927	106	10.8	120	16.4	52.8	2.87	-	10.3
860311	860415	1394	115	13.0	437	22.9	70.6	3.45	-	9.6
860415	860513	1575	118	13.2	596	17.7	59.9	2.97	-	9.0
860513	860604	2284	168	21.2	1021	24.9	66.0	3.32	-	8.5
860604	860715	2328	186	23.0	960	27.8	73.7	3.27	-	7.9
860715	860806	988	111	13.6	393	14.2	32.3	1.40	-	9.5
860806	860909	1694	144	18.1	744	19.9	52.7	2.53	-	8.7
860909	861015	1016	104	12.6	369	7.57	28.6	1.31	-	8.4
861015	861113	812	87.5	10.5	232	12.2	29.6	1.47	-	9.4
861113	861209	-	-	-	-	-	-	-	-	-
870121	870217	1214	123	14.2	168	20.8	75.2	3.66	-	9.7
870217	870310	1095	110	12.3	172	19.5	61.1	3.16	-	10.7
870310	870407	1069	95.1	10.9	200	9.89	60.0	3.21	-	9.4
870407	870505	2239	156	20.6	1041	17.9	62.7	2.79	-	8.5
870616	870714	2154	166	21.2	843	28.4	67.7	2.84	-	8.0
870714	870827	2264	184	22.1	924	22.9	51.9	2.96	-	7.6
870827	870922	1391	181	21.9	412	20.6	42.8	1.80	-	8.7
870922	871020	1063	137	16.2	323	14.6	37.4	1.67	-	8.4
871020	871117	1212	107	13.1	436	21.6	36.7	1.86	-	8.8
871117	871215	1114	124	13.6	230	34.7	49.5	2.46	-	9.8
871215	880106	1144	136	14.2	191	20.9	54.7	2.84	-	9.9
880106	880202	-	-	-	-	-	-	-	-	-
880202	880329	960	65.7	7.57	313	14.5	32.9	1.64	-	10.8
880329	880426	1643	132	14.2	736	15.0	46.9	2.30	-	11.1
880426	880525	2066	152	16.4	914	19.1	45.2	2.35	-	10.1
880525	880628	2021	149	16.0	830	20.6	36.7	1.87	-	9.2
880628	880809	1343	118	13.5	437	19.5	41.0	1.69	-	9.0
880809	880917	1779	153	17.0	671	29.8	39.1	1.52	-	8.2
880917	881018	1130	99.0	11.7	454	20.4	32.5	1.51	-	8.4
881018	881116	871	93.3	10.2	183	19.4	37.7	1.87	-	9.9
881116	881213	825	93.4	9.83	136	20.6	40.0	2.03	-	10.2
881213	890105	1078	117	13.8	177	22.1	47.9	2.54	-	10.0
890105	890131	690	75.9	8.66	114	14.5	33.6	1.77	-	10.6
890131	890307	1039	104	11.8	143	24.5	55.5	2.68	-	10.6
890307	890404	1346	106	12.8	398	17.4	54.8	2.82	-	10.4
890404	890502	1769	136	15.6	727	23.8	47.7	2.41	-	9.4
890502	890606	1721	126	15.2	662	22.2	45.1	2.30	-	8.4
890606	890705	3493	217	26.2	1381	36.9	60.3	2.81	-	7.9
890705	890829	1687	213	21.7	482	18.9	44.0	1.80	-	8.3

Table H.2: Sediment-trap fluxes measured at station JV-3: 300 m.

start	end	mass	OC	N	BSi	$CaCO_3$	Al	Ti	$\delta^{13}C$	$\delta^{15}N$
ddmmyy		mg m^{-2} day^{-1}								
850808	850918	4007	202	23.4	999	68.4	224	9.70	-21.2	7.6
850918	851009	4268	217	24.9	947	55.1	246	11.9	-21.5	7.6
851009	851105	6472	329	34.3	1294	97.7	389	19.2	-22.3	7.5
851217	860128	2362	154	16.5	368	36.9	135	7.00	-22.2	8.3
860311	860415	2023	119	12.8	521	29.1	97.1	4.81	-22.4	7.5
860415	860513	2369	130	15.0	756	28.0	104	5.03	-21.9	8.0
860513	860604	2610	153	18.1	919	27.0	96.8	4.56	-22.1	6.8
860604	860715	2765	178	21.3	931	31.8	117	5.41	-21.1	6.7
860715	860806	1308	109	12.8	360	20.5	54.7	2.63	-20.8	6.9
860806	860909	2001	125	13.7	652	29.3	87.8	4.06	-21.2	6.8
860909	861015	1853	119	14.0	594	23.9	81.2	3.82	-20.9	7.5
861015	861113	2375	136	16.5	546	37.7	125	6.21	-21.7	8.3
861113	861209	-	-	-	-	-	-	-	-	-
870121	870217	2317	144	16.5	337	32.5	144	6.84	-22.1	9.2
870217	870310	1780	122	12.8	273	19.9	109	4.92	-22.4	8.5
870310	870407	1898	112	11.9	354	17.0	102	5.07	-22.5	8.3
870407	870505	2679	141	16.6	1032	18.6	93.4	4.46	-22.2	6.4
870616	870714	2754	162	18.7	826	29.7	104	5.10	-21.2	6.7
870714	870827	3107	193	23.0	1051	21.9	101	4.42	-20.5	6.5
870827	870922	1944	161	18.6	502	22.7	75.5	3.19	-21.1	7.2
870922	871020	1972	136	17.4	467	29.8	85.7	4.04	-21.5	7.4
871020	871117	2485	134	16.8	609	35.3	107	5.44	-21.8	8.6
871117	871215	2000	133	15.4	399	37.0	99.5	4.77	-21.7	8.5
871215	880106	2159	143	16.5	368	32.9	108	5.41	-21.9	10.1
880106	880202	-	-	-	-	-	-	-	-	-
880202	880329	1313	74.5	8.27	351	20.5	55.7	2.54	-22.1	8.6
880329	880426	2289	116	12.9	810	21.7	81.4	3.92	-21.9	8.7
880426	880525	2402	143	16.2	1007	24.1	81.7	3.98	-21.4	8.0
880525	880628	2491	153	15.6	894	28.5	65.2	3.20	-21.4	8.0
880628	880809	1847	122	13.7	452	23.6	72.0	3.22	-21.5	7.8
880809	880917	2488	149	16.9	747	32.1	88.9	3.73	-21.7	7.7
880917	881018	2468	134	16.8	639	33.1	118	5.11	-21.8	7.4
881018	881116	3486	194	22.2	609	50.2	173	8.94	-22.1	8.8
881116	881213	2457	154	17.4	395	47.3	118	5.94	-22.1	9.5
881213	890105	2142	138	15.9	327	50.9	105	5.27	-21.9	9.7
890105	890131	1540	103	12.0	234	24.4	78.6	4.11	-22.1	9.7
890131	890307	1749	117	13.9	265	39.8	90.9	4.38	-22.0	9.3
890307	890404	2293	124	14.0	622	29.7	96.3	4.86	-21.9	8.5
890404	890502	2190	120	13.8	757	25.1	83.7	3.94	-22.1	7.7
890502	890606	2005	120	14.5	652	39.3	61.9	2.90	-21.8	7.5
890606	890705	3221	189	23.6	1098	30.9	67.6	3.04	-20.5	7.0
890705	890829	2136	191	19.7	537	29.1	74.0	3.22	-20.6	7.1

Table H.3: Sediment-trap fluxes measured at station JV-3: 600 m.

start ddmmyy	end ddmmyy	mass	OC	N	BSi	$CaCO_3$	Al	Ti	$\delta^{13}C$	$\delta^{15}N$
		mg m^{-2} day^{-1}								
850328	850424	1715	197	24.7	813	120	20.5	1.03	-21.5	6.7
850424	850522	1728	307	46.4	607	481	10.8	0.444	-23.6	-
850522	850704	2442	604	85.4	912	49.8	19.5	0.927	-21.5	-
850704	850808	1385	281	39.1	357	368	9.41	0.471	-21.5	11.8
850808	850919	1127	153	20.4	609	86.5	9.03	0.449	-22.4	9.0
850919	851009	1740	169	23.0	1262	56.6	7.26	0.359	-24.5	9.5
851009	851105	1142	113	12.4	184	41.6	55.9	2.92	-24.9	7.6
851105	851217	250	40.8	4.79	45.1	13.5	8.48	0.536	-24.1	8.5
851217	860128	844	69.7	7.95	48.4	12.2	52.6	2.69	-23.3	9.3
860128	860311	1033	111	14.2	66.1	16.8	59.6	2.85	-23.4	11.7
860311	860415	989	244	30.2	91.3	22.7	33.8	1.55	-23.0	11.8
860415	860513	1742	610	78.9	356	31.5	11.6	0.513	-22.8	11.8
860513	860604	3972	453	59.1	865	27.0	138	6.74	-22.7	9.3
860604	860715	1931	376	48.2	732	11.9	25.7	1.17	-21.2	9.3
860715	860806	998	212	27.8	327	12.5	15.2	0.714	-21.8	10.0
860806	860909	1994	482	65.5	788	7.98	11.7	0.515	-20.8	11.6
860909	861015	688	174	22.4	205	16.2	6.15	0.414	-22.5	9.8
861015	861113	844	231	30.0	220	11.8	16.7	0.979	-22.3	11.8
861113	861209	988	248	27.4	170	16.4	24.2	1.24	-23.2	11.6
861209	870121	1352	118	10.9	71.7	16.2	82.0	3.76	-24.3	9.6
870121	870217	344	54.6	6.16	32.6	11.0	14.8	0.800	-23.3	10.6
870217	870310	587	50.8	5.55	25.8	6.37	36.4	1.63	-23.8	9.8
870310	870407	735	253	39.9	47.9	3.79	10.1	0.554	-22.2	14.0
870407	870505	912	164	24.6	344	11.8	12.8	0.589	-23.5	11.7
870505	870616	1412	204	28.9	521	12.0	30.7	1.64	-22.3	11.0
870714	870827	1306	164	21.7	615	60.1	13.8	0.686	-20.6	7.8
870827	870922	822	163	19.6	233	20.5	8.83	0.501	-21.6	10.6
870922	871020	401	87.5	11.6	135	16.1	4.30	0.258	-24.3	7.6
871020	871117	619	80.9	10.1	205	9.16	17.2	0.838	-25.2	7.9
871117	871215	297	62.6	6.22	25.3	14.3	11.7	0.578	-23.8	9.8
871215	880106	257	51.2	6.19	43.5	20.6	6.59	0.342	-	9.6
880106	880202	381	62.7	7.09	50.3	21.5	13.9	0.691	-23.8	10.0
880202	880301	316	50.9	6.45	79.9	7.59	9.20	0.587	-23.4	6.6
880301	880329	940	137	16.6	394	22.0	12.3	0.601	-22.1	7.6
880329	880426	1149	140	16.5	869	10.7	7.50	0.347	-22.2	-
880426	880525	1634	190	19.3	611	25.6	28.4	1.21	-21.6	8.8
880525	880628	1094	137	16.0	439	24.8	20.4	0.976	-21.3	7.6
880628	880809	1125	165	20.8	371	47.9	17.1	0.783	-23.1	7.6
880809	880917	606	108	13.5	149	50.1	7.76	0.403	-24.4	7.2
880917	881018	693	101	13.9	301	92.1	6.17	0.383	-24.9	6.8
881018	881116	1040	98.6	9.41	81.1	42.4	49.5	2.32	-24.7	9.8
881116	881213	433	87.8	9.32	51.1	34.5	16.7	0.874	-24.0	-
881213	890105	336	72.9	9.56	32.4	18.6	9.57	0.560	-23.9	10.9
890105	890131	348	60.4	6.80	29.5	16.1	13.1	0.725	-23.8	-
890404	890502	1076	130	15.8	322	25.0	21.6	1.02	-23.7	8.6
890502	890606	1291	180	20.3	351	11.1	23.4	1.00	-24.1	10.2
890606	890705	2225	247	30.2	950	58.4	21.9	1.10	-21.1	8.4
890705	890829	737	163	18.8	148	57.0	9.14	0.486	-21.7	10.6
890829	891011	421	73.2	7.27	282	9.23	2.75	0.143	-19.9	7.4
891011	891219	1077	87.5	7.76	84.7	12.4	68.3	2.94	-24.3	7.3

Table H.4: Sediment-trap fluxes measured at station JV-7: 50 m.

start ddmmyy	end ddmmyy	mass	OC	N	BSi	$CaCO_3$	Al	Ti	$\delta^{13}C$	$\delta^{15}N$
		mg m^{-2} day^{-1}								
850328	850424	1512	120	15.1	658	35.1	33.2	1.61	-	7.5
850424	850522	810	90.2	12.2	296	34.4	21.8	0.944	-	-
850522	850704	1602	149	19.1	753	29.4	39.6	1.61	-	7.8
850704	850808	1188	132	17.5	483	26.4	24.0	1.09	-	7.9
850808	850919	1005	104	13.5	468	37.1	19.5	0.998	-	8.2
850919	851009	1215	90.4	11.2	753	8.02	16.6	0.800	-	7.1
851009	851105	1301	97.4	10.0	375	8.83	58.8	2.85	-	7.4
851105	851217	577	59.9	6.64	123	5.45	25.2	1.35	-	7.7
851217	860128	732	49.4	5.17	76.6	6.31	42.5	2.18	-	8.0
860128	860311	1120	90.8	9.12	99.0	10.6	70.3	3.22	-	8.5
860311	860415	978	98.6	12.9	113	7.37	53.2	2.56	-	9.9
860415	860513	843	104	12.5	193	11.8	32.3	1.57	-	9.9
860513	860604	2838	189	22.4	730	22.6	135	6.74	-	7.5
860604	860715	1841	140	17.5	767	10.2	57.7	2.65	-	8.0
860715	860806	1000	113	14.8	254	32.1	35.1	1.65	-	7.9
860806	860909	1497	130	15.6	786	14.0	32.0	1.53	-	7.5
860909	861015	1061	108	12.6	435	20.7	32.0	1.48	-	8.0
861015	861113	665	77.6	9.68	193	5.31	25.9	1.33	-	8.0
861113	861209	1822	121	13.4	506	39.0	84.1	3.90	-	7.8
861209	870121	1441	104	9.36	128	8.91	95.5	4.86	-	8.1
870121	870217	778	72.8	7.76	79.3	7.87	41.0	2.15	-	9.4
870217	870310	1095	92.7	9.46	91.3	7.93	66.9	2.94	-	9.1
870310	870407	738	72.2	8.20	77.5	0.78	45.7	1.90	-	9.1
870407	870505	674	71.8	9.28	182	2.82	28.1	1.27	-	9.0
870505	870616	-	-	-	-	-	-	-	-	-
870714	870827	1667	133	15.8	594	7.57	27.3	1.35	-	-
870827	870922	1175	152	18.6	374	5.19	21.5	1.09	-	7.9
870922	871020	495	80.5	10.9	110	14.7	10.7	0.578	-	7.9
871020	871117	723	79.1	9.85	229	9.22	23.6	1.09	-	7.2
871117	871215	577	75.2	8.09	84.1	8.60	24.4	1.18	-	8.9
871215	880106	447	64.8	7.21	62.3	6.16	16.1	0.863	-	9.2
880106	880202	617	81.2	9.29	97.6	16.1	25.4	1.18	-	9.0
880202	880301	-	-	-	-	-	-	-	-	-
880301	880329	-	-	-	-	-	-	-	-	-
880329	880426	1247	118	13.3	585	10.7	24.6	1.17	-	-
880426	880525	2034	163	17.8	768	12.4	34.4	1.57	-	7.7
880525	880628	955	110	11.9	270	11.2	27.1	1.21	-	8.2
880628	880809	1128	117	13.5	303	21.1	24.8	1.28	-	7.9
880809	880917	852	118	14.1	226	26.6	20.6	0.964	-	8.0
880917	881018	776	85.7	10.9	256	22.7	18.9	0.763	-	7.3
881018	881116	1278	108	9.84	161	10.5	57.4	2.57	-	6.0
881116	881213	540	64.2	6.50	80.5	15.0	25.8	1.21	-	8.4
881213	890105	565	71.1	7.58	71.6	18.3	24.9	1.18	-	7.9
890105	890131	491	63.0	7.06	68.2	21.1	18.5	0.990	-	10.9
890404	890502	870	88.5	10.5	262	16.2	31.8	1.31	-	9.4
890502	890606	1806	130	15.2	705	23.3	39.0	1.65	-	-
890606	890705	2024	156	18.7	794	22.1	32.5	1.54	-	7.6
890705	890829	960	136	14.4	229	19.4	19.1	0.943	-	8.2
890829	891011	982	125	12.2	402	5.65	12.1	0.589	-	6.5
891011	891219	1264	88.6	7.51	128	6.01	77.5	3.36	-	6.4

Table H.5: Sediment-trap fluxes measured at station JV-7: 200 m.

start ddmmyy	end	mass	OC	N	BSi	$CaCO_3$	Al	Ti	$\delta^{13}C$	$\delta^{15}N$
					mg m^{-2} day^{-1}					
850328	850424	2424	134	16.6	1077	26.5	60.4	3.17	-21.0	8.3
850424	850522	1404	87.1	10.6	406	27.7	52.9	2.44	-21.7	-
850522	850704	2231	149	18.8	643	39.2	88.3	3.83	-21.2	7.8
850704	850808	1722	137	18.3	560	14.0	55.1	2.48	-21.1	8.3
850808	850919	1801	125	16.1	572	51.4	64.8	2.94	-21.4	-
850919	851009	2376	147	20.2	702	32.8	90.9	4.04	-21.7	9.4
851009	851105	3329	181	20.0	776	53.4	162	8.05	-23.1	7.9
851105	851217	1444	104	12.5	261	20.2	67.6	3.51	-22.8	8.3
851217	860128	1529	104	12.4	211	36.9	73.2	3.70	-22.9	9.1
860128	860311	1834	115	12.0	201	29.6	102	4.78	-23.4	8.4
860311	860415	1845	121	12.4	250	21.5	115	5.49	-23.2	9.0
860415	860513	1272	90.4	9.48	287	20.7	69.8	3.26	-23.6	7.8
860513	860604	3491	185	20.6	875	12.5	189	9.16	-22.6	6.4
860604	860715	1974	115	13.5	643	6.97	83.9	3.71	-22.0	6.2
860715	860806	1192	87.2	10.4	297	7.69	51.9	2.30	-22.4	8.2
860806	860909	1867	117	12.7	619	11.2	55.4	2.53	-21.6	7.7
860909	861015	1341	113	15.0	482	12.1	43.1	1.94	-21.2	8.9
861015	861113	1485	105	13.4	332	20.3	66.8	3.18	-22.1	7.7
861113	861209	1844	121	12.7	225	4.00	74.5	3.47	-22.6	9.8
861209	870121	2457	149	14.6	315	26.2	132	6.60	-23.5	8.9
870121	870217	1492	100	10.8	188	14.2	83.7	3.86	-23.0	8.4
870217	870310	1780	127	14.4	213	18.0	97.5	4.47	-22.9	9.4
870310	870407	1329	85.9	8.31	161	5.57	81.3	3.47	-23.7	7.4
870407	870505	948	66.4	6.86	188	4.93	49.4	2.21	-24.1	7.2
870505	870616	-	-	-	-	-	-	-	-	-
870714	870827	1855	115	13.2	572	6.29	50.0	2.28	-21.5	6.3
870827	870922	1570	120	14.4	522	9.8	52.0	2.69	-21.7	7.2
870922	871020	966	82.9	9.94	213	10.9	38.0	1.74	-22.2	7.7
871020	871117	1347	89.9	11.0	329	16.0	53.7	2.58	-23.3	7.2
871117	871215	1315	92.2	10.1	229	13.6	57.4	2.65	-23.5	7.8
871215	880106	1126	92.9	11.2	187	13.3	48.7	2.32	-22.8	8.1
880106	880202	1422	105	11.2	243	13.3	64.8	2.80	-23.2	8.4
880202	880301	-	-	-	-	-	-	-	-	-
880301	880329	1422	100	10.8	351	13.9	53.4	2.47	-23.2	7.9
880329	880426	1621	115	13.1	566	6.12	50.8	2.31	-22.3	-
880426	880525	2485	160	17.0	973	10.1	54.6	2.24	-21.3	7.5
880525	880628	1360	93.2	10.3	317	7.29	48.2	2.09	-	6.8
880628	880809	1537	106	11.7	342	14.3	50.7	2.12	-22.2	7.4
880809	880917	1293	96.5	10.1	289	11.6	41.1	1.84	-23.0	7.5
880917	881018	1438	97.9	11.7	348	31.4	54.4	2.38	-21.3	7.2
881018	881116	2783	175	17.7	397	45.2	136	6.55	-23.3	7.4
881116	881213	1748	122	14.8	273	50.9	82.4	3.66	-22.4	8.9
881213	890105	1508	118	15.4	213	35.7	61.1	2.81	-22.1	10.3
890105	890131	1467	102	11.9	215	22.2	62.8	2.88	-22.7	9.3
890404	890502	1164	78.2	8.79	246	9.09	56.6	2.13	-23.3	7.5
890502	890606	1404	96.7	11.4	507	17.9	45.5	1.96	-22.9	6.7
890606	890705	2005	127	15.1	662	13.5	58.8	2.43	-21.7	6.9
890705	890829	1147	110	12.0	285	9.25	38.3	1.70	-22.1	7.3
890829	891011	1490	147	13.8	466	7.76	35.1	1.61	-20.3	6.6
891011	891219	2280	136	13.0	273	28.1	142	6.18	-23.3	-

Table H.6: Sediment-trap fluxes measured at station JV-7: 450 m.